

# Development of Functionalized Metal-Organic Frameworks for Gas Storage and Fluorescence Sensing Applications



*A Dissertation Submitted to the  
Indian Institute of Technology Guwahati  
as Partial Fulfillment for the Degree of*

**DOCTOR of PHILOSOPHY**

*by*

**Amlan Buragohain**

**DEPARTMENT OF CHEMISTRY  
INDIAN INSTITUTE OF TECHNOLOGY GUWAHATI  
GUWAHATI, INDIA**

**April 2017**

# Development of Functionalized Metal-Organic Frameworks for Gas Storage and Fluorescence Sensing Applications

*A Dissertation Submitted to the  
Indian Institute of Technology Guwahati  
as Partial Fulfillment for the Degree of*

**DOCTOR of PHILOSOPHY**

*by*

**Amlan Buragohain  
Roll No: 136122029**



**Department of Chemistry  
Indian Institute of Technology Guwahati  
Guwahati – 781039, Assam, India  
April 2017**

## STATEMENT

I hereby declare that this thesis entitled, “**Development of Functionalized Metal-Organic Frameworks for Gas Storage and Fluorescence Sensing Applications**” is the outcome of research work carried out by me under the supervision of Dr. Shyam P. Biswas, at the Department of Chemistry, Indian Institute of Technology Guwahati, Guwahati, Assam, India.

In keeping with the general practice of reporting scientific observations, due acknowledgement has been made whenever work described here has been based on the findings of other investigators.

IIT Guwahati

April 2017

Amlan Buragohain

Candidate

*Dr. Shyam P. Biswas*  
*Assistant Professor*



*Department of Chemistry  
Indian Institute of Technology Guwahati  
Guwahati – 781039, India  
Tel: +91 – 361 – 258 3309  
Email: [sbiswas@iitg.ernet.in](mailto:sbiswas@iitg.ernet.in)*

---

## Certificate

Certified that the work described in this thesis entitled “**Development of Functionalized Metal-Organic Frameworks for Gas Storage and Fluorescence Sensing Applications**” by Mr. Amlan Buragohain, Department of Chemistry, Indian Institute of Technology Guwahati has been carried out under my supervision and has not been submitted elsewhere for a degree.

IIT Guwahati  
April 2017

Shyam P. Biswas  
Thesis supervisor  
Department of Chemistry  
Indian Institute of Technology Guwahati  
Guwahati – 781039, Assam, India

## ACKNOWLEDGEMENT

---

*The successful outcome of my thesis works has many supporting hands without which it would not have been possible to make it a reality. At the very onset, with a deepest sense of gratitude, I wish to express my sincere thanks to my supervisor, Dr. Shyam P. Biswas for his proficient guidance, inspiration, creative and scientific ideas which helped me to explore the domain of my work assembled in this thesis.*

*Besides my supervisor, I would also like to extend my heartiest thanks to the doctoral committee members, Prof. Gopal Das, Dr. Chandan Mukherjee and Dr. Kingsuk Mahata for their periodic evaluation of my work and valuable suggestions. I would like to thank all faculty members and staff members of Chemistry department. My sincere thanks to the staffs of Central Instruments Facility, for their help and in hand guidance to several analytical instruments, required during my research work.*

*I wish to express my sincere gratitude to IIT Guwahati for all the facilities that were made available to me and the Ministry of Human Resource Development (MHRD), India for the financial support.*

*I would like to thank all my present group members Rana, Mostakim, Aniruddha, Soutick, and Chiranjib for their timely help, support and for creating a pleasant atmosphere in the lab.*

*I extend my sincere thanks to all my friends for their constant unfailing support, their encouragement and all the help they extended whenever required. I also wish to thank Nilotpal, Hiranya, Jugal, Tridip, Abhijit Da, Pingal, Romen, Anupal, Saurav, Rupinder for the joyful & special moments shared with me during my course of PhD and their support.*

*No words would suffice to express my feelings for my teachers to whom I owe my obligations for all their great teachings and philosophy to be a good human; Nayanmoni Sir, AKP Sir, Ruli Ma'am, Nandita Ma'am, Pushpa Sir, Basdev Sir and the entire fraternity from my school, college and university who gave me the direction and insightful information to march forward in this field.*

*Finally, my Ph. D. endeavor could not have been completed without the endless love, endless support, tolerance and blessings from my family. I would like to express my deepest gratitude to my parents for all the unconditional love and sacrifices they have made for the sake of my upbringing. I am also grateful to my brother Dipu, Mahi, Apa, Bardeuta, Barma and Ishani for their affection and deep concern for my career.*

*Still many names are missing whose contribution and help is worth mentioning.*

*Amlan*

---

*Dedicated to My Father & Mother*

---



# TABLE OF CONTENTS

---

<b>SYNOPSIS</b>	<b>i</b>
<b>CHAPTER 1: INTRODUCTION AND BRIEF HISTORY OF FUNCTIONALIZED METAL-ORGANIC FRAMEWORKS (MOFs)</b>	
1.1 INTRODUCTION	1
1.2 BASIC DESIGN PRINCIPLES	2
1.2.a Node-and-Spacer Strategy	2
1.2.b Vertex-Linked Polygons or Polyhedra (VLPP) Strategy	4
1.2.c SBU Strategy	5
1.3 SYNTHETIC METHODS	7
1.3.1 Hydro/Solvothermal Synthesis	9
1.3.2 Microwave-Assisted and Sonochemical Synthesis	9
1.3.3 Electrochemical and Mechanochemical Synthesis	10
1.3.4 Post-Synthetic Modification	10
1.4 HISTORY	10
1.5 MOFs AS CHEMICAL SENSORS	14
1.5.1 MOFs for Sensing of Nitroaromatic Explosives	15
1.5.2 MOFs for Sensing of Hydrogen Sulphide	20
1.6 MOFs FOR CO <sub>2</sub> ADSORPTION	20
1.7 MOTIVATION AND OBJECTIVES	26
1.8 REFERENCES	27
<b>CHAPTER 2: IMPROVED SYNTHESIS OF ZIRCONIUM(IV) MUCONATE MOF: CHARACTERIZATION, STABILITY AND GAS SORPTION PROPERTIES</b>	
2.1 INTRODUCTION	39
2.2 EXPERIMENTAL SECTION	40
2.2.1 Materials and General Methods	40
2.2.2 Synthesis of [Zr <sub>6</sub> O <sub>4</sub> (OH) <sub>4</sub> (C <sub>6</sub> H <sub>4</sub> O <sub>4</sub> ) <sub>6</sub> ].1.5DMF.10H <sub>2</sub> O (1-H <sub>2</sub> O-AS)	40
2.2.3 Synthesis of [Zr <sub>6</sub> O <sub>4</sub> (OH) <sub>4</sub> (C <sub>6</sub> H <sub>4</sub> O <sub>4</sub> ) <sub>6</sub> ].1.3DMF.8H <sub>2</sub> O (1-HCl-AS)	41
2.2.4 Activation of the Compounds	41
2.3 RESULTS AND DISCUSSIONS	41
2.3.1 Synthesis, Activation and FT-IR Analysis	41

---

## TABLE OF CONTENTS

---

2.3.2	Structure Description	45
2.3.3	Thermal and Chemical Stability	47
2.3.4	Gas Sorption Properties	49
2.4	CONCLUSIONS	50
2.5	REFERENCES	50

### **CHAPTER 3: 3D LUMINESCENT AMIDE-FUNCTIONALIZED CADMIUM TETRAZOLATE FRAMEWORK FOR SELECTIVE DETECTION OF 2,4,6-TRINITROPHENOL**

3.1	INTRODUCTION	55
3.2	EXPERIMENTAL SECTION	56
3.2.1	Materials and General Methods	56
3.2.2	Synthesis	57
3.2.3	Activation of the Compound	58
3.2.4	Single-Crystal X-Ray Diffraction	58
3.2.5	Fluorescence Quenching Titration Experiments	60
3.3	RESULTS AND DISCUSSIONS	60
3.3.1	Synthesis	60
3.3.2	Structure Description	61
3.3.3	X-ray Powder Diffraction and FT-IR Analysis	66
3.3.4	Thermal Stability	66
3.3.5	Photoluminescence Properties	68
3.3.6	Sensing of Nitroaromatic Explosives	70
3.3.7	Estimation of Quenching Constant and Detection Limit for TNP	74
3.3.8	Response Time of 1' towards the Detection of TNP	77
3.3.9	Mechanisms for the Detection of Nitroaromatic Explosives	79
3.4	CONCLUSIONS	82
3.5	REFERENCES	82

### **CHAPTER 4: CERIUM BASED AZIDE- AND NITRO-FUNCTIONALIZED UIO-66 FRAMEWORKS AS FLUORESCENT TURN-ON PROBES FOR THE SENSING OF H<sub>2</sub>S**

4.1	INTRODUCTION	87
-----	--------------	----

---

## TABLE OF CONTENTS

---

4.2	EXPERIMENTAL SECTION	89
4.2.1	Materials and General Methods	89
4.2.2	Synthesis of Ce-UiO-66-N <sub>3</sub> (1-N <sub>3</sub> )	89
4.2.3	Synthesis of Ce-UiO-66-NO <sub>2</sub> (2-NO <sub>2</sub> )	90
4.2.4	Activation of the Compounds	90
4.2.5	Preparation of the Medium for Fluorescence Studies	90
4.2.6	Fluorescence Titration Experiments	90
4.3	RESULTS AND DISCUSSIONS	91
4.3.1	Synthesis and Characterization	91
4.3.2	Thermal and Chemical Stability	94
4.3.3	Fluorescence Turn-On Experiments: Sensing of H <sub>2</sub> S	97
4.3.4	Recyclability Test	107
4.3.5	Gas Adsorption Properties	107
4.4	CONCLUSIONS	109
4.5	REFERENCES	110
 <b>CHAPTER 5: SYNTHESIS AND GAS ADSORPTION PROPERTIES OF NEW FUNCTIONALIZED AL-MIL-101-X (X = -CH<sub>3</sub>, -NO<sub>2</sub>, -OCH<sub>3</sub>, -C<sub>6</sub>H<sub>4</sub>, -F<sub>2</sub>, -(CH<sub>3</sub>)<sub>2</sub>, -(OCH<sub>3</sub>)<sub>2</sub>) MATERIALS</b>		
5.1	INTRODUCTION	113
5.2	EXPERIMENTAL SECTION	114
5.2.1	Materials and General Methods	114
5.2.2	Synthesis	115
5.2.3	Activation of the As-Synthesized Al-MIL-101-X-CE Materials	117
5.3	RESULTS AND DISCUSSIONS	118
5.3.1	Synthesis and Activation	118
5.3.2	Structure Description	121
5.3.3	Infrared Spectroscopy	128
5.3.4	Thermal Stability	130
5.3.5	Gas Adsorption Properties	132
5.4	CONCLUSIONS	135
5.5	REFERENCES	135

---

## TABLE OF CONTENTS

---

<b>CHAPTER 6: SYNTHESIS, CHARACTERIZATION AND SORPTION PROPERTIES OF FUNCTIONALIZED CR-MIL-101-X (X = -F, -Cl, -Br, -CH<sub>3</sub>, -C<sub>6</sub>H<sub>4</sub>, -F<sub>2</sub>, -(CH<sub>3</sub>)<sub>2</sub>) MATERIALS</b>	
6.1 INTRODUCTION	141
6.2 EXPERIMENTAL SECTION	142
6.2.1 Materials and General Methods	142
6.2.2 Synthesis	144
6.2.3 Activation of the As-Synthesized Cr-MIL-101-X Compounds	145
6.3 RESULTS AND DISCUSSIONS	145
6.3.1 Synthesis and Activation	145
6.3.2 Structure Description	147
6.3.3 DRIFT Analysis	148
6.3.4 Thermal Stability	149
6.3.5 Sorption Properties	150
6.4 CONCLUSIONS	155
6.5 REFERENCES	156
<b>CONCLUSIONS AND OUTLOOK</b>	159
<b>ANNEXURE-I</b>	163
<b>ANNEXURE-II</b>	167
<b>ANNEXURE-III</b>	173
<b>ANNEXURE-IV</b>	177
<b>LIST OF PUBLICATIONS AND CONFERENCES ATTENDED</b>	181

**Thesis Title:** Development of functionalized metal-organic frameworks for gas storage and fluorescence sensing applications

**Name of the Candidate:** Shri Amlan Buragohain

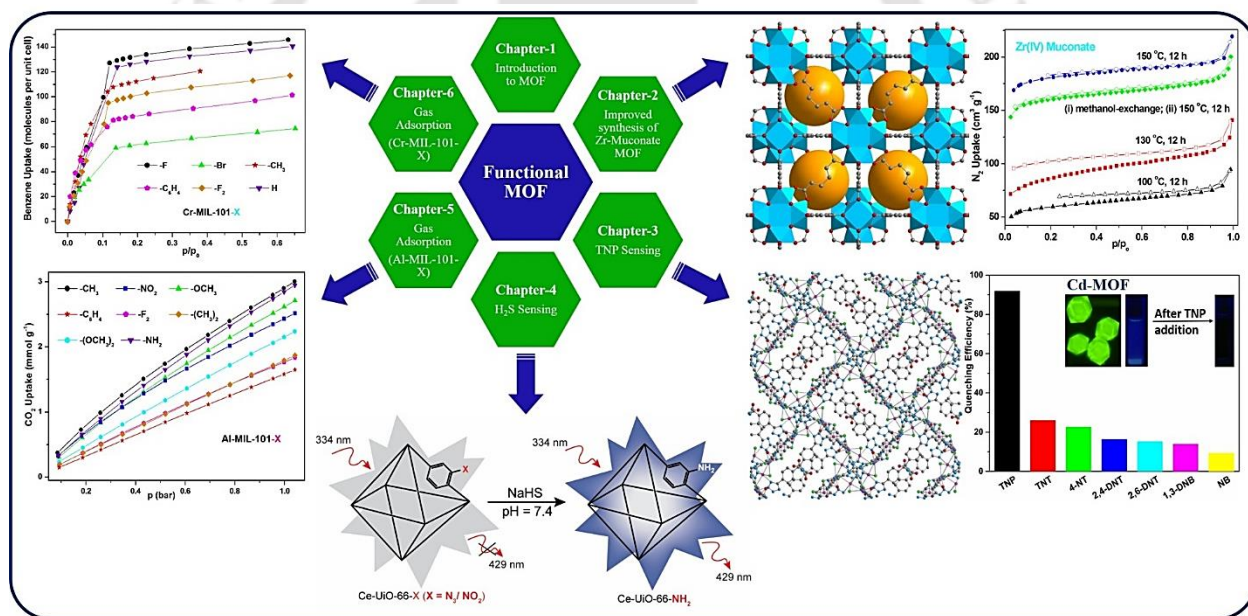
**Registration Number:** 136122029

**Thesis Supervisor:** Dr. Shyam P. Biswas

**Department:** Chemistry

**Institute:** Indian Institute of Technology Guwahati, Assam – 781039, India.

## Thesis Overview:



**Chapter 1** describes potential applications of MOFs in gas (H<sub>2</sub>, CO<sub>2</sub>, CH<sub>4</sub>, CO, etc.) storage and fluorescence sensing of a wide variety of analytes (cations, anions, biomolecules, small molecules, volatile organic compounds, nitro explosive materials, etc.). Functionalization of MOFs has been demonstrated as a promising strategy to enhance the physicochemical stability (air, water, acid-base, heat, etc.) as well as gas storage and separation properties of the resulting MOFs. The attached functional groups can act as interaction sites for specific gas molecules (during gas adsorption) and analytes (during fluorescence sensing), thus increasing the selectivity of the MOF

material towards the target gas or analyte. In this chapter, recent advancements in rational design and synthesis of various functional MOFs in gas storage and fluorescence sensing behavior have been discussed.

**Chapter 2** presents an improved synthesis procedure for the preparation of the previously reported Zr(IV) *trans,trans*-muconate framework compound. Instead of using non-commercial Zr<sub>6</sub>-methacrylate oxocluster as the metal source, the same MOF material was successfully synthesized by using commercially available ZrCl<sub>4</sub> as the Zr source. During the synthesis, small amounts of H<sub>2</sub>O (**1-H<sub>2</sub>O-AS**) or concd. HCl (**1-HCl-AS**) were used as additives in DMF. The effect of ZrCl<sub>4</sub>/additive molar ratio on the crystallinity of the compounds has been systematically examined. The phase purity of the materials having optimum crystallinity was investigated by a combination of XRPD analysis (Figure 1), FT-IR spectroscopy, thermogravimetric and elemental analyses. The physicochemical stability of the materials was examined. According to the thermogravimetric analyses, the two materials are stable up to ~250 °C in air atmosphere. As confirmed by the XRPD analyses, the **1-HCl** material is unstable in acetic acid, 1M HCl and 1M NaOH solutions. The crystallinity of the materials deteriorated slowly when they were exposed to water as well as moisture (from air), suggesting gradual structural collapse of the framework over time.

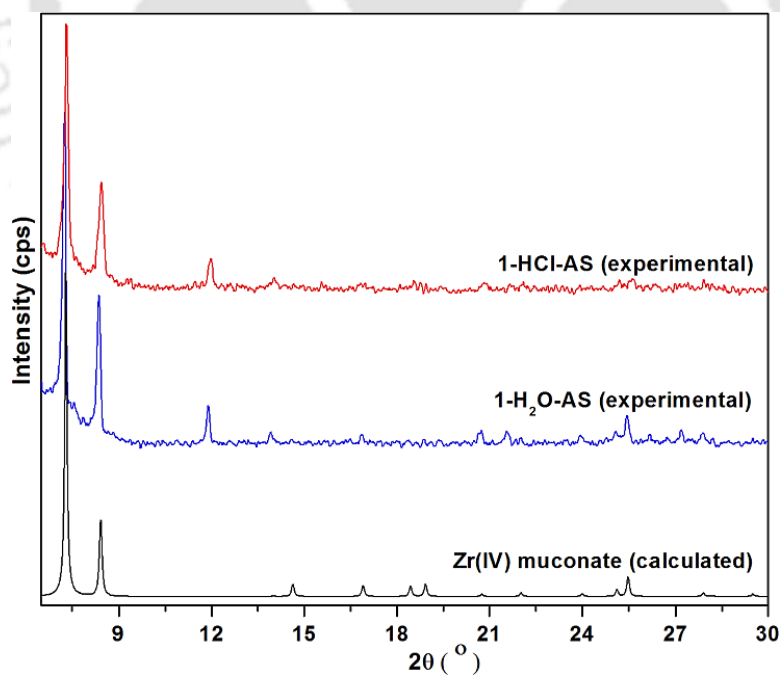


**Figure 1.** Calculated (black) XRPD pattern of Zr(IV) muconate, and experimental XRPD patterns of **1-H<sub>2</sub>O-AS** (blue) and **1-HCl-AS** (red).

The effect of activation temperature on the BET surface area of the materials was also examined. As corroborated by the N<sub>2</sub> sorption measurements, the optimally activated **1-HCl** exhibited BET surface area of 557 m<sup>2</sup> g<sup>-1</sup> (Figure 2), which is lower than the isostructural UiO-66 (950 m<sup>2</sup> g<sup>-1</sup>) but close to the literature value (705 m<sup>2</sup> g<sup>-1</sup>) of Zr(IV) muconate. The moderate physicochemical stability along with significant porosity of the material will make it a promising candidate in the field of gas storage and separation.

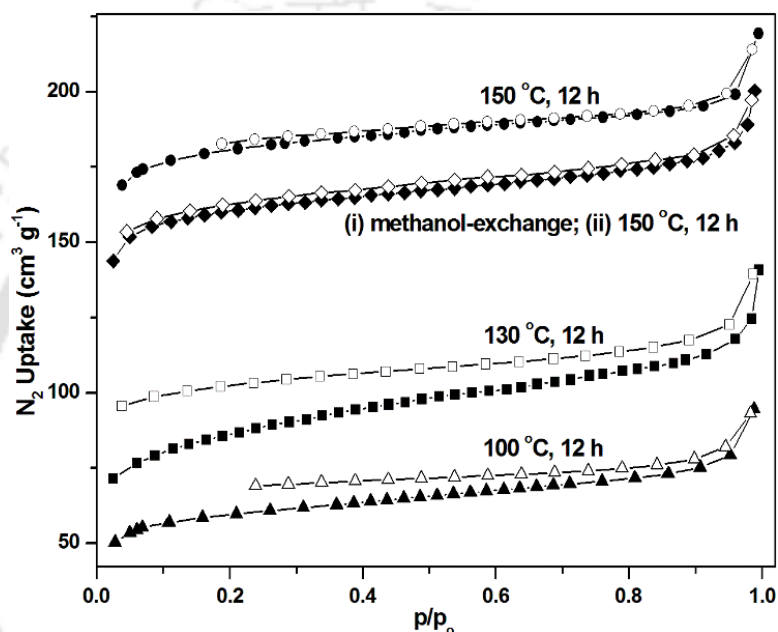


**Figure 2.** N<sub>2</sub> adsorption (filled symbols) and desorption (empty symbols) isotherms of thermally activated samples of **1-HCl** measured at  $-196\text{ }^{\circ}\text{C}$ . The sample was heated at  $150\text{ }^{\circ}\text{C}$  under vacuum for 12 h before the sorption measurement. The sorption isotherms of a sample of **1-HCl**, which was activated in two steps (exchange of guest molecules with methanol, followed by thermal activation at  $150\text{ }^{\circ}\text{C}$  under vacuum for 12 h), are also shown for comparison. (*Eur. J. Inorg. Chem.*, 2015, 2463)

**Chapter 3** presents a successful synthesis of strongly fluorescent 3D Cd(II)-based MOF (**1**) incorporating a highly  $\pi$ -conjugated amide-functionalized ditopic tetrazolate-based organic ligand under solvothermal conditions (Figure 3). Selective detection of TNP by activated compound (**1'**) with a very high rate of response was confirmed by the steady-state fluorescence titration experiments (Figure 4). It was found that the selective detection of TNP was also possible in presence of other potentially interfering nitroaromatic explosives. The detection limit of **1'** for the sensing of TNP was estimated to be  $1.87 \times 10^{-7}\text{ M}$  (42.84 ppb), which is comparable with other MOF-based fluorescence sensors reported until today. The recyclability experiments indicate high

photostability and reusability of **1'** for long-term in-field detection of nitroaromatic explosive materials. The combination of experimental and theoretical results provides indications in favour of both energy and electron transfer mechanisms for the highest quenching efficiency of TNP. Moreover, the enhanced selectivity of **1'** for sensing of TNP can be intuitively attributed to the existence of electrostatic interactions between the N-H moiety of the ligand and the hydroxyl group of TNP. The outstanding sensing performance renders the material as a promising sensing device for the practical detection of TNP.

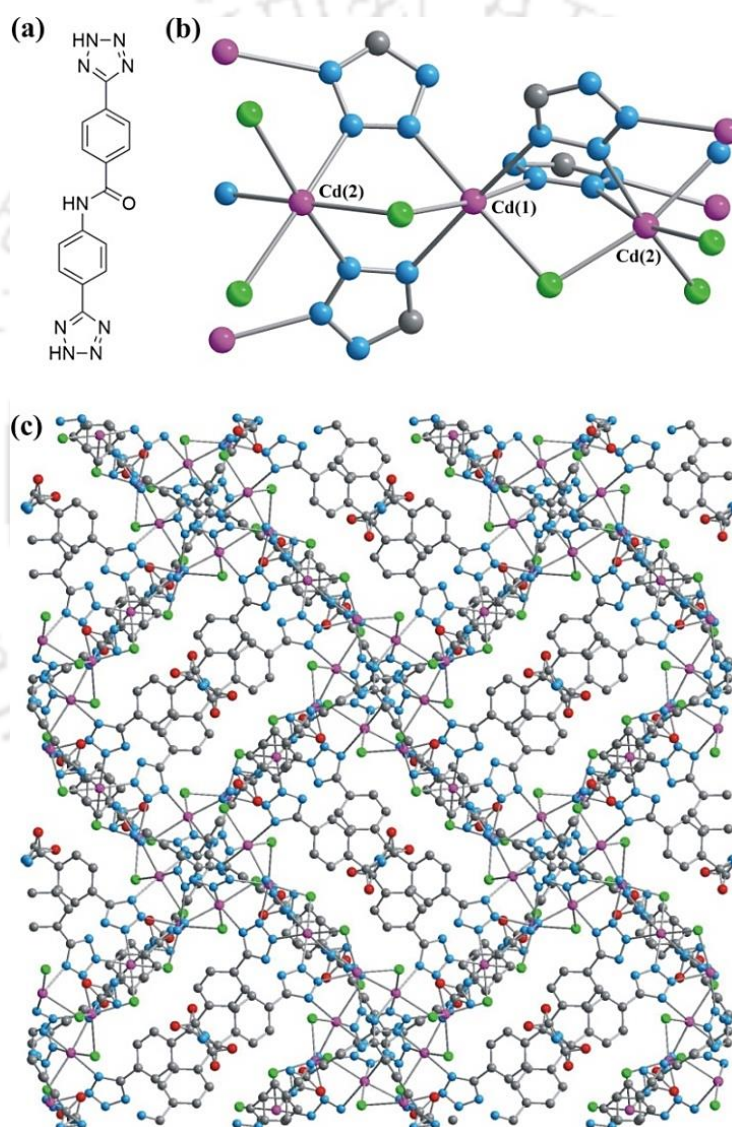


**Figure 3.** (a) Structure of  $H_2L$  ligand employed for synthesizing **1**. (b) Ball-and-stick representation showing the coordination environment around of  $Cd^{2+}$  ions in **1**. (c) The same representation of the 3D framework structure of **1**. Color codes: Cd, magenta; N, cyan; Cl, green; C, gray; O, red. The guest molecules and hydrogen atoms have been removed from the structural plots for clarity.

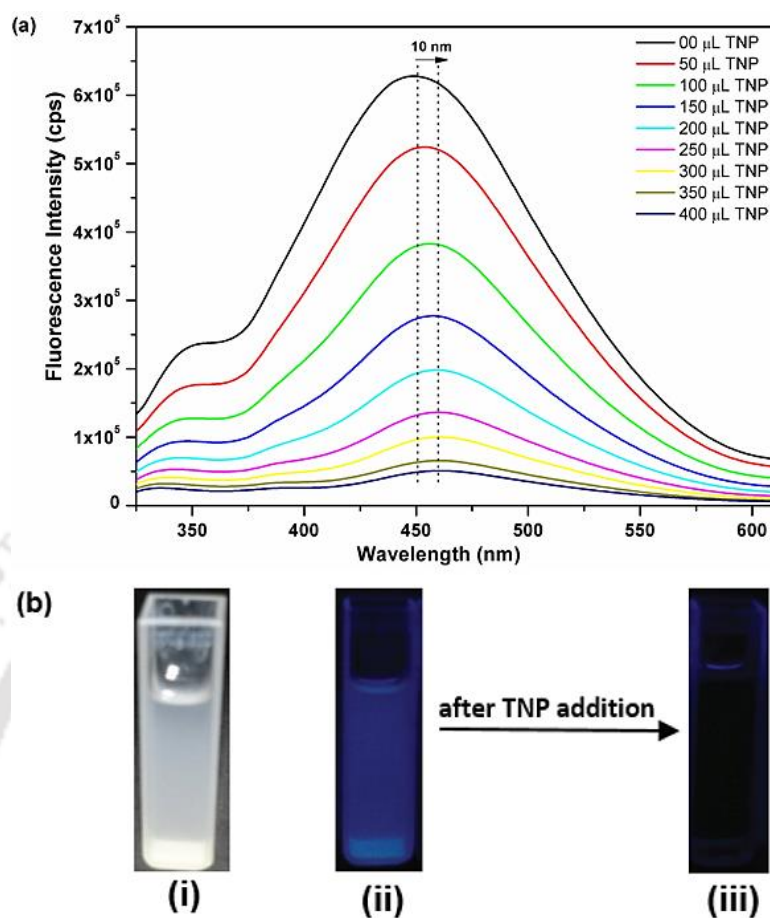


**Figure 4.** (a) Quenching of fluorescence intensity of **1'** by incremental addition of 1 mM TNP solution to a 3 mL suspension of **1'** in ethanol ( $\lambda_{\text{ex}} = 315$  nm and  $\lambda_{\text{max}} = 450$  nm). (b) Photographs of fluorescence cuvettes containing ethanol suspensions of **1'** under visible light (i), UV light before TNP addition (ii) and UV light after TNP addition (iii). (*Cryst. Growth Des.*, 2016, 16, 842)

**Chapter 4** presents a new (**1'-N<sub>3</sub>**) and an existing (**2'-NO<sub>2</sub>**) Ce(IV)-based MOF with UiO-66 framework topology for the first time as fluorescence turn-on probes for the detection of H<sub>2</sub>S under physiological conditions (Figure 5). Both compounds have demonstrated promising potentials towards highly selective, sensitive (detection limits: 12.2  $\mu\text{M}$  for **1'-N<sub>3</sub>** and 34.8  $\mu\text{M}$  for **2'-NO<sub>2</sub>**) and fast detection of H<sub>2</sub>S. It was found that the Ce-based UiO-66 MOFs exhibited improved fluorescence response towards H<sub>2</sub>S than their Zr-based counterparts. Owing to their extraordinary selectivity towards sensing of H<sub>2</sub>S even in the presence of other potentially interfering biomolecules, these compounds could be promising candidates for the real-time monitoring of H<sub>2</sub>S in biological systems. Besides the rapid, selective and sensitive detection of H<sub>2</sub>S, both of these compounds can effectively adsorb considerable amounts CO<sub>2</sub> at 0 °C and in pressure range of 0 to 1 bar. As a consequence, they are also excellent materials in the field of CO<sub>2</sub> capture.

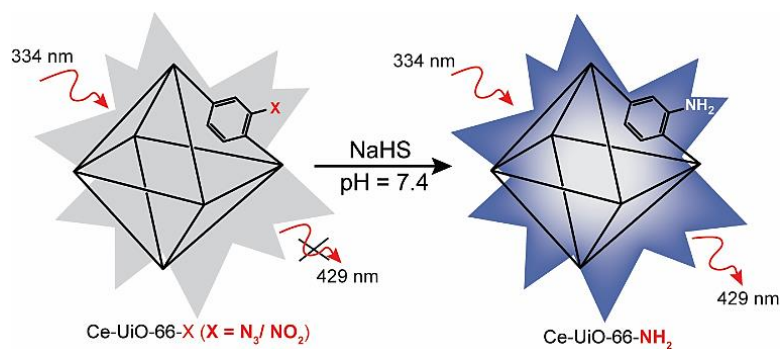


**Figure 5.** Fluorescent turn-on probes resulting from the NaHS-mediated reduction of Ce-UiO-66-X (X = N<sub>3</sub> or NO<sub>2</sub>) MOFs to Ce-UiO-66-NH<sub>2</sub>. (*CrystEngComm*, 2016, 18, 4374)

**Chapter 5** presents the facile synthesis, full characterization and gas adsorption properties of seven new functionalized Al-MIL-101-X (X = -CH<sub>3</sub>, -NO<sub>2</sub>, -OCH<sub>3</sub>, -C<sub>6</sub>H<sub>4</sub>, -F<sub>2</sub>, -(CH<sub>3</sub>)<sub>2</sub>, -(OCH<sub>3</sub>)<sub>2</sub>) materials. The seven new materials along with the previously reported Al-MIL-101-NH<sub>2</sub> compound were prepared by using stoichiometric mixtures of Al(ClO<sub>4</sub>)<sub>3</sub>·9H<sub>2</sub>O and H<sub>2</sub>BDC-X linkers in DEF under similar solvothermal conditions (130 °C, 3-12 h) with conventional electric (CE) heating. The Al-MIL-101-X materials with X = -CH<sub>3</sub>, -OCH<sub>3</sub>, -C<sub>6</sub>H<sub>4</sub> and -(OCH<sub>3</sub>)<sub>2</sub> were also prepared under identical microwave-assisted solvothermal conditions (170 °C, 10 min, 150 W) by employing similar reaction mixtures as those used during the syntheses with CE heating. A substantial reduction in the reaction time was observed in the microwave irradiation method as compared to the solvothermal technique. To confirm the phase purity of the materials, XRPD analysis, FT-IR spectroscopy, thermogravimetric and elemental analysis were performed. It was observed that Al-MIL-101-X materials can sustain up to 260-430 °C in an air atmosphere. The thermally activated forms of all the materials show significant porosity, as revealed by the N<sub>2</sub> (S<sub>BET</sub> in the range of 1328-2398 m<sup>2</sup> g<sup>-1</sup>) (Figure 6) and CO<sub>2</sub> (uptake values in the range of 1.6-3.0 mmol g<sup>-1</sup> at 0 °C and 1 bar) (Figure 7) sorption analysis. The N<sub>2</sub> adsorption capacities of the materials are reliant on the size of the attached functional groups, whereas the CO<sub>2</sub> uptake values of the materials are dependent on both the size and nature of attached functional groups, resulting in various CO<sub>2</sub>-framework interactions. The high thermal and moisture stability of the light-weight, non-toxic Al-MIL-101-X-CE materials along with the considerably high porosity would make them potential candidates for applications in gas storage and separation.

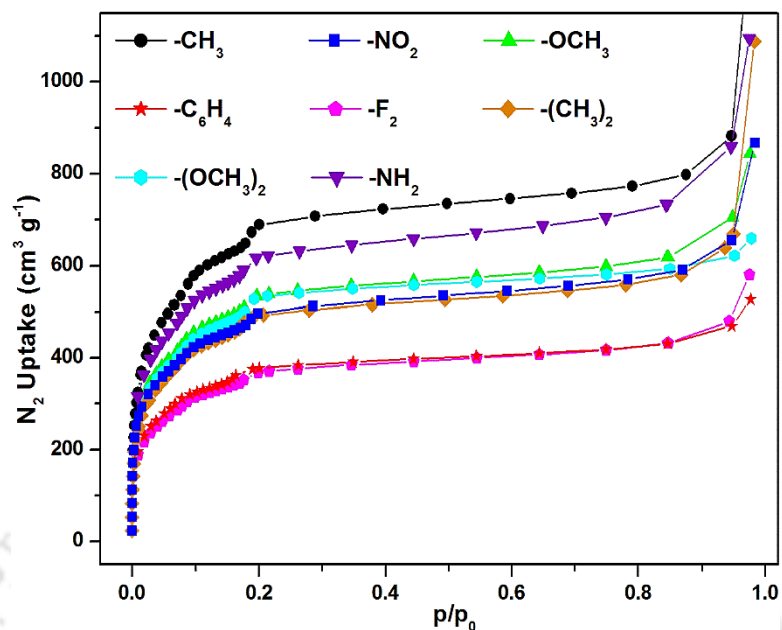


**Figure 6.**  $N_2$  adsorption isotherms of the thermally activated 1- $CH_3$  (black, circles), 2- $NO_2$  (blue, squares), 3- $OCH_3$  (green, triangles), 4- $C_6H_4$  (red, stars), 5- $F_2$  (magenta, pentagons), 6- $(CH_3)_2$  (orange, rotated squares), 7- $(OCH_3)_2$  (cyan, hexagons) and Al-MIL-101- $NH_2$  (violet, upside-down triangles) synthesized by solvothermal method. The adsorption curves were recorded at  $-196\text{ }^\circ\text{C}$ .

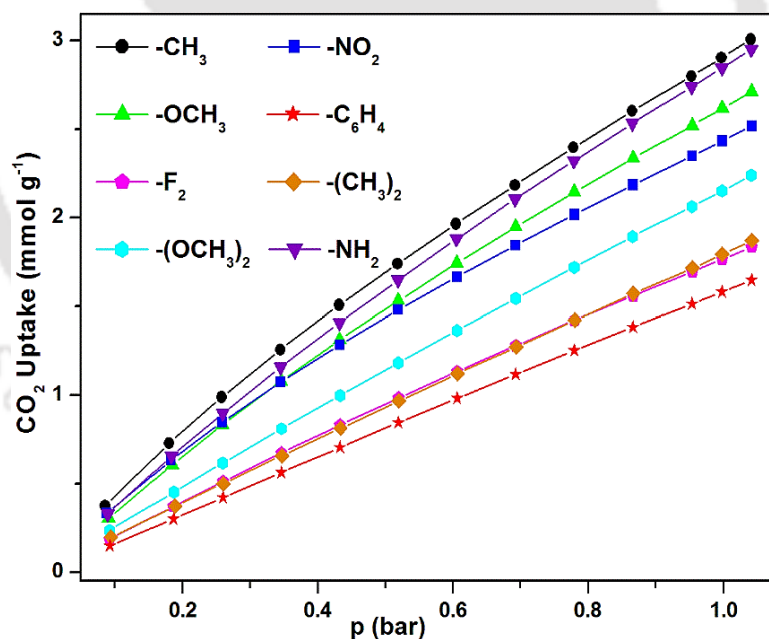


**Figure 7.**  $CO_2$  adsorption isotherms of the thermally activated 1- $CH_3$  (black, circles), 2- $NO_2$  (blue, squares), 3- $OCH_3$  (green, triangles), 4- $C_6H_4$  (red, stars), 5- $F_2$  (magenta, pentagons), 6- $(CH_3)_2$  (orange, rotated squares), 7- $(OCH_3)_2$  (cyan, hexagons) and Al-MIL-101- $NH_2$  (violet, upside-down triangles) synthesized by solvothermal method. The adsorption curves were measured at  $0\text{ }^\circ\text{C}$ . (*Microporous Mesoporous Mater.*, 2015, 215, 91)

**Chapter 6** demonstrates the hydrothermal synthesis, complete characterization and sorption behavior of functionalized Cr-MIL-101-X (X = -F, -Cl, -Br, -CH<sub>3</sub>, -C<sub>6</sub>H<sub>4</sub>, -F<sub>2</sub>, -(CH<sub>3</sub>)<sub>2</sub>) materials. All of the functionalized compounds except Cr-MIL-101-C<sub>6</sub>H<sub>4</sub> were obtained by reacting the mixtures of CrO<sub>3</sub>, H<sub>2</sub>BDC-X linkers, conc. HCl and water with a molar ratio of 1:1:3.9:222.2 at 180 °C for 144 h. On the other hand, the Cr-MIL-101-X compounds with X = -Cl, -Br and -C<sub>6</sub>H<sub>4</sub> was synthesized in a shorter reaction times (12-18 h at 180-210 °C). The phase purity of the materials is confirmed by a combination of XRPD analysis, DRIFT spectroscopy and thermogravimetric analysis. TG analyses shows that all the Cr-MIL-101-X compounds exhibit high thermal stability up to 270-300 °C in an air atmosphere. All the thermally activated materials exhibit significant porosity, as verified by the N<sub>2</sub> ( $S_{\text{BET}}$  in the 1273-2135 m<sup>2</sup> g<sup>-1</sup> range) (Figure 8), CO<sub>2</sub> (uptake values in the 1.7-2.9 mmol g<sup>-1</sup> range at 0 °C and 1 bar) (Figure 9) and benzene (adsorption capacities in the 66.2-139.5 molecules per unit cell range at 50 °C and p/p<sub>0</sub> = 0.35) (Figure 10) sorption analyses. The N<sub>2</sub> uptake values of the materials are dependent on the size of the attached functional groups whereas, their CO<sub>2</sub> and benzene adsorption capacities are dependent both on the size and the nature of grafted functional groups, resulting in different adsorptive-framework interactions. Specially, the mono- and di-fluorinated Cr-MIL-101 materials displayed enhanced CO<sub>2</sub> adsorption capacities. Moreover, Cr-MIL-101-F exhibited higher benzene uptake value compared to the non- and methyl-functionalized Cr-MIL-101, indicating that the fluorination induced more hydrophobicity in Cr-MIL-101 as compared to the methylation. The high thermal and hydrolytic stability as well as noticeably high porosity would make the Cr-MIL-101-X compounds as potential candidates for applications in gas/liquid storage and separation.

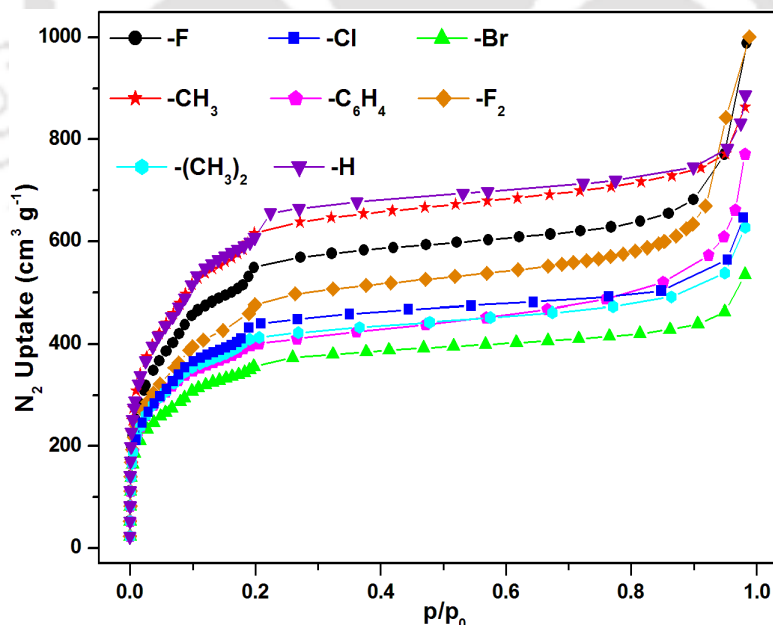


**Figure 8.** N<sub>2</sub> adsorption isotherms of the thermally activated **1-F** (black, circles), **2-Cl** (blue, squares), **3-Br** (green, triangles), **4-CH<sub>3</sub>** (red, stars), **5-C<sub>6</sub>H<sub>4</sub>** (magenta, pentagons), **6-F<sub>2</sub>** (orange, rotated squares), **7-(CH<sub>3</sub>)<sub>2</sub>** (cyan, hexagons) and Cr-MIL-101 (violet, upside-down triangles) recorded at -196 °C.

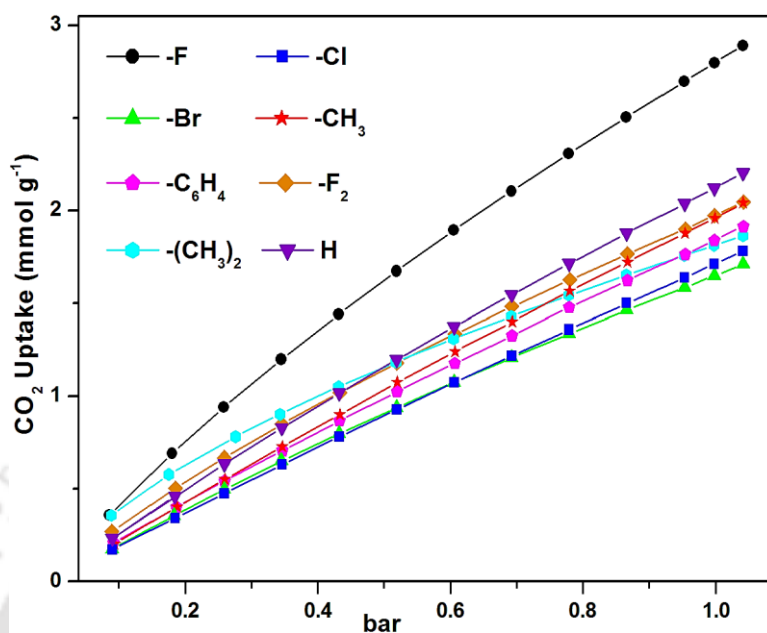


**Figure 9.** CO<sub>2</sub> adsorption isotherms of the thermally activated **1-F** (black, circles), **2-Cl** (blue, squares), **3-Br** (green, triangles), **4-CH<sub>3</sub>** (red, stars), **5-C<sub>6</sub>H<sub>4</sub>** (magenta, pentagons), **6-F<sub>2</sub>** (orange, rotated squares), **7-(CH<sub>3</sub>)<sub>2</sub>** (cyan, hexagons) and Cr-MIL-101 (violet, upside-down triangles) measured at 0 °C.

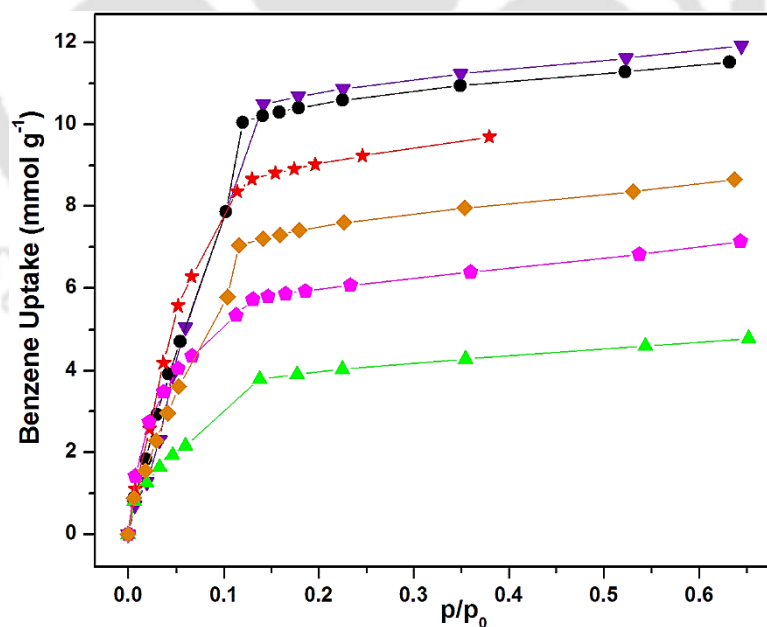
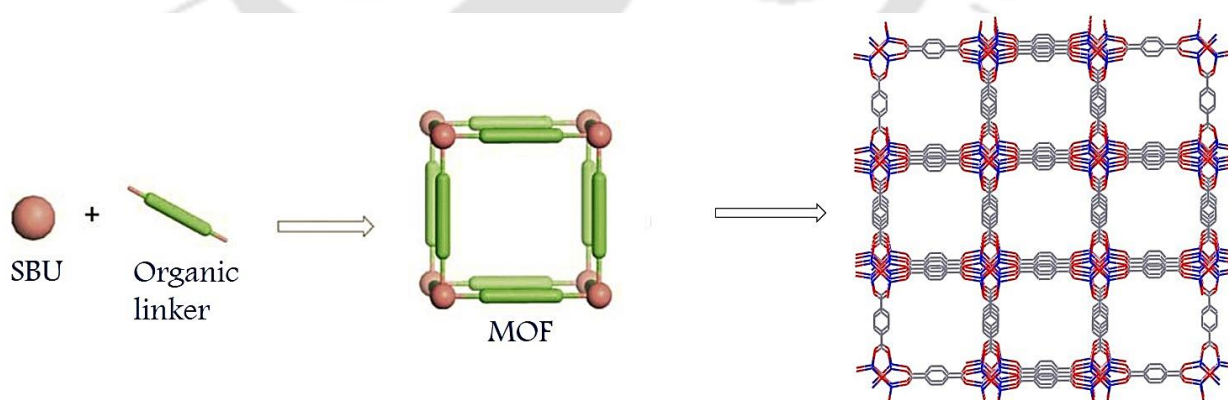


**Figure 10.** Benzene adsorption isotherms of the thermally activated **1-F** (black, circles), **3-Br** (green, triangles), **4-CH<sub>3</sub>** (red, stars), **5-C<sub>6</sub>H<sub>4</sub>** (magenta, pentagons), **6-F<sub>2</sub>** (orange, rotated squares) and Cr-MIL-101 (violet, upside-down triangles) recorded at 50 °C. (*J. Solid State Chem.*, 2016, 238, 195)

## Introduction and Brief History of Functionalized Metal-Organic Frameworks (MOFs)

*This chapter presents recent advancements in rational design and synthesis of various functionalized MOFs for potential application in gas ( $H_2$ ,  $CO_2$ ,  $CH_4$ ,  $CO$ , etc.) storage and fluorescence sensing of wide variety of analytes (cations, anions, biomolecules, small molecules, volatile organic compounds, nitro explosive materials, etc.). Functionalization of MOFs has been demonstrated as a promising strategy to enhance the physicochemical stability (air, water, acid-base, heat, etc.) as well as gas storage and separation properties of the resulting MOFs. The attached functional groups can act as interaction sites for specific gas molecules (during gas adsorption) and analytes (during fluorescence sensing), thus increasing the selectivity of the MOF material towards the target gas or analyte.*



## 1.1 INTRODUCTION

Porous materials have attracted great scientific interest because of their enormous application scopes as host molecules in the field of separation and storage,<sup>1</sup> molecular sensing,<sup>2,3</sup> catalysis,<sup>4,5</sup> asymmetric synthesis,<sup>6</sup> and as host templates for preparing composite materials (e.g., organic/inorganic templates for embedded arrays of nanowires/polymers etc).<sup>7-9</sup> Two types of porous solids are found: amorphous solids (e.g., plastics and gels) and crystalline solids (e.g., nanoporous silicas and zeolites). Based on the size of the pores, these porous solids can be divided into three categories: microporous (pore diameter, < 2 nm), mesoporous (pore diameter, 2 – 50 nm) and macroporous (pore diameter, > 50 nm).

Metal-Organic Frameworks (MOFs)<sup>10-14</sup> are a new class of highly crystalline porous coordination polymers which are composed of metal-containing secondary building units (SBUs) interconnected by rigid or semi-rigid polytopic organic linkers. The topology of the framework can be tuned by changing the length or geometry of the linkers,<sup>15</sup> and also the geometry and connectivity of SBUs show a significant effect to the design of directionality for the construction of MOFs with larger surface area and tailorability.<sup>16, 17</sup> Moreover, the grafting of different functional groups into the organic linker<sup>18-21</sup> would provide an excellent way to produce MOFs having exceptional chemical and physical properties. Owing to their extraordinary porous behaviour and tunable framework characteristics, MOFs have received remarkable research interests towards a wide range of potential applications including gas storage/separation,<sup>22-24</sup> catalysis,<sup>25, 26</sup> drug delivery,<sup>27-30</sup> sensing<sup>31-36</sup> etc., over traditional porous adsorbents such as zeolites, mesoporous silicas, carbon nanotubes and activated carbons. Owing to the accessibility of an almost infinite combination of metal ions and organic linkers, a large variety of MOF architectures bearing different types of pore systems as well as chemical and physical properties have been reported till date (Figure 1.1). However, there are still some ongoing challenges regarding the low physiochemical stabilities (moisture, thermal, and acid-base) of MOFs. Indeed, several MOFs have displayed promising gas adsorption/separation behavior, but these types of stability issues hinder their applications in industrial level. Several investigations on the chemical and thermal stability of MOFs have revealed that the framework stability is dependent upon various factors such as oxidation state of the metal ion, lability of metal-ligand bonds, etc.<sup>37</sup> It has been found that the successful construction of MOFs having high hydrolytic stability is possible

by using metal ions with higher oxidation states, e.g. Cr(III),<sup>38</sup> Al(III),<sup>39, 40</sup> Fe(III),<sup>41</sup> Zr(IV),<sup>42</sup> Ti(IV).<sup>43</sup>

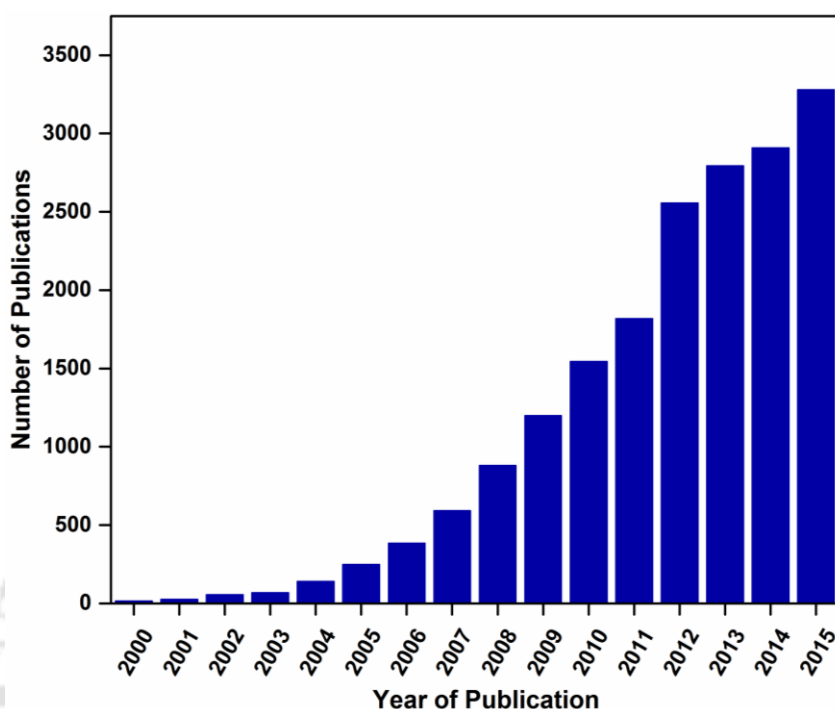


**Figure 1.1** Number of publications containing the key word “Metal Organic Framework” in the past 15 years (source: Sci Finder Scholar until 2015).

## 1.2 BASIC DESIGN PRINCIPLES

MOFs are highly crystalline inorganic-organic framework solids. The network structures are constructed by accumulation of metal-containing clusters with organic molecules which serve as ligands coordinating via covalent bond. Three different types of strategies have been generally used to direct the synthesis of MOFs, which are mainly: (a) node-and-spacer, (b) vertex-linked polygons or polyhedra (VLPP), and (c) secondary building unit (SBU) approach. A brief description of each of these strategies is provided in this section.

### (a) Node-and-Spacer Strategy

The originally reported ‘node-and-spacer’ approach describes that the nets are usually constructed from organic ligands as linear ‘spacers’ and metal cations as ‘nodes’. The shapes of the spacers and nodes could be square, tetrahedral, octahedral, etc. During the synthesis of MOFs, the same strategy can be applied to construct extended framework structures, where both metal

centers and organic ligands can appropriately function as either nodes or spacers.<sup>44</sup> Figure 1.2 illustrates some representative examples of organic ligands with linear, angular, trigonal and tetrahedral shapes. In the node-and-spacer approach, the metal cluster serves as the node, while the multidentate organic ligand is the spacer. Availability of different possible combination of metal centers and organic molecules can lead to the design of a diverse arrangement of metal-organic architectures ranging from 0D discrete nanostructures to 3D infinite networks (Figure 1.3).

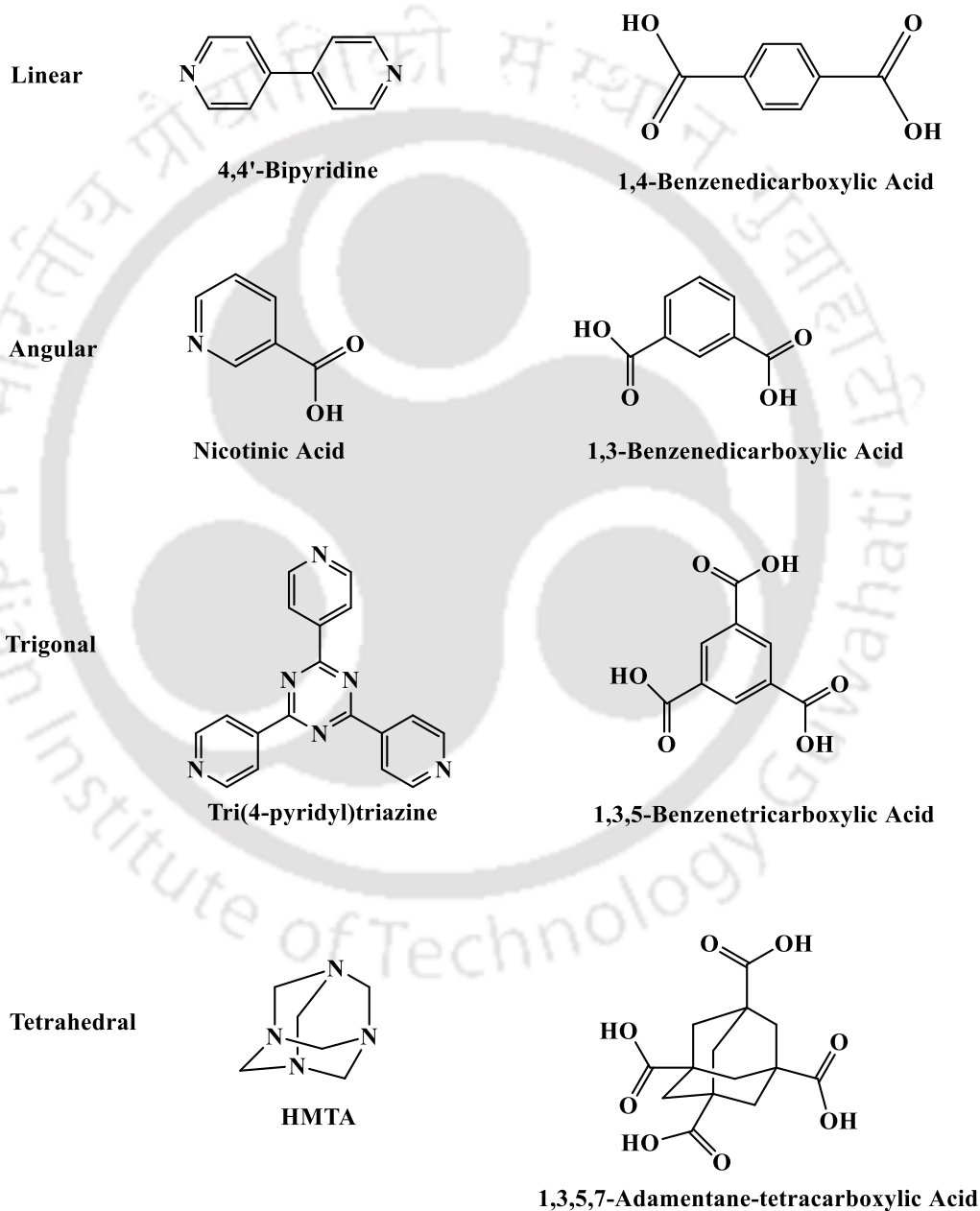


**Figure 1.2** Representative examples of organic ligands employed for the construction of MOFs (HMTA = hexamethylenetetramine).

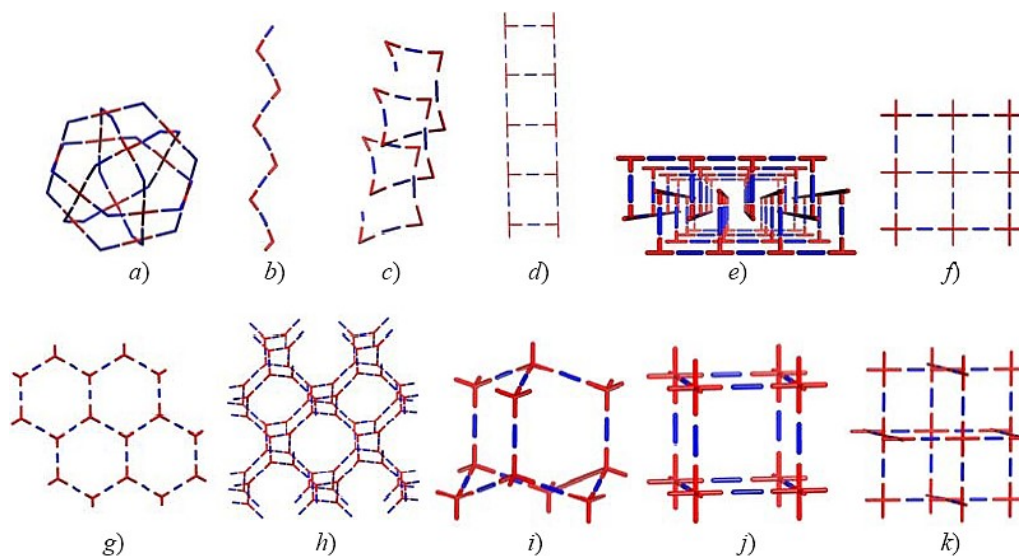


**Figure 1.3** “Node-and-spacer” representations of metal-organic frameworks: (a) 0D nanoball; (b) 1D zigzag chain; (c) 1D helix; (d) 1D ladder; (e) 2D bilayers; (f) 2D square grid; (g) 2D honeycomb; (h) 3D (10,3)-a net; (i) 3D diamondoid net; (j) 3D primitive cubic net; (k) 3D NbO net. The diagrams have been adopted from ref. 45.

#### (b) Vertex-Linked Polygons or Polyhedra (VLPP) Strategy

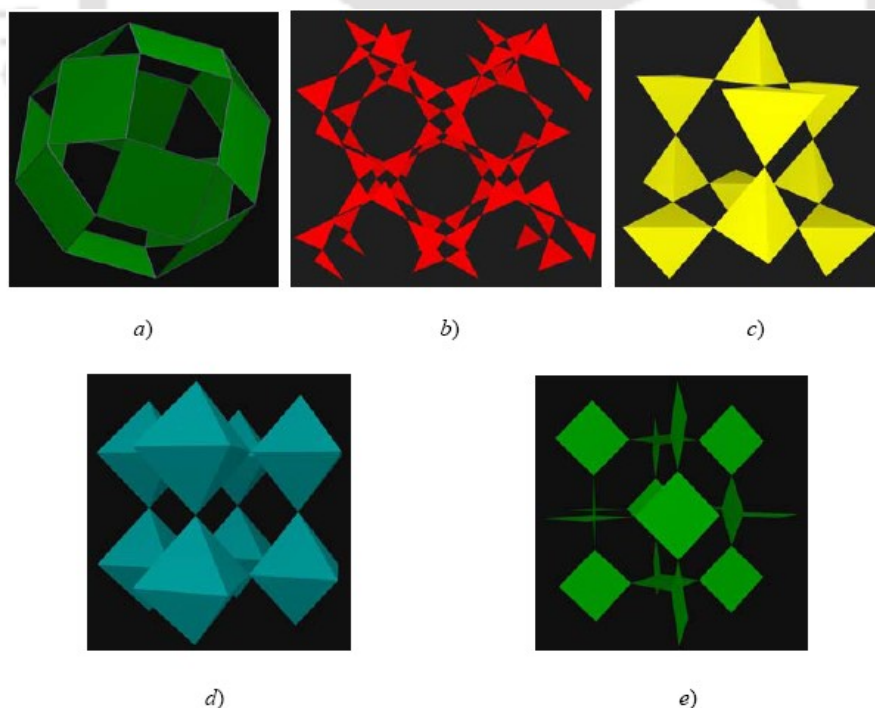


**Figure 1.4** “Vertex-linked Polygons or Polyhedra” (VLPP) representations of metal-organic frameworks: a) 0D nanoball; b) 3D (10,3)-a net; c) 3D diamondoid net; d) 3D primitive cubic net; e) 3D NbO net. The diagrams have been adopted from ref.45.

Based on geometrical principles, another approach was presented which involves the definite shapes of the building blocks and represents the nets as being sustained by vertex-linked polygons or polyhedra (VLPP)<sup>46-49</sup> (Figure 1.4). Notably, the nets shown in Figure 1.3 can also be similarly well represented in the VLPP fashion (Figure 1.5). Node-and-spacer approach seems more straightforward in cases of linear spacers, whereas VLPP approach reveals more fundamental geometrical relationship between various building units.

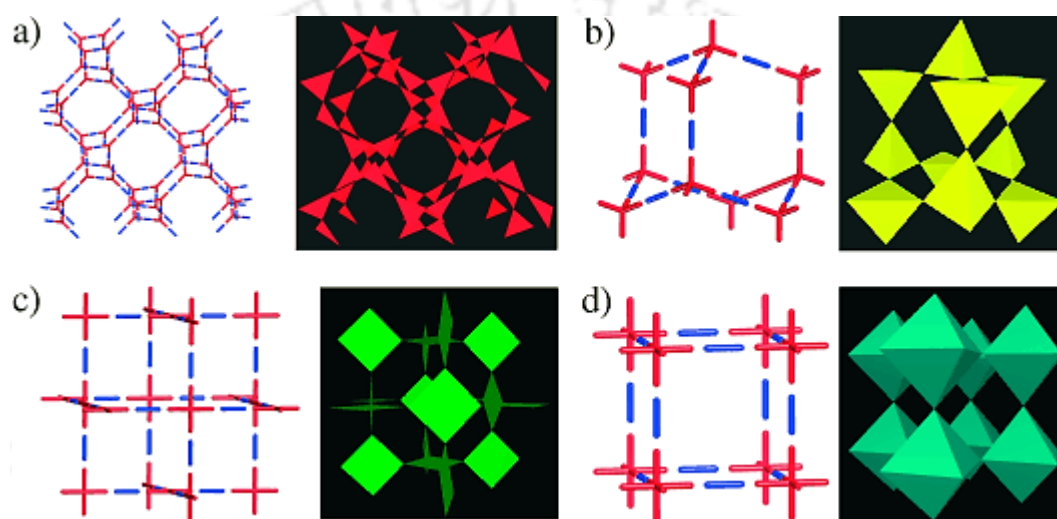


**Figure 1.5** Four unitary nets represented in both node-and-spacer and VLPP format: a) (10,3)-a net, b) diamondoid net, c) NbO net, d) primitive cubic net. The diagrams have been adopted from ref.45.

### (c) SBU Strategy

The term ‘secondary building unit’ was initially used in zeolite chemistry where SBUs are denoted to common structural motifs occurring in various tetrahedral frameworks.<sup>50</sup> Yaghi and co-workers have extended this idea and introduced the so-called ‘secondary building unit (SBU)’ strategy for the construction of rigid and porous frameworks.<sup>16, 17, 51</sup> These SBUs are constructed from metal containing clusters formed by the aggregation of metal ions and multidentate linkers possessing well-defined and highly symmetric coordination geometries. The SBUs serve as rigid vertices which are connected through organic linkers to form robust framework with high structural stability and permanent porosity.

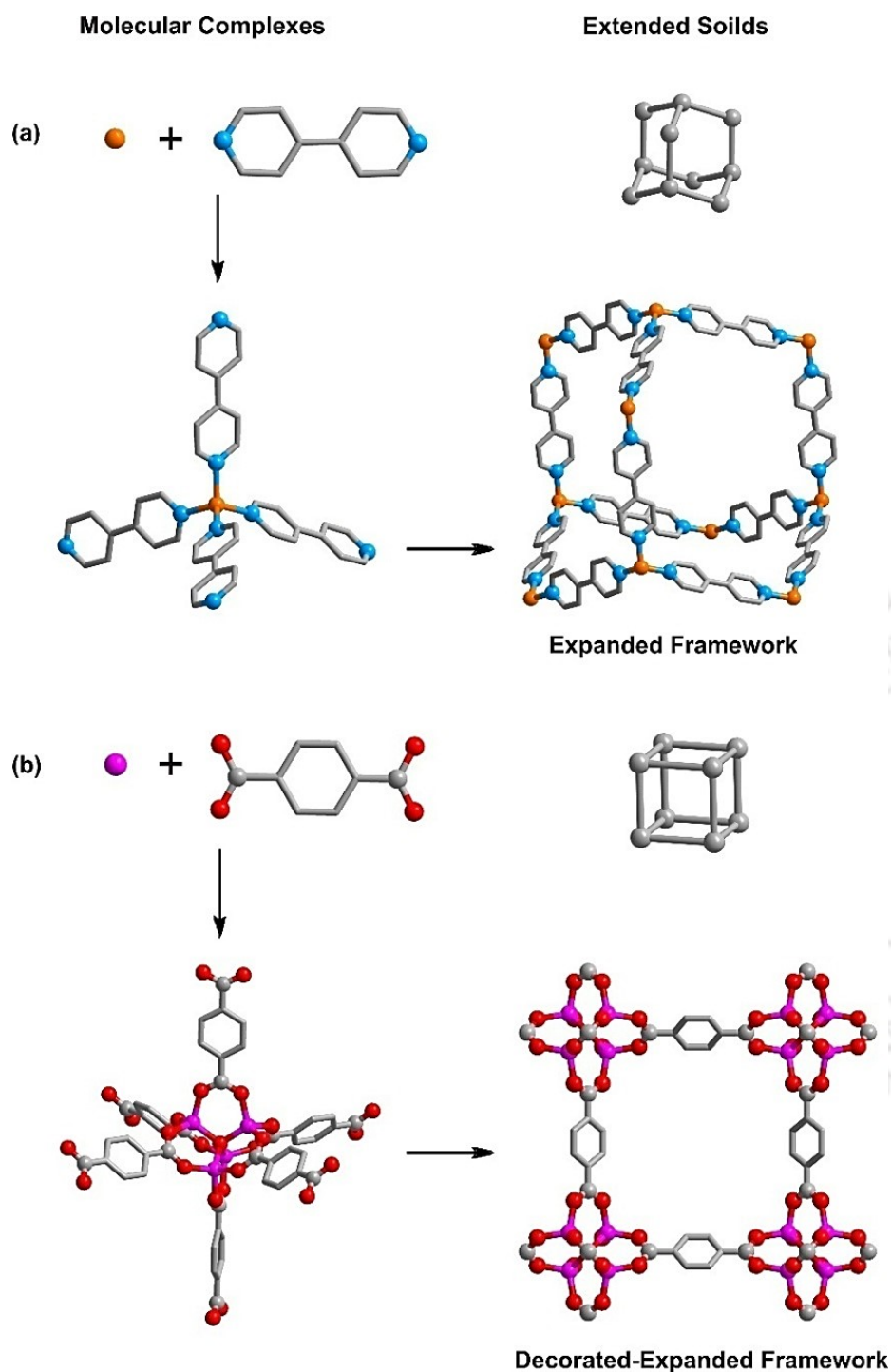


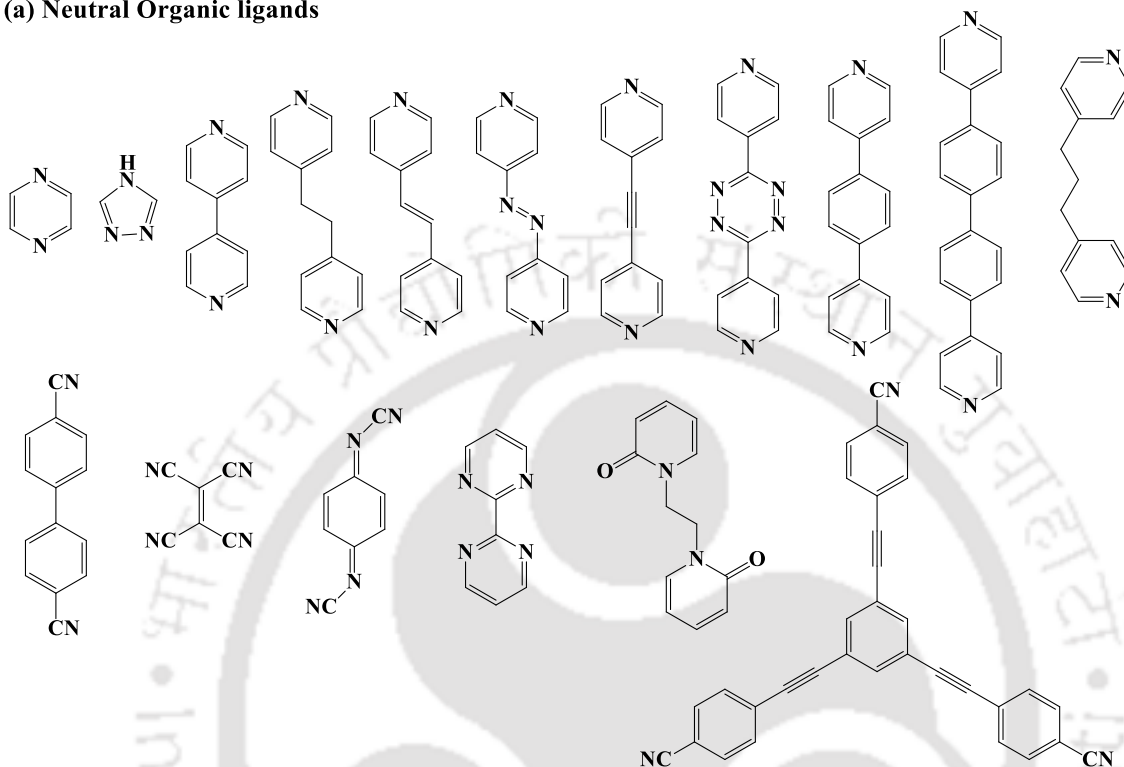
**Figure 1.6** Assembly of metal-organic frameworks (MOFs) by the copolymerization of metal ions with organic linkers to give (a) flexible metal-bipyridine structures with expanded diamond topology, and (b) rigid metal-carboxylate coordination units that can be linked by benzene “struts” to form rigid extended frameworks in which the M-O-C core (SBU) of each coordination unit acts as a large octahedron decorating a 6-connected vertex in a cube. All hydrogen atoms have been omitted for clarity. In (a): M, orange; C, grey; N, blue; in (b): M, pink; O, red; C, grey. The diagram has been adopted from ref.52.

### 1.3 SYNTHETIC METHODS

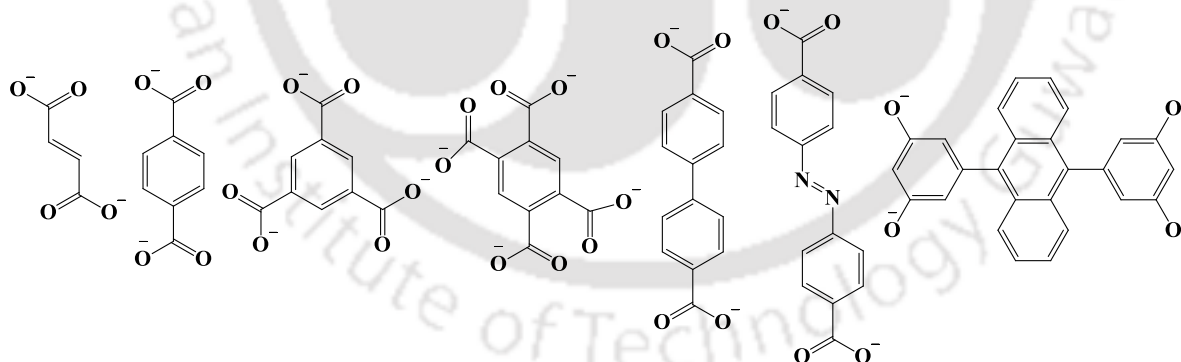
Apart from those geometric principles considered for designing MOFs, several factors also need crucial attention for maintaining the structural integrity of the building blocks during synthesis. The synthetic conditions must be mild enough to retain the functionality and conformation of the rigid organic linker, however at the same time they have to be reactive enough to generate the desired SBU to construct the framework structure via establishment of coordinative bonds. In general, synthesis of MOFs involves a chemical reaction between organic linkers and metal ions as an inorganic component in a polar solvent under mild temperatures (up to 200 °C) and autogenous pressures (up to 100 atm). Transition metal ions are often used as the inorganic components which prefer different coordination numbers and geometries, such as linear, T- or Y-shaped, tetrahedral, square planar, square pyramidal, trigonal bipyramidal, octahedral, trigonal prismatic and pentagonal bipyramidal. A wide variety of organic linkers including electronically neutral, cationic, or anionic have been used for the synthesis of MOFs (Figure 1.7). Preferably, those linkers with rigid backbones are frequently used, because the rigidity makes it easier to predict the network geometry in advance of synthesis. Moreover, it also helps to preserve the open-pore structure after the removal of the occluded solvent molecules. Since most products are considered to be thermodynamically or kinetically controlled, factors such as solubility of the organic linker and metal salt, solvent polarity, ionic strength of the medium, pH, temperature or pressure can play key roles in determining the nature of the products. It has been found that change of the crystal quality as well as yield of the reaction or even formation of new phases can occur upon variation of these parameters. Several techniques have been applied to produce highly crystalline MOF materials by reducing the rate of crystallite nucleation, which include slow evaporation of a solution of the precursors, layering of solutions or slow diffusion of one component solution into another through a membrane or an immobilizing gel. Prior to coordination with the metal ions, ligands such as polycarboxylic acids need to be deprotonated. In cases where deprotonation of the organic linker molecule is necessary, amide co-solvents which undergo thermal decomposition on heating such as alkyl formamides and pyrrolidinones are very useful for gradual neutralization of the solution. In order to increase the crystallinity, modulated synthesis of several MOFs have been carried by using common mono carboxylic acids (e.g., acetic acid, formic acid, trifluoroacetic acid and benzoic acid) and HCl as modulators. These modulators are assumed to play two important roles during the synthesis: (i) facilitate the formation of metal clusters and

the growth of crystals; (ii) slow down the crystal growth rate by competing with organic linker molecules for the coordination sites at the metal centers.<sup>53, 54</sup>

(a) Neutral Organic ligands



(b) Anionic Organic ligands



(c) Cationic Organic ligands

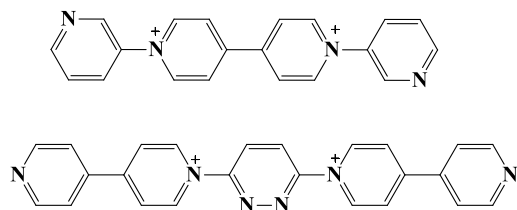


**Figure 1.7** Representative examples of neutral, cationic and anionic linkers used for the synthesis of MOFs.

Several synthetic procedures including room temperature synthesis, conventional electric (CE) heating, microwave (MW) heating, electrochemistry (EC), mechanochemistry (MC) and ultrasonic (US) methods have been employed for the synthesis of MOFs.<sup>55</sup> Various well-known MOFs have been synthesized at room temperature by just mixing the reactants, e.g., MOF-5, MOF-74, MOF-177, HKUST-1 or ZIF-8.<sup>56-58</sup>

### 1.3.1 Hydro/Solvothermal Synthesis

MOFs have mostly been synthesized by solvothermal methods in stainless steel autoclaves or sealed Pyrex tubes at high temperature and pressure using conventional electric (CE) heating.<sup>12, 59, 60</sup> In hydrothermal synthesis, only water is used as the solvent. On the other hand, solvothermal synthesis includes various solvents other than water that are heated above the boiling point of the solvent. Moreover, mixtures of solvents other than pure solvents also have been used for synthesizing various MOFs. In order to prepare a robust and stable MOF, hydrothermal techniques play a more important role compared to the solution reactions.<sup>61</sup> Unlike solution reactions, hydrothermal reactions are performed at high temperature and pressure in sealed reaction vessels which increases the solubility of the reactants and allows the reactions that do not occur at lower temperatures. However, this method usually involves long reaction times (sometimes several hours up to several days) depending upon the MOF of interest and other factors including reaction solvent, reaction temperature, reagent concentrations, etc.

### 1.3.2 Microwave-Assisted and Sonochemical Synthesis

Synthesis using microwave (MW) irradiation has been widely applied for the rapid synthesis of MOFs under hydrothermal conditions. Besides fast crystallization,<sup>62-64</sup> direct interaction of the microwave radiation with the solution/reactants allows MW-assisted technique to provide a very energy efficient method of heating with phase selectivity<sup>65</sup> and decreased size<sup>66</sup>.

Sonochemical or ultrasonic methods via homogeneous and accelerated nucleation upon application of high-energy ultrasound to the reaction mixture can also result in a decrease in crystallization time and considerably smaller particle size than those obtained by the conventional solvothermal synthesis.<sup>67</sup>

### 1.3.3 Electrochemical and Mechanochemical Synthesis

In order to develop an environmentally friendly process, MOFs have also been synthesized under solvent-free conditions using electrochemical<sup>68</sup> and mechanochemical<sup>69, 70</sup> techniques. In electrochemical synthesis, the metal ions are continuously introduced through anodic dissolution rather than the addition of metal salts, which react with the medium containing dissolved linker molecules and a conducting salt. In addition, mechanochemical synthesis involves the mechanical breakage of intramolecular bonds followed by a chemical transformation of metal oxides and organic linkers at room temperature.

### 1.3.4 Post-Synthetic Modification

Tuning of chemical/physical properties of MOFs for various applications can be achieved by integrating functional groups to the organic linker, which allows control in framework-guest molecule interactions leading to tailored properties. However, the introduction of functional group for a desired application is sometimes difficult to achieve during synthesis of MOFs owing to the high sensitivity and reactivity of the additional functionality during the formation of MOFs. Nevertheless, initially synthesizing the desired framework with linkers featuring inert functional groups and subsequently transforming those into reactive functional groups has led to the formation of several functionalized MOFs. Such post-synthetic modifications (PSMs) are emerging as a promising route to the tailor host-guest interactions for more specific and enhanced properties of MOFs.<sup>71</sup>

## 1.4 HISTORY

It is well established that the reaction of  $Zn^{2+}$  ions with carboxylic acid produces a centered tetrazinc cluster,  $[Zn_4O(RCOO)_6]$  where the four  $Zn^{2+}$  ions are bridged together by the  $\mu_4$ -oxo group and six bridging carboxylates. For the first time, Yaghi and coworkers showed that it is possible to interconnect such tetrazinc clusters into an infinite polymeric cubic network by employing a rigid linear dicarboxylic acid instead of a monocarboxylic acid. Thus, the reaction of  $Zn(OAc)_2 \cdot 2H_2O$  with terephthalic acid in presence of a non-coordinating base such as  $Et_3N$  yields a highly robust cubic 3-dimensional MOF,  $Zn_4O(BDC)_3$  (BDC = 1,4-benzenedicarboxylate). This coordination framework features an exceptionally high surface area of  $3909 \text{ m}^2\text{g}^{-1}$  and it is popularly abbreviated as MOF-5.<sup>72</sup> A series of Cr(III), Al(III) and Zr(IV) based MOFs have been

thoroughly investigated and among those UiO-66,<sup>42</sup> MIL-101<sup>38, 39</sup> and MIL-53<sup>38, 73</sup> are very well known for their extraordinary physiochemical stability and potential applications. Since the preparation of MOFs having the ability to survive when exposed to moist air in order to avoid framework collapse is a challenging goal and requires research attention, herein we have aimed to synthesize new Al(III), Cr(III) and Zr(IV) based MOFs that can overcome these drawbacks with retention of their chemical and physical properties.

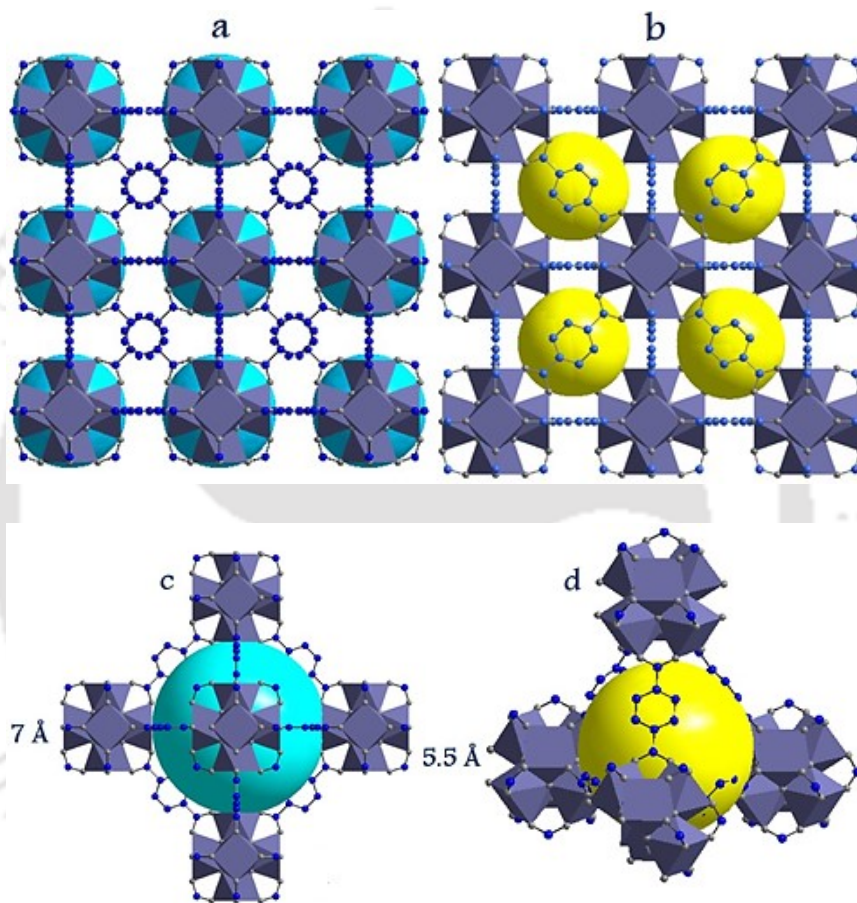


**Figure 1.8** Ball-and-stick representation of the 3D cubic framework structure of UiO-66. (a,b) Spatial arrangement of the octahedral (cyan spheres) and tetrahedral (yellow spheres) cages in the framework. (c,d) Magnified representation of the octahedral and tetrahedral cages. Zr atoms are shown as octahedra (colour codes: Zr, blue; C, blue; O, dark grey). The hydrogen atoms and guest molecules have been removed from all structural plots for clarity. The figure was drawn by using atomic coordinates provided in ref.74.

The Zr(IV)-based MOF called UiO-66 (UiO = University of Oslo)<sup>42</sup> has attracted notable attention in recent years owing to its high thermal and chemical stability as well as potential properties for CO<sub>2</sub>/CH<sub>4</sub> gas separation.<sup>75, 76</sup> The 3D cubic framework of this MOF is built up of hexanuclear [Zr<sub>6</sub>O<sub>4</sub>(OH)<sub>4</sub>]<sup>12+</sup> building units in which the triangular faces of the Zr<sub>6</sub>-octahedron are

alternatively capped by  $\mu_3$ -O and  $\mu_3$ -OH groups (Figure 1.8). All the  $[\text{Zr}_6\text{O}_4(\text{OH})_4]^{12+}$  building units are interconnected by the carboxylate groups of twelve 1,4-benzenedicarboxylate (BDC) dianions leading to the formation of  $[\text{Zr}_6\text{O}_4(\text{OH})_4(\text{BDC})_6]$  framework having octahedral (Figure 1.8 c) and tetrahedral (Figure 1.8 d) cages. Each Zr atom exists in a square-antiprismatic geometry and coordinates with eight O atoms. One square face of the square antiprism comprises of O atoms from the carboxylate groups, whereas the O atoms from the  $\mu_3$ -O and  $\mu_3$ -OH groups construct the other face of the square antiprism.

The synthesis of UiO-66 was performed by using commercially available  $\text{ZrCl}_4$  and 1,4-benzenedicarboxylic acid ( $\text{H}_2\text{BDC}$ ) applying *N,N'*-dimethylformamide (DMF) as solvent medium at 120 °C in a pre-heated oven for 24 h. This coordination framework exhibits an exceptionally high Langmuir surface area of 1187  $\text{m}^2 \text{g}^{-1}$ . Extending the length of the linker to two and three benzene ring dicarboxylic acids resulted in two more very potential MOFs popularly abbreviated as UiO-67 and UiO-68 with increased surface area of 3000 and 4170  $\text{m}^2 \text{g}^{-1}$ , respectively. The structural integrity of UiO-66 against different solvents like water, DMF, benzene and acetone, confirmed by X-ray powder diffraction (XRPD) measurements, also proved the efficacy of this material for industrial applications. Functionalization of UiO-66 framework through attachment of different functional groups to the BDC ligand (UiO-66-X, X =  $-\text{CH}_3$ ,  $-(\text{CH}_3)_2$ ,  $-\text{NO}_2$ ,  $-\text{NH}_2$ ,  $-\text{OH}$ ,  $-\text{CO}_2\text{H}$ ,  $-\text{SO}_3\text{H}$ ) enhanced the  $\text{CO}_2$  uptake compared to that of the un-functionalized UiO-66 material.<sup>21</sup> Moreover, the modulated synthesis of the MOF materials having UiO-66 framework topology by the addition of different modulators/additives (e.g., benzoic acid, acetic acid, formic acid, conc. HCl and  $\text{H}_2\text{O}$ )<sup>77, 78</sup> have been carried out in order to investigate their effect on the crystallinity of the MOF materials.

Ferey and coworkers have developed a very interesting series of MOFs known as the MIL-n (MIL = Material of the Institute Lavoisier) which possess very high thermal and chemical stability in addition to their remarkable porosity.<sup>38, 39</sup> Cr-MIL-101 is the most popular amongst these MOFs on account of its high moisture stability, high thermal stability (up to 400 °C) and extraordinarily high surface area of 4100  $\text{m}^2 \text{g}^{-1}$ .<sup>38, 79</sup> This chromium terephthalate MOF having formula of  $[\text{Cr}_3\text{F}(\text{H}_2\text{O})_2\text{O}(\text{BDC})_3] \cdot n\text{H}_2\text{O}$  (where  $n \sim 25$ ) were synthesized by the reaction of  $\text{Cr}(\text{NO}_3)_3 \cdot 9\text{H}_2\text{O}$  with  $\text{H}_2\text{BDC}$  ligand and HF in  $\text{H}_2\text{O}$  under hydrothermal conditions (at 220 °C for 8 h).

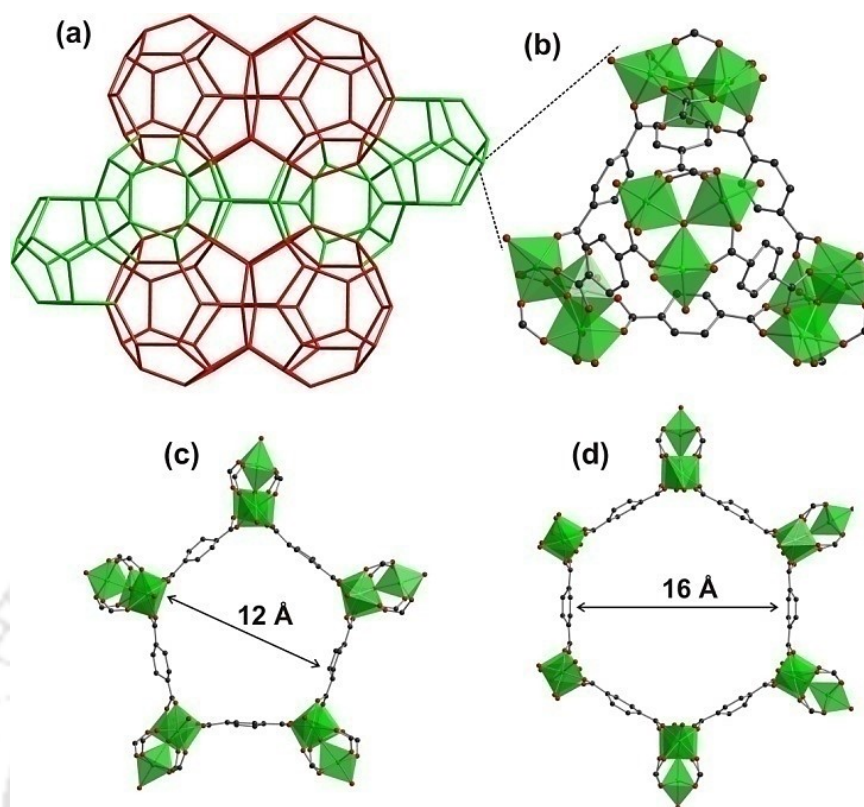


**Figure 1.9** (a) Framework structure of Cr-MIL-101 having MTN topology and consisting of smaller (green) and larger (red) mesoporous cages. The structure is derived from (b) supertetrahedra (ST), which consist of trimeric oxido-centered  $[\text{Cr}_3(\mu_3\text{-O})(\text{F})(\text{H}_2\text{O})_2]^{6+}$  building units at the vertices cross-linked by the BDC linkers. The smaller and larger cages possess only pentagonal (c) or a combination of pentagonal (c) and hexagonal (d) windows, respectively. Colour codes: Cr, green octahedra; C, gray; O, red. The MTN framework (a) and the portions of Cr-MIL-101 network (b-d) have been drawn by using the atomic coordinates provided in “Database of Zeolite Structures”<sup>80</sup> and ref.38, respectively.

The framework structure of Cr-MIL-101 is constructed from the linkage of BDC dianions with inorganic trimeric  $[\text{Cr}_3\text{O}(\text{H}_2\text{O})_2\text{F}(\text{CO}_2)_6]$  building units. Within the trimeric secondary building units, the three Cr atoms are in an octahedral environment and the six coordination sites are occupied by four O atoms from the bridging bidentate dicarboxylates, one  $\mu_3\text{-O}$  atom and one O atom from the terminal water or fluorine group. The structure of Cr-MIL-101 features corner-sharing supertetrahedra which are made from the linkage of inorganic trimers and BDC dianions. The framework has two types of quasi-spherical cages limited by 12 pentagonal faces for the smaller (29 Å) and by 16 faces (12 pentagonal and 4 hexagonal) for the larger (34 Å) (Figure 1.9). Besides the parent and functionalized Cr-MIL-101-X (X = -H, -F, -Cl, -Br, -I, -CH<sub>3</sub>, -NO<sub>2</sub>, -NH<sub>2</sub>, -OH, -CO<sub>2</sub>H, -SO<sub>3</sub>H, etc.)<sup>81</sup> MOFs, several other hydrolytically stable Fe-based MIL-101-X (X =

-H, -Cl, -NH<sub>2</sub> and -(CH<sub>3</sub>)<sub>2</sub>)<sup>82, 83</sup> materials were also reported. The synthesis of non- and amino-functionalized vanadium-based materials MIL-101 materials has been reported by the groups of Van Der Voort and Zou.<sup>84</sup> Nevertheless, the rate of exchange of linkers by water molecules for both V(III) and Fe(III)-based MIL-101 materials made them highly sensitive to moisture. Apart from the parent and functionalized Cr(III), Fe(III) and V(III)-based MIL-101 materials, the synthesis, thermal and chemical properties of Al-MIL-101-NH<sub>2</sub> compound have been also studied.<sup>40, 85, 86</sup> However, the synthesis procedures of Al-MIL-101 derivatives having any other functional group than amino is so far unknown.

## 1.5 MOFs AS CHEMICAL SENSORS

Recently, the development of porous crystalline luminescent MOF materials have attracted great interest over other sensor materials for sensitive and selective detection of various analytes for a range of applications including chemical threat detection, medical diagnostics, industrial process management, food quality control and environmental monitoring.<sup>87-95</sup> The tunability of the specific surface area and pore volume of MOFs offers a high degree of molecular specificity and selectivity for the detection of analytes. Most notably, the large surface areas of MOFs along with the sustainable pores within the framework increase the chances of guest-host interactions and allow the confinement of analytes within their pores, which leads to high sensitivity detection of the analytes. Moreover, functional groups within the framework, such as Lewis acidic or basic and open metal sites, can serve as specific recognition sites for the detection of different analytes.<sup>94, 96-98</sup> The selective accumulation of the targeted analyte within the cavities of MOFs by these recognition sites can result in increased detection performance with lower detection limit up to single molecule level. In addition, the incorporation of organic ligands with aromatic moieties or extended  $\pi$  systems in the rigid frameworks of MOFs leads to stronger fluorescence emissions that might be visible to the naked eye. Most of the luminescent MOF materials display high thermal and chemical stability, which is necessary for the practical application of a sensor material. Above all, the availability of a huge combination of metal ions and organic ligands allows fine-tuning of valance and/or conduction band (and hence optical band gap) of MOFs, which is very important for sensing applications. Inspired by the above-mentioned advantages, a broad variety of MOF materials have been synthesized and examined for the detection of a wide range of analytes

including cations, anions, biomolecules, small molecules, volatile organic compounds and nitro explosive materials.<sup>87-95</sup>

The mechanism of generating fluorescence in MOFs can be explained in different ways based on their mode of fluorescence behavior. Such mode of mechanisms includes linker-based luminescence (ligand-localized emission), ligand-to-metal charge transfer (LMCT), metal-to-ligand charge transfer (MLCT), metal-based emission, antennae effects, adsorbate-based emission, sensitization, excimer/exciple emission and surface functionalization.<sup>99, 100</sup> In principle, for turn-off or turn-on sensing experiments, the change in fluorescence intensity of a luminescent MOF (LMOF) can be considered as change in their spectroscopic characteristics, which can potentially be used as a sensing signal. Depending on the electronic nature of the analyte molecule, electron transfer or energy transfer between the analyte molecule and the LMOF or a combination of the two can occur, which leads to either quenching or enhancement of the luminescence. Owing to their high electron affinity, nitroaromatic explosives are known as strong quencher molecules<sup>101-103</sup> whereas paramagnetic metal ions, such as  $Mn^{2+}$ ,  $Co^{2+}$ ,  $Ni^{2+}$  and  $Cu^{2+}$  also show quenching efficiency via LMCT and by relaxation of the excitation energy through a non-radiative pathway. Conversely, electronically rich benzene and its derivatives with electron donating substituents can enhance fluorescence, probably due to their ability to donate electrons from the excited-state to the LUMO or conduction band (CB) of the LMOF.<sup>104</sup> On the other hand, in turn-on fluorescence experiments, the addition of analyte molecules results in the shift of an emission peak or a new emission peak (typically in the visible range) evolving from a previously dark background. For instance, the selective binding of analyte molecules can post-synthetically trigger the strong emission of an originally low-emitting or non-emitting MOF, which is known as guest-induced emission.<sup>105</sup> In order to act as a useful sensor, a MOF material must possess few properties: (i) it must exhibit some change when allowed to interact with an analyte, (ii) it must show selectivity towards the targeted analyte, (iii) the change must be detectable.

### 1.5.1 MOFs for Sensing of Nitroaromatic Explosives

The rapid and selective detection of nitroaromatic explosive compounds is very important for security screening, homeland security, environmental safety and human health. The major industrial explosives are 2,4,6-trinitrotoluene (TNT), 2,4-dinitrotoluene (2,4-DNT), 2,6-dinitrotoluene (2,6-DNT) and 2,4,6-trinitrophenol (TNP). 2,4,6-Trinitrophenol (TNP), which is

more powerful explosive than its well-known counterpart 2,4,6-trinitrotoluene (TNT), has been extensively used in the manufacture of landmines, rocket fuels, fireworks and matches.<sup>106, 107</sup> It is also commonly used in leather, pharmaceutical and dye industries. TNP has become a major environmental pollutant due to its extensive use. Uncontrolled exposure of TNP to the environment from chemical industries rigorously affects the soil and aquatic system, causing various problems for wildlife and humans. In addition, mutagenic and/or carcinogenic activities of TNP can cause various health problems and fatal environmental pollution. Therefore, discriminative sensing of TNP from other nitroaromatic explosives having a very low detection limit is a vital task for reduction of its detrimental effects on the environment. Current in-field detection techniques for explosives use sophisticated instruments, which possess many disadvantages such as low selectivity, limited portability, high cost and enormous complexity. The fluorescent MOF materials, which have been employed so far as sensors for detecting nitroaromatic explosives, consists of various metal ion. When the electronically rich luminescent MOFs interact with the electron-deficient nitroaromatic explosives, the electron transfer takes place from the MOF to the nitroaromatic explosive compound. This electron transfer process leads to a “turn-off” effect due to the reduction of the luminescence emission intensity. In the following, several examples of luminescent MOFs containing three different types of metal ions and exhibiting fluorescence sensing properties towards nitroaromatic explosives, are presented.<sup>108</sup>

#### (a) Transition Metal Based Luminescent MOFs

MOF materials constructed from  $\pi$ -electron rich ligands can be easily quenched by electron-poor nitroaromatic explosive guests due to their suitably confined environment for efficient electron transfer from electron-rich ligands to the guest molecules. Transition metal ions, especially Zn(II) and Cd(II) with  $d^{10}$  electronic configuration, are very promising candidates for the construction of ligand-centered luminescent MOFs due to their excellent luminescent behavior. A large number Zn-based luminescent MOFs have been reported until today for the detection of nitroaromatic explosives.<sup>104, 109-120</sup> For example, a 3D Zn(II)-based MOF having molecular formula  $[Zn_4O(cpi)_2(H_2O)_3] \cdot 3DMA \cdot 3EtOH \cdot 6H_2O$  ( $H_3cpi = 5$ -(4-carboxyphenylethynyl)isophthalic acid) has been built up of  $\pi$ -conjugated  $H_3cpi$  ligand. This shows significant quenching efficiencies for various nitroaromatic explosives such as NB, NT, NP, DNT and TNT (Figure. 1.10).<sup>119</sup> Besides Zn(II)-based luminescence MOFs, a wide variety of

Cd(II)-based luminescent MOF materials have been also examined for the sensing of highly explosive nitroaromatic compounds (Figure 1.11).<sup>121-124,125-128</sup>

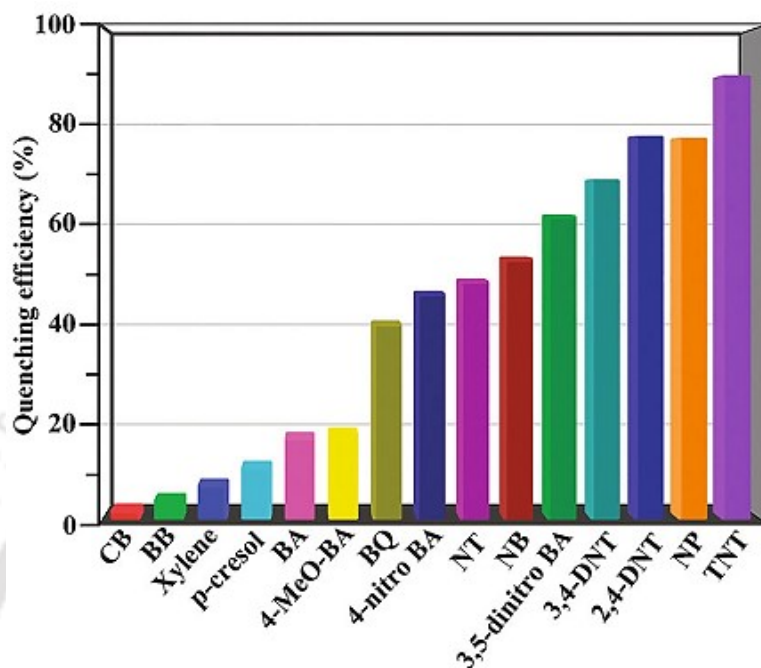


**Figure 1.10** Reduction in fluorescence intensity of Zn(II)-based MOF (plotted as quenching efficiency) observed upon the addition of several quenchers. CB = chlorobenzene, BB = bromobenzene, BA = benzoic acid, 4-MeO-BA = 4-methoxybenzoic acid, BQ = benzoquinone. Reproduced with permission from ref.119. Copyright 2011 Royal Society of Chemistry.

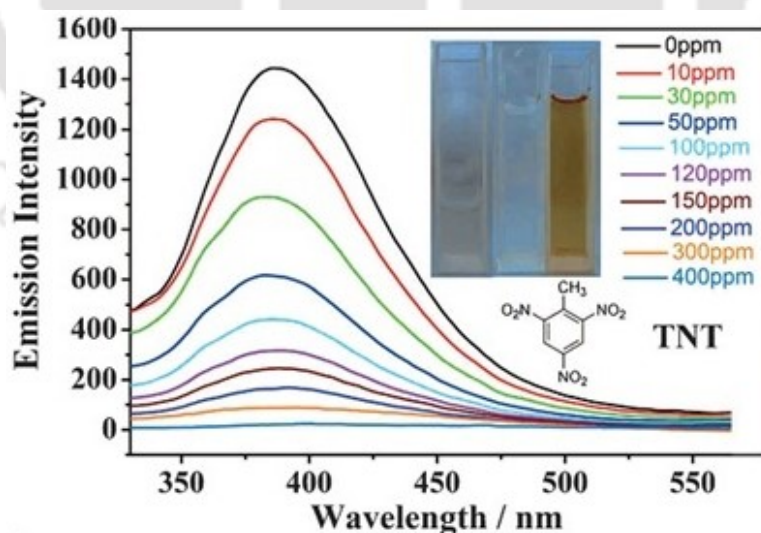


**Figure 1.11** Emission spectra of NENU-503 at different concentrations of TNT (inset: color changes upon incremental addition of TNT solution. The photos from left to right are TNT, NENU-503 in DMA, NENU-503 in DMA containing TNT, respectively). Reproduced with permission from ref.121. Copyright 2014 John Wiley and Sons.

Moreover, several other transition metal based MOFs have been developed for the fluorimetric detection of nitroaromatic explosives.<sup>129-131</sup> A Zr(IV)-based MOF having composition  $Zr_6O_4(OH)_4(ppdc)_6$  ( $ppdc = 2\text{-phenylpyridine-5,4'-dicarboxylic}$ ) having Lewis basic pyridyl sites have been demonstrated for the rapid, selective and sensitive detection of TNP in aqueous medium (Figure 1.12).<sup>96</sup> Another 3D Zr-MOF also provides selective sensing ability towards TNP where the guest-accessible Lewis basic N-donor sites of thienothiophene moieties can act as recognition sites for TNP via electrostatic interactions (Figure 1.13).<sup>132</sup>

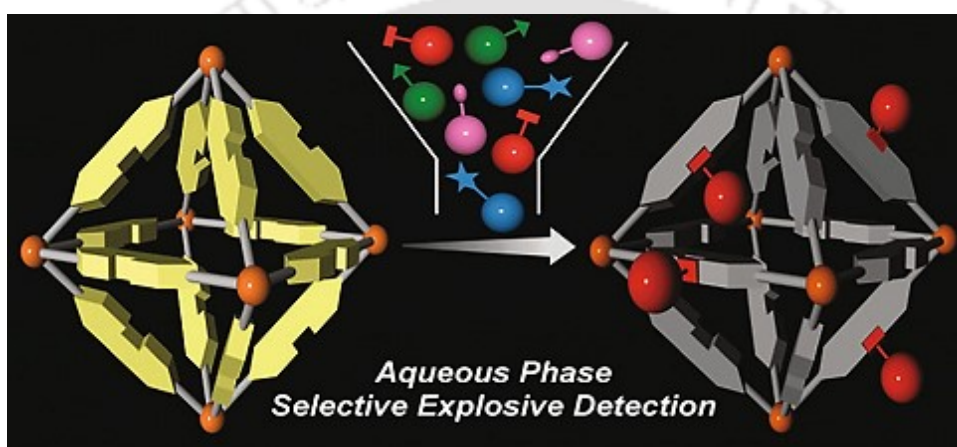


**Figure 1.12** Highly selective detection of nitroaromatic explosives by  $Zr_6O_4(OH)_4(ppdc)_6$  in aqueous phase. Reproduced with permission from ref.96. Copyright 2014 Royal Society of Chemistry.

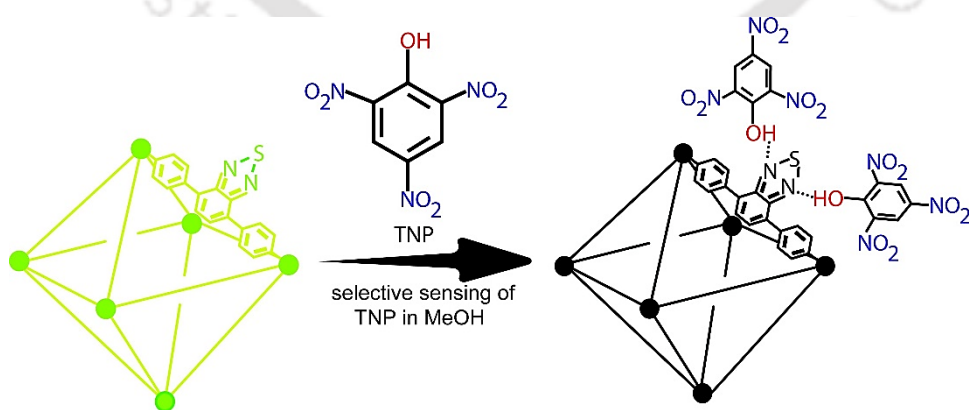


**Figure 1.13** Fluorescent Zr(IV)-based MOF with attached amine functionality for highly selective detection of TNP in aqueous phase.<sup>132</sup>

### (b) Lanthanide Based Luminescent MOFs

Indeed, a huge number of Zn(II) and Cd(II)-based luminescent MOFs have been applied for the detection of nitro explosives. However, the major drawback of these sensors is the small Stokes shift, which prevents the detection by naked eye as there is not much difference in color between excitation light. Lanthanide based MOF sensors with large Stokes shift exhibit excellent luminescence properties. Hence, they open up another potential way of for the fluorimetric sensing of nitroaromatic explosives. Especially,  $Tb^{3+}$ <sup>133-137</sup> and  $Eu^{3+}$ <sup>120, 138-142</sup> (Figure 1.14) based MOFs have been found to be very promising as sensor materials for the selective detection of nitroaromatic explosives.

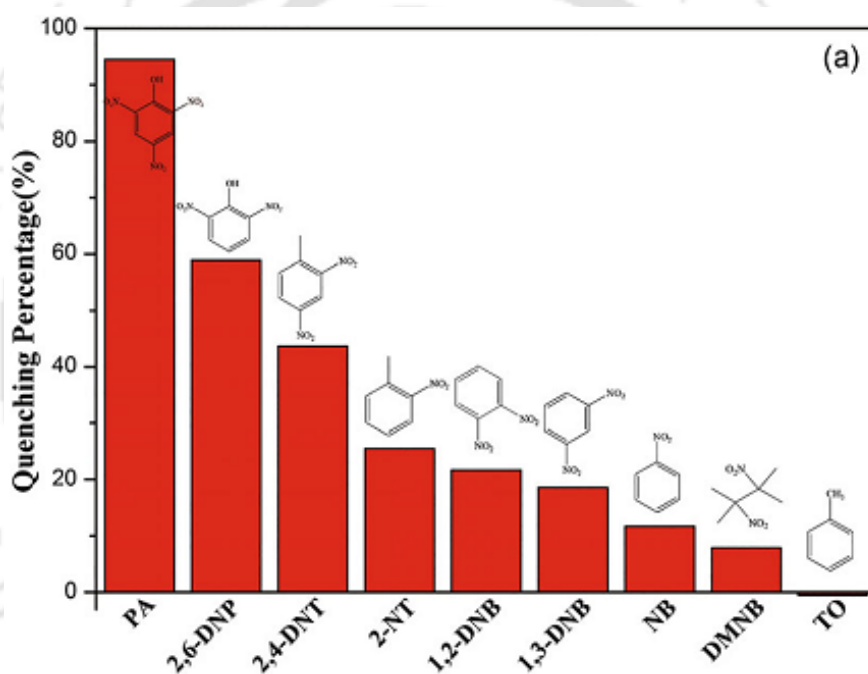


**Figure 1.14** Luminescence quenching percentage when the MOF having composition  $Eu_3(H_{0.75}MHFDA)_4(NO_3)_4 \cdot 5.5DMF$  ( $H_2MHFDA = 9\text{-methyl-9-hydroxy-fluorene-2,7-dicarboxylic acid}$ ) was dispersed in eight different nitro explosives and toluene solutions in DMF. Reproduced with permission from ref.139. Copyright 2015 Royal Society of Chemistry.

### (c) Main Group and Metalloligand Based Luminescent MOFs

In addition to these two types of MOFs, main group-based luminescent MOFs<sup>143-146</sup> and MOFs with metalloligands<sup>147-149</sup> (as metal-containing complexes instead of pure organic ligands) are widely used for the fluorescence-based selective and sensitive detection of nitro explosive compounds. For example, an In(III)-based MOF having molecular formula  $[In_2(tdmm)]$

$[\text{NH}_2(\text{CH}_3)_2]_2 \cdot (\text{DMF})_4(\text{H}_2\text{O})_{16}$  (tdmm = tetrakis[(3,5-dicarboxyphenoxy) methyl]methane) have displayed highly selective and sensitive sensing properties towards nitrobenzene (NB).<sup>146</sup> Furthermore, a highly luminescent heteronuclear MOF having composition  $\text{Zn}[\text{L}]_2 \cdot 3\text{DMF} \cdot 5\text{H}_2\text{O}$  { $\text{L} = [\text{Ir}(\text{ppy})_2(\text{dcbpy})_2]$ }; ppy = 2-phenylpyridine, dcbpy = 2,2'-bipyridine-4,4'-dicarboxylate, based on a highly light-harvesting cyclo-metalated iridium(III) unit, have featured highly selective sensing of TNT on the ppm scale.<sup>150</sup>

Although a large number of MOF-based fluorescent sensor materials<sup>87-95</sup> have been investigated until today for the detection of nitroaromatic explosive compounds, only a few of them<sup>151-160</sup> have exhibited rapid and selective sensing properties towards TNP.

### 1.5.2 MOFs for Sensing of Hydrogen Sulphide

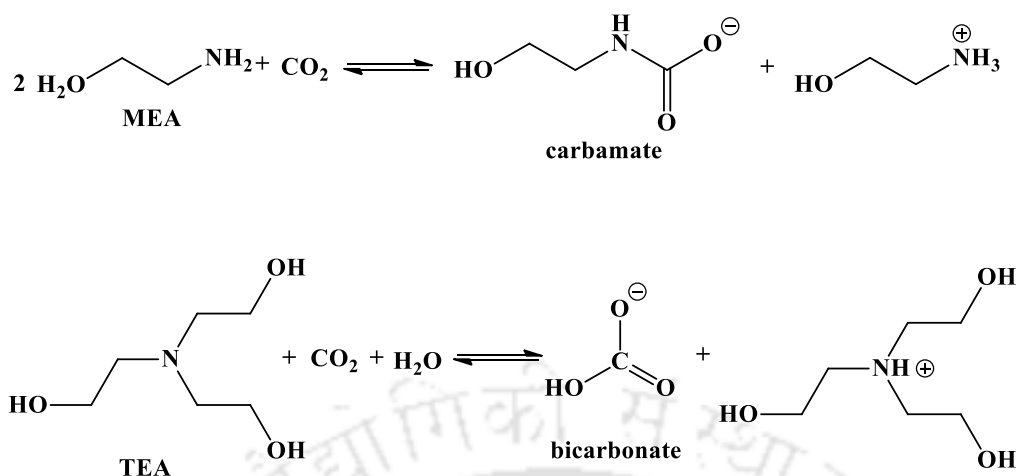
MOF-based turn-on fluorescent probes with improved sensitivity over other traditional methods would be a promising strategy for the prompt detection and real-time monitoring of  $\text{H}_2\text{S}$ . Only a few MOF materials (nitro-, azide-, malonitrile-functionalized and metalloporphyrin-based) have been reported as a fluorescence turn-on probe for the selective sensing of  $\text{H}_2\text{S}$  under physiological conditions.<sup>161-165</sup> These MOF-based fluorescent probes for detection of  $\text{H}_2\text{S}$  can be classified into three categories based on their different fluorescence turn-on mechanism. (i) Probes containing azide/nitro group can be converted to turn-on fluorescence probe from their initial turn-off state by  $\text{H}_2\text{S}$ -facilitated reduction of azide/nitro functional group to amine.<sup>161-163</sup> (ii) Probes incorporating reactive metal centers which can act as recognition sites for  $\text{H}_2\text{S}$  within the framework. For example, Cu/Al-nano-MOF based on porphyrin acted as a fluorescent turn-on probe when treated with  $\text{H}_2\text{S}$  as a consequence of leaching of Cu as CuS and simultaneous release of the fluorescent MOF.<sup>165</sup> (iii) Probes with specific functional groups can efficiently uptake and respond to thiol-containing species. For example, malonitrile units in malonitrile-functionalized ZIF-90 MOF acted as recognition sites for thiol moieties by increasing the photoluminescence behavior as a result of the reaction between the malonitrile units and thiol compounds.<sup>164</sup>

## 1.6 MOFs FOR $\text{CO}_2$ ADSORPTION

The declining climate condition due to global warming caused by the rising of atmospheric  $\text{CO}_2$  level resulting from anthropogenic emissions is a matter of widespread public concern. The

increasing dependency on combustion fossil fuels (coal, petroleum and natural gas) is a major source of CO<sub>2</sub> emission, which contributes 86% of anthropogenic greenhouse gas emissions.<sup>166</sup> The annual global emission of CO<sub>2</sub> has been increased by approximately 80% between 1970 and 2004. It is expected to continue to increase in the future due to economic growth and industrial development, particularly in the developing nations. Therefore, the urgent need of strategies to reduce the atmospheric CO<sub>2</sub> levels has urged action from national and international governments and industries. Several methods have been proposed for the effective capture and sequestration/separation of CO<sub>2</sub> (CCS) including membrane separation, chemical absorption with solvents, adsorption with solid adsorbents, cryogenic separation, electrochemical separation and fuel cells.<sup>167</sup> The most essential parameter for any CO<sub>2</sub> capture material is high selectivity toward CO<sub>2</sub> in order to completely remove the CO<sub>2</sub> component of the flue gas for subsequent sequestration. However, the affinity of the material toward CO<sub>2</sub> is also a crucial parameter which controls and optimizes the interaction of CO<sub>2</sub> with the material and energy penalty of capture. If the interaction is too strong, a high energy will be required for desorption of the captured CO<sub>2</sub>. On the other hand, a weak interaction although lowers the regeneration cost but it would afford low selectivity for CO<sub>2</sub> over the other components of the flue gas. In addition, the material should exhibit a high stability under the conditions of capture and regeneration. It should also adsorb CO<sub>2</sub> at a high density.

The CO<sub>2</sub> adsorptive capacity of a porous material can be measured by both gravimetric and volumetric methods. The gravimetric CO<sub>2</sub> uptake reveals the quantity of CO<sub>2</sub> adsorbed within a unit mass of the material whereas the volumetric uptake refers to how densely CO<sub>2</sub> can be stored within the material. Porous materials are chosen as potential candidates for CO<sub>2</sub> adsorption due to their porosity and high internal surface areas. The CO<sub>2</sub> adsorption within the pores of the material depends on various factors including structural effects to surface functionalization. Besides porous materials, aqueous alkanol amine solutions (e.g., monoethanolamine, triethanolamine, N-methyldiethanolamine) show very high affinity towards CO<sub>2</sub> due to the presence of amine functional groups, which participate in nucleophilic attack at the C atom of CO<sub>2</sub> to form a C–N bond resulting in the formation of carbamate or bicarbonate species, as shown in Scheme 1.1.<sup>168</sup>



**Scheme 1.1** Reaction of  $\text{CO}_2$  with monoethanolamine (MEA) to give carbamate product (upper), and the corresponding reaction with triethanolamine (TEA) resulting in a bicarbonate species (lower).

Despite the affinity for  $\text{CO}_2$ , alkanolamine has also some major disadvantages as absorbent. First, the full regeneration of  $\text{CO}_2$  from the adsorbent materials is not possible because the solution of alkanolamine is relatively unstable towards heating which limits the regeneration. Secondly, the performance of the absorbent material deteriorates over time. Therefore, the lifetime of the solutions is reduced due to decomposition of the amines. In addition, the corrosive nature of the amines is a major drawback for this type of adsorbents, which prevents their practical applications. A large number of solid physical adsorbents have been reported so far for  $\text{CO}_2$  capture including carbon-based sorbents, zeolites, chemically modified mesoporous materials, metal oxides, hydrotalcite-like compounds and organic solids such as covalent organic frameworks (COFs).<sup>146</sup> The solid adsorbents are promising candidates for  $\text{CO}_2$  adsorption because the smaller heat capacities of solids may reduce the functional temperature required for regeneration. Utilization of the solid adsorbents would also minimize the corrosion issues resulting from the use of aqueous amines. Zeolite LTA, a porous and low-cost solid adsorbent material, has shown a significant impact on the rapid and effective  $\text{CO}_2$  adsorption.<sup>169</sup> However, the hydrophilic nature of the zeolites leads to ready adsorption of water vapor, which reduces the  $\text{CO}_2$  adsorption capacity of the materials. Furthermore, the large enthalpy of adsorption of  $\text{CO}_2$  limits their practical applications by increasing the  $\text{CO}_2$  desorption temperature (ca. 135 °C). Later, these difficulties were overcome by using highly porous and hydrophobic activated carbons, which exhibit effective  $\text{CO}_2$  adsorption compared to zeolites with reduced effect of water vapor on the adsorbent.<sup>170</sup> Therefore, the development of new materials combining the high affinity of amines and the

advantages of using a porous solid adsorbent to improve the CO<sub>2</sub> uptake capacity is very crucial task. In last two decades, a new class of porous crystalline materials known as metal-organic frameworks (MOFs) has shown remarkable progress in CO<sub>2</sub> adsorption.<sup>171</sup> These materials have attracted much attention due to their unique structural properties including robustness, high internal surface areas, high chemical and thermal stabilities, high void volumes and low densities. In addition to the adsorption capacity, the selectivity is a principal property relevant to adsorptive gas separation, and is determined by interplay of factors including molecular sieving effect, thermodynamic equilibrium effect and kinetic effect. The high tunability of the framework design of MOFs allows greater functionality with reduced adsorbent mass and volume compared to conventional solid adsorbents. In addition, the presence of coordinatively unsaturated metal centers (open metal sites) along the pore surfaces provides Lewis acidity to the framework. Besides large surface areas and pore volumes, the available open metal sites in some MOFs (e.g., M<sub>2</sub>-dobdc or M-MOF-74; M = Mg, Mn, Fe, Co, Ni, Zn; dobdc<sup>4-</sup> = 2,5-dioxido-1,4-benzenedicarboxylate) make them potential candidates for CO<sub>2</sub> adsorption.<sup>172</sup> The majority of the known MOFs, which have been investigated for CO<sub>2</sub> adsorption, are catalogued in Table 1.1.

**Table 1.1** Summary of known MOFs investigated for CO<sub>2</sub> adsorption.

MOFs	Conditions	Adsorbed amount (mmol/g)	Ref.
Mg/DOBDC / MOF-74 (Mg) / CPO-27-Mg	298 K, 1 bar	8.48	173
HKUST-1 / Cu-BTC	298 K, 1 bar, 4% hydrated	8.18	174
Mg/DOBDC / MOF-74 (Mg) / CPO-27-Mg	296 K, 1 atm	8.00	175
Co/DOBDC / MOF-74 (Co) / CPO-27-Co	298 K, 1 bar	7.55	173
Ni/DOBDC / MOF-74 (Ni) / CPO-27-Ni	298 K, 1 bar	7.15	173
Co/DOBDC / MOF-74 (Co) / CPO-27-Co	296 K, 1 atm	6.95	175
Mg/DOBDC / MOF-74 (Mg) / CPO-27-Mg	298 K, 1 atm	6.82	176
Ni/DOBDC / MOF-74 (Ni) / CPO-27-Ni	298 K, 1 atm	6.82	176
bio-MOF-11	273 K, 1 bar	6.00	177

MOFs	Conditions	Adsorbed amount (mmol/g)	Ref.
Ni/DOBDC / MOF-74 (Ni) / CPO-27-Ni	296 K, 1 atm	5.82	175
Zn/DOBDC / MOF-74 (Zn) / CPO-27-Zn	296 K, 1 atm	5.54	175
Ni/DOBDC / MOF-74 (Ni) / CPO-27-Ni	303 K, 1 atm	5.00	178
HKUST-1 / Cu-BTC	298 K, 1 bar, dehydrated	5.00	174
HKUST-1 / Cu-BTC	295.25 K, 1 bar	4.20	179
bio-MOF-11	298 K, 1 bar	4.10	177
HKUST-1 / Cu-BTC	298 K, 1 bar	4.07	180
CUK-1	298 K, 760 torr	3.48	181
YO-MOF	273 K, 1 atm	3.39	182
SNU-M10	273 K, 1 atm	3.3	183
H <sub>3</sub> [(Cu <sub>4</sub> Cl) <sub>3</sub> -(BTTri) <sub>8</sub> ]	298 K, 1 bar	3.25	184
USO-2-Ni-A	303 K, 1 atm	3.18	185
USO-1-Al-A	303 K, 1 atm	2.73	185
ZIF-69	273 K, 1 atm	2.62	1
HKUST-1 / Cu-BTC	318.15 K, 1 bar	2.60	179
Ni-STA-12	298 K, 1 bar	2.60	186
[Pd(m-F-PYMO-N <sup>1</sup> ,N <sup>3</sup> ) <sub>2</sub> ·(H <sub>2</sub> O) <sub>m</sub> ] <sub>n</sub>	293 K, 650 torr	2.49	187
[Fe(PZ)Ni(CN) <sub>4</sub> ]	298 K, 1 bar	2.48	188
MIL-53(Cr)	303 K, 0.1 Mpa	2.39	189
USO-1-Al	303 K, 1 atm	2.27	185
MOF-5 / IRMOF-1	296 K, 1 bar	2.10	190
SNU-M10	298 K, 1 atm	2.10	183
USO-2-Ni	303 K, 1 atm	2.05	185
MIL-47	298 K, 1 bar	2.00	173
Amino-MIL-53(Al)	288 K, 1 bar	2.00	191
MIL-53	304 K, 1 bar	2.00	192
UoC-1'	273 K, 1 bar	2.00	193

MOFs	Conditions	Adsorbed amount (mmol/g)	Ref.
MOF-5 / IRMOF-1	298 K, 1 bar	1.92	190
HKUST-1 / Cu-BTC	295.25 K, 1 bar	1.80	179
[Cu <sub>2</sub> (IMTA)(DMSO) <sub>2</sub> ·2H <sub>2</sub> O]	298 K, 1 bar	1.80	194
ZIF-100	273 K, 1 atm	1.70	195
[Pd(2-PYMO) <sub>2</sub> ] <sub>n</sub>	298 K, 1 atm	1.68	196
[Pd(m-H-PYMO-N <sup>1</sup> ,N <sup>3</sup> ) <sub>2</sub> ·(H <sub>2</sub> O) <sub>m</sub> ] <sub>n</sub>	293 K, 650 torr	1.64	187
HKUST-1 / Cu-BTC	318.15 K, 1 bar	1.50	179
MOF-5 / IRMOF-1	273 K, 1 bar	1.50	193
H <sub>3</sub> [(Cu <sub>4</sub> Cl) <sub>3</sub> (BTTri) <sub>8</sub> ](en)	298 K, 1 bar	1.25	184
SNU-9	273 K, 1 atm	1.25	197
Zn <sub>2</sub> (tetrakis[4-(carboxyphenyl)oxamethyl]methane)(4,4'-bipyridine)	298 K, 1 bar	1.14	198
MOF-5 / IRMOF-1	298 K, 1 bar	1.13	190
MOF-5 / IRMOF-1	298 K, 1 bar	1.12	190
ZIF-8	298 K, 1 bar	1.02	173
[Cu <sub>2</sub> (HBTB) <sub>2</sub> (H <sub>2</sub> O)(EtOH)]·H <sub>2</sub> O·EtOH	298 K, 1 bar	1.00	199
ZIF-100	298 K, 1 atm	0.96	195
USO-3-Ni	303 K, 1 atm	0.91	185
UMCM-1	298 K, 1 bar	0.91	173
[Cu(2-PYMO) <sub>2</sub> ] <sub>n</sub>	298 K, 1 atm	0.90	187
MOF-5 / IRMOF-1	298 K, 1 bar	0.83	173
[Cu <sub>3</sub> (m-TATB) <sub>2</sub> Py(CH <sub>3</sub> OH) <sub>2</sub> ]	273 K, 1 atm	0.82	200
[Pd(m-Br-PYMO-N <sup>1</sup> ,N <sup>3</sup> ) <sub>2</sub> ·(H <sub>2</sub> O) <sub>m</sub> ] <sub>n</sub>	293 K, 650 torr	0.74	187
[Zn <sub>2</sub> (4,4',4'',4'''-benzene-1,2,4,5-tetrayltetrabenzoic acid)(py-R) <sub>2</sub> ] <sub>n</sub>	298 K, 1 bar	0.62	201
[Zn <sub>2</sub> (4,4',4'',4'''-benzene-1,2,4,5-tetrayltetrabenzoic acid)(DMF) <sub>2</sub> ] <sub>n</sub>	298 K, 1 bar	0.60	201

MOFs	Conditions	Adsorbed amount (mmol/g)	Ref.
MOF-2	298 K, 1 bar	0.57	180
$[\text{Pd}(\text{m-I-PYMO-N}^1, \text{N}^3)_2 \cdot (\text{H}_2\text{O})_m]_n$	293 K, 650 torr	0.41	187
$[\text{Mg}(\text{HCOO})_2 \cdot 2\text{H}_2\text{O}]$	298 K, 700 torr	0.30	202
ZIF-20	273 K, 760 torr	0.16	203

Ligand abbreviations: BTC = benzenetricarboxylate; BTri = 1,3,5-tris(1H-1,2,3-triazol-5-yl)benzene; F-PYMO = 5-fluoropyrimidin-2-olate; PZ = pyrazine; H-PYMO = pyrimidin-2-olate; TATB = 4',4',4''-s-triazine-2,4,6-triyl-tribenzoate; IMTA = imidazolium tetracarboxylic acid; BTB = 1,3,5-tris(4-carboxyphenyl)benzene.

## 1.7 MOTIVATION AND OBJECTIVES

So far, a large number of MOFs have shown application potentials in gas ( $\text{H}_2$ ,  $\text{CO}_2$ ,  $\text{CH}_4$ ,  $\text{CO}$ , etc.) storage and fluorescence sensing of a wide variety of analytes (cations, anions, biomolecules, small molecules, volatile organic compounds, nitro explosive materials, etc.). Functionalization of MOFs has been performed by using pre-functionalized ligands during the synthesis or by using the post-synthetic modification approach. The functional groups introduced in either strategy have been demonstrated to affect the physicochemical stability (air, water, acid-base, heat, etc.)<sup>204</sup> as well as gas storage and separation<sup>205, 206</sup> properties of the resulting MOFs. The attached functional groups can act as interaction sites for specific gas molecules (during gas adsorption) and analytes (during fluorescence sensing), thus increasing the selectivity of the MOF material towards the target gas or analyte. In this thesis, the synthesis, characterization, gas storage and fluorescence sensing behavior of new MOFs possessing different functional groups will be presented. The synthesis of air- and moisture-stable MOFs bearing desired functional groups is still a key challenge. Some of the well-known MOF materials<sup>207, 208</sup> displaying application potentials in adsorption, separation or catalysis collapse after prolonged exposure towards moisture from air. This type of instability hampers their practical applications. For enhancing their hydrolytic stabilities, hydrophobic functional groups (e.g., -F, - $\text{CH}_3$ , - $\text{CF}_3$ , - $\text{OCF}_3$ , etc.) have been incorporated in their frameworks. In addition, the use of metal ions with higher oxidation states than divalent ions (e.g. Al(III),<sup>20, 209</sup> Cr(III),<sup>38</sup> Ti(IV),<sup>43</sup> Zr(IV),<sup>42</sup> Ce(IV),<sup>210</sup> etc.) has been demonstrated to be a successful approach, which results in MOFs having relatively higher

physiochemical stabilities (air, water, heat, acid-base, etc.). In this dissertation, the gas adsorption and fluorescence sensing applications of highly stable MOFs bearing metal ions in high oxidation states (Al(III), Cr(III), Zr(IV) and Ce(IV)-based MOFs including one Cd(II)-based MOF) will be presented.

## 1.8 REFERENCES

1. R. Banerjee, A. Phan, B. Wang, C. Knobler, H. Furukawa, M. O'Keeffe and O. M. Yaghi, *Science*, 2008, **319**, 939.
2. B. Chen, L. Wang, Y. Xiao, F. R. Fronczek, M. Xue, Y. Cui and G. Qian, *Angew. Chem. Int. Ed.*, 2009, **48**, 500.
3. B. Chen, L. Wang, F. Zapata, G. Qian and E. B. Lobkovsky, *J. Am. Chem. Soc.*, 2008, **130**, 6718.
4. M. H. Alkordi, Y. Liu, R. W. Larsen, J. F. Eubank and M. Eddaoudi, *J. Am. Chem. Soc.*, 2008, **130**, 12639.
5. R.-Q. Zou, H. Sakurai and Q. Xu, *Angew. Chem. Int. Ed.*, 2006, **45**, 2542.
6. R. J. Kuppler, D. J. Timmons, Q.-R. Fang, J.-R. Li, T. A. Makal, M. D. Young, D. Yuan, D. Zhao, W. Zhuang and H.-C. Zhou, *Coord. Chem. Rev.*, 2009, **253**, 3042.
7. B. Liu, H. Shioyama, H. Jiang, X. Zhang and Q. Xu, *Carbon*, 2010, **48**, 456.
8. W. Wang, Y. Li, R. Zhang, D. He, H. Liu and S. Liao, *Catal. Commun.*, 2011, **12**, 875.
9. B. Liu, H. Shioyama, T. Akita and Q. Xu, *J. Am. Chem. Soc.*, 2008, **130**, 5390.
10. Themed issue on MOFs: *Chem. Soc. Rev.*, 2009, **38**, 1201.
11. Special issue on MOFs: *Chem. Rev.*, 2012, **112**, 673.
12. G. Férey, *Chem. Soc. Rev.*, 2008, **37**, 191.
13. O. M. Yaghi, M. O'Keeffe, N. W. Ockwig, H. K. Chae, M. Eddaoudi and J. Kim, *Nature*, 2003, **423**, 705.
14. S. Kitagawa, R. Kitaura and S. Noro, *Angew. Chem. Int. Ed.*, 2004, **43**, 2334.
15. M. Eddaoudi, J. Kim, N. Rosi, D. Vodak, J. Wachter, M. O'Keeffe and O. M. Yaghi, *Science*, 2002, **295**, 469.
16. D. J. Tranchemontagne, J. L. Mendoza-Corte's, M. O'Keeffe and O. M. Yaghi, *Chem. Soc. Rev.*, 2009, **38**, 1257.

17. M. Eddaoudi, D. B. Moler, H. Li, B. Chen, T. M. Reineke, M. O'Keeffe and O. M. Yaghi, *Acc. Chem. Res.*, 2001, **34**, 319.
18. S. Biswas, D. E. P. Vanpoucke, T. Verstraelen, M. Vandichel, S. Couck, K. Leus, Y.-Y. Liu, M. Waroquier, V. Van Speybroeck, J. F. M. Denayer and P. V. D. Voort, *J. Phys. Chem. C*, 2013, **117**, 22784.
19. S. Biswas, J. Zhang, Z. Li, Y.-Y. Liu, M. Grzywa, L. Sun, D. Volkmer and P. V. D. Voort, *Dalton Trans.*, 2013, **42**, 4730.
20. S. Biswas, T. Ahnfeldt and N. Stock, *Inorg. Chem.*, 2011, **50**, 9518.
21. S. Biswas and P. V. D. Voort, *Eur. J. Inorg. Chem.*, 2013, **2013**, 2154.
22. J. R. Li, R. J. Kuppler and H. C. Zhou, *Chem. Soc. Rev.*, 2009, **38**, 1477.
23. L. Hamon, P. L. Llewellyn, T. Devic, A. Ghoufi, G. Clet, V. Guillerm, G. D. Pirngruber, G. Maurin, C. Serre, G. Driver, W. van Beek, E. Jolimaître, A. Vimont, M. Daturi and G. Férey, *J. Am. Chem. Soc.*, 2009, **131**, 17490.
24. L. J. Murray, M. Dinca and J. R. Long, *Chem. Soc. Rev.*, 2009, **38**, 1294.
25. J. Lee, O. K. Farha, J. Roberts, K. A. Scheidt, S. T. Nguyen and J. T. Hupp, *Chem. Soc. Rev.*, 2009, **38**, 1450.
26. L. Ma, C. Abney and W. Lin, *Chem. Soc. Rev.*, 2009, **38**, 1248.
27. K. M. L. Taylor-Pashow, J. Della Rocca, Z. G. Xie, S. Tran and W. B. Lin, *J. Am. Chem. Soc.*, 2009, **131**, 14261.
28. M. Vallet-Regí, F. Balasm and D. Arcos, *Angew. Chem. Int. Ed.*, 2007, **46**, 7548.
29. P. Horcajada, C. Serre, M. Vallet-Regí, M. Sebban, F. Taulelle and G. Férey, *Angew. Chem. Int. Ed.*, 2006, **45**, 5974.
30. P. Horcajada, T. Chalati, C. Serre, B. Gillet, C. Sebrie, T. Baati, J. F. Eubank, D. Heurtaux, P. Clayette, C. Kreuz, J. S. Chang, Y. K. Hwang, V. Marsaud, Y.-N. Bories, L. Cynober, S. Gil, G. Férey, P. Couvreur and R. Gref, *Nat. Mater.*, 2010, **9**, 172.
31. S. Dang, E. Ma, Z.-M. Sun and H. Zhang, *J. Mater. Chem.*, 2012, **22**, 16920.
32. W. Yang, J. Feng and H. Zhang, *J. Mater. Chem.*, 2012, **22**, 6819.
33. Z. C. Liu, Z. Y. Yang, T. R. Li, B. D. Wang, Y. Li, D. D. Qin, M. F. Wang and M. H. Yan, *Dalton Trans.*, 2011, **40**, 9370.
34. S. Liu, Z. Xiang, Z. Hu, X. Zheng and D. Cao, *J. Mater. Chem.*, 2011, **21**, 6649.

35. S. Bai, T. Sheng, C. Tan, Q. Zhu, Y. Huang, H. Jiang, S. Hu, R. Fu and X. Wu, *J. Mater. Chem.*, 2013, **1**, 2970.
36. Y. Liu, V. Kravtsov, R. Larsen and M. Eddaoudi, *Chem. Commun.*, 2006, 1488.
37. M. Bosch, M. Zhang and H.-C. Zhou, *Adv. Chem.*, 2014, **2014**, 1.
38. G. Férey, C. Mellot-Draznieks, C. Serre, F. Millange, J. Dutour, S. Surble and I. Margiolaki, *Science*, 2005, **309**, 2040.
39. T. Loiseau, C. Serre, C. Huguenard, G. Fink, F. Taulelle, M. Henry, T. Bataille and G. Férey, *Chem.–Eur. J.*, 2004, **10**, 1373.
40. P. Serra-Crespo, E. V. Ramos-Fernandez, J. Gascon and F. Kapteijn, *Chem. Mater.*, 2011, **23**, 2565.
41. H. Chevreau, T. Devic, F. Salles, G. Maurin, N. Stock, C. and Serre, *Angew. Chem. Int. Ed.*, 2013, **52**, 5056.
42. J. H. Cavka, S. Jakobsen, U. Olsbye, N. Guillou, C. Lamberti, S. Bordiga and K. P. Lillerud, *J. Am. Chem. Soc.*, 2008, **130**, 13850.
43. M. Dan-Hardi, C. Serre, T. Frot, L. Rozes, G. Maurin, C. Sanchez and G. Férey, *J. Am. Chem. Soc.*, 2009, **131**, 10857.
44. G. S. Papaefstathiou and L. R. MacGillivray, *Angew. Chem. Int. Ed.*, 2002, **41**, 2070.
45. Z. Wang, PhD Thesis, University of South Florida, 2006.
46. Z. Wang, V. C. Kravtsov and M. J. Zaworotko, *Angew. Chem. Int. Ed.*, 2005, **44**, 2877.
47. J. J. Lu, A. Mondal, B. Moulton and M. J. Zaworotko, *Angew. Chem. Int. Ed.*, 2001, **40**, 2113.
48. S. A. Bourne, J. J. Lu, A. Mondal, B. Moulton and M. J. Zaworotko, *Angew. Chem. Int. Ed.*, 2001, **40**, 2111.
49. B. Moulton, J. Lu, A. Mondal and M. J. Zaworotko, *Chem. Commun.*, 2001, 863.
50. C. Baerlocher, L. B. McCusker and D. H. Olson, *Atlas of Zeolite Framework Types*, Elsevier, Amsterdam, The Netherlands, 6th rev. edn. edn., 2007.
51. J. Kim, B. Chen, T. M. Reineke, H. Li, M. Eddaoudi, D. B. Moler, M. O’Keeffe and O. M. Yaghi, *J. Am. Chem. Soc.*, 2001, **123**, 8239.
52. S. Biswas, PhD Thesis, University of Ulm, 2010.
53. Z. Hu, Y. Peng, Z. Kang, Y. Qian and D. Zhao, *Inorg. Chem.*, 2015, **54**, 4862.

54. A. Schaate, P. Roy, A. Godt, J. Lippke, F. Waltz, M. Wiebcke and P. Behrens, *Chem. Eur. J.*, 2011, **17**, 6643.
55. N. Stock and S. Biswas, *Chem. Rev.*, 2012, **112**, 933.
56. J. Cravillon, S. Münzer, S. J. Lohmeier, A. Feldhoff, K. Huber and M. Wiebcke, *Chem. Mater.*, 2009, **21**, 1410.
57. D. Tranchemontagne, J. Hunt and O. M. Yaghi, *Tetrahedron*, 2008, **64**, 8553.
58. L. Huang, H. Wang, J. Chen, Z. Wang, J. Sun, D. Zhao and Y. Yan, *Microporous Mesoporous Mater.*, 2003, **58**, 105.
59. S. Kitagawa, R. Kitaura and S.-I. Noro, *Angew. Chem. Int. Ed.*, 2004, **116**, 2388.
60. O. M. Yaghi, M. O'Keeffe, N. W. Ockwig, H. K. Chae, M. Eddaoudi and J. Kim, *Nature*, 2003, **423**, 705.
61. X.-X. Zhao, J.-P. Ma, Y.-B. Dong and R.-Q. Huang, *Cryst. Growth Des.*, 2007, **7**, 1058.
62. Z. Ni and R. I. Masel, *J. Am. Chem. Soc.*, 2006, **128**, 12394.
63. J. Y. Choi, J. Kim, S. H. Jhung, H. K. Kim, J. S. Chang and H. K. Chae, *Bull. Korean Chem. Soc.*, 2006, **27**, 1523.
64. S. H. Jhung, J.-H. Lee and J.-S. Chang, *Bull. Korean Chem. Soc.*, 2005, **26**, 880.
65. S. H. Jhung, J.-H. Lee, P. M. Forster, G. Férey, A. K. Cheetham and J.-S. Chang, *Chem. Eur. J.*, 2006, **12**, 7899.
66. S. H. Jhung, J. Lee, J. W. Yoon, C. Serre, G. Férey and J.-S. Chang, *Adv. Mater.*, 2007, **19**, 121.
67. W.-J. Son, J. Kim, J. Kim and W.-S. Ahn, *Chem. Commun.*, 2008, 6336.
68. U. Mueller, H. Puetter, M. Hesse, M. Schubert, H. Wessel, J. Huff and M. Guzmán, U.S. Pat. No. 8163949, 2012.
69. A. Pichon and S. L. James, *CrystEngComm*, 2008, **10**, 1839.
70. A. Pichon, A. Lazuen-Garay and S. L. James, *CrystEngComm*, 2006, **8**, 211.
71. K. K. Tanabe and S. M. Cohen, *Chem. Soc. Rev.*, 2011, **40**, 498.
72. H. Li, M. Eddaoudi, M. O'Keeffe and O. M. Yaghi, *Nature*, 1999, **402**, 276.
73. F. Millange, C. Serre and G. Férey, *Chem. Commun.*, 2002, 822.
74. V. Guillermin, S. Gross, C. Serre, T. Devic, M. Bauer and G. Férey, *Chem. Commun.*, 2010, **46**, 767.

75. Q. Yang, A. D. Wiersum, H. Jobic, V. Guillerm, C. Serre, P. L. Llewellyn and G. Maurin, *J. Phys. Chem. C*, 2011, **115**, 13768.
76. Q. Yang, H. Jobic, F. Salles, D. Kolokolov, V. Guillerm, C. Serre and G. Maurin, *Chem. Eur. J.*, 2011, **17**, 8882.
77. M. J. Katz, Z. J. Brown, Y. J. Colón, P. W. Siu, K. A. Scheidt, R. Q. Snurr, J. T. Hupp and O. K. Farha, *Chem. Commun.*, 2013, **49**, 9449.
78. A. Schaate, P. Roy, A. Godt, J. Lippke, F. Waltz, M. Wiebcke and P. Behrens, *Chem. Eur. J.*, 2011, **17**, 6643.
79. J. Juan-Alcañiz, E. V. Ramos-Fernandez, U. Lafont, J. Gascon and F. Kapteijn, *J. Catal.*, 2010, **269**, 229.
80. <http://www.iza-structure.org/databases/>.
81. M. Lammert, S. Bernt, F. Vermoortele, D. E. De Vos and N. Stock, *Inorg. Chem.*, 2013, **52**, 8521.
82. P. Horcajada, H. Chevreau, D. Heurtaux, F. Benyettou, F. Salles, T. Devic, A. Garcia-Marquez, C. Yu, H. Lavrard, C. L. Dutson, E. Magnier, G. Maurin, E. Elkaim and C. Serre, *Chem. Commun.*, 2014, **50**, 6872.
83. B. Wu, X. Lin, L. Ge, L. Wu and T. Xu, *Chem. Commun.*, 2013, **49**, 143.
84. S. Biswas, S. Couck, M. Grzywa, J. F. M. Denayer, D. Volkmer and P. Van Der Voort, *Eur. J. Inorg. Chem.*, 2012, **2012**, 2481.
85. F. Carson, J. Su, A. E. Platero-Prats, W. Wan, Y. Yun, L. Samain and X. Zou, *Cryst. Growth Des.*, 2013, **13**, 5036.
86. M. Hartmann and M. Fischer, *Microporous Mesoporous Mater.*, 2012, **164**, 38.
87. K. Müller-Buschbaum, F. Beuerle and C. Feldmann, *Microporous Mesoporous Mater.*, 2015, **216**, 171.
88. Z. Hu, B. J. Deibert and J. Li, *Chem. Soc. Rev.*, 2014, **43**, 5815.
89. M. D. Allendorf, C. A. Bauer, R. K. Bhakta and R. J. T. Houk, *Chem. Soc. Rev.*, 2009, **38**, 1330.
90. Y. Cui, Y. Yue, G. Qian and B. Chen, *Chem. Rev.*, 2012, **112**, 1126.
91. L. E. Kreno, K. Leong, O. K. Farha, M. Allendorf, R. P. Van Duyne and J. T. Hupp, *Chem. Rev.*, 2012, **112**, 1105.
92. Y. Cui, B. Chen and G. Qian, *Coord. Chem. Rev.*, 2014, **76**, 273.

93. L. V. Meyer, F. Schonfeld and K. Muller-Buschbaum, *Chem. Commun.*, 2014, **50**, 8093.
94. B. Chen, S. Xiang and G. Qian, *Acc. Chem. Res.*, 2010, **43**, 1115.
95. J. Lei, R. Qian, P. Ling, L. Cui and H. Ju, *Trends Analyt. Chem.*, 2014, **58**, 71.
96. S. S. Nagarkar, A. V. Desai and S. K. Ghosh, *Chem. Commun.*, 2014, **50**, 8915.
97. S. S. Nagarkar, B. Joarder, A. K. Chaudhari, S. Mukherjee and S. K. Ghosh, *Angew. Chem. Int. Ed.*, 2013, **52**, 2881.
98. S. S. Nagarkar, A. V. Desai, P. Samanta and S. K. Ghosh, *Dalton Trans.*, 2015, **44**, 15175.
99. M. D. Allendorf, C. A. Bauer, R. K. Bhakta and R. J. T. Houk, *Chem. Soc. Rev.*, 2009, **38**, 1330.
100. Y. Cui, Y. Yue, G. Qian and B. Chen, *Chem. Rev.*, 2011, **112**, 1126.
101. S. Pramanik, C. Zheng, X. Zhang, T. J. Emge and J. Li, *J. Am. Chem. Soc.*, 2011, **133**, 4153.
102. M. E. Germain and M. J. Knapp, *Chem. Soc. Rev.*, 2009, **38**, 2543.
103. S. J. Toal and W. C. Trogler, *J. Mater. Chem.*, 2006, **16**, 2871.
104. Z. Hu, B. J. Deibert and J. Li, *Chem. Soc. Rev.*, 2014, **43**, 5815.
105. H. Xu, X. Rao, J. Gao, J. Yu, Z. Wang, Z. Dou, Y. Cui, Y. Yang, B. Chen and G. Qian, *Chem. Commun.*, 2012, **48**, 7377.
106. G. He, H. Peng, T. Liu, M. Yang, Y. Zhang and Y. Fang, *J. Mater. Chem.*, 2009, **19**, 7347.
107. Y. Peng, A.-J. Zhang, M. Dong and Y.-W. Wang, *Chem. Commun.*, 2011, **47**, 4505.
108. T. Cheng, J. Hu, C. Zhou, Y. Wang and M. Zhang, *Sci. Chin. Chem.*, 2016, **59**, 929.
109. A. K. Chaudhari, S. S. Nagarkar, B. Joarder and S. K. Ghosh, *Cryst. Growth Des.*, 2013, **13**, 3716.
110. Z. Hu, S. Pramanik, K. Tan, C. Zheng, W. Liu, X. Zhang, Y. J. Chabal and J. Li, *Cryst. Growth Des.*, 2013, **13**, 4204.
111. S. Pramanik, Z. Hu, X. Zhang, C. Zheng, S. Kelly and J. Li, *Chem. Eur. J.*, 2013, **19**, 15964.
112. S. Sanda, S. Parshamoni, S. Biswas and S. Konar, *Chem. Commun.*, 2015, **51**, 6576.
113. Z. Q. Shi, Z. J. Guo, H. G. Zheng and S. Konar, *Chem. Commun.*, 2015, **51**, 8300.
114. X. Jiang, Y. Liu, P. Wu, L. Wang, Q. Wang, G. Zhu, X. Li and J. Wang, *RSC Adv.*, 2014, **4**, 47357.
115. D. Singh and C. M. Nagaraja, *Dalton Trans.*, 2014, **43**, 17912.
116. G. Liu, Y. Qin, L. Jing, G. Wei and H. Li, *Chem. Commun.*, 2013, **49**, 1699.

117. D. Ma, B. Li, X. Zhou, Q. Zhou, K. Liu, G. Zeng, G. Li, Z. Shi and S. Feng, *Chem. Commun.*, 2013, **49**, 8964.
118. M. Guo and Z. M. Sun, *J. Mater. Chem.*, 2012, **22**, 15939.
119. B. Gole, A. K. Bar and P. S. Mukherjee, *Chem. Commun.*, 2011, **47**, 12137.
120. M. Jurcic, W. J. Peveler, C. N. Savory, D. O. Scanlon, A. J. Kenyon and I. P. Parkin, *J. Mater. Chem. A*, 2015, **3**, 6351.
121. S. R. Zhang, D. Y. Du, J. S. Qin, S. J. Bao, S. L. Li, W. W. He, Y. Q. Lan, P. Shen and Z. M. Su, *Chem. Eur. J.*, 2014, **20**, 3589.
122. F. Y. Yi, Y. Wang, J. P. Li, D. Wu, Y. Q. Lan and Z. M. Sun, *Mater. Horiz.*, 2015, **2**, 245.
123. H. He, Y. Song, F. Sun, N. Zhao and G. Zhu, *Cryst. Growth Des.*, 2015, **15**, 2033.
124. A. K. Chaudhari, S. S. Nagarkar, B. Joarder, S. Mukherjee and S. K. Ghosh, *Inorg. Chem.*, 2013, **52**, 12784.
125. D. Tian, Y. Li, R. Y. Chen, Z. Chang, G. Y. Wang and X. H. Bu, *J. Mater. Chem. A*, 2014, **2**, 1465.
126. S. S. Nagarkar, B. Joarder, A. K. Chaudhari, S. Mukherjee and S. K. Ghosh, *Angew. Chem. Int. Ed.*, 2013, **125**, 2953.
127. M. V. enkateswarulu, A. Pramanik and R. R. Koner, *Dalton Trans.*, 2015, **44**, 6348.
128. X. L. Hu, F. H. Liu, C. Qin, K. Z. Shao and Z. M. Su, *Dalton Trans.*, 2015, **44**, 7822.
129. S. Shanmugaraju, S. A. Joshi and P. S. Mukherjee, *Inorg. Chem.*, 2011, **50**, 11736.
130. J. F. Song, Y. Li, R. S. Zhou, T. P. Hu, Y. L. Wen, J. Shao and X. B. Cui, *Dalton Trans.*, 2016, **45**, 545.
131. S. Barman, J. A. Garg, O. Blacque, K. V. Enkatesan and H. Berke, *Chem. Commun.*, 2012, **48**, 11127.
132. M. SK and S. Biswas, *CrystEngComm*, 2016, **18**, 3104.
133. D. K. Singha, S. Bhattacharya, P. Majee, S. K. Mondal, M. Kumar and P. Mahata, *J. Mater. Chem. A*, 2014, **2**, 20908.
134. J. Wang, W. Sun, S. Chang, H. Liu, G. Zhang, Y. Wang and Z. Liu, *RSC Adv.*, 2015, **5**, 48574.
135. W. Sun, J. Wang, H. Liu, S. Chang, X. Qin and Z. Liu, *Mater. Lett.*, 2014, **126**, 189.
136. J. J. Qian, L. G. Qiu, Y. M. Wang, Y. P. Yuan, A. J. Xie and Y. H. Shen, *Dalton Trans.*, 2014, **43**, 3978.

137. J. D. Xiao, L. G. Qiu, F. Ke, Y. P. Yuan, G. S. Xu, Y. M. Wang and X. Jiang, *J. Mater. Chem. A*, 2013, **1**, 8745.
138. S. N. Zhao, X. Z. Song, M. Zhu, X. Meng, L. L. Wu, S. Y. Song, C. Wang and H. J. Zhang, *RSC Adv.*, 2015, **5**, 93.
139. A. Li, L. Li, Z. Lin, L. Song, Z. H. Wang, Q. Chen, T. Yang, X. H. Zhou, H. P. Xiao and X. J. Yin, *New J. Chem.*, 2015, **39**, 2289.
140. X. Zhou, H. Li, H. Xiao, L. Li, Q. Zhao, T. Yang, J. Zuo and W. Huang, *Dalton Trans.*, 2013, **42**, 5718.
141. X. H. Zhou, L. Li, H. H. Li, A. Li, T. Yang and W. Huang, *Dalton Trans.*, 2013, **42**, 12403.
142. H. Xu, F. Liu, Y. Cui, B. Chen and G. Qian, *Chem. Commun.*, 2011, **47**, 3153.
143. T. K. Kim, J. H. Lee, D. Moon and H. R. Moon, *Inorg. Chem.*, 2013, **52**, 589.
144. S. Xie, H. Wang, Z. Liu, R. Dai and L. Huang, *RSC Adv.*, 2015, **5**, 7121.
145. Y. Yuan, H. Ren, F. Sun, X. Jing, K. Cai, X. Zhao, Y. Wang, Y. Wei and G. Zhu, *J. Mater. Chem.*, 2012, **22**, 24558.
146. Y. S. Xue, Y. He, L. Zhou, F. J. Chen, Y. Xu, H. B. Du, X. Z. You and B. Chen, *J. Mater. Chem. A*, 2013, **1**, 4525.
147. M. C. Das, S. Xiang, Z. Zhang and B. Chen, *Angew. Chem. Int. Ed.*, 2011, **50**, 10510.
148. M. C. Das, Q. Guo, Y. He, J. Kim, C. G. Zhao, K. Hong, S. Xiang, Z. Zhang, K. M. Thomas, R. Krishna and B. Chen, *J. Am. Chem. Soc.*, 2012, **134**, 8703.
149. S. Kitagawa, R. Kitaura and S. Noro, *Angew. Chem. Int. Ed.*, 2004, **43**, 2334.
150. L. Li, S. Zhang, L. Xu, L. Han, Z.-N. Chen and J. Luo, *Inorg. Chem.*, 2013, **52**, 12323.
151. B. Joarder, A. V. Desai, P. Samanta, S. Mukherjee and S. K. Ghosh, *Chem. Eur. J.*, 2015, **21**, 965.
152. S. S. Nagarkar, B. Joarder, A. K. Chaudhari, S. Mukherjee and S. K. Ghosh, *Angew. Chem. Int. Ed.*, 2013, **52**, 2881.
153. C. Zhang, L. Sun, Y. Yan, J. Li, X. Song, Y. Liu and Z. Liang, *Dalton Trans.*, 2014, **44**.
154. X. Z. Song, S. Y. Song, S. N. Zhao, Z. M. Hao, M. Zhu, X. Meng, L. L. Wu and H. J. Zhang, *Adv. Funct. Mater.*, 2014, **24**, 4034.
155. Y.-N. Gong, L. Jiang and T.-B. Lu, *Chem. Commun.*, 2013, **49**, 11113.
156. X. H. Zhou, L. Li, H. H. Li, A. Li, T. Yang and W. Huang, *Dalton Trans.*, 2013, **42**, 12403.

157. L. Zhao, J. Ye, W. Li, R. F. Bogale, B. Wang, W. Gong and G. Ning, *Inorg. Chem. Commun.*, 2014, **46**, 212.
158. J.-D. Xiao, L.-G. Qiu, F. Ke, Y.-P. Yuan, G.-S. Xu, Y.-M. Wang and X. Jiang, *J. Mater. Chem. A*, 2013, **1**, 8745.
159. S. S. Nagarkar, A. V. Desai and S. K. Ghosh, *Chem. Commun.*, 2014, **50**, 8915.
160. S. S. Nagarkar, A. V. Desai, P. Samanta and S. K. Ghosh, *Dalton Trans.*, 2015, **44**, 15175
161. S. S. Nagarkar, A. V. Desai and S. K. Ghosh, *Chem. Eur. J.*, 2015, **21**, 9994.
162. X. Zhang, J. Zhang, Q. Hu, Y. Cui, Y. Yang and G. Qian, *Appl. Surf. Sci.*, 2015, **355**, 814.
163. S. S. Nagarkar, T. Saha, A. V. Desai, P. Talukdar and S. K. Ghosh, *Sci Rep.*, 2014, **4**, 7053.
164. H. Li, X. Feng, Y. Guo, D. Chen, R. Li, X. Ren, X. Jiang, Y. Dong and B. Wang, *Sci Rep.*, 2014, **4**, 4366.
165. Y. Ma, H. Su, X. Kuang, X. Li, T. Zhang and B. Tang, *Anal. Chem.*, 2014, **86**, 11459.
166. Carbon Dioxide Capture and Storage, B. Metz, O. Davidson, H. de Coninck, M. Loos, L. Meyer (eds), Cambridge University Press, Cambridge, UK.
167. Z. Zhang, Y. Zhao, Q. Gong, Z. Li and J. Li, *Chem. Commun.*, 2013, **49**, 653.
168. E. F. d. Silva and H. F. Svendsen, *Int. J. Greenhouse Gas Control*, 2007, **1**, 151.
169. M. Palomino, A. Corma, F. Rey and S. Valencia, *Langmuir*, 2010, **26**, 1910.
170. M. G. Plaza, S. García, F. Rubiera, J. J. Pis and C. Pevida, *Chem. Eng. J.*, 2010, **163**, 41.
171. K. Sumida, D. L. Rogow, J. A. Mason, T. M. McDonald, E. D. Bloch, Z. R. Herm, T.-H. Bae and J. R. Long, *Chem. Rev.*, 2012, **112**, 724.
172. T. G. Glover, G. W. Peterson, B. J. Schindler, D. Britt and O. M. Yaghi, *Chem. Eng. Sci.*, 2011, **66**, 163.
173. A. O. Yazaydin, R. Q. Snurr, T. H. Park, K. Koh, J. Liu, M. D. LeVan, A. I. Benin, P. Jakubczak, M. Lanuza, D. B. Galloway, J. J. Low and R. R. Willis, *J. Am. Chem. Soc.*, 2009, **131**, 18198.

174. A. O. Yazaydin, A. I. Benin, S. A. Faheem, P. Jakubczak, J. J. Low, R. R. Willis and R. Q. Snurr, *Chem. Mater.*, 2009, **21**, 1425.
175. S. R. Caskey, A. G. Wong-Foy and A. J. Matzger, *J. Am. Chem. Soc.*, 2008, **130**, 10870.
176. P. D. C. Dietzel, V. Besikiotis and R. Blom, *J. Mater. Chem.*, 2009, **19**, 7362.
177. J. An, S. J. Geib and N. L. Rosi, *J. Am. Chem. Soc.*, 2009, **132**, 38.
178. P. D. C. Dietzel, R. E. Johnsen, H. Fjellvag, S. Bordiga, E. Groppo, S. Chavan and R. Blom, *Chem. Commun.*, 2008, 5125.
179. P. Chowdhury, C. Bikkina, D. Meister, F. Dreisbach and S. Gumma, *Microporous Mesoporous Mater.*, 2009, **117**, 406.
180. A. R. Millward and O. M. Yaghi, *J. Am. Chem. Soc.*, 2005, **127**, 17998.
181. J. W. Yoon, S. H. Jung, Y. K. Hwang, S. M. Humphrey, P. T. Wood and J. S. Chang, *Adv. Mater.*, 2007, **19**, 1830.
182. K. L. Mulfort, O. K. Farha, C. D. Malliakas, M. G. Kanatzidis and J. T. Hupp, *Chem. Eur. J.*, 2009, **16**, 276.
183. H. S. Choi and M. P. Suh, *Angew. Chem. Int. Ed.*, 2009, **48**, 6865.
184. A. Demessence, D. M. D'Alessandro, M. L. Foo and J. R. Long, *J. Am. Chem. Soc.*, 2009, **131**, 8784.
185. B. Arstad, H. Fjellvag, K. O. Kongshaug, O. Swang and R. Blom, *Adsorption*, 2008, **14**, 755.
186. S. R. Miller, G. M. Pearce, P. A. Wright, F. Bonino, S. Chavan, S. Bordiga, I. Margiolaki, N. Guillou, G. Feerey, S. Bourrelly and P. L. Llewellyn, *J. Am. Chem. Soc.*, 2008, **130**, 15967.
187. J. A. R. Navarro, E. Barea, J. M. Salas, N. Masciocchi, S. Galli, A. Sironi, C. O. Ania and J. B. Parra, *J. Mater. Chem.*, 2007, **17**, 1939.
188. P. D. Southon, L. Liu, E. A. Fellows, D. J. Price, G. J. Halder, K. W. Chapman, B. Moubaraki, K. S. Murray, J. F. Letard and C. J. Kepert, *J. Am. Chem. Soc.*, 2009, **131**, 10998.
189. L. Hamon, P. L. Llewellyn, T. Devic, A. Ghoufi, G. Clet, V. Guillermin, G. D. Pirngruber, G. Maurin, C. Serre, G. Driver, W. v. Beek, E. Jolimaitre, A. Vimont, M. Daturi and G. Ferey, *J. Am. Chem. Soc.*, 2009, **131**, 17490.

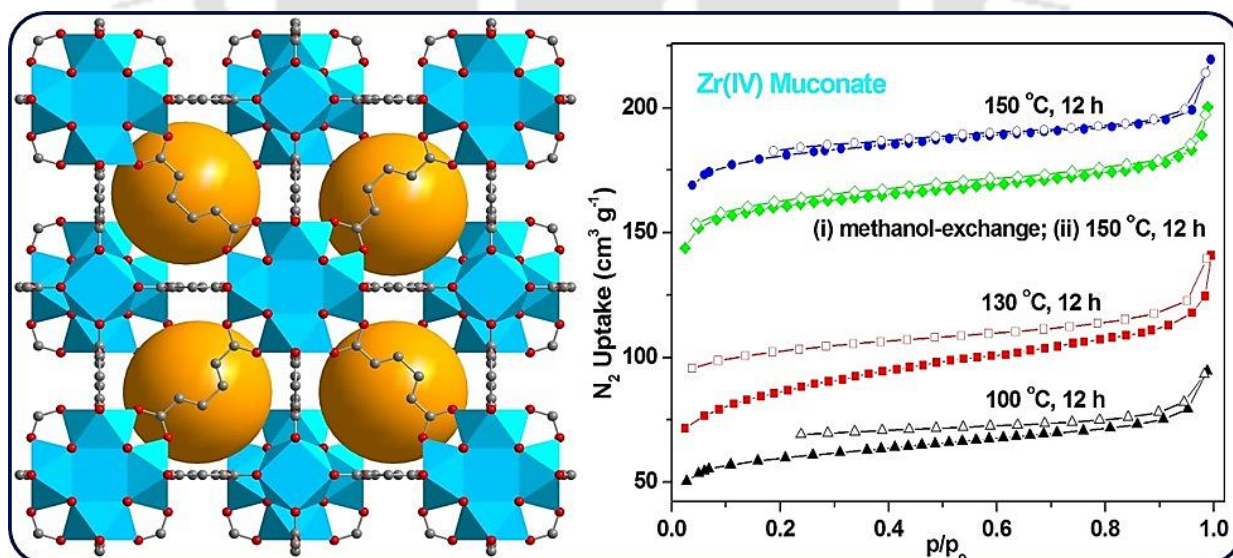
190. Z. X. Zhao, Z. Li and Y. S. Lin, *Ind. Eng. Chem. Res.*, 2009, **48**, 10015.
191. S. Couck, J. F. M. Denayer, G. V. Baron, T. Remy, J. Gascon and F. Kapteijn, *J. Am. Chem. Soc.*, 2009, **131**, 6326.
192. C. Serre, S. Bourrelly, A. Vimont, N. A. Ramsahye, G. Maurin, P. L. Llewellyn, M. Daturi, Y. Filinchuk, O. Leynaud, P. Barnes and G. Ferey, *Adv. Mater.*, 2007, **19**, 2246.
193. E. Neofotistou, C. D. Malliakas and P. N. Trikalitis, *Chem. Eur. J.*, 2009, **15**, 4523.
194. J. Y. Lee, J. M. Roberts, O. K. Farha, A. A. Sarjeant, K. A. Scheidt and J. T. Hupp, *Inorg. Chem.*, 2009, **48**, 9971.
195. B. Wang, A. P. Cote, H. Furukawa, M. O'Keeffe and O. M. Yaghi, *Nature*, 2008, **453**, 207.
196. J. A. R. Navarro, E. Barea, J. M. Salas, N. Masciocchi, S. Galli, A. Sironi, C. O. Ania and J. B. Parra, *Inorg. Chem.*, 2006, **45**, 2397.
197. H. J. Park and M. P. Suh, *Chem. Commun.*, 2010, **46**, 610.
198. P. K. Thallapally, J. Tian, M. R. Kishan, C. A. Fernandez, S. J. Dalgarno, P. B. McGrail, J. E. Warren and J. L. Atwood, *J. Am. Chem. Soc.*, 2008, **130**, 16842.
199. B. Mu, F. Li and K. S. Walton, *Chem. Commun.*, 2009, 2493.
200. Z. Y. Guo, J. B. Yu, G. H. Li, Z. J. Si, H. D. Guo and H. J. Zhang, *CrystEngComm*, 2009, **11**, 2254.
201. Y. S. Bae, O. K. Farha, J. T. Hupp and R. Q. Snurr, *J. Mater. Chem.*, 2009, **19**, 2131.
202. A. Rossin, A. Ienco, F. Costantino, T. Montini, B. D. Credico, M. Caporali, L. Gonsalvi, P. Fornasiero and M. Peruzzini, *Cryst. Growth Des.*, 2008, **8**, 3302.
203. H. Hayashi, A. P. Cote, H. Furukawa, M. O'Keeffe and O. M. Yaghi, *Nat. Mater.*, 2007, **6**, 501.
204. M. Kandiah, M. H. Nilsen, S. Usseglio, S. Jakobsen, U. Olsbye, M. Tilset, C. Larabi, E. A. Quadrelli, F. Bonino and K. P. Lillerud, *Chem. Mater.*, 2010, **22**, 6632.
205. R. Custelcean and M. G. Gorbunova, *J. Am. Chem. Soc.*, 2005, **127**, 16362.
206. V. Colombo, C. Montoro, A. Maspero, G. Palmisano, N. Masciocchi, S. Galli, E. Barea and J. A. R. Navarro, *J. Am. Chem. Soc.*, 2012, **134**, 12830.
207. J. A. Greathouse and M. D. Allendorf, *J. Am. Chem. Soc.*, 2006, **128**, 10678.

208. L. M. Huang, H. T. Wang, J. X. Chen, Z. B. Wang, J. Y. Sun, D. Y. Zhao and Y. S. Yan, *Microporous Mesoporous Mater.* , 2003, **58**, 105.
209. T. Loiseau, C. Serre, C. Huguenard, G. Fink, F. Taulelle, M. Henry, T. Bataille and G. Ferey, *Chem. Eur. J.* , 2004, **10**, 1373.
210. M. Lammert, M. T. Wharmby, S. Smolders, B. Bueken, A. Lieb, K. A. Lomachenko, D. D. Vos and N. Stock, *Chem. Commun.*, 2015, **51**, 12578.



## Improved Synthesis of Zirconium(IV) Muconate MOF: Characterization, Stability and Gas Sorption Properties

*This chapter presents an improved synthesis procedure for the preparation of the previously reported Zr(IV) trans,trans-muconate framework compound. Instead of using non-commercial Zr<sub>6</sub>-methacrylate oxocluster as the metal source, the same MOF material was successfully synthesized by using commercially available ZrCl<sub>4</sub> as the Zr source. The N<sub>2</sub> sorption isotherms confirm the microporous nature of the thermally activated Zr(IV) muconate compound. The moderate physicochemical stability along with significant porosity of the material will make it a potential candidate in the field of gas storage and separation.*



## 2.1 INTRODUCTION

Metal-organic frameworks (MOFs) are highly porous and crystalline materials which are composed of metal ions or metal clusters cross-linked by rigid, polytopic organic ligand molecules.<sup>1-5</sup> Owing to their structural tunability because of a huge combination of metal ions and organic ligands and improved chemical as well as physical properties compared to other traditional porous materials (e.g. zeolites, mesoporous silicas and activated carbons), MOFs have gained a remarkable attention for application in several areas including gas storage and separation,<sup>6, 7</sup> sensing,<sup>8-16</sup> catalysis<sup>6, 17</sup> and drug delivery<sup>18-21</sup> etc. A large variety of porous MOF structures possessing different types of pore systems have been reported until today. Several well-known MOFs<sup>22-26</sup> have exhibited strong possibilities for adsorption/separation. However, their industrial application is limited due to low physicochemical stabilities (air, water, thermal, acid-base, etc.). MOFs with transition metal ions having higher oxidation states (e.g. Ti(IV),<sup>27</sup> Zr(IV),<sup>28</sup> etc.) have shown higher physicochemical stabilities. The popularly known UiO-66 (UiO = University of Oslo)<sup>28</sup> MOF with Zr(IV) metal ions has attracted tremendous attention in recent years due to its high thermal and chemical stability as well as potential properties for CO<sub>2</sub>/CH<sub>4</sub> gas separation.<sup>29, 30</sup> The 3D cubic framework of this MOF is constructed from a centric octahedral cage linked to eight corner tetrahedral cages by means of trigonal windows and 1,4-benzenedicarboxylate (BDC) dianions as ligand molecules. The Zr(IV) *trans,trans*-muconate network (Figure 2.5)<sup>31</sup> possesses the same structural topology as the UiO-66 compound. The Zr(IV) muconate material bears moderate physicochemical stabilities, whereas the aromatic BDC ligands impart high physicochemical stabilities to the UiO-66 material.

In order to increase the crystallinity of the resulting Zr(IV)-based MOF materials having UiO-66 framework topology, several modulators and/or additives<sup>32</sup> have been employed during the synthesis.<sup>33-60</sup> Typically, the solvothermal reaction of a Zr(IV) salt with the respective ligand in a polar amide solvent in presence of a modulator/additive results in the formation of highly crystalline and porous Zr(IV)-based MOF compound. The Zr(IV) *trans,trans*-muconate material (**1**) was prepared for the first time by exchanging the methacrylate anions of the oxocluster [Zr<sub>6</sub>O<sub>4</sub>(OH)<sub>4</sub>(OMc)<sub>6</sub>] (Mc = methacrylate) by *trans,trans*-muconate dianions.<sup>31</sup> Indeed, this “precursor approach”<sup>32</sup> allowed the modulation of the size of the MOF nanoparticles as a function of reaction time. However, the starting “precursor” compound is commercially

unavailable and the preparation of this precursor requires inert atmosphere for handling of the reactants.<sup>61</sup> In the original report,<sup>31</sup> the researchers could not succeed to synthesize the Zr(IV) muconate compound by using commercially available ZrCl<sub>4</sub> as the precursor and by varying the reaction conditions. In this work, we show that the same MOF material can be successfully prepared by employing cheap, commercially available ZrCl<sub>4</sub> as the Zr(IV) source and small quantities of H<sub>2</sub>O (**1-H<sub>2</sub>O-AS**; AS = as-synthesized) or concd. HCl (**1-HCl-AS**) as additives in *N,N*-dimethylformamide (DMF). Herein, we present the improved synthetic procedure, characterization, thermal and chemical stability, and gas sorption behavior of the Zr(IV) muconate compound.

## 2.2 EXPERIMENTAL SECTION

### 2.2.1 Materials and General Methods

All the starting materials were of reagent grade and used as received from the commercial suppliers. Fourier transform infrared (FT-IR) spectra were recorded in the region of 440-4000 cm<sup>-1</sup> with a Perkin Elmer Spectrum Two FT-IR spectrometer. The following indications are used to characterize absorption bands: very strong (vs), strong (s), medium (m), weak (w), shoulder (sh), and broad (br). Elemental analyses (C, H, N) were carried out on a Eurovector EA3000 CHNS-O analyzer. Thermogravimetric analysis (TGA) was performed with a Mettler-Toledo TGA/SDTA 851e thermogravimetric analyzer in a temperature range of 25-750 °C under air atmosphere at a heating rate of 5 °C min<sup>-1</sup>. Ambient temperature X-Ray powder diffraction (XRPD) patterns were recorded on a Bruker D2 Phaser X-ray diffractometer operated at 30 kV, 10 mA using Cu-K $\alpha$  ( $\lambda = 1.5406 \text{ \AA}$ ). The nitrogen sorption isotherms up to 1 bar were measured using a Quantachrome Autosorb iQ-MP gas sorption analyzer at -196 °C. Prior to the sorption experiments, the compounds were degassed at 150 °C for 12 h under dynamic vacuum.

### 2.2.2 Synthesis of [Zr<sub>6</sub>O<sub>4</sub>(OH)<sub>4</sub>(C<sub>6</sub>H<sub>4</sub>O<sub>4</sub>)<sub>6</sub>] $\cdot$ 1.5DMF $\cdot$ 10H<sub>2</sub>O (**1-H<sub>2</sub>O-AS**)

A mixture of ZrCl<sub>4</sub> (100 mg, 0.43 mmol), *trans,trans*-muconic acid (61 mg, 0.43 mmol) and H<sub>2</sub>O (20  $\mu$ L, 1.11 mmol) in 3 mL of DMF was heated in a sealed glass tube at 150 °C for 24 h using a block heater. After spontaneous cooling to room temperature, the white precipitate was collected by filtration, washed with acetone and dried in air. The yield was 114 mg (0.07 mmol, 92%) based on the Zr salt. Anal. Calcd for C<sub>40.5</sub>H<sub>54.5</sub>N<sub>1.5</sub>O<sub>39.5</sub>Zr<sub>6</sub>: C, 27.92 H, 3.15 N, 1.20.

Found: C, 27.97 H, 2.82 N, 1.50%. FT-IR (KBr,  $\text{cm}^{-1}$ ): 3420 (br), 2926 (sh), 1618 (vs), 1554 (sh), 1388 (vs), 1291 (sh), 1187 (w), 999 (m), 865 (w), 731 (sh), 658 (s), 585 (sh), 488 (w).

### 2.2.3 Synthesis of $[\text{Zr}_6\text{O}_4(\text{OH})_4(\text{C}_6\text{H}_4\text{O}_4)_6]\cdot 1.2\text{DMF}\cdot 12\text{H}_2\text{O}$ (1-HCl-AS)

A mixture of  $\text{ZrCl}_4$  (100 mg, 0.43 mmol), *trans,trans*-muconic acid (61 mg, 0.43 mmol) and concd. HCl (36  $\mu\text{L}$ , 0.43 mmol) in 3 mL of DMF was heated in a sealed glass tube at 150  $^\circ\text{C}$  for 24 h using a block heater. After spontaneous cooling to room temperature, the white precipitate was collected by filtration, washed with acetone and dried in air. The yield was 116 mg (0.07 mmol, 96%). Anal. Calcd for  $\text{C}_{39.9}\text{H}_{49.1}\text{N}_{1.3}\text{O}_{37.3}\text{Zr}_6$ : C, 28.33 H, 2.92 N, 1.07. Found: C, 27.93 H, 2.73 N, 1.12%. FT-IR (KBr,  $\text{cm}^{-1}$ ): 3431 (br), 2927 (sh), 1613 (vs), 1558 (sh), 1382 (vs), 1297 (sh), 1193 (w), 1005 (m), 865 (w), 731 (sh), 658 (s), 585 (sh), 488 (w).

### 2.2.4 Activation of The Compounds

The as-synthesized compounds were activated by employing two procedures. In one procedure, which is similar to the previous report,<sup>31</sup> the as-synthesized samples were directly heated under vacuum at different temperatures (100, 130 and 150  $^\circ\text{C}$ ) for 12 h. In the other procedure, the as-synthesized samples were activated in two steps. In the first step, the as-synthesized samples (0.3 g) were stirred in methanol (50 mL) under ambient conditions for 24 h. In the second step, the methanol-exchanged forms of the materials were heated at 150  $^\circ\text{C}$  under vacuum for 12 h.

## 2.3 RESULTS AND DISCUSSIONS

### 2.3.1 Syntheses, Activation and FT-IR Analysis

The optimization of the synthesis conditions for Zr(IV) muconate compound was performed by performing reactions of *trans, trans*-muconic acid ligand with Zr(IV) salts ( $\text{ZrCl}_4$ ,  $\text{ZrO}(\text{NO}_3)_2\cdot x\text{H}_2\text{O}$  or  $\text{ZrOCl}_2\cdot 8\text{H}_2\text{O}$ ) in presence of modulators/additives ( $\text{H}_2\text{O}$ , concd. HCl, benzoic acid, formic acid, acetic acid or trifluoroacetic acid) in polar amide solvents such as DMF, *N,N*-diethylformamide (DEF) and *N,N*-dimethylacetamide (DMA). Reactions in all possible combinations (Table 2.1) of the Zr(IV) salts, modulators/additives and solvents were carried out. Zr(IV) muconate compounds with very high crystallinity were achieved when  $\text{ZrCl}_4$  was used as the metal source and water/concd. HCl was employed as the additive in DMF. The

optimized  $\text{ZrCl}_4/\text{ligand}/\text{H}_2\text{O}$  and  $\text{ZrCl}_4/\text{ligand}/\text{HCl}$  molar ratios correspond to 1:1:2.6 (**1-H<sub>2</sub>O-AS**) and 1:1:1 (**1-HCl-AS**). The influence of  $\text{ZrCl}_4/\text{additive}$  molar ratio on the crystallinity of the Zr(IV) muconate material was investigated by varying the  $\text{ZrCl}_4/\text{H}_2\text{O}$  and  $\text{ZrCl}_4/\text{HCl}$  molar ratios in the ranges 1:1.3-1:100 (Figure 2.1) and 1:1-1:10 (Figure 2.2), respectively. It was observed that the excess of additives than the optimized molar ratio had a detrimental effect on the crystallinity of the compounds. The reactions in the presence of monocarboxylic acids (formic, acetic and trifluoroacetic acid) as modulators also produced crystalline products. However, none of these products corresponded to the Zr(IV) muconate phase, as verified by the XRPD measurements.

**Table 2.1** The 18 possible combinations of reactants for the synthesis of the Zr(IV) muconate compound employing  $\text{ZrCl}_4$  and *trans, trans*-muconic acid ligand at 150 °C.

Solvent \ Additive	water	concd. HCl	benzoic acid	formic acid	acetic acid	trifluoro- acetic acid
<i>N,N'</i> -dimethylformamide	○	○	○	○	○	○
<i>N,N'</i> -diethylformamide	○	○	○	○	○	○
<i>N,N'</i> -dimethylacetamide	○	○	○	○	○	○

In the literature, Zr(IV) muconate solid was synthesized using the non-commercial  $\text{Zr}_6$ -methacrylate oxocluster as the metal source, since the researchers failed to prepare the MOF initially with commercially available  $\text{ZrCl}_4$ .<sup>31</sup> Herein, we demonstrate that the same Zr(IV) muconate material can be successfully synthesized by employing commercially available  $\text{ZrCl}_4$  as the Zr(IV) source and following the above-mentioned optimized reaction conditions.

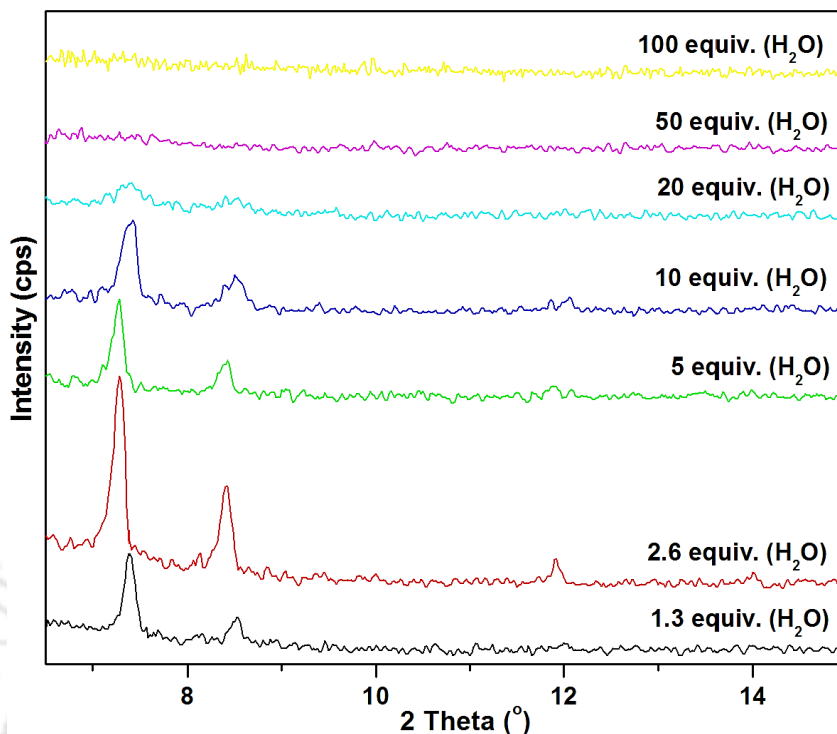


**Figure 2.1.** XRPD patterns of Zr(IV) muconate samples prepared with different equivalents (with respect to ZrCl<sub>4</sub>) of H<sub>2</sub>O as an additive.

The as-synthesized forms of **1-H<sub>2</sub>O** and **1-HCl** were washed with sufficient amounts of acetone after filtration for the removal of the physisorbed DMF molecules from the external surface of the samples. In order to optimize the conditions for thermal activation (i.e., removal of the occluded molecules from the pores of the compounds), two independent methods were employed and surface area analyses (*cf.* Gas Sorption Properties section) were carried out with all the samples obtained by using the two procedures. In one method, the as-synthesized samples were directly heated under vacuum at different temperatures (100, 130 and 150 °C) for 12 h. The optimum BET surface area was obtained when the sample was heated at 150 °C. This temperature was employed in the second method, which consisted of two steps. In the first step, the guest solvent (H<sub>2</sub>O and DMF) molecules within the pores were exchanged with more volatile methanol molecules. In the second step, the methanol-exchanged form of the compound was heated at 150 °C under vacuum in order to remove the methanol molecules from the pores. Both of the methanol-exchanged and thermally activated compounds displayed similar XRPD patterns (Figure 2.3) as the as-synthesized compounds, verifying structural integrity of the **1-HCl** compound upon treatment with methanol and heat, respectively.

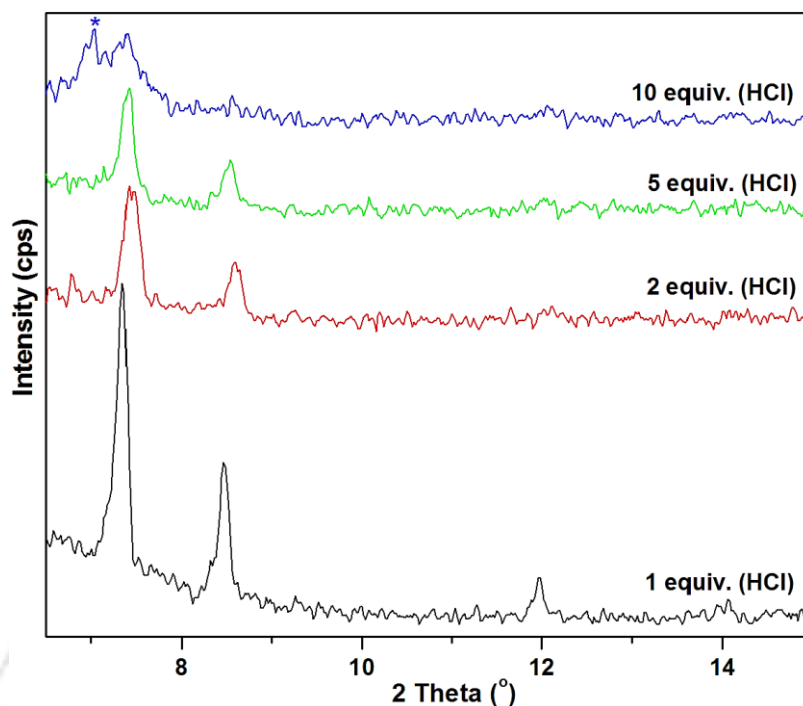


**Figure 2.2.** XRPD patterns of Zr(IV) muconate samples prepared with different equivalents (with respect to  $ZrCl_4$ ) of concd. HCl as an additive. Note that an additional peak (marked with a blue asterisk) for an impure phase was observed when 10 equivalents of HCl was used.

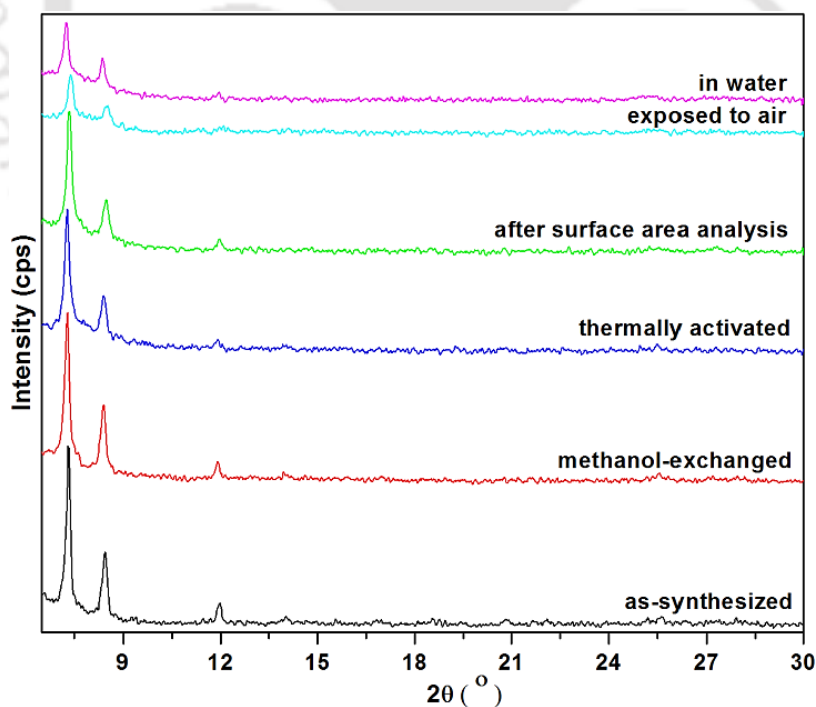


**Figure 2.3** XRPD patterns of **1-HCl** in different forms: as-synthesized (black), methanol-exchanged (red), thermally activated (blue), after surface area analysis (green), exposed to air for 7 days (cyan), and treated with water (magenta).

The FT-IR spectra of the thermally activated forms of structurally related **1-H<sub>2</sub>O** and **1-HCl** (Figure 2.4) are similar, as expected. In the FT-IR spectra, the strong absorption bands owing to the asymmetric and symmetric  $\text{-CO}_2$  stretching vibrations of the coordinated *trans,trans*-muconate ligand molecules are located at around 1615 and 1385  $\text{cm}^{-1}$ , respectively.<sup>62</sup>

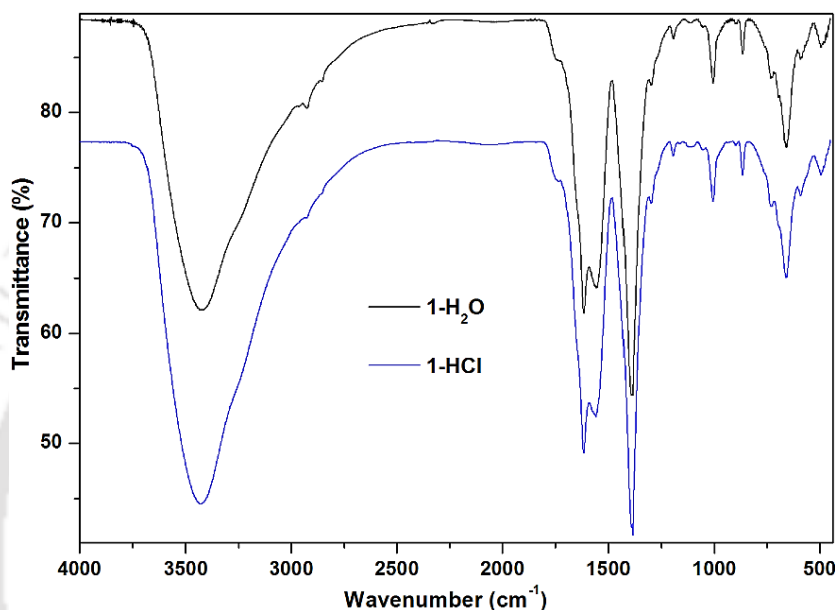


**Figure 2.4.** FT-IR spectra of the thermally activated forms of **1-H<sub>2</sub>O** (black) and **1-HCl** (blue) compounds.

### 2.3.2 Structure Description

The refined unit cell parameters (Table 2.2) of **1-H<sub>2</sub>O-AS** and **1-HCl-AS** compounds were determined from the corresponding XRPD patterns collected at ambient conditions. The values of lattice parameters match closely with those reported in the literature for Zr(IV) muconate material.<sup>31</sup> The experimental XRPD patterns (Figure 2.6) are very similar to those documented in the literature and they match well with the simulated XRPD patterns. The slight discrepancy between the calculated and experimental XRPD patterns might be owing to the fact that the simulated patterns correspond to the dehydroxylated form whereas the experimental patterns relate to the as-synthesized (i.e. hydroxylated) form of the compound. As described in the earlier report,<sup>31</sup> the hydroxylated form of Zr(IV) muconate framework is constructed from hexanuclear  $[\text{Zr}_6\text{O}_4(\text{OH})_4]$  building units in which the triangular faces of the  $\text{Zr}_6$  octahedron are alternatively capped by  $\mu_3\text{-O}$  and  $\mu_3\text{-OH}$  groups.

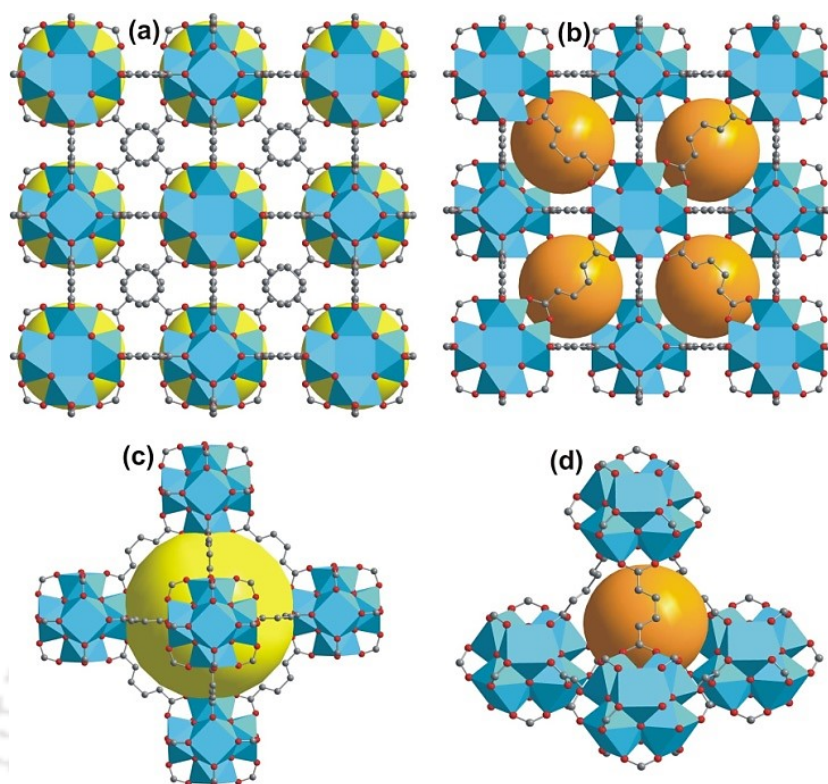


**Figure 2.5** Ball-and-stick representation of the 3D cubic framework structure of Zr(IV) muconate. (a,b) Spatial arrangement of the octahedral (yellow spheres) and tetrahedral (orange spheres) cages in the framework. (c,d) Magnified representation of the octahedral and tetrahedral cages. Zr atoms are shown as octahedra (color codes: Zr, blue; C, gray; O, red). The hydrogen atoms and guest molecules have been removed from all the structural plots for clarity. The figure was drawn by using atomic coordinates provided in ref. 31.

The  $Zr_6$  polyhedra are interconnected along the edges by carboxylate groups of twelve *trans,trans*-muconate ligand molecules. This structural connectivity results in the formation of a cubic, three-dimensional (3D) framework exhibiting both octahedral and tetrahedral microporous cages (Figure 2.5a, b). Each Zr atom coordinates with eight O atoms and resides in a square-antiprismatic geometry. One square face of the square antiprism is constructed from O atoms from carboxylate groups. The second square face is built up of O atoms from the  $\mu_3$ -O and  $\mu_3$ -OH groups. In the microporous framework, each centric octahedral cage (Figure 2.5c, free diameter:  $\sim 12$  Å) is coordinated with eight corner tetrahedral cages (Figure 2.5d, free diameter:  $\sim 7.5$  Å) through trigonal windows. During the reaction, a surprising change in the geometry (*cis-trans* isomerism) of the ligand molecule occurs, resulting in the formation of disordered *cis,cis*-muconate molecule in the framework from starting *trans,trans*-muconic acid molecule in the reaction mixture.

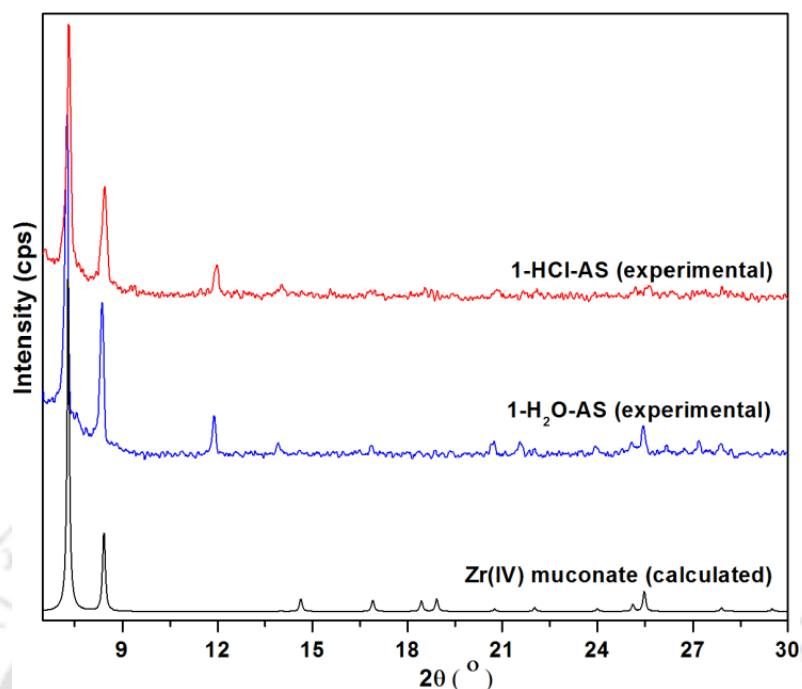


**Figure 2.6** Calculated (black) XRPD pattern of Zr(IV) muconate, and experimental XRPD patterns of **1-H<sub>2</sub>O-AS** (blue) and **1-HCl-AS** (red).

**Table 2.2.** Refined lattice parameters for the as-synthesized **1-H<sub>2</sub>O** and **1-HCl** compounds having cubic unit cells.

Compound	$a$ (Å)	$V$ (Å <sup>3</sup> )	Figures of Merit
<b>1-H<sub>2</sub>O-AS</b>	20.950(9)	9194.5(14)	$F_{10} = 21.7$ (0.014, 34)
<b>1-HCl-AS</b>	21.082(7)	9369.8(22)	$F_9 = 45.8$ (0.007, 30)
Zr(IV) muconate <sup>31</sup>	20.818(1)	9022.6(7)	$F_{25} = 20$ (0.0070, 103)

### 2.3.3 Thermal and Chemical Stability

In order to investigate the thermal stability of the two compounds, thermogravimetric analyses (TGA) were carried out with the as-synthesized samples in air atmosphere. According to the TG analyses (Figure 2.7), **1-H<sub>2</sub>O-AS** and **1-HCl-AS** compounds are thermally stable up to  $\sim 250$  °C, which is comparable with the literature value.<sup>31</sup> Thus, the thermal stabilities of **1-H<sub>2</sub>O-AS** and **1-HCl-AS** are considerably lower compared to those of nonfunctionalized (430 °C) and functionalized UiO-66 compounds.<sup>33,37</sup> The lower thermal stability of Zr(IV) muconate compound compared to that of UiO-66 has been formerly ascribed to the easier thermal decomposition of the olefinic muconate ligand compared to the aromatic terephthalate ligand.<sup>31</sup> In

the TG curves of **1-H<sub>2</sub>O-AS** and **1-HCl-AS** (Figure 2.7), the first weight loss steps (10.3 wt%, **1-H<sub>2</sub>O-AS**; 11.7 wt%, **1-HCl-AS**) in the range 25-130 °C can be assigned to the removal of 10 and 12 occluded H<sub>2</sub>O molecules per formula unit (calcd: 10.5 wt%, **1-H<sub>2</sub>O-AS**; 11.8 wt%, **1-HCl-AS**), respectively. The second weight loss steps (6.7 wt%, **1-H<sub>2</sub>O-AS**; 4.4 wt%, **1-HCl-AS**) in the range 130-250 °C can be attributed to the removal of 1.5 and 1.2 guest DMF molecules per formula unit (calcd: 6.3 wt%, **1-H<sub>2</sub>O-AS**; 4.8 wt%, **1-HCl-AS**), respectively. Above 250 °C, the compounds start to decompose due to the loss of organic ligand molecules from the frameworks.

In order to determine the chemical stabilities, samples of **1-HCl** were stirred at ambient conditions in water, acetic acid, 1M HCl and 1M NaOH solutions for 12 h. After that the material was collected by filtration and their crystallinity was examined by XRPD experiments (Figure 2.3). The crystallinity of the **1-HCl** compound significantly deteriorated after treatment with water solutions. Drastic reduction in the crystallinity was also observed when the thermally activated samples were exposed to moisture (from air) for 7 days. After treatment with acetic acid, 1M HCl and 1M NaOH solutions, the materials lost their crystallinity and became totally amorphous. Therefore, the **1-HCl** sample possess significantly lower chemical stabilities compared to the pristine<sup>28</sup> and functionalized UiO-66 materials.<sup>33,34, 37, 64</sup>

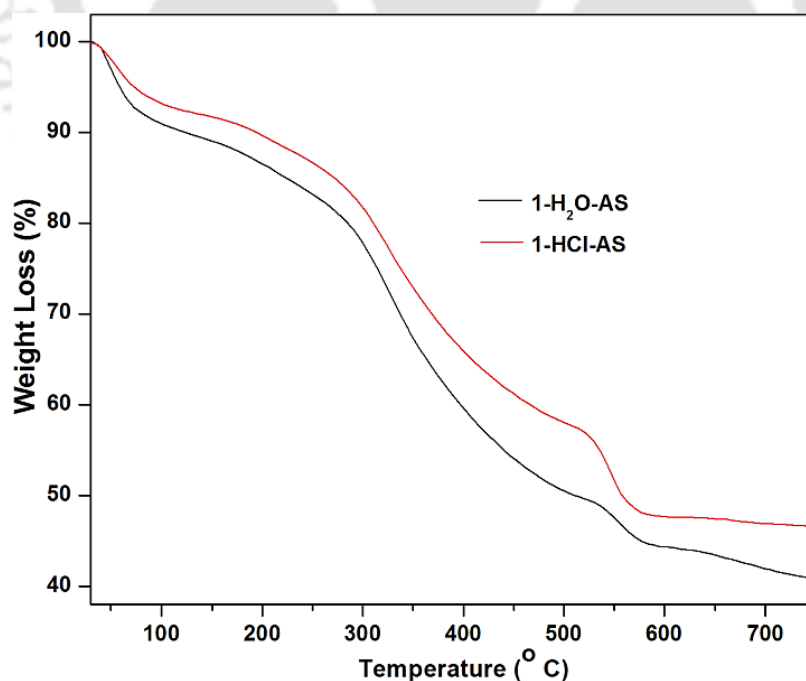


**Figure 2.7** TG curves of **1-H<sub>2</sub>O-AS** (black) and **1-HCl-AS** (red) recorded in air atmosphere in the temperature range 25-750 °C.

### 2.3.4 Gas Sorption Properties

$N_2$  adsorption and desorption experiments were carried out with the thermally activated **1-HCl** compound. The  $N_2$  sorption isotherms (Figure 2.8) exhibit type-I behavior, confirming microporous nature of the thermally activated Zr(IV) muconate compound. The optimization of the activation temperature was performed by utilizing the results of  $N_2$  sorption measurements. The BET surface areas were calculated from the  $N_2$  adsorption isotherms. The BET surface areas of samples of **1-HCl** were found to be 186 and 282  $m^2 g^{-1}$ , when the samples were heated directly at 100 and 130  $^{\circ}C$  under vacuum for 12 h, respectively. The highest BET surface area of 557  $m^2 g^{-1}$  (micropore volume of 0.34  $cm^3 g^{-1}$  at  $p/p_0 = 0.9$ ) was obtained when the sample was heated directly at 150  $^{\circ}C$  under vacuum for 12 h. Similar BET surface area (496  $m^2 g^{-1}$ ; micropore volume of 0.31  $cm^3 g^{-1}$  at  $p/p_0 = 0.9$ ) was obtained with a sample of **1-HCl**, which was activated in two steps: exchange of guest molecules with methanol, followed by heating at 150  $^{\circ}C$  under vacuum for 12 h. The thermally activated compound retained their crystallinity after the sorption analyses, as confirmed by the XRPD experiments (Figure 2.3).

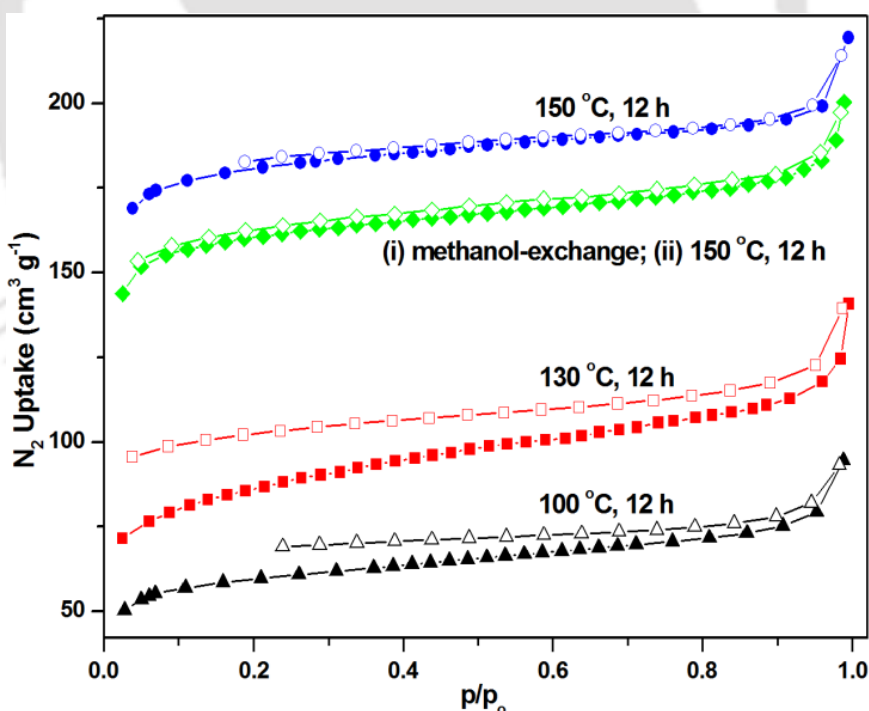


**Figure 2.8**  $N_2$  adsorption (filled symbols) and desorption (empty symbols) isotherms of thermally activated samples of **1-HCl** measured at  $-196^{\circ}C$ . The samples were heated directly at 100, 130 and 150  $^{\circ}C$  under vacuum for 12 h before the sorption measurement. The sorption isotherms of a sample of **1-HCl**, which was activated in two steps (exchange of guest molecules with methanol, followed by thermal activation at 150  $^{\circ}C$  under vacuum for 12 h), are also shown for comparison.

Noticeably, the highest BET surface area of **1-HCl** is considerably lower compared to UiO-66 (ca.  $950 \text{ m}^2 \text{ g}^{-1}$ ) but it is close to the value reported in the literature (ca.  $705 \text{ m}^2 \text{ g}^{-1}$ ) for Zr(IV) muconate compound.<sup>31</sup> The lower BET surface area of Zr(IV) muconate compared to that of UiO-66 was formerly attributed to the lower stability of the former compound upon removal of the guest solvent molecules compared to the high thermal and chemical stability of the later compound.<sup>31</sup>

## 2.4 CONCLUSIONS

An improved synthesis procedure has been developed for the preparation of the previously reported Zr(IV) *trans,trans*-muconate framework compound. Instead of non-commercial  $\text{Zr}_6$ -methacrylate oxocluster as the metal source, the present investigation demonstrates the successful synthesis of the same MOF material by using commercially available  $\text{ZrCl}_4$  as the Zr source. During the synthesis, small amounts of  $\text{H}_2\text{O}$  (**1-H<sub>2</sub>O-AS**) or concd. HCl (**1-HCl-AS**) were used as additives in DMF. The effect of  $\text{ZrCl}_4$ /additive molar ratio on the crystallinity of the compounds has been systematically examined. The phase purity of the materials having optimum crystallinity was investigated by a combination of XRPD analysis, FT-IR spectroscopy, thermogravimetric and elemental analyses. The physicochemical stability of the materials was investigated. According to the thermogravimetric analyses, the two materials are stable up to  $\sim 250 \text{ }^\circ\text{C}$  in air atmosphere. As confirmed by the XRPD analyses, the **1-HCl** material is unstable in acetic acid, 1M HCl and 1M NaOH solutions. The crystallinity of the materials deteriorated slowly when they were exposed to water as well as moisture (from air), suggesting a gradual structural collapse of the framework over time. The effect of activation temperature on the BET surface area of the materials was also examined. As corroborated by the  $\text{N}_2$  sorption measurements, the optimally activated **1-HCl** exhibited BET surface area of  $557 \text{ m}^2 \text{ g}^{-1}$ , which is lower than the isostructural UiO-66 ( $950 \text{ m}^2 \text{ g}^{-1}$ ) but it is close to the literature value ( $705 \text{ m}^2 \text{ g}^{-1}$ ) of Zr(IV) muconate. The moderate physicochemical stability along with significant porosity of the material will make it a promising candidate in the field of gas storage and separation.

## 2.5 REFERENCES

1. Themed issue on MOFs: *Chem. Soc. Rev.*, 2009, **38**, 1201.

2. Special issue on MOFs: *Chem. Rev.*, 2012, **112**, 673.
3. G. Férey, *Chem. Soc. Rev.*, 2008, **37**, 191.
4. O. M. Yaghi, M. O’Keeffe, N. W. Ockwig, H. K. Chae, M. Eddaoudi and J. Kim, *Nature*, 2003, **423**, 705.
5. S. Kitagawa, R. Kitaura and S. Noro, *Angew. Chem. Int. Ed.*, 2004, **43**, 2334.
6. L. Ma, C. Abney and W. Lin, *Chem. Soc. Rev.*, 2009, **38**, 1248.
7. L. J. Murray, M. Dinca and J. R. Long, *Chem. Soc. Rev.*, 2009, **38**, 1294.
8. K. Müller-Buschbaum, F. Beuerle and C. Feldmann, *Microporous Mesoporous Mater.*, 2015, **216**, 171.
9. Z. Hu, B. J. Deibert and J. Li, *Chem. Soc. Rev.*, 2014, **43**, 5815.
10. M. D. Allendorf, C. A. Bauer, R. K. Bhakta and R. J. T. Houk, *Chem. Soc. Rev.*, 2009, **38**, 1330.
11. Y. Cui, Y. Yue, G. Qian and B. Chen, *Chem. Rev.*, 2012, **112**, 1126.
12. L. E. Kreno, K. Leong, O. K. Farha, M. Allendorf, R. P. Van Duyne and J. T. Hupp, *Chem. Rev.*, 2012, **112**, 1105.
13. Y. Cui, B. Chen and G. Qian, *Coord. Chem. Rev.*, 2014, **76**, 273.
14. L. V. Meyer, F. Schonfeld and K. Muller-Buschbaum, *Chem. Commun*, 2014, **50**, 8093.
15. B. Chen, S. Xiang and G. Qian, *Acc. Chem. Res.*, 2010, **43**, 1115.
16. J. Lei, R. Qian, P. Ling, L. Cui and H. Ju, *Trends Analyt. Chem.*, 2014, **58**, 71.
17. J. Lee, O. K. Farha, J. Roberts, K. A. Scheidt, S. T. Nguyen and J. T. Hupp, *Chem. Soc. Rev.*, 2009, **38**, 1450.
18. K. M. L. Taylor-Pashow, J. Della Rocca, Z. G. Xie, S. Tran and W. B. Lin, *J. Am. Chem. Soc.*, 2009, **131**, 14261.
19. P. Horcajada, T. Chalati, C. Serre, B. Gillet, C. Sebrie, T. Baati, J. F. Eubank, D. Heurtaux, P. Clayette, C. Kreuz, J. S. Chang, Y. K. Hwang, V. Marsaud, Y.-N. Bories, L. Cynober, S. Gil, G. Férey, P. Couvreur and R. Gref, *Nat. Mater.*, 2010, **9**, 172.
20. M. Vallet-Regí, F. Balasm and D. Arcos, *Angew. Chem. Int. Ed.*, 2007, **46**, 7548.
21. P. Horcajada, C. Serre, M. Vallet-Regí, M. Sebban, F. Taulelle and G. Férey, *Angew. Chem. Int. Ed.*, 2006, **45**, 5974.
22. L. M. Huang, H. T. Wang, J. X. Chen, Z. B. Wang, J. Y. Sun, D. Y. Zhao and Y. S. Yan, *Microporous Mesoporous Mater.*, 2003, **58**, 105.

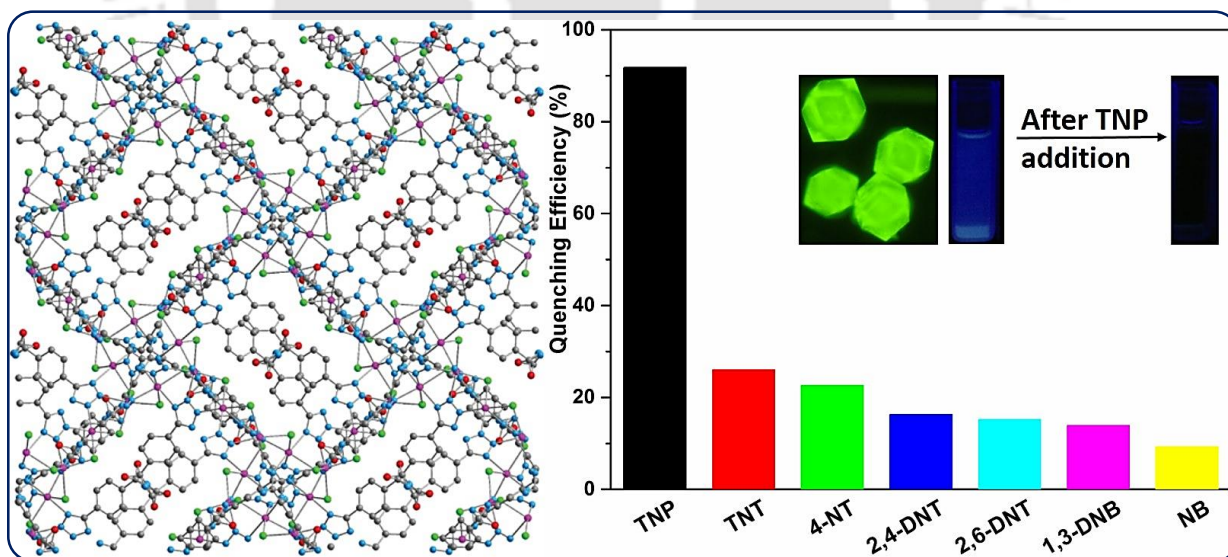
23. J. A. Greathouse and M. D. Allendorf, *J. Am. Chem. Soc.*, 2006, **128**, 10678.
24. Y. Li and R. T. Yang, *Langmuir*, 2007, **23**, 12937.
25. S. S. Kaye, A. Dailly, O. M. Yaghi and J. R. Long, *J. Am. Chem. Soc.*, 2007, **129**, 14176.
26. D. Ma, Y. Li and Z. Li, *Chem. Commun.*, 2011, **47**, 7377.
27. M. Dan-Hardi, C. Serre, T. Frot, L. Rozes, G. Maurin, C. Sanchez and G. Férey, *J. Am. Chem. Soc.*, 2009, **131**, 10857.
28. J. H. Cavka, S. Jakobsen, U. Olsbye, N. Guillou, C. Lamberti, S. Bordiga and K. P. Lillerud, *J. Am. Chem. Soc.*, 2008, **130**, 13850.
29. Q. Yang, H. Jobic, F. Salles, D. Kolokolov, V. Guillerm, C. Serre and G. Maurin, *Chem. Eur. J.*, 2011, **17**, 8882.
30. Q. Yang, A. D. Wiersum, H. Jobic, V. Guillerm, C. Serre, P. L. Llewellyn and G. Maurin, *J. Phys. Chem. C*, 2011, **115**, 13768.
31. V. Guillerm, S. Gross, C. Serre, T. Devic, M. Bauer and G. Férey, *Chem. Commun.*, 2010, **46**, 767.
32. N. Stock and S. Biswas, *Chem. Rev.*, 2012, **112**, 933.
33. S. Biswas, J. Zhang, Z. Li, Y.-Y. Liu, M. Grzywa, L. Sun, D. Volkmer and P. V. D. Voort, *Dalton Trans.*, 2013, **42**, 4730.
34. Y. Huang, W. Qin, Z. Li and Y. Li, *Dalton Trans.*, 2012, **41**, 9283.
35. C. Zlotea, D. Phanon, M. Mazaj, D. Heurtaux, V. Guillerm, C. Serre, P. Horcajada, T. Devic, E. Magnier, F. Cuevas, G. Férey, P. L. Llewellyn and M. Latroche, *Dalton Trans.*, 2011, **40**, 4879.
36. M. L. Foo, S. Horike, T. Fukushima, Y. Hijikata, Y. Kubota, M. Takataf and S. Kitagawa, *Dalton Trans.*, 2012, **41**, 13791.
37. S. Biswas and P. V. D. Voort, *Eur. J. Inorg. Chem.*, 2013, 2154.
38. F. Vermoortele, M. Vandichel, B. Van de Voorde, R. Ameloot, M. Waroquier, V. Van Speybroeck, D. E. De and Vos, *Angew. Chem., Int. Ed.*, 2012, **51**, 4887.
39. F. Vermoortele, R. Ameloot, A. Vimont, C. Serre and D. D. Vos, *Chem. Commun.*, 2011, **47**, 1521.
40. C. Wang, Z. Xie, K. E. deKrafft and W. Lin, *J. Am. Chem. Soc.*, 2011, **133**, 13445.
41. A. Schaate, S. Dühnen, G. Platz, S. Lilienthal, A. M. Schneider and P. Behrens, *Eur. J. Inorg. Chem.*, 2012, 790.

42. V. Guillerm, F. Ragon, M. Dan-Hardi, T. Devic, M. Vishnuvarthan, B. Campo, A. Vimont, G. Clet, Q. Yang, G. Maurin, G. Férey, A. Vittadini, S. Gross and C. Serre, *Angew. Chem. Int. Ed.*, 2012, **51**, 9267.
43. A. Schaate, P. Roy, A. Godt, J. Lippke, F. Waltz, M. Wiebcke and P. Behrens, *Chem.–Eur. J.*, 2011, **17**, 6643.
44. C. Wang, K. E. deKrafft and W. Lin, *J. Am. Chem. Soc.*, 2012, **134**, 7211.
45. S. Chavan, J. G. Vitillo, D. Gianolio, O. Zavorotynska, B. Civalleri, S. Jakobsen, M. H. Nilsen, L. Valenzano, C. Lamberti, K. P. Lillerud and S. Bordiga, *Phys. Chem. Chem. Phys.*, 2012, **14**, 1614.
46. G. Wißmann, A. Schaate, S. Lilienthal, I. Bremer, A. M. Schneider and P. Behrens, *Microporous Mesoporous Mater.*, 2012, **152**, 64.
47. Q. Yang, V. Guillerm, F. Ragon, A. D. Wiersum, P. L. Llewellyn, C. Zhong, T. Devic, C. Serre and G. Maurin, *Chem. Commun.*, 2012, **48**, 9831.
48. A. D. Wiersum, E. Soubeyrand-Lenoir, B. M. Q. Yang, V. Guillerm, M. B. Yahia, S. Bourrelly, A. Vimont, S. Miller, C. Vagner, M. Daturi, G. Clet, C. Serre, G. Maurin and P. L. Llewellyn, *Chem. Asian J.*, 2011, **6**, 3270.
49. D. A. Gomez-Gualdron, O. V. Gutov, V. Krungleviciute, B. Borah, J. E. Mondloch, J. T. Hupp, T. Yildirim, O. K. Farha and R. Q. Snurr, *Chem. Mater.*, 2014, **26** 5632.
50. X.-L. Lv, M. Tong, H. Huang, B. Wang, Lei Gan, Q. Yang, C. Zhong and J.-R. Li, *J. Solid State Chem.*, 2015, **223**, 104.
51. W. Morris, B. Voloskiy, S. Demir, F. Gándara, P. L. McGrier, H. Furukawa, D. Cascio, J. F. Stoddart and O. M. Yaghi, *Inorg. Chem.*, 2012, **51**, 6443.
52. V. Bon, V. Senkovskyy, I. Senkovska and S. Kaskel, *Chem. Commun.*, 2012, **48**, 8407.
53. K. Manna, T. Zhang, M. Carboni, C. W. Abney and W. Lin, *J. Am. Chem. Soc.*, 2014, **136**, 13182.
54. H. Furukawa, F. Gándara, Y.-B. Zhang, J. Jiang, W. L. Queen, M. R. Hudson and O. M. Yaghi, *J. Am. Chem. Soc.*, 2014, **136**, 4369.
55. P. Xydias, I. Spanopoulos, E. Klontzas, G. E. Froudakis and P. N. Trikalitis, *Inorg. Chem.*, 2014, **53**, 679.
56. V. Bon, I. Senkovska, I. A. Baburin and S. Kaskel, *Cryst. Growth Des.*, 2013, **13**, 1231.

57. B. Bueken, H. Reinsch, N. Reimer, I. Stassen, F. Vermoortele, R. Ameloot, N. Stock, C. E. A. Kirschhock and D. D. Vos, *Chem. Commun.*, 2014, **50**, 10055.
58. C. Wang, J.-L. Wang and W. Lin, *J. Am. Chem. Soc.*, 2012, **134**, 19895.
59. W. Zhang, H. Huang, D. Liu, Q. Yang, Y. Xiao, Q. Ma and C. Zhong, *Microporous Mesoporous Mater.*, 2013, **171**, 118.
60. G. Zahn, H. A. Schulze, J. Lippke, S. König, U. Sazama, M. Fröba and P. Behrens, *Microporous Mesoporous Mater.*, 2015, **203**, 186.
61. G. Kickelbick and U. Schubert, *Chem. Ber.*, 1997, **130**, 473.
62. S. Biswas, T. Ahnfeldt and N. Stock, *Inorg. Chem.*, 2011, **50**, 9518.
63. S. Biswas, D. E. P. Vanpoucke, T. Verstraelen, M. Vandichel, S. Couck, K. Leus, Y.-Y. Liu, M. Waroquier, V. Van Speybroeck, J. F. M. Denayer and P. V. D. Voort, *J. Phys. Chem. C*, 2013, **117**, 22784.
64. M. Kandiah, M. H. Nilsen, S. Usseglio, S. Jakobsen, U. Olsbye, M. Tilset, C. Larabi, E. A. Quadrelli, F. Bonino and K. P. Lillerud, *Chem. Mater.*, 2010, **22**, 6632.

## 3D Luminescent Amide-Functionalized Cadmium Tetrazolate Framework for Selective Detection of 2,4,6-Trinitrophenol

*This chapter presents the successful synthesis of strongly fluorescent 3D Cd(II)-based MOF incorporating a highly  $\pi$ -conjugated amide-functionalized ditopic tetrazolate-based organic ligand under solvothermal conditions. Selective detection of TNP by this compound with a very high rate of response was confirmed by the steady-state fluorescence titration experiments. It was found that the selective detection of TNP was also possible in presence of other potentially interfering nitroaromatic explosives. The outstanding sensing performance renders the material as a promising sensing device for the practical detection of TNP.*



### 3.1 INTRODUCTION

The prompt and selective detection of nitroaromatic explosive compounds is very vital for security screening, environmental safety, homeland security and human health.<sup>1-3</sup> 2,4,6-trinitrotoluene (TNT), 2,4-dinitrotoluene (2,4-DNT), 2,6-dinitrotoluene (2,6-DNT) and 2,4,6-trinitrophenol (TNP) are considered as major industrial explosives.<sup>4</sup> Compared to the well-known counterpart 2,4,6-trinitrotoluene (TNT), TNP or 2,4,6-trinitrophenol (more commonly known as picric acid) is a more powerful explosive which has been widely used in the manufacture of landmines, rocket fuels, fireworks and matches.<sup>5, 6</sup> and also frequently used in leather, pharmaceutical and dye industries. Consequently, TNP has become a major environmental pollutant owing to its widespread use. Uncontrolled exposure of TNP to the environment from chemical industries severely disturbs the soil and aquatic system, triggering various problems for wildlife and humans. Furthermore, mutagenic and/or carcinogenic activities of TNP can cause several health problems along with fatal environmental pollution. Therefore, discriminatory detection of TNP from other nitroaromatic explosives with a very low detection limit is an essential task in order to decrease its detrimental effects on the environment. Existing on-site detection methods for explosives employ sophisticated instruments, which suffer from low selectivity, limited portability, high cost and enormous complexity.<sup>4</sup> Fluorescence-based detection techniques for nitroaromatic explosives have attracted increasing attention in recent years due to their high sensitivity, portability, simplicity, low cost, short response times and dual compatibility in solid and solution media. The fluorescent sensor materials including conjugated polymers,<sup>1-3</sup> nanoparticles,<sup>7, 8</sup> and metal-organic frameworks (MOFs)<sup>9-17</sup> have been employed so far for the sensing of nitroaromatic explosives.

The porous crystalline structures of luminescent MOF materials and their ability to tune the sorption properties provide a high degree of molecular specificity and selectivity for the detection of targeted analytes over other sensor materials.<sup>9-17</sup> Besides the size-selectivity, the large surface areas of MOFs along with confinement of the analytes inside their pores can potentially result in high sensitivity detection of analytes. Additionally, the functional sites such as Lewis acidic or basic and open metal sites within porous MOFs can function as specific recognition sites for the detection of different analytes.<sup>16, 18-20</sup> This lead to increased detection performance via selective accumulation of the targeted analyte within MOF cavities by those recognition sites.

Furthermore, the incorporation of organic ligands in the rigid frameworks of MOFs results in stronger fluorescence emissions. Luminescent MOF materials are found to exhibit high physicochemical stability (air, water, heat, acid-base, etc.), which is desirable for the practical application of a sensor material. In addition, the availability of a huge combination of metal ions and organic ligands exclusively allows the fine-tuning of valance and/or conduction band (and hence optical band gap) of MOFs, which makes them more versatile for sensing applications. Encouraged by the above-mentioned advantages, several MOF materials have been synthesized and examined for the detection of a wide range of analytes including cations, anions, biomolecules, small molecules, volatile organic compounds and nitroaromatic explosive materials.<sup>9-17</sup>

Indeed, a large number of MOF-based fluorescent sensor materials<sup>9-17</sup> have been investigated until today for the detection of nitroaromatic explosive compounds but only a few of them<sup>18-26</sup> have displayed rapid and selective sensing behaviour towards TNP. Herein, we present a new fluorescent Cd(II)-based MOF having molecular formula  $[\text{Cd}_5\text{Cl}_6(\text{L})(\text{HL})_2] \cdot 7\text{H}_2\text{O}$  (**1**)  $\{\text{H}_2\text{L} = 4\text{-}(1H\text{-tetrazol-5-yl})\text{-N-[4-(1H-tetrazol-5-yl)phenyl]benzamide}\}$  and incorporating the amide-functionalized luminescent ditopic tetrazolate-based  $\text{H}_2\text{L}$  ligand. The activated form of the compound (denoted as **1'** hereafter) shows its potential for the highly selective, sensitive and rapid detection of TNP, even in the presence of other potentially interfering nitroaromatic explosive compounds. The collective experimental and theoretical study described herein suggests that energy and electron transfer processes as well as electrostatic interactions of the MOF material with TNP play important roles in determining the extraordinary selective quenching.

## 3.2 EXPERIMENTAL SECTION

### 3.2.1 Materials and General Methods

All the starting materials were of reagent grade and used as received from the commercial suppliers. The organic ligand  $\text{H}_2\text{L}$  was prepared by following a previously published procedure.<sup>27</sup> Fourier transform infrared (FT-IR) spectra were recorded in the region of  $440\text{-}4000\text{ cm}^{-1}$  with a Perkin Elmer Spectrum Two FT-IR spectrometer. The following indications are used to characterize absorption bands: very strong (vs), strong (s), medium (m), weak (w), shoulder (sh) and broad (br). Thermogravimetric analysis (TGA) was performed with a SDT Q600 V20.9 Build 20 thermogravimetric analyser in a temperature ranges of  $25\text{-}900\text{ }^\circ\text{C}$  under air atmosphere at a

heating rate of  $5\text{ }^{\circ}\text{C min}^{-1}$ . Ambient temperature X-Ray powder diffraction (XRPD) patterns were recorded on a Bruker D2 Phaser X-ray diffractometer operated at 30 kV, 10 mA using Cu-K $\alpha$  ( $\lambda = 1.5406\text{ \AA}$ ). The nitrogen sorption isotherms up to 1 bar were measured using a Quantachrome Autosorb iQ-MP gas sorption analyzer at  $-196\text{ }^{\circ}\text{C}$ . Prior to the sorption experiments, the compound was degassed at  $120\text{ }^{\circ}\text{C}$  for 12 h under dynamic vacuum. The UV-vis absorption spectra in solution were recorded with a PerkinElmer LAMBDA 750 UV-Vis spectrophotometer. The solid-state UV-Vis absorption spectra were collected on a JASCO V-650 UV-Vis spectrophotometer by using a 150 mm integrating sphere. BaSO<sub>4</sub> was used as an internal standard. Fluorescence emission studies were carried out with a HORIBA JOBIN YVON Fluoromax-4 spectrofluorometer. Fluorescence lifetimes were measured using time correlated single-photon counting (TCSPC) method on an Edinburgh Instrument Life-Spec II instrument. The samples were excited at 308 nm keeping the emission wavelength at 450 nm using a pulsed diode laser. The fluorescence decays were analysed by reconvolution method using the FAST software provided by Edinburgh Instruments.

Safety note! *Metal azides, tetrazolate compounds, TNP and TNT are potentially explosive, and caution should be exercised when dealing with such materials.* However, the small quantities used in this study were not found to present a hazard.

### 3.2.2 Synthesis

Synthesis of  $[\text{Cd}_5\text{Cl}_6(\text{L})(\text{HL})_2]\cdot 7\text{H}_2\text{O}$  (**1**):  $\text{CdCl}_2\cdot\text{H}_2\text{O}$  (24 mg, 0.12 mmol) and  $\text{H}_2\text{L}$  (20 mg, 0.06 mmol) ligand were dissolved in a mixture of DMF (1.5 mL) and MeOH (1.5 mL) by sonication for 15 min. After that two drops of conc. HCl were added to the solution. The resulting solution was heated in a sealed glass tube at  $80\text{ }^{\circ}\text{C}$  for 2 days using a block heater. After spontaneous cooling to room temperature, colorless prism-shaped crystals were collected by filtration, washed with DMF (10 mL) and methanol (10 mL) and dried in air. The yield was 14 mg (0.007 mmol, 31%) based on the Cd salt. Anal. calcd for  $\text{C}_{45}\text{H}_{43}\text{N}_{27}\text{O}_{10}\text{Cd}_5\text{Cl}_6$  (1896.77): C, 28.83 H, 2.94 N, 19.76. Found: C, 28.50 H, 2.28 N, 19.93%. FT-IR (KBr,  $\text{cm}^{-1}$ ): 3443 (br), 3350 (w), 3049-2776 (w), 1665 (vs), 1601 (m), 1544 (s), 1529 (sh), 1458 (s), 1417 (m), 1389 (w), 1327 (m), 1257 (w), 1157 (w), 1101 (w), 1009 (s), 900 (w), 861 (sh), 842 (m), 748 (m), 663 (w).

### 3.2.3 Activation of the Compound

The as-synthesized form of **1** was heated at 120 °C under vacuum for 12 h in order to get the activated form of the compound (**1'**).

### 3.2.4 Single-Crystal X-Ray Diffraction

Structure of **1** was determined from single-crystal X-ray diffraction data. Single-crystal X-ray diffraction intensities of **1** was recorded at 175 K on a Bruker D8 Quest diffractometer with a Photon 100 CMOS detector equipped with an Oxford Cryosystems 700 series cooler, a TRIUMPH monochromator and a MoK $\alpha$  fine-focused sealed tube ( $\lambda = 0.71073$  Å). Crystals collected at lower temperatures appeared to crack in the cryostream. Initial structures were solved by XT and refined by full-matrix least-squares techniques based on  $F^2$  using the SHELXTL package (version 6.14).<sup>28</sup> Statistical information of the single-crystal data collection and refinement of **1** are summarized in Table 3.1. The structure of **1** was found to be disordered at the six-membered ring and amide group. The entire ligand lies on a two-fold rotation axis, which causes the disorder. Several attempts to split the disorder into separate parts were unsuccessful (atoms became non-positive definite and refinement was unstable). In the end, the six-membered ring was refined using anisotropic parameters while a FRAG command was used to fix the coordinates of the amide. The amide itself was left isotropic as all other attempts to split the amide or refine it anisotropically also proved unsuccessful. Disordered water molecule was found solvated within the structure. The oxygen atom of the water molecule lies on a three-fold rotation axis and residual electron density surrounding the oxygen atom was refined as H atoms. Subsequent refinement placed both H atoms along the three-fold symmetry causing deviated H-O-H bond angles and O-H distances but further treatment using a combination of restraints gave poor results (again, atoms went non-positive definite and refinement was unstable). The H atoms were left in the refinement for the purpose of proper formulation of the water molecule. It should be noted that a lower symmetry space group,  $P2_13$  was attempted in order to remove the two-fold rotation along the amide group, however the amide was still clearly disordered. No indication of the presence of counter ions was observed in the difference Fourier map or from the elemental analysis. The structural model having no counter ions indicates that two-thirds of the tetrazole units of the ligands are protonated in order to maintain the electrostatic neutrality of the framework.

**Table 3.1.** Single-crystal X-ray data and structure refinement parameters for compound **1**.

Formula	$C_{48}H_{27}Cd_5Cl_6N_{27}O_3 \cdot 2(H_2O)$
Formula mass	1840.70
$T/K$	175(2)
$\lambda/\text{\AA}$	0.71073
Crystal dimensions/mm	0.25×0.15×0.10
Crystal system	Cubic
Space group	$P 4_132$
$a/\text{\AA}$	20.8320(11)
$V/\text{\AA}^3$	9040.5(14)
$Z$	4
$D_c/g\text{ cm}^{-3}$	1.352
$\mu/\text{mm}^{-1}$	1.382
$F(000)$	3560
$\theta$ Range/ $^\circ$	3.092-27.097
Measured reflections	105333
Independent reflections/ $R_{\text{int}}$	3341/0.0638
Data/restraints/parameters	3341/12/115
$R_1 (I > 2\sigma(I))^a$	0.0476
$wR_2$ (all data) <sup>b</sup>	0.1513
Goodness-of-fit on $F^2$	1.188
$\Delta\rho_{\text{max, min}}/e\text{ \AA}^{-3}$	1.625, -0.837

$$^a R_1 = \sum ||F_o| - |F_c|| / \sum |F_o|, \quad ^b wR_2 = \{ \sum [w(F_o^2 - F_c^2)^2] / \sum [w(F_o^2)^2] \}^{1/2}$$

Although protonation could not be observed in the difference Fourier map, it can be implied from elemental analysis and IR spectroscopy that protonation does occur. The bonding scheme as determined by the X-ray structure indicates that protonation occurs at N(2) atom. Therefore, it is reasonable to assume that the ligand resides in the  $\text{HL}^-/\text{L}^{2-}$  deprotonation states. Similar deprotonation states have been formerly<sup>29</sup> observed in two manganese MOFs incorporating ditopic tetrazolate-based ligands. CCDC-1420421 contains the supplementary crystallographic data for this structure.

### 3.2.5 Fluorescence Quenching Titration Experiments

In order to make a stable suspension, 1.5 mg of **1'** was stirred in 3 mL of ethanol for 30 min and subsequently sonicated for 30 min. The resulting suspensions were allowed to stand undisturbed for one day before the fluorescence titration experiments. The fluorescence titration measurements were carried out by the gradual addition of 1 mM solution of various nitroaromatic explosives (up to 400  $\mu\text{L}$ ) to a 3 mL well-dispersed ethanol suspension of **1'**. The solid-state fluorescence emission measurements were performed by exciting the compound at 356 nm. For all the fluorescence titration measurements, the excitation wavelength ( $\lambda_{\text{ex}}$ ) was 315 nm. The quenching efficiency was calculated by using  $(1-I/I_0) \times 100\%$ , where  $I_0$  is the initial fluorescence intensity of **1'** dispersed in ethanol and  $I$  is the fluorescence intensity after addition of the analyte.

## 3.3 RESULTS AND DISCUSSIONS

### 3.3.1 Synthesis

In order to obtain the single-crystal crystals of **1**, reactions were performed in various combinations of reactants at different temperatures. Two cadmium salts, namely  $\text{CdCl}_2 \cdot \text{H}_2\text{O}$  and  $\text{Cd}(\text{NO}_3)_2 \cdot 4\text{H}_2\text{O}$ , were employed. The solvents, which were used for these reactions, included DMF, *N,N*-dimethylacetamide (DMA), ethanol, methanol, DMF/ethanol, DMF/methanol, DMA/ethanol and DMA/methanol. The reaction temperatures ranged from 60 to 140 °C. Various metal salt/ligand molar ratios (1:1, 2:1, 3:1 and 4:1) were used. Very small crystals were obtained when a mixture of  $\text{CdCl}_2 \cdot \text{H}_2\text{O}$  and  $\text{H}_2\text{L}$  in a 2:1 molar ratio was heated at 80 °C in DMF/methanol (50:50, v/v) mixture. For increasing the size of the crystals, the same reaction was performed by adding various amounts (1-6 drops) of conc. HCl to the reaction mixture. Fortunately, the reaction

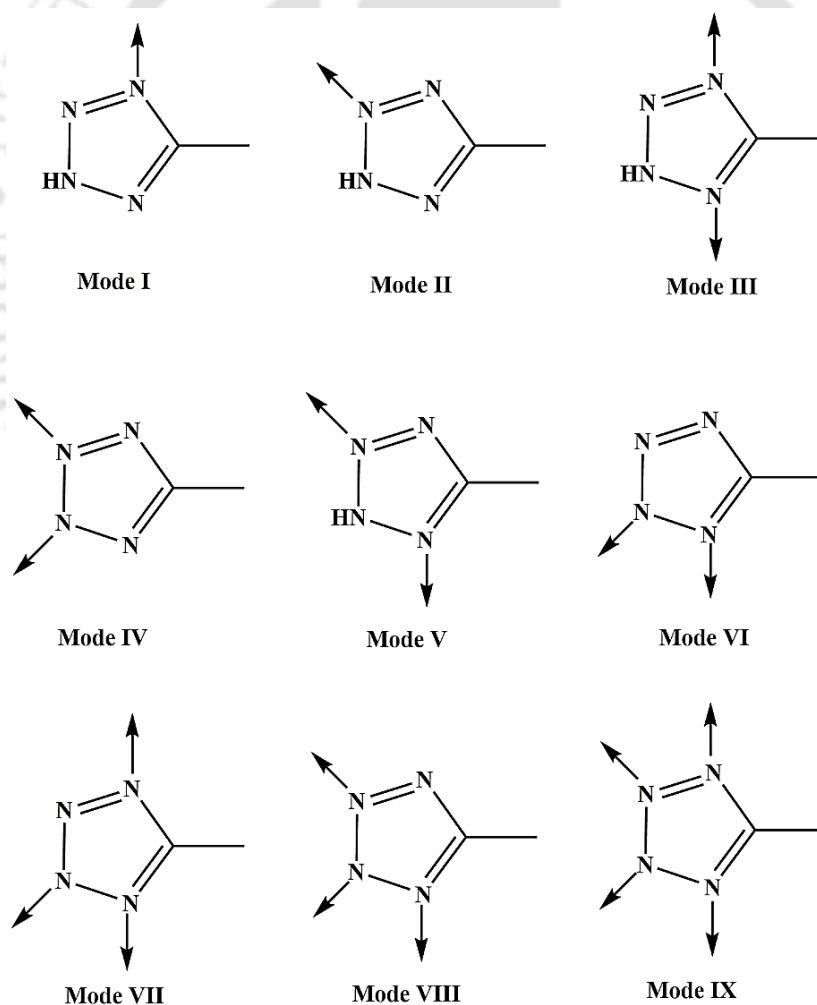
mixture containing 2 drops of conc. HCl resulted in the formation of prism-shaped single-crystals, which were suitable for single-crystal XRD measurement. The addition of more than 2 drops of conc. HCl led to decrease in yield of the product. Good quality single-crystals having similar shape were also achieved with  $\text{Cd}(\text{NO}_3)_2 \cdot 4\text{H}_2\text{O}$  by applying the same procedure, except 3 drops of conc. HCl were added instead of 2 drops.

The as-synthesized crystals of **1** were thoroughly washed with DMF after filtration for the removal of the physisorbed DMF molecules from the external surface. After that the compound was heated at 120 °C under vacuum in order to remove the occluded water molecules from the pores. In this way, the activated form of the compound (**1'**) was obtained.

### 3.3.2 Structure Description

Single-crystal X-ray diffraction analysis disclosed that **1** crystallizes in a cubic crystal system within space group  $P4_132$  and features a three-dimensional (3D) framework structure (Figure 3.1d). The asymmetric unit of compound **1** (Figure 3.2) consists of two crystallographically independent  $\text{Cd}^{2+}$  ions ( $\text{Cd}(1)$  lies on a two-fold rotation axis with occupancy of 1/2 whereas  $\text{Cd}(2)$  lies on a three-fold rotation axis with occupancy of 1/3), half of  $\text{H}_2\text{L}$  ligand molecule (Figure 3.1a) and one  $\mu_2$ -Cl atom. Each  $\text{Cd}^{2+}$  ion resides in a distorted octahedral environment. The two types of  $\text{Cd}^{2+}$  ions are arranged in an alternative fashion having two different types of coordination environments (Figure 3.1b). In the first type of coordination environment, which contains  $\text{CdCl}_2\text{N}_4$  unit, each  $\text{Cd}(1)$  atom is coordinated with two  $\mu_2$ -Cl atoms and four N atoms from four different  $\text{H}_2\text{L}$  ligand molecules. On the other hand, the second type of coordination environment consists of  $\text{CdCl}_3\text{N}_3$  unit where every  $\text{Cd}(2)$  atom is connected with three  $\mu_2$ -Cl atoms and three N atoms from three different  $\text{H}_2\text{L}$  ligand molecules. Each ditopic tetrazolate-based ligand molecule is bound with six  $\text{Cd}^{2+}$  ions through three N atoms of each tetrazolate ring. Thus, each  $\text{H}_2\text{L}$  ligand molecule shows  $\eta^3:\mu_6$  coordinating motif. As shown in Scheme 3.1, only one type of binding mode (Mode VIII) is present in the structure of compound **1** among all possible binding modes of tetrazole ring.<sup>30</sup> Such binding mode of the tetrazole moiety has been reported in the literature for only few metal-tetrazolate coordination polymers.<sup>31, 32</sup> The adjacent  $\text{Cd}^{2+}$  ions are interconnected by the bridging Cl atoms and ligand molecules, resulting in a non-interpenetrated 3D network structure (Figure 3.1c). If the bridging ligand molecules are omitted, the resulting framework structure (Figure 3.1d) can be imagined to possess larger oval-

and smaller square-shaped pores. The selected bond distances and angles are shown in Table 3.2. The Cd-N bond distances vary from 2.343(7) to 2.489(8) Å, whereas the two kinds of Cd-Cl bond distances are 2.601(2) and 2.596(2) Å. The Cd-N bond distances observed in the present compound are in agreement with the formerly reported Cd-tetrazolate MOFs.<sup>33-46</sup> According to the program PLATON,<sup>47</sup> the total potentially accessible void volume is 3521.7 Å<sup>3</sup>, which is 39% of the unit cell volume (9040.5 Å<sup>3</sup>). Under ambient conditions, these void regions of the network are occupied by seven water molecules per formula unit, which is in agreement with the thermogravimetric (TG) and elemental analysis. Despite having considerable pore volume, the N<sub>2</sub> sorption analysis (Figure 3.3) indicated that compound **1** is non-porous towards N<sub>2</sub> (specific BET surface area: 4 m<sup>2</sup> g<sup>-1</sup>). This fact can be related to the very small pore apertures, which restricts the passage of relatively larger N<sub>2</sub> molecules into the framework of compound **1**.



**Scheme 3.1.** All possible coordination modes of tetrazole ring.

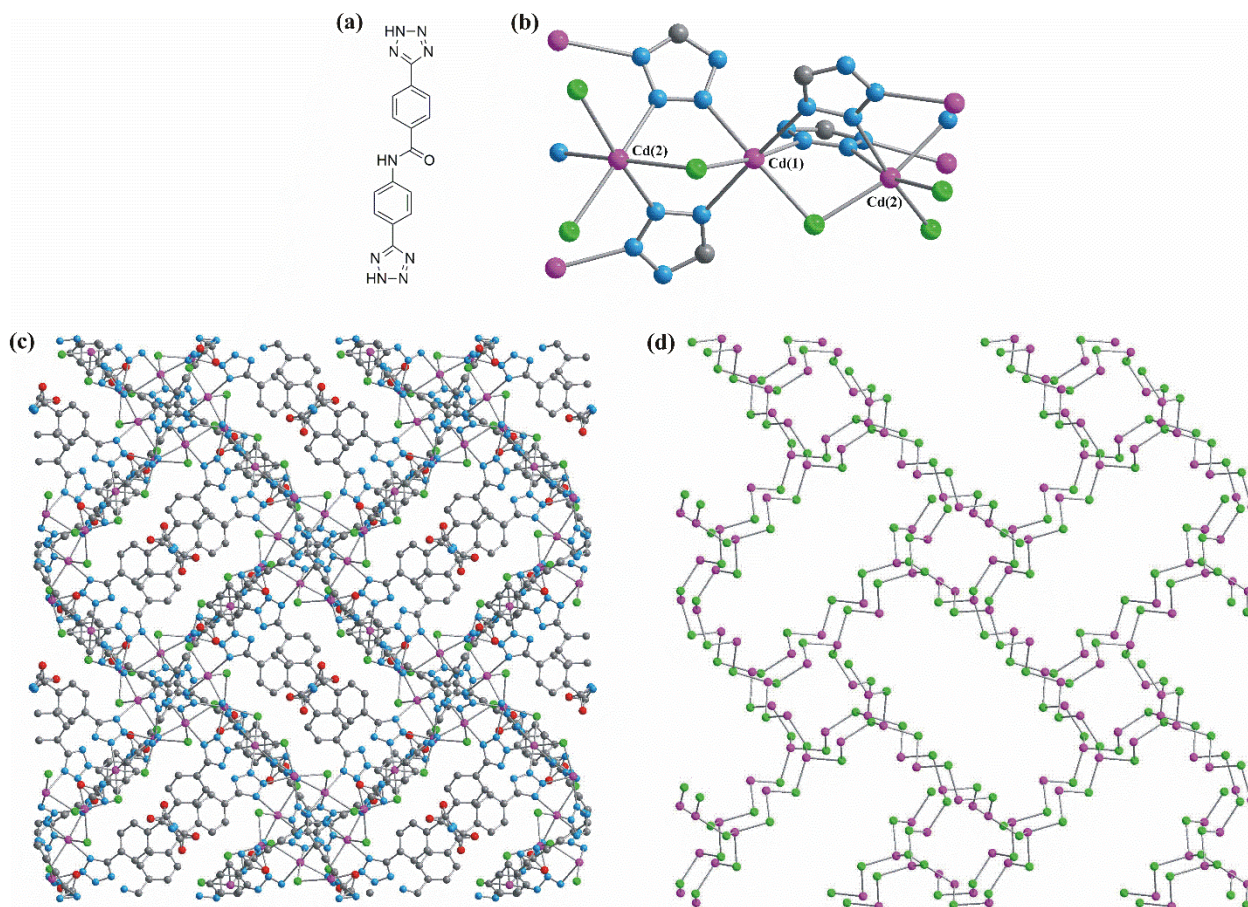


**Figure 3.1** (a) Structure of H<sub>2</sub>L ligand employed for synthesizing **1**. (b) Ball-and-stick representation showing the coordination environment around of Cd<sup>2+</sup> ions in **1**. (c) The same representation of the 3D framework structure of **1**. (d) The network of **1** with the ligand molecules omitted. Color codes: Cd, magenta; N, cyan; Cl, green; C, gray; O, red. The guest molecules and hydrogen atoms have been removed from the structural plots for clarity.

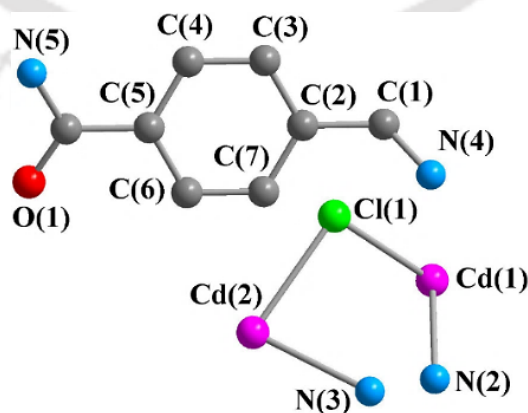


**Figure 3.2** Ball-and-stick representation of the asymmetric unit of **1**.

**Table 3.2** Selected bond distances (Å) and angles (°) for **1**.

Bond	Distances (Å)	Bond	Angles (°)
Cd(1)-N(1)	2.343(7)	N(1)-Cd(1)-N(1)#1	87.4(4)
Cd(1)-N(1)#1	2.343(7)	N(1)-Cd(1)-N(4)#1	97.1(3)
Cd(1)-N(4)#1	2.489(8)	N(1)#1-Cd(1)-N(4)#1	86.1(3)
Cd(1)-N(4)	2.489(8)	N(1)-Cd(1)-N(4)	86.1(3)
Cd(2)-N(3)	2.381(7)	N(1)#1-Cd(1)-N(4)	97.1(3)
Cd(2)-N(3)#2	2.381(7)	N(4)#1-Cd(1)-N(4)	175.6(4)
Cd(2)-N(3)#3	2.381(7)	N(1)-Cd(1)-Cl(1)#1	86.51(19)
Cd(1)-Cl(1)#1	2.601(2)	N(1)#1-Cd(1)-Cl(1)#1	173.4(2)
Cd(1)-Cl(1)	2.601(2)	N(4)#1-Cd(1)-Cl(1)#1	91.96(19)
Cd(2)-Cl(1)#3	2.596(2)	N(4)-Cd(1)-Cl(1)#1	85.19(18)
Cd(2)-Cl(1)#2	2.596(2)	N(1)-Cd(1)-Cl(1)	173.4(2)
Cd(2)-Cl(1)	2.596(2)	N(1)#1-Cd(1)-Cl(1)	86.52(19)
		N(4)#1-Cd(1)-Cl(1)	85.19(18)
		N(4)-Cd(1)-Cl(1)	91.96(19)
		Cl(1)#1-Cd(1)-Cl(1)	99.65(10)
		N(3)-Cd(2)-N(3)#2	85.3(3)
		N(3)-Cd(2)-N(3)#3	85.3(3)
		N(3)#2-Cd(2)-N(3)#3	85.3(3)
		N(3)-Cd(2)-Cl(1)#3	86.38(18)
		N(3)#2-Cd(2)-Cl(1)#3	166.67(18)

Bond	Distances (Å)	Bond	Angles (°)
		N(3)#3-Cd(2)-Cl(1)#3	83.61(17)
		N(3)-Cd(2)-Cl(1)#2	166.67(18)
		N(3)#2-Cd(2)-Cl(1)#2	83.61(17)
		N(3)#3-Cd(2)-Cl(1)#2	86.38(18)
		Cl(1)#3-Cd(2)-Cl(1)#2	103.05(6)
		N(3)-Cd(2)-Cl(1)	83.61(17)
		N(3)#2-Cd(2)-Cl(1)	86.38(18)
		N(3)#3-Cd(2)-Cl(1)	166.67(18)
		Cl(1)#3-Cd(2)-Cl(1)	103.05(6)
		Cl(1)#2-Cd(2)-Cl(1)	103.05(6)
		Cd(2)-Cl(1)-Cd(1)	97.50(8)

Symmetry transformations used to generate equivalent atoms:

#1  $y-1/4, x+1/4, -z+9/4$  #2  $y-1/2, -z+3/2, -x+1$  #3  $-z+1, x+1/2, -y+3/2$

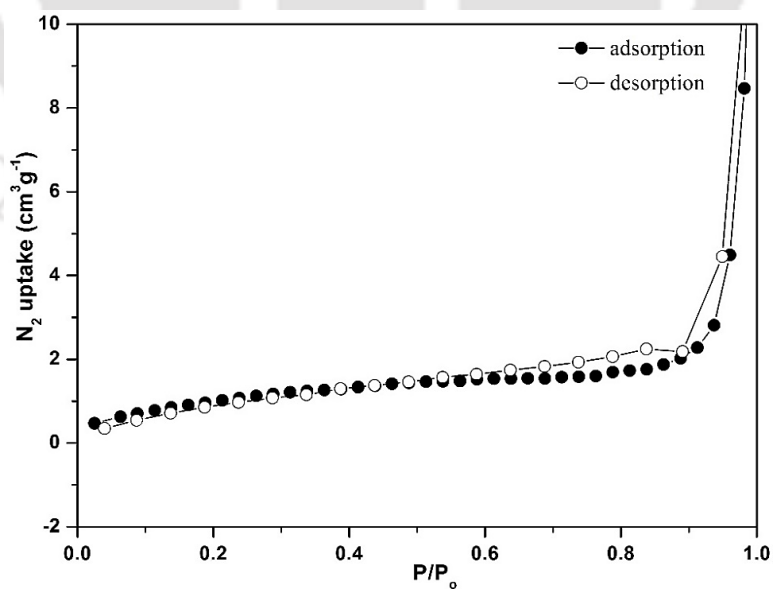


**Figure 3.3** N<sub>2</sub> adsorption (filled circles) and desorption (empty circles) isotherms of thermally activated **1'** measured at  $-196$  °C. The samples were heated at  $120$  °C under vacuum for 12 h before the sorption measurement.

### 3.3.3 X-ray Powder Diffraction and FT-IR Analysis

The phase purity of **1** was verified by using XRPD patterns recorded from as-synthesized **1** at ambient conditions. The experimental XRPD pattern (Figure 3.4) of as-synthesized **1** matches closely with the simulated XRPD pattern obtained from the single-crystal X-ray diffraction data. The thermally activated **1'** retains its crystallinity, as corroborated from the XRPD patterns (Figure 3.4) of the corresponding sample.

In the FT-IR spectrum (Figure 3.5) of **1**, the strong absorption band at  $1665\text{ cm}^{-1}$  can be assigned to the C=O stretching vibration of the amide group of the ligand molecules. The absorption bands owing to the N-H stretching and bending vibrations of the amide group of the ligand molecules are located at  $3350$  and  $1544\text{ cm}^{-1}$ , respectively.<sup>48, 49</sup>

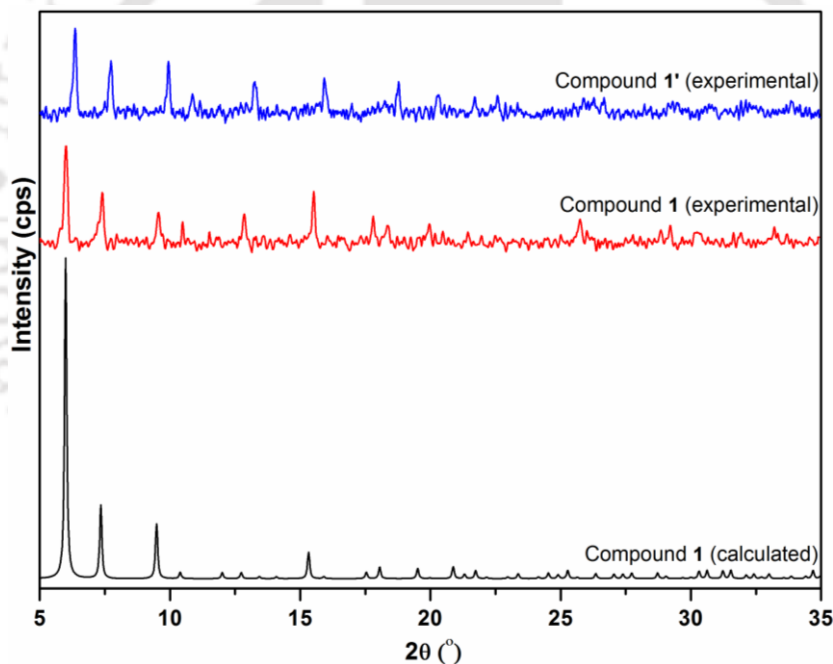


**Figure 3.4** Calculated and experimental XRPD patterns of **1** and **1'**.

### 3.3.4 Thermal Stability

In order to investigate the thermal stability of **1**, thermogravimetric analysis (TGA) was performed in the temperature range of 25-900 °C in an air atmosphere. According to the TG analysis, **1** is stable up to 300 °C. In the TG curve of **1** (Figure 3.6), the first weight loss step of 6.1 wt% in the temperature range of 25-80 °C can be attributed to the removal of seven guest water molecules per formula unit (calcd.: 6.6 wt%). No further weight loss step is observed below the

decomposition temperature (300 °C) of **1**. Above 300 °C, the compound starts to decompose due to the loss of the organic linker molecules from the framework. In the TG trace of **1'**, the one weight loss step below the decomposition temperature can be ascribed to the removal of absorbed water molecules. The exposure of **1'** to air after thermal activation presumably resulted in the hydration of the compound.

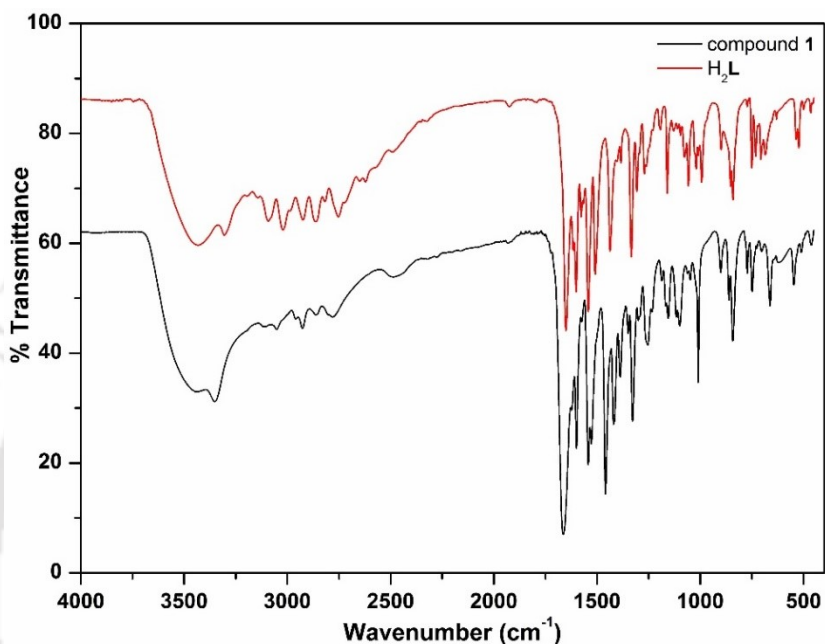


**Figure 3.5** FT-IR spectra of **1** (black) and  $H_2L$  (red).

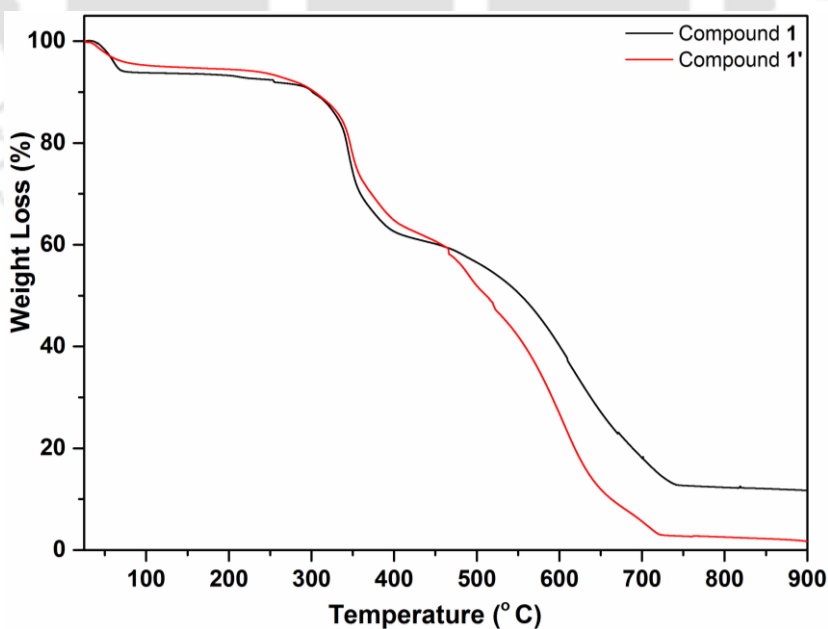


**Figure 3.6** TG curves of **1** and **1'** recorded in an air atmosphere in the temperature range of 25-900 °C with a heating rate of 5 °C/min.

The high thermal stability of **1'** was also verified by variable temperature XRPD experiments (Figure 3.7), which disclosed that the compound is stable up to 300 °C. This result is in agreement with that obtained from the thermogravimetric analyses.

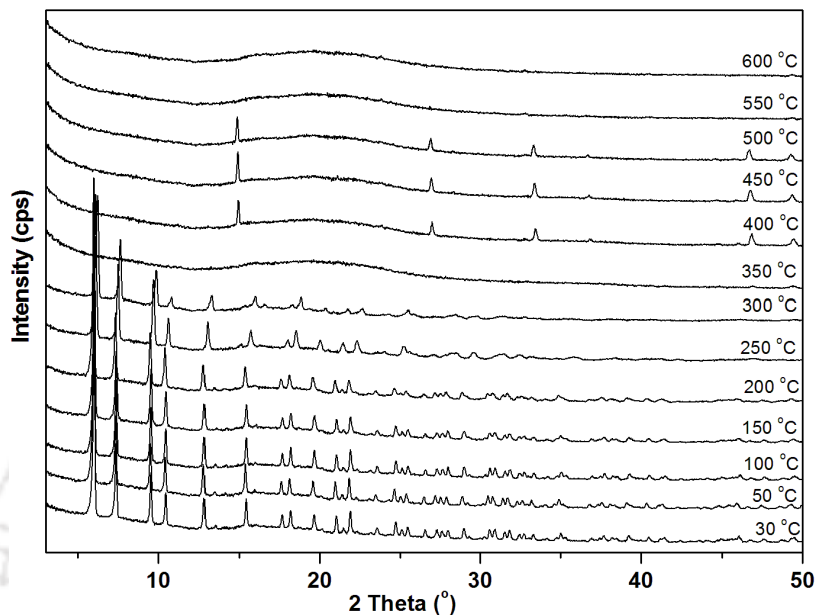


**Figure 3.7** Variable temperature XRPD patterns of compound **1** recorded in an air atmosphere in the temperature range of 30-600 °C with a heating rate of 5 °C/min.

### 3.3.5 Photoluminescence Properties

MOFs based on  $d^{10}$  metal ions with  $\pi$ -conjugated aromatic ligands are well known for their excellent luminescence behaviour and thus regarded as potential candidates for applications as fluorescent sensors.<sup>11</sup> Since **1'** is constructed from  $d^{10}$  ( $\text{Cd}^{2+}$ ) metal ions and  $\pi$ -electron rich conjugated organic ligand, it was hypothesized to be a potential fluorophore with tremendous photoluminescence (PL) properties. The solid-state fluorescence emission spectrum of the  $\text{H}_2\text{L}$  ligand (Figure 3.8) shows an emission maximum at 456 nm upon excitation at 344 nm, which can be ascribed to the intra-ligand  $\pi$ - $\pi^*$  transition of the aromatic rings.<sup>11</sup> On the other hand, **1'** (Figure 3.8) displays an emission maximum at 470 nm in the solid-state upon excitation at 356 nm. The similarity between the emission bands of  $\text{H}_2\text{L}$  ligand and **1'** indicates that the photoluminescence behaviour of **1'** is mainly due to ligand-centred electronic excitation.<sup>50</sup> However, a red shift (14 nm) of the emission band of the compound compared to the parent ligand is observed, which can be attributed to the perturbation caused by the complexation of the ligand with  $\text{Cd}^{2+}$  ions.<sup>50, 51</sup>

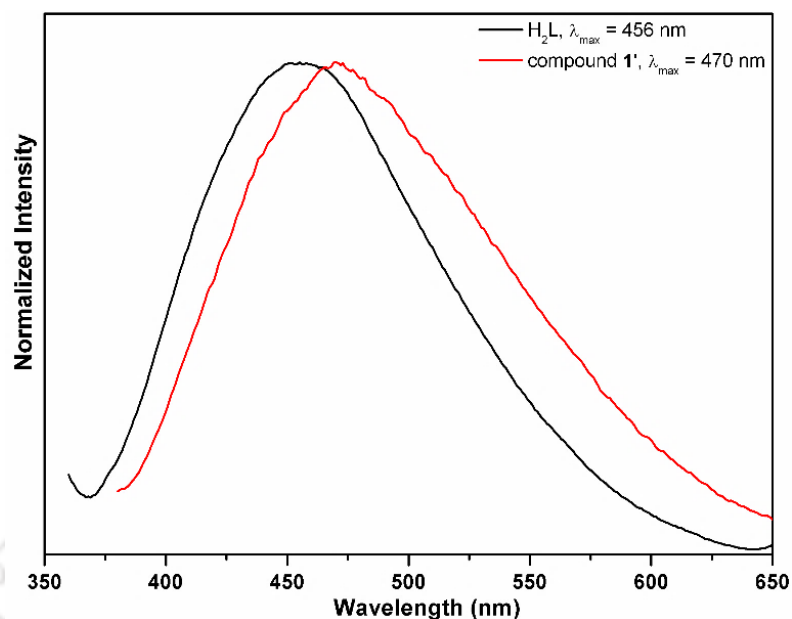


**Figure 3.8** Solid-state fluorescence emission spectra of  $H_2L$  ligand ( $\lambda_{ex} = 344$  nm) and  $1'$  ( $\lambda_{ex} = 356$  nm) measured at room temperature.

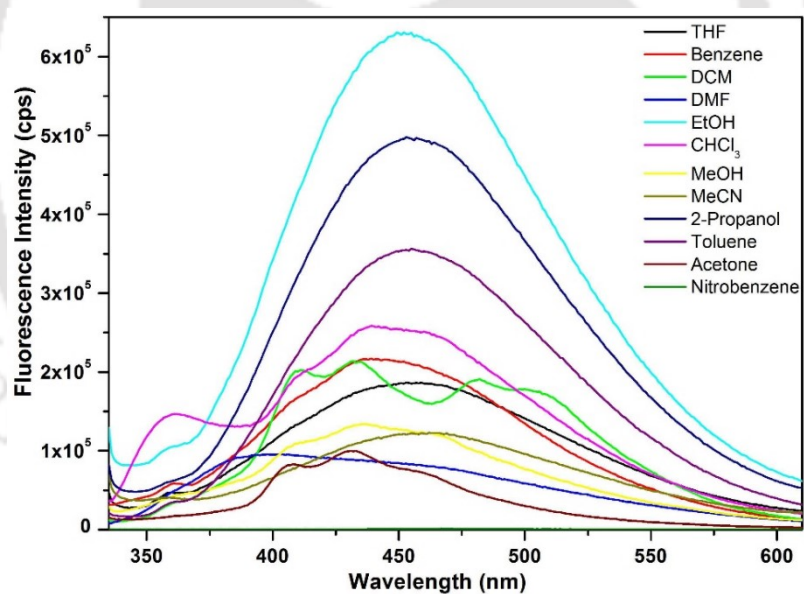


**Figure 3.9** Fluorescence emission spectra of  $1'$  in common organic solvents ( $\lambda_{ex} = 315$  nm).

The photoluminescence behaviour of  $1'$  (Figure 3.9) in common organic solvents (tetrahydrofuran, benzene, dichloromethane, DMF, ethanol, chloroform, methanol, acetonitrile, 2-propanol, toluene, acetone and nitrobenzene) and in water was also investigated. All the fluorescence emission experiments were performed with a stable suspension of  $1'$  (1.5 mg) in different organic solvents (3 mL). An ethanol suspension of  $1'$  showed the strongest emission band

at 450 nm upon excitation at 315 nm at room temperature. Hence, all the fluorescent experiments were performed in ethanol. Due to the instability of **1'** in water (as revealed from the XRPD analysis), the luminescence behavior of the compound in water was not investigated.

### 3.3.6 Sensing of Nitroaromatic Explosives

The highly fluorescent nature of **1'** in both solution and solid-state inspired us to explore its potential applications as a sensor for the detection of nitroaromatic explosives (NAEs). In order to investigate the applicability of electron rich **1'** as a promising detecting device for electron-deficient NAEs, the fluorescence sensing behavior of **1'** in presence of the NAEs were examined.

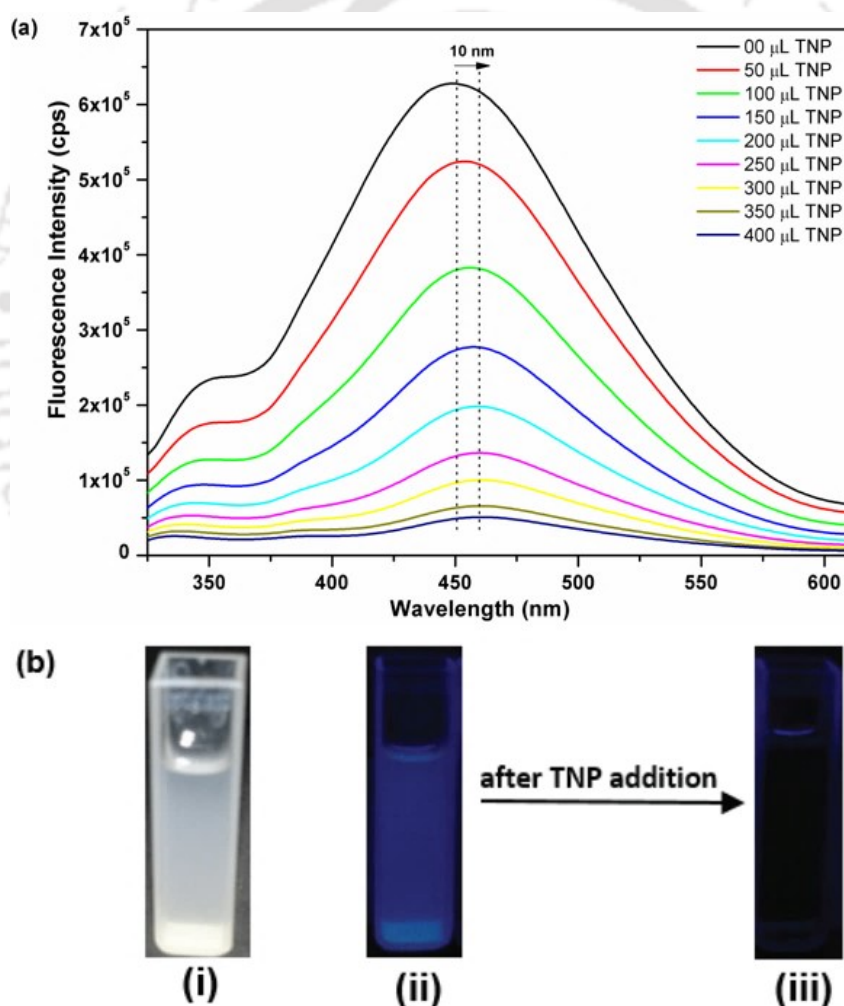


**Figure 3.10** (a) Quenching of fluorescence intensity of **1'** by incremental addition of 1 mM TNP solution to a 3 mL suspension of **1'** in ethanol ( $\lambda_{\text{ex}} = 315$  nm and  $\lambda_{\text{max}} = 450$  nm). (b) Photographs of fluorescence cuvettes containing ethanol suspensions of **1'** under visible light (i), UV light before TNP addition (ii) and UV light after TNP addition (iii).

The NAEs, which were used for this work, included 2,4,6-trinitrophenol (TNP; commonly known as picric acid), 2,4-dinitrophenol (DNP), *p*-nitrophenol (PNP), 2,4,6-trinitrotoluene (TNT), 2,4-dinitrotoluene (2,4-DNT), 2,6-dinitrotoluene (2,6-DNT), 4-nitrotoluene (4-NT), 1,3-dinitrobenzene (1,3-DNB) and nitrobenzene (NB). For this purpose, fluorescent titration measurements were performed by the gradual addition of 1 mM ethanol solution of the NAEs to the well-dispersed suspensions of **1'** in ethanol. A successive quenching of the fluorescence intensity of **1'** was observed upon incremental addition of the analytes. It is remarkable that the visible light blue emission of **1'** under UV light disappeared after addition of 400  $\mu$ L of 1 mM TNP solution, which resulted in nearly 92% quenching of the initial fluorescence intensity (Figure 3.10). A small red shift (10 nm) of the emission band upon increasing addition of TNP solution could be a consequence of energy transfer mechanism occurring between the analyte and the compound.<sup>51</sup> The detection performance of **1'** for other nitroaromatic explosives (Figure 3.11) was very low and the lowest quenching efficiency was observed for NB. The quenching efficiencies for the selected analytes decreased in the sequence: TNP > PNP > DNP > TNT > 4-NT > 2,4-DNT > 2,6-DNT > 1,3-DNB > NB. This sequence is not completely in agreement with the trend of electron-deficient nitro groups present in the analytes.

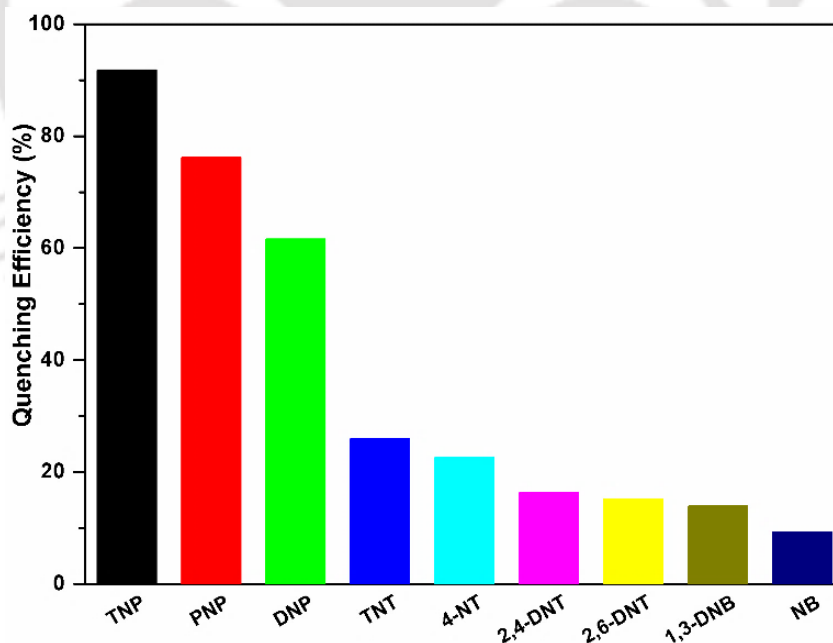


**Figure 3.11** Quenching efficiencies of different nitroaromatic explosives at  $1.18 \times 10^{-4}$  M concentration ( $\lambda_{\text{ex}} = 315$  nm and  $\lambda_{\text{max}} = 450$  nm).

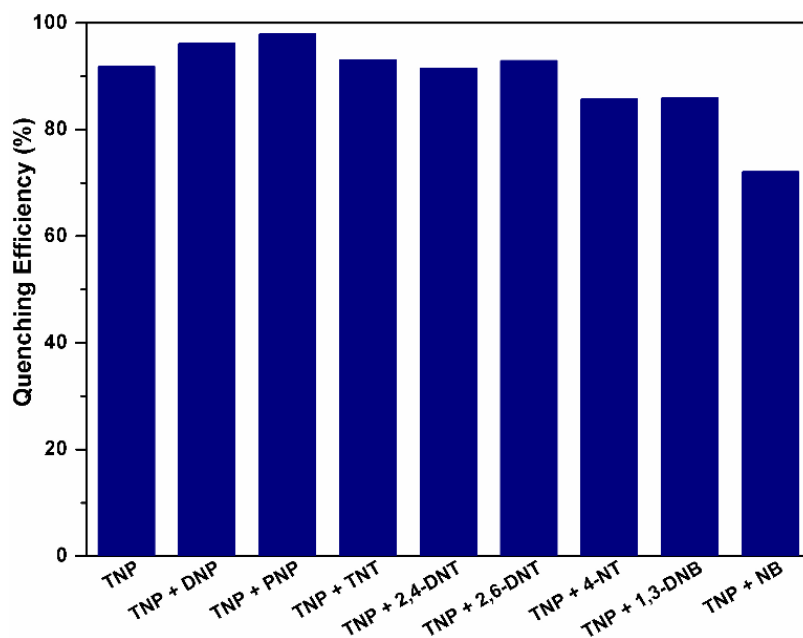


**Figure 3.12** Quenching efficiencies of TNP ( $1.43 \times 10^{-4}$  M) in presence of other nitroaromatic explosives ( $1.43 \times 10^{-4}$  M).

In order to study the quenching efficiency of TNP in presence of other NAEs, fluorescence titration experiments were carried out by the gradual addition of  $1.43 \times 10^{-4}$  M TNP solution to the suspension of **1'** containing  $1.43 \times 10^{-4}$  M solution of other NAEs. As shown in Figure 3.12, the quenching efficiency of TNP remains almost same in presence of other NAEs, except for NB where quenching efficiency decreases by nearly 20%. These results clearly show the high selectivity of **1'** for TNP, even in the existence of a higher concentration of other NAEs. For effective quenching, a compound must show a defined and assessable response to the analytes at a specific concentration. In Figure 3.13, the change of fluorescence quenching efficiencies upon incremental addition of different analytes is shown. The figure discloses that the quenching efficiencies increase considerably at lower concentrations, but they increase slightly at higher concentrations.

In order to investigate the recyclability of **1'**, the material was recovered after every fluorescence titration experiment by centrifugation, followed by washing with ethanol for several times. Remarkably, the compound almost regains its initial fluorescence intensity and quenching efficiency over 5 cycles of repetition (Figure 3.14). As verified by the XRPD measurements (Figure 3.15), **1'** maintained its crystallinity (and hence structural integrity) after 5 repeated cycles of fluorescence titration experiments with 1 mM TNP solution. These results imply high

photostability and reusability of the material, making it potentially applicable for long-term in-field detection of nitroaromatic explosive compounds.

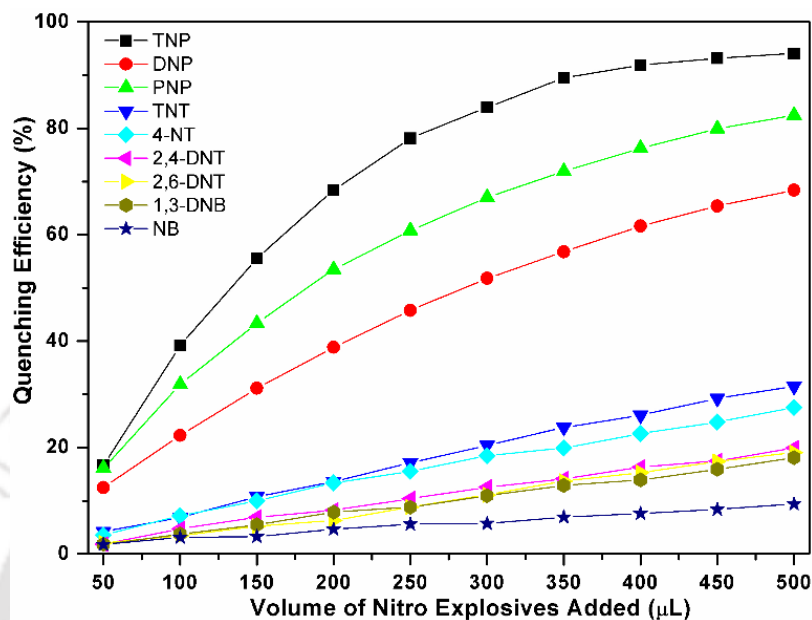


**Figure 3.13** Change of fluorescence quenching efficiencies upon gradual addition of 1 mM solution of different nitroaromatic explosives to a 3 mL suspension of **1'** in ethanol.

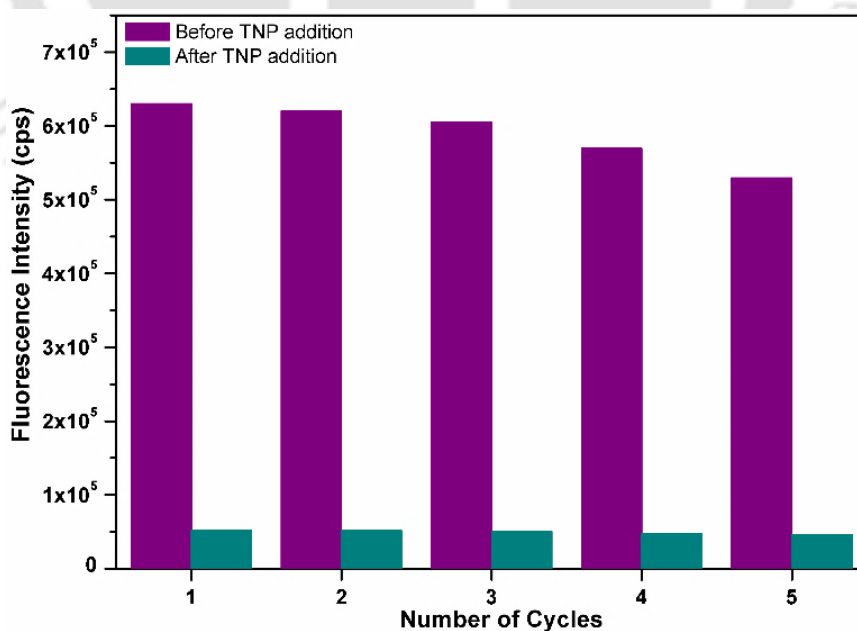


**Figure 3.14** Reproducibility of the quenching efficiency of the ethanol suspension of **1'** towards 1 mM TNP solution.

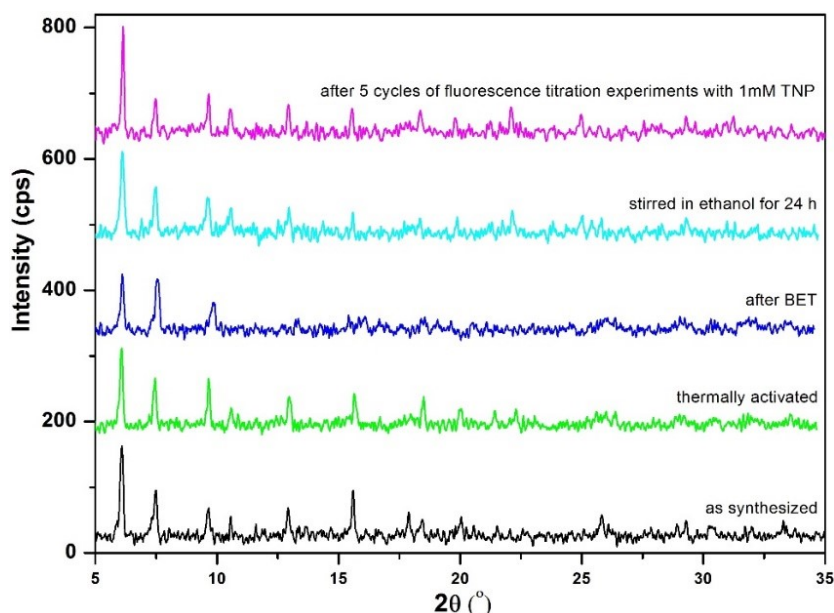


**Figure 3.15** XRPD patterns of **1** in different forms: as-synthesized (black); thermally activated (green); after BET measurement (blue); in ethanol (cyan); after 5 cycles of fluorescence titration experiments with 1 mM TNP solution (magenta).

### 3.3.7 Estimation of Quenching Constant and Detection Limit for TNP

Quenching of fluorescence intensity can occur by two quenching processes: collisional or dynamic quenching and complex formation or static quenching. Dynamic quenching takes place when the excited fluorophore comes in contact with the quencher molecule, which facilitates non-radiative transition to the ground state. This process leads to quenching of the fluorescence intensity. On the other hand, the static quenching involves the formation of a non-fluorescent stable complex (dark complex) between the fluorophore and the quencher molecule.<sup>52, 53</sup> If only one type of quenching process is taking place, the quenching can be expressed by the Stern-Volmer (S-V) equation,  $(I_0/I) = K_{sv} [A] + 1$ , where  $I_0$  is the initial fluorescence intensity before addition of analyte,  $I$  is the fluorescence intensity after addition of analyte,  $[A]$  is the molar concentration of analyte and  $K_{sv}$  is the quenching constant (in  $M^{-1}$ ). In order to determine the Stern-Volmer binding constant ( $K_{sv}$ ), a steady state fluorescence measurement was performed. The S-V plot for TNP at low concentrations (Figure 3.16) showed a linear curve, indicating that either dynamic or static quenching is taking place. But the deviation of the S-V plot from linearity at higher concentrations (inset of Figure 3.16) suggests the presence of both dynamic and static quenching processes. The  $K_{sv}$  value determined from the linear portion of the S-V plot for TNP towards luminescent **1'** was estimated to be  $4.05 \times 10^4 M^{-1}$ . This is among the highest values reported<sup>18, 19, 21-23, 26, 51, 52</sup> (Table

3.3) until today for MOF-based sensor materials. The distinction between the two quenching mechanisms can be predicted by performing time-resolved fluorescence measurement of photoluminescence decays of the fluorophore at different concentrations of the quencher. If the fluorescence lifetime of the sensor material decreases, the quenching process is regarded as dynamic because additional relaxation of the excited-state lifetime in this process is resulted by collision with the quencher. However, if the fluorescence lifetime of the sensor material remains unchanged after gradual addition of the quencher, it is considered as a static quenching process. The time-resolved fluorescence experiments (Figure 3.17) revealed that the average excited state lifetimes ( $\langle\tau\rangle$ ) of **1'** are 1.12 ns and 1.09 ns (Table 3.4) before and after addition of 400  $\mu$ L TNP, respectively. These average lifetime values indicate that the quenching process is mainly static in nature.

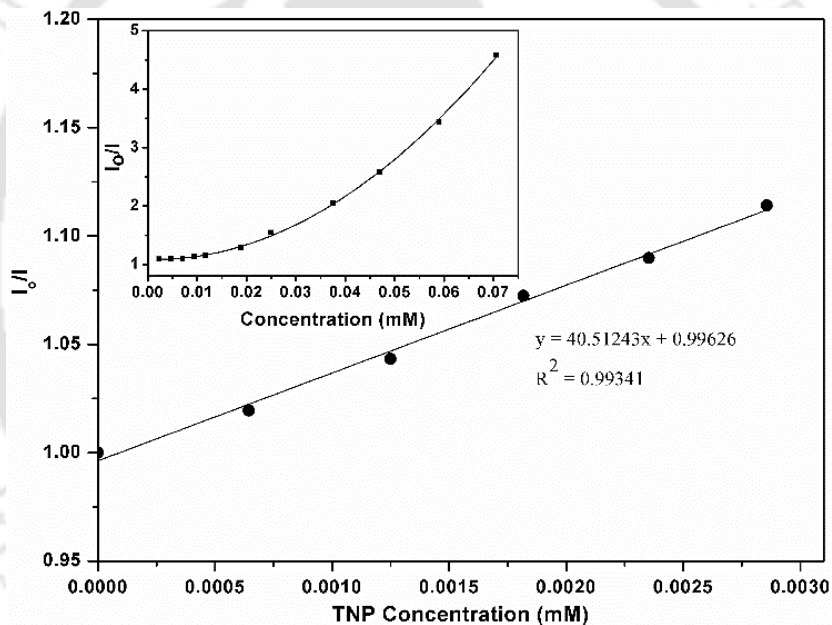


**Figure 3.16** Stern-Volmer plot for the fluorescence quenching of **1'** upon addition of TNP. Inset: non-linearity of the plot at higher concentrations of TNP.

**Table 3.3** A comparison of the Stern-Volmer constant ( $K_{sv}$ ), detection limit and medium used for TNP detection for MOFs reported until today.

Sl. No.	MOF	$K_{sv} (\times 10^4 \text{ M}^{-1})$	Detection Limit	Medium Used	Ref.
1	$[\text{Cd}_5\text{Cl}_6(\text{L})(\text{HL})_2] \cdot 7\text{H}_2\text{O}$	4.05	$1.87 \times 10^{-7} \text{ M}$ (42.84 ppb)	Ethanol	This work

Sl. No.	MOF	$K_{sv} (\times 10^4 M^{-1})$	Detection Limit	Medium Used	Ref.
2	$[Cd_3(TPT)_2(DMF)_2] \cdot (H_2O)_{0.5}$	6.56		Ethanol	22
3	$Zr_6O_4(OH)_4(L)_6(UiO-67@N)$	2.9		Water	18
4	$Cd(NDC)_{0.5}(PCA)$	3.5		Acetonitrile	19
5	$[Zn_2(NDC)_2(bpy)] \cdot G_x$	0.422		Ethanol	54
6	Bio-MOF-1	4.6	2.9 ppb	Water	21
7	$[Tb(1,3,5-BTC)]$	3.41	$8.1 \times 10^{-8} M$	Ethanol	26
8	$Zn_2(PAM)_2(1,3-PDA)_2$		$1.27 \times 10^{-8} M$	DMSO	55
9	$[Eu_2(MFDA)_2(HCOO)_2(H_2O)_6] \cdot (H_2O)_n$		$4.5 \times 10^{-7} M$	DMF	6

Ligand abbreviation: TPT = p-terphenyl-3,4,5-tricarboxylic acid; NDC = 2,6-naphthalenedicarboxylic acid; PCA=4-pyridinecarboxylic acid; bpy = 4,4-bipyridine; G = guest solvent molecules; BTC = 1,3,5-benzenetricarboxylic acid; PAM = 4,4'-methylenebis (3-hydroxy-2-naphthalenecarboxylic acid); PDA = 1,3-propanediamine; MFDA = 9,9-dimethylfluorene-2,7-dicarboxylic acid.

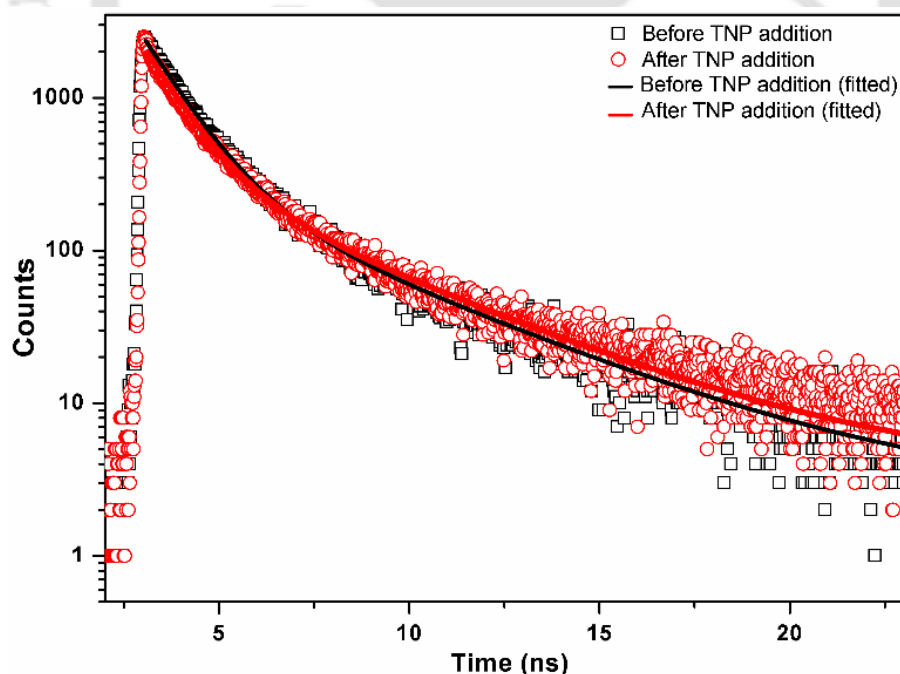


**Figure 3.17** Fluorescence lifetime decay profile of **1'** before and after addition of 400  $\mu$ L TNP solution ( $\lambda_{ex}$  = 308 nm,  $\lambda_{em}$  = 450 nm).

**Table 3.4** Average excited-state lifetime ( $\langle\tau\rangle$ ) values of **1'** before and after addition of different volume of 1 mM TNP solution ( $\lambda_{\text{ex}} = 308 \text{ nm}$ ,  $\lambda_{\text{em}} = 450 \text{ nm}$ )

Volume of TNP added ( $\mu\text{L}$ )	$B_1$	$B_2$	$a_1$	$a_2$	$\tau_1$ (ns)	$\tau_2$ (ns)	$\langle\tau\rangle^*$ (ns)
00	0.413	0.012	0.97	0.03	1.029	4.2	1.12
100	0.494	0.014	0.97	0.03	0.959	3.91	1.04
200	0.459	0.014	0.97	0.03	0.974	4.09	1.07
300	0.468	0.014	0.97	0.03	0.947	4.16	1.04
400	0.377	0.013	0.97	0.03	0.98	4.2	1.09

$$*\langle\tau\rangle = a_1\tau_1 + a_2\tau_2$$

### 3.3.8 Response Time of **1'** towards the Detection of TNP

For determination of the response time for the sensing of TNP by **1'**, time-dependent fluorescence investigations were performed at four different concentrations of TNP (100, 200, 300 and 400  $\mu\text{L}$  of 1 mM TNP solutions added to a 3 mL suspension of **1'** in ethanol). At a particular concentration of TNP, the fluorescence intensity of **1'** was monitored at regular time intervals up to 320 s of exposure time. The plots of quenching efficiencies versus exposure times (Figure 3.18) reveal that the addition of 400  $\mu\text{L}$  of TNP to the ethanol suspension of **1'** leads to very fast detection of the former. At this concentration of TNP, it takes only a few seconds ( $<25 \text{ s}$ ) to attain almost complete quenching (92%) of the preliminary fluorescence emission intensity of **1'**.

In order to obtain the limit of detection for TNP towards **1'**, very low concentrations of TNP ( $\mu\text{M}$ ) solution were added incrementally to **1'** dispersed in ethanol and the fluorescence quenching was monitored. The plot of change in fluorescence intensity versus concentration of TNP exhibited a linear curve (Figure 3.19) with a slope ( $K$ ) of  $2 \times 10^{10}$  and correlation coefficient ( $R^2$ ) of 0.9965. The limit of detection (LOD) was calculated by using the equation:  $\text{LOD} = 3\sigma/K$ , where  $\sigma$  is the standard deviation of initial intensity of **1'** without analyte and  $K$  denotes the slope of the above-mentioned linear curve. The detection limit of **1'** for sensing of TNP was found to be

$1.87 \times 10^{-7}$  M (42.84 ppb), which compares well with other reported<sup>18, 19, 21-23, 26, 51, 52</sup> (Table 3.3) MOF-based sensor materials.

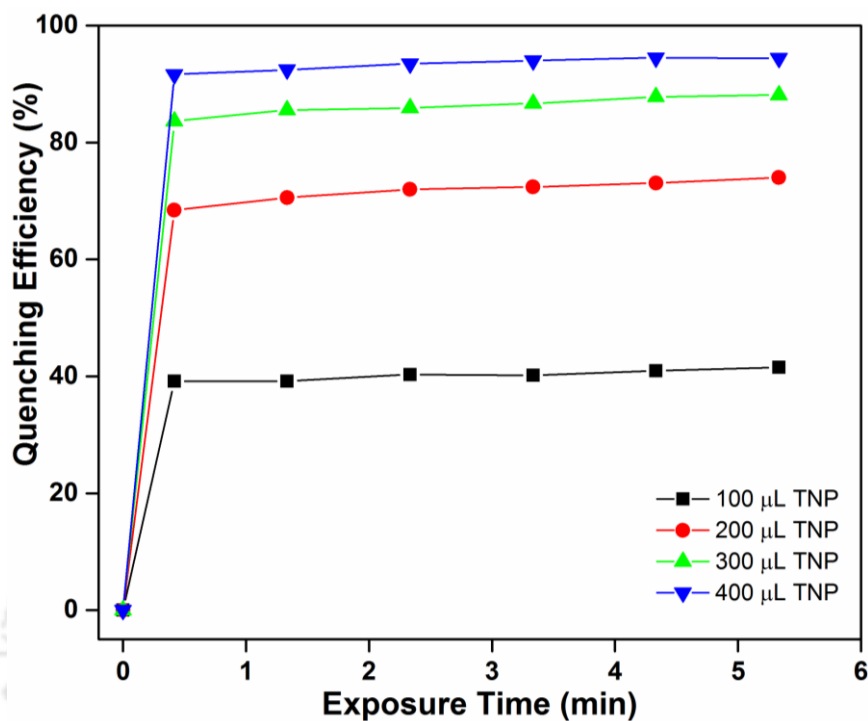


**Figure 3.18** Quenching efficiency as a function of exposure time at four different concentrations of TNP (100, 200, 300, and 400  $\mu\text{L}$  of 1 mM TNP solutions added to a 3 mL suspension of **1'** in ethanol).

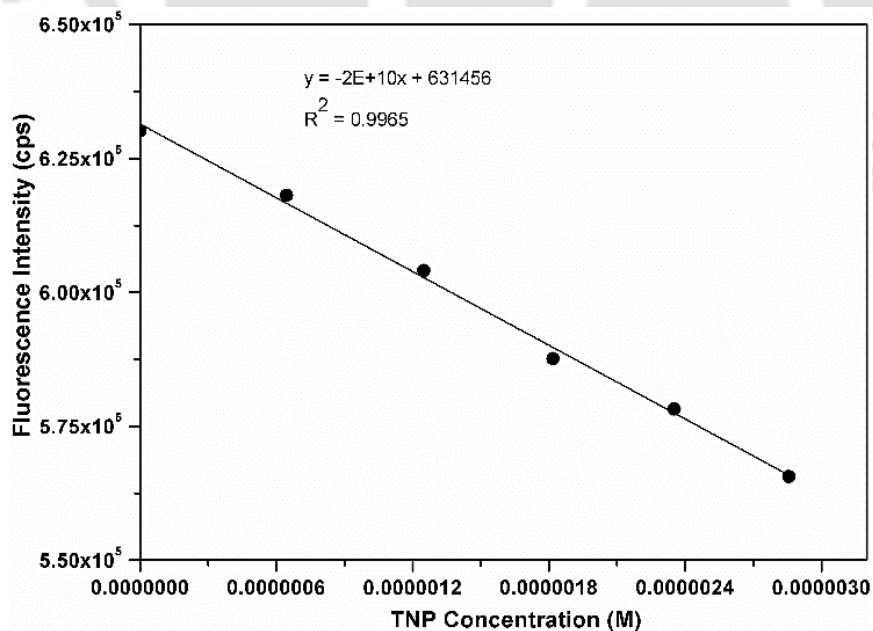


**Figure 3.19** Change in the fluorescence intensity of **1'** at different concentrations of TNP.

### 3.3.9 Mechanisms for the Detection of Nitroaromatic Explosives

The sensing mechanism was investigated for understanding the high selectivity of **1'** for TNP. For all the nitroaromatic explosives (NAEs), only surface adsorption is anticipated to occur due to the smaller pore apertures of the framework structure of **1'**. A photo-induced electron transfer mechanism can be proposed for the highly selective sensing of NAEs by **1'**.<sup>9-14</sup> Despite their extended framework structures, MOFs often bear definite band gap energies owing to the highly localized electronic structures (especially for MOFs with  $d^{10}$  metal ions).<sup>56</sup> Usually, the lowest unoccupied MOs (LUMOs) of the electron-deficient NAEs reside between the valence band (VB) and conduction band (CB) of the luminescent MOFs.<sup>57</sup> Efficient transfer of electrons can occur from the CB of **1'** to the LUMO of NAEs, leading to quenching of the fluorescence intensity upon excitation. The HOMO and LUMO orbital energies (Table 3.5) for the H<sub>2</sub>L ligand and the selected analytes are depicted in Figure 3.20. These values were calculated by the density functional theory (DFT) at B3LYP/6-31G\* accuracy level using Gaussian 09 package of programs<sup>58</sup>. Figure 3.7 reveals that the photoluminescence behaviour of **1'** is ligand-centred. The LUMO energy of the electron-rich H<sub>2</sub>L ligand was estimated to be -1.8757 eV, which is higher than those of the selected NAEs (-2.2213 to -3.898 eV).

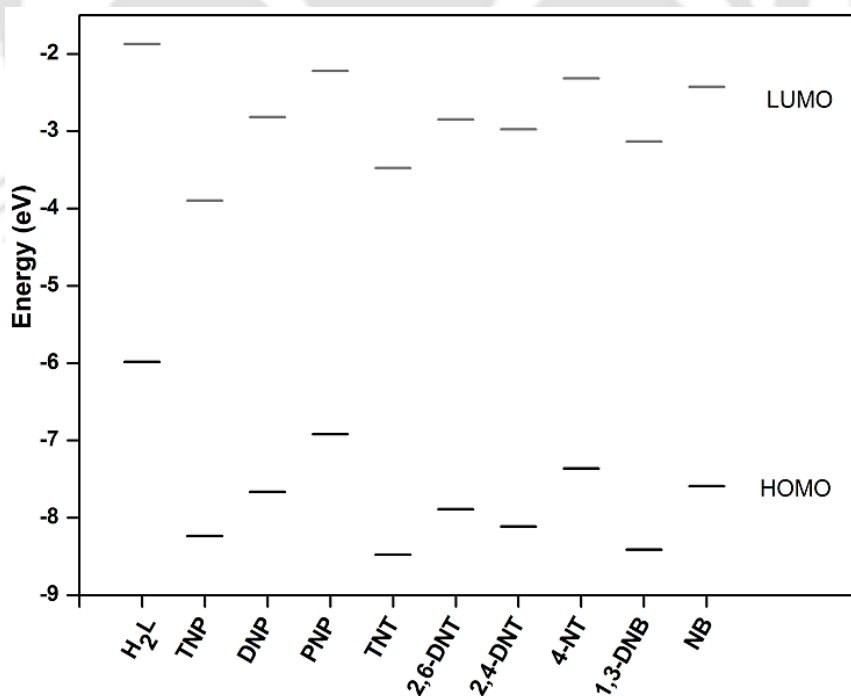


**Figure 3.20** HOMO and LUMO energies for H<sub>2</sub>L ligand and selected analytes.

These LUMO energy values indicate that the excited-state electron transfers from **1'** to the NAEs can take place efficiently. The calculated LUMO energy values of the analytes increase in the order: TNP < TNT < DNB < 2,4-DNT < 2,6-DNT < DNP < NB < 4-NT < PNP. The ease of electron transfer to the electron-deficient analytes should follow the opposite trend. Thus, the lowest LUMO energy value of TNP is in good agreement with the maximum quenching observed for this analyte. However, the order of experimental quenching efficiencies (i.e., TNP > PNP > DNP > TNT > 4-NT > 2,4-DNT > 2,6-DNT > 1,3-DNB > NB) is not completely in agreement with the LUMO energies of other NAEs. Therefore, it can be inferred that the photo-induced electron transfer is not the only mechanism for the observed quenching. Long-range energy transfer might also be operative in the quenching process.

**Table 3.5** HOMO and LUMO energy levels of H<sub>2</sub>L ligand and analytes calculated by density functional theory (DFT) at B3LYP/6-31G\* accuracy level using Gaussian 09 package of programs<sup>58</sup>.

Analytes	HOMO (eV)	LUMO (eV)	Band Gap (eV)
H <sub>2</sub> L	-5.9865	-1.8757	4.1108
TNP	-8.2374	-3.898	4.3394
DNP	-7.6644	-2.8202	4.8442
PNP	-6.9207	-2.2213	4.6994
TNT	-8.4793	-3.479	5.0003
4-NT	-7.3626	-2.3171	5.0455
2,4-DNT	-8.1131	-2.9769	5.1362
2,6-DNT	-7.8913	-2.8501	5.0412
1,3-DNB	-8.4129	-3.135	5.2779
NB	-7.5917	-2.4294	5.1623

Resonance energy transfer from the fluorophore of the organic ligand to non-emissive analytes can take place if the absorption bands of the analytes have an efficient overlap with the emission band of the fluorophore. The effective energy transfer increases the fluorescence quenching efficiency of the analyte. It is noticed from Figure 3.21 that the absorption band of TNP has a large overlap with the emission band (450 nm) of **1'**, whereas other analytes have less or almost no overlap. The maximum overlap between the absorption band of TNP and the emission band of **1'** (as compared to other analytes) is in agreement with the highest quenching efficiency of TNP. From the spectral overlap, it can be proposed that the fluorescence quenching by TNP occurs by an energy transfer mechanism. This mechanism can be also supported by the red shift of the fluorescent intensity (Figure 3.9) observed during gradual addition of TNP solution to a suspension of **1'**. Evidence in support of energy transfer mechanism can also be obtained from the non-linearity of the S-V plots (inset of Figure 3.16) at higher concentrations.

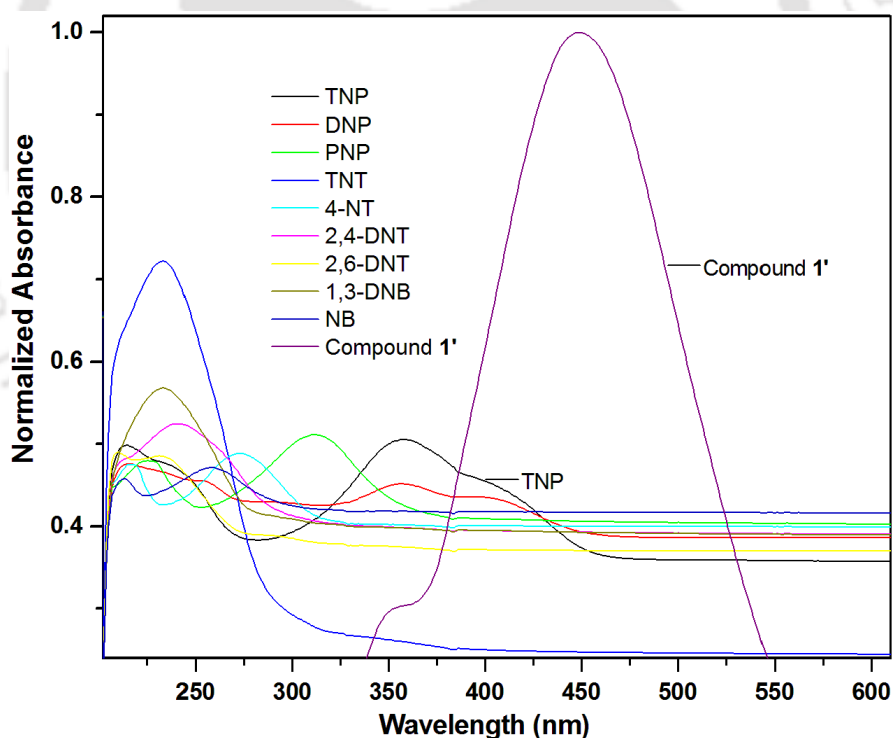


**Figure 3.21** Spectral overlap between the absorption spectra of the analytes and emission spectrum of **1'** in ethanol.

The highest quenching efficiency of TNP may also be related to the strong electrostatic interactions between the Lewis basic amide group of H<sub>2</sub>L ligand and the highly acidic hydroxyl group of TNP.<sup>19</sup> The presence of amide group in H<sub>2</sub>L ligand enhances the surface area of interaction of **1'** with the acidic hydroxyl group of TNP via hydrogen bonding and ionic interaction. This increase in surface interaction between the host and the analyte leads to a turn-off fluorescence response for TNP.<sup>59, 60</sup> Other analytes (except DNP and PNP) do not possess any acidic hydroxyl group in order to interact with the free basic amide sites of the ligand. Thus, the above-mentioned electrostatic interactions are absent in the other analytes, resulting in significantly lower quenching performances. Overall, the combined effects of energy and electron transfer mechanisms as well as electrostatic interactions may be ascribed for the high selectivity of **1'** for the detection of TNP.

### 3.4 CONCLUSIONS

A strongly fluorescent 3D Cd(II)-based MOF (**1**) incorporating a highly  $\pi$ -conjugated amide-functionalized ditopic tetrazolate-based organic ligand has been successfully synthesized under solvothermal conditions. The activated compound (**1'**) can selectively detect TNP with a very high rate of response, as verified by the steady-state fluorescence titration experiments. The selective detection of TNP in presence of other potentially interfering nitroaromatic explosives has also been demonstrated. The detection limit of **1'** for the sensing of TNP was estimated to be  $1.87 \times 10^{-7}$  M (42.84 ppb), which is comparable with other MOF-based fluorescence sensors reported until today. The recyclability experiments imply high photostability and reusability of **1'** for long-term in-field detection of nitroaromatic explosive materials. The combination of experimental and theoretical results provides indications in favour of both energy and electron transfer mechanisms for the highest quenching efficiency of TNP. Moreover, the enhanced selectivity of **1'** for sensing of TNP can be intuitively attributed to the existence of electrostatic interactions between the N-H moiety of the ligand and the hydroxyl group of TNP. The outstanding sensing performance renders the material as a promising sensing device for the practical detection of TNP.

### 3.5 REFERENCES

1. Y. Salinas, R. Martinez-Manez, M. D. Marcos, F. Sancenon, A. M. Costero, M. Parraad and S. Gil, *Chem. Soc. Rev.*, 2012, **41**, 1261.

2. D. T. McQuade, A. E. Pullen and T. M. Swager, *Chem. Rev.*, 2000, **100**, 2537.
3. S. W. Thomas, G. D. Joly and T. M. Swager, *Chem. Rev.*, 2007, **107**, 1339.
4. M. E. Germain and M. J. Knapp, *Chem. Soc. Rev.*, 2009, **38**, 2543.
5. G. He, H. Peng, T. Liu, M. Yang, Y. Zhang and Y. Fang, *J. Mater. Chem.*, 2009, **19**, 7347.
6. Y. Peng, A.-J. Zhang, M. Dong and Y.-W. Wang, *Chem. Commun*, 2011, **47**, 4505.
7. D. Gao, Z. Wang, B. Liu, L. Ni, M. Wu and Z. Zhang, *Anal. Chem.*, 2008, **80**, 8545.
8. Y. Jiang, H. Zhao, N. Zhu, Y. Lin, P. Yu and L. Mao, *Angew. Chem., Int. Ed.*, 2008, **47**, 8601.
9. K. Müller-Buschbaum, F. Beuerle and C. Feldmann, *Microporous Mesoporous Mater.*, 2015, **216**, 171.
10. Z. Hu, B. J. Deibert and J. Li, *Chem. Soc. Rev.*, 2014, **43**, 5815.
11. M. D. Allendorf, C. A. Bauer, R. K. Bhakta and R. J. T. Houk, *Chem. Soc. Rev.*, 2009, **38**, 1330.
12. Y. Cui, Y. Yue, G. Qian and B. Chen, *Chem. Rev.*, 2012, **112**, 1126.
13. L. E. Kreno, K. Leong, O. K. Farha, M. Allendorf, R. P. Van Duyne and J. T. Hupp, *Chem. Rev.*, 2012, **112**, 1105.
14. Y. Cui, B. Chen and G. Qian, *Coord. Chem. Rev.*, 2014, **76**, 273.
15. L. V. Meyer, F. Schonfeld and K. Muller-Buschbaum, *Chem. Commun*, 2014, **50**, 8093.
16. B. Chen, S. Xiang and G. Qian, *Acc. Chem. Res.*, 2010, **43**, 1115.
17. J. Lei, R. Qian, P. Ling, L. Cui and H. Ju, *Trends Analyt. Chem.*, 2014, **58**, 71.
18. S. S. Nagarkar, A. V. Desai and S. K. Ghosh, *Chem. Commun.*, 2014, **50**, 8915.
19. S. S. Nagarkar, B. Joarder, A. K. Chaudhari, S. Mukherjee and S. K. Ghosh, *Angew. Chem. Int. Ed.*, 2013, **52**, 2881.
20. S. S. Nagarkar, A. V. Desai, P. Samanta and S. K. Ghosh, *Dalton Trans.*, 2015, **44**, 15175.
21. B. Joarder, A. V. Desai, P. Samanta, S. Mukherjee and S. K. Ghosh, *Chem. Eur. J.*, 2015, **21**, 965.
22. C. Zhang, L. Sun, Y. Yan, J. Li, X. Song, Y. Liu and Z. Liang, *Dalton Trans.*, 2015, **44**, 230.
23. Y.-N. Gong, L. Jiang and T.-B. Lu, *Chem. Commun.*, 2013, **49**, 11113.
24. X. H. Zhou, L. Li, H. H. Li, A. Li, T. Yang and W. Huang, *Dalton Trans.*, 2013, **42**, 12403.

25. L. Zhao, J. Ye, W. Li, R. F. Bogale, B. Wang, W. Gong and G. Ning, *Inorg. Chem. Commun.*, 2014, **46**, 212.
26. J.-D. Xiao, L.-G. Qiu, F. Ke, Y.-P. Yuan, G.-S. Xu, Y.-M. Wang and X. Jiang, *J. Mater. Chem. A*, 2013, **1**, 8745.
27. F. Makovec, W. Peris, L. Revel, R. Giovanetti, D. Redaelli and L. C. Rovati, *J. Med. Chem.*, 1992, **35**, 3633.
28. G. M. Sheldrick, *Acta Crystallogr. Sect. A*, 2008, **64**, 112.
29. S. Jeong, X. Song, S. Jeong, M. Oh, X. Liu, D. Kim, D. Moon and M. S. Lah, *Inorg. Chem.*, 2011, **50**, 12133.
30. H. Zhao, Z.-R. Qu, H.-Y. Ye and R.-G. Xiong, *Chem. Soc. Rev.*, 2008, **37**, 84.
31. X.-S. Wang, Y.-Z. Tang, X.-F. Huang, Z.-R. Qu, C.-M. Che, P. W. H. Chan and R.-G. Xiong, *Inorg. Chem.*, 2005, **44**, 5278.
32. X.-S. Wang, Y.-Z. Tang and R.-G. Xiong, *Chin. J. Inorg. Chem.*, 2005, **21**, 1025.
33. Y.-T. Yang, F.-H. Zhao, Y.-X. Che and J.-M. Zheng, *Inorg. Chem. Commun.*, 2011, **14**, 1855.
34. Y.-Q. Liu, G.-J. Ren, Y.-H. Zhang, J. Xu and X.-H. Bu, *Dalton Trans.*, 2015, **44**, 20361.
35. A. J. Calahorra, G. Zaragoza, A. S.-Castillo, J. M. Seco and A. R.-Diéguez, *Polyhedron*, 2014, **80**, 228.
36. D.-C. Zhong, Y.-Q. Wen, J.-H. Deng, X.-Z. Luo, Y.-N. Gong and T.-B. Lu, *Angew. Chem. Int. Ed.*, 2015, **54**, 11795.
37. R.-G. Xiong, X. Xue, H. Zhao, X.-Z. You, B. F. Abrahams and Z. Xue, *Angew. Chem. Int. Ed.*, 2002, **41**, 3800.
38. L. Sun, L. Ma, J.-B. Cai, L. Liang and H. Deng, *CrystEngComm*, 2012, **14**, 890.
39. P. Pachfule and R. Banerjee, *Cryst. Growth Des.*, 2011, **11**, 5176.
40. J.-D. Lin, S.-H. Wang, L.-Z. Cai, F.-K. Zheng, G.-C. Guo and J.-S. Huang, *CrystEngComm*, 2013, **15**, 903.
41. T.-W. Tseng, T.-T. Luo, S.-Y. Chen, C.-C. Su, K.-M. Chi and K.-L. Lu, *Cryst. Growth Des.*, 2013, **13**, 510.
42. X. He, C.-Z. Lu and D.-Q. Yuan, *Inorg. Chem.*, 2006, **45**, 5760.
43. C. S. Collins, D. Sun, W. Liu, J.-L. Zuo and H.-C. Zhou, *J. Mol. Struct.*, 2008, **890**, 163.
44. Y.-L. Yao, L. Xue, Y.-X. Che and J.-M. Zheng, *Cryst. Growth Des.*, 2009, **9**, 606.

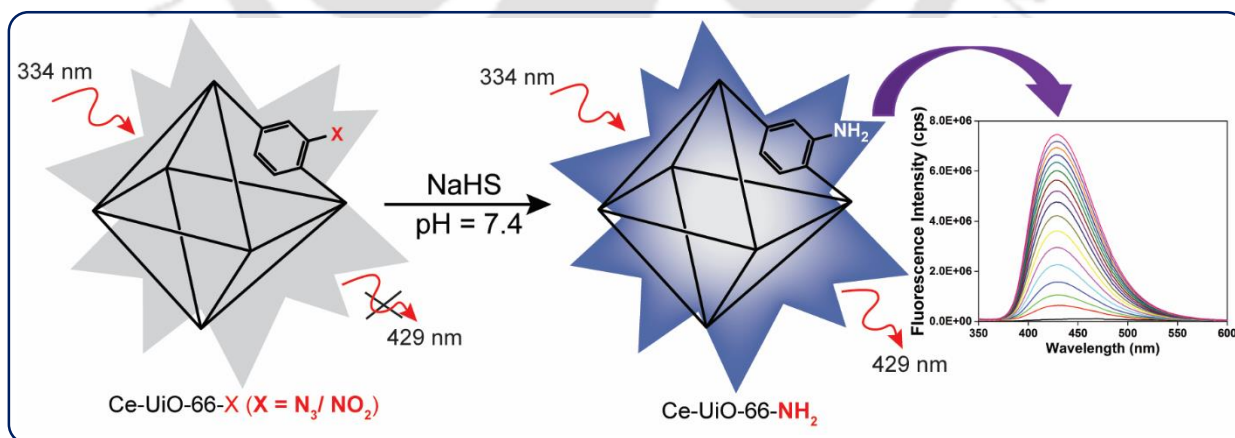
45. K. Darling, W. Ouellette, S. Pellizzeri, T. Smith, J. Vargas, S. Tomaszfski, C. J. O'Connor and J. Zubieta, *Inorganica Chimica Acta*, 2012, **392**, 417.
46. H. Xiang, W.-Y. Gao, D.-C. Zhong, L. Jiang and T.-B. Lu, *CrystEngComm*, 2011, **13**, 5825.
47. A. L. Spek, *Acta Crystallogr., Sect. D*, 2009, **65**, 148.
48. J. Světlík, A. Martvoň and J. Leško, *Chem. Zvesti.*, 1979, **33**, 521.
49. N. A. Matveeva, N. I. Suschko, N. I. Makarevich, P. N. Gaponik, O. A. Ivashkevich and A. O. Koren, *J. Appl. Spectrosc.*, 1992, **57**, 845.
50. G.-Y. Wang, L.-L. Yang, Y. Li, H. Song, W.-J. Ruan, Z. Chang and X.-H. Bu, *Dalton Trans.*, 2013, **42**, 12865.
51. K. S. Asha, K. Bhattacharyya and S. Mandal, *J. Mater. Chem. C*, 2014, **2**, 10073.
52. B. Gole, A. K. Bar and P. S. Mukherjee, *Chem. Eur. J.*, 2014, **20**, 13321.
53. B. Gole, A. K. Bar and P. S. Mukherjee, *Chem. Eur. J.*, 2014, **20**, 2276.
54. K. S. Asha, K. Bhattacharyya and S. Mandal, *J. Mater. Chem. C*, 2014, **2**, 10073.
55. S. S. Nagarkar, A. V. Desai, P. Samanta and S. K. Ghosh, *Dalton Trans.*, 2015, **44**, 15175.
56. Special issue on MOFs: *Chem. Rev.*, 2012, **112**, 673.
57. S. Pramanik, C. Zheng, X. Zhang, T. J. Emge and J. Li, *J. Am. Chem. Soc.*, 2011, **133**, 4153.
58. M. J. Frisch, G. W. Trucks, H. B. Schlegel, G. E. Scuseria, M. A. Robb, J. R. Cheeseman, G. Scalmani, V. Barone, B. Mennucci, G. A. Petersson, H. Nakatsuji, M. Caricato, X. Li, H. P. Hratchian, A. F. Izmaylov, J. Bloino, G. Zheng, J. L. Sonnenberg, M. Hada, M. Ehara, K. Toyota, R. Fukuda, J. Hasegawa, M. Ishida, T. Nakajima, Y. Honda, O. Kitao, H. Nakai, T. Vreven, J. J. A. Montgomery, J. E. Peralta, F. Ogliaro, M. Bearpark, J. J. Heyd, E. Brothers, K. N. Kudin, V. N. Staroverov, R. Kobayashi, J. Normand, K. Raghavachari, A. Rendell, J. C. Burant, S. S. Iyengar, J. Tomasi, M. Cossi, N. Rega, J. M. Millam, M. Klene, J. E. Knox, J. B. Cross, V. Bakken, C. Adamo, J. Jaramillo, R. Gomperts, R. E. Stratmann, O. Yazyev, A. J. Austin, R. Cammi, C. Pomelli, J. W. Ochterski, R. L. Martin, K. Morokuma, V. G. Zakrzewski, G. A. Voth, P. Salvador, J. J. Dannenberg, S. Dapprich, A. D. Daniels, O. Farkas, J. B. Foresman, J. V. Ortiz, J. Cioslowski and D. J. Fox, *Gaussian 09, Revision A.1*, Gaussian, Inc., Wallingford CT, 2009.

59. S. Mukherjee, A. V. Desai, B. Manna, A. I. Inamdar and S. K. Ghosh, *Cryst. Growth Des.*, 2015, **15**, 4627.
60. P. Vishnoi, M. G. Walawalkar, S. Sen, A. Datta, G. N. Patwari and R. Murugavel, *Phys. Chem. Chem. Phys.*, 2014, **16**, 10651.



## Cerium Based Azide- and Nitro-Functionalized UiO-66 Frameworks as Fluorescent Turn-On Probes for the Sensing of H<sub>2</sub>S

This chapter presents a new and an existing Ce(IV)-based MOF with UiO-66 framework topology for the first time as fluorescence turn-on probes for the detection of H<sub>2</sub>S under physiological conditions. Both compounds have demonstrated promising potentials towards highly selective, sensitive and fast detection of H<sub>2</sub>S. Owing to their extraordinary selectivity towards sensing of H<sub>2</sub>S even in the presence of other potentially interfering biomolecules, these compounds could be promising candidates for the real-time monitoring of H<sub>2</sub>S in biological systems. Besides the rapid, selective and sensitive detection of H<sub>2</sub>S, both of these compounds can effectively adsorb considerable amounts CO<sub>2</sub> and hence could be an excellent material in the field of CO<sub>2</sub> capture.

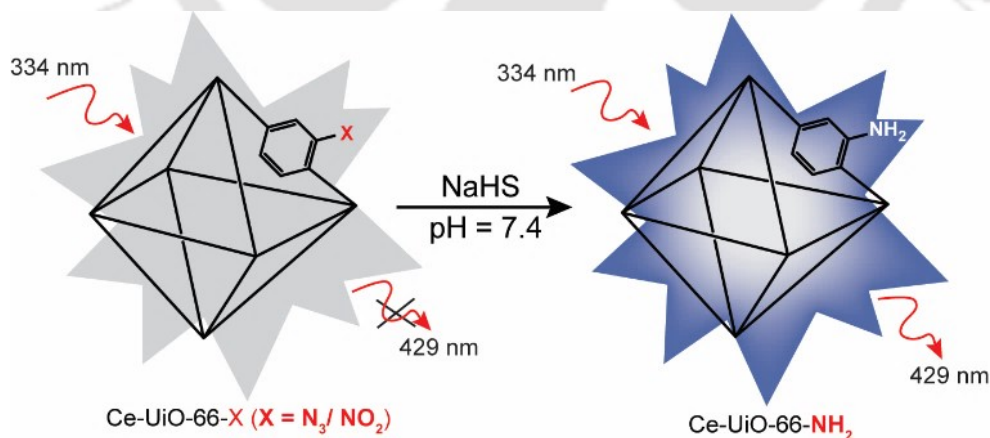


## 4.1 INTRODUCTION

Hydrogen sulphide ( $\text{H}_2\text{S}$ ), a colorless stinky gas present in the environment and industrial processing,<sup>1, 2</sup> has been usually considered as a toxic gas. The overexposure to  $\text{H}_2\text{S}$  causes lethal effect on living systems due to its catastrophic nature.<sup>1, 3</sup> However, after nitric oxide (NO) and carbon monoxide (CO),  $\text{H}_2\text{S}$  is identified as the third endogenous gaseous signaling molecule.<sup>4-8</sup> This third endogenous gas, produced by enzymatic reactions,<sup>9</sup> is involved in various physiological processes such as modulation of blood pressure,<sup>10</sup> neurotransmission,<sup>11</sup> anti-inflammatory action,<sup>12</sup> antioxidation,<sup>13</sup> angiogenesis,<sup>14</sup> and apoptosis<sup>15</sup>. Furthermore,  $\text{H}_2\text{S}$  also provides protection against ischemia/reperfusion injury,<sup>16</sup> but failure of  $\text{H}_2\text{S}$  homeostasis could be a key reason for many pathological processes in human body such as Alzheimer's disease,<sup>17</sup> diabetes,<sup>18</sup> Down's syndrome,<sup>19</sup> liver cirrhosis,<sup>20</sup> and cancer<sup>21</sup>. Due to its significant role in living systems, controlling of  $\text{H}_2\text{S}$  level is a vital task which makes it a potential target in the diagnostic and treatment of these diseases. As a consequence, detection of  $\text{H}_2\text{S}$  in living systems for investigation and better understanding of its physiological and pathological functions is very essential and has become a crucial subject of scientific research. Several traditional methods have been applied to monitor the  $\text{H}_2\text{S}$  level including gas chromatography,<sup>22</sup> colorimetry,<sup>23, 24</sup> electrochemical analysis,<sup>25</sup> and metal-induced sulphide precipitation<sup>26</sup>. Although, these traditional techniques have shown remarkable achievement in  $\text{H}_2\text{S}$  detection but prerequisite post-mortem processing or even destruction of living cells or tissues in order to perform the analysis prevent these methods from in-situ detection of  $\text{H}_2\text{S}$  in living bio systems. Moreover, due to its high diffusible and reactive properties, selective and real-time detection of endogenous  $\text{H}_2\text{S}$  is still a major challenge and depends on sample preparation and detection method<sup>27, 28</sup>. Owing to its high sensitivity, simplicity, short response time, non-invasive nature, real-time monitoring and easy sample preparation, fluorescence-based detection methods have been gaining notable attention for the selective and precise detection of endogenous  $\text{H}_2\text{S}$ .<sup>29, 30</sup> Notably, change in fluorescence intensity in response to  $\text{H}_2\text{S}$ , high selectivity over other interfering biological substances, rapid interaction (within minutes or even seconds) with  $\text{H}_2\text{S}$  and cell permeability are the primary requirements of an ideal fluorescent probe.<sup>27, 28</sup> In particular, fluorescence turn-on probes are always favored to avoid false detection and enhanced signal to noise ratio as the detection takes place relative to dark background.<sup>8</sup> Indeed, several turn-on type

fluorescent probes for the rapid detection of H<sub>2</sub>S have been reported, however, the development of an efficient fluorescent probe combining all these properties is a challenging task. Recently, fluorescent turn-on probes based on the reduction of hydroxyl amide, nitro and azide groups have attracted much more attention towards the fast and selective detection of H<sub>2</sub>S.<sup>27, 31-44</sup>

The application of MOF-based fluorescent turn-on probes with enhanced sensitivity over other traditional methods would be a promising strategy for the rapid detection and real-time monitoring of H<sub>2</sub>S. Only a few MOFs with nitro and azide functionalities have been reported till date as fluorescent turn-on probes for the selective detection of H<sub>2</sub>S under physiological conditions.<sup>32, 33, 44</sup> Indeed, cerium is the most abundant of the rare earth elements and has various applications including catalysis, yet cerium-based MOFs are still rare. Only two Ce(IV)-based MOFs (one for CO<sub>2</sub> sorption and another for catalysis),<sup>45, 46</sup> and three luminescent Ce(III)-based MOFs<sup>47-49</sup> have been reported till date. Herein, we present a new azide-functionalized and an existing nitro-functionalized<sup>46</sup> Ce(IV)-based MOF as fluorescent turn-on probes for detection of H<sub>2</sub>S under physiological conditions. We have also compared the detection performances of the two Ce-based MOFs with their Zr-based counterparts. Since H<sub>2</sub>S-facilitated reduction of azide and nitro groups to amine functionalities (Scheme 4.1) is a widespread practice<sup>50-53</sup> for designing fluorescent turn-on probes, we aim to use NaHS as a source of H<sub>2</sub>S in this present work.



**Scheme 4.1** Fluorescent turn-on probes resulting from the NaHS-mediated reduction of Ce-UiO-66-X (X = N<sub>3</sub> or NO<sub>2</sub>) MOFs to Ce-UiO-66-NH<sub>2</sub>.

## 4.2 EXPERIMENTAL SECTION

### 4.2.1 Materials and General Methods

Synthesis of H<sub>2</sub>BDC-N<sub>3</sub> linker was carried out by following the previously published procedure.<sup>54</sup> Zr-UiO-66-N<sub>3</sub><sup>55</sup> and Zr-UiO-66-NO<sub>2</sub><sup>32</sup> MOFs were prepared by following the earlier reported procedures. All other chemicals were commercially available and used without further purification. Fourier transform infrared (FT-IR) spectra were recorded in the region of 440-4000 cm<sup>-1</sup> with a Perkin Elmer Spectrum Two FT-IR spectrometer. The following indications are used to characterize absorption bands: very strong (vs), strong (s), medium (m), weak (w), shoulder (sh) and broad (br). Thermogravimetric analyses (TGA) were performed with a SDT Q600 V20.9 Build 20 thermogravimetric analyzer in a temperature range of 25-650 °C under air atmosphere at a heating rate of 5 °C min<sup>-1</sup>. Ambient temperature X-Ray powder diffraction (XRPD) patterns were recorded on a Bruker D2 Phaser X-ray diffractometer operated at 30 kV, 10 mA using Cu-K $\alpha$  ( $\lambda = 1.5406 \text{ \AA}$ ). Lattice parameters were determined by using the DICVOL program<sup>56</sup> and refined by using STOE's WinXPow<sup>57</sup> software package. The nitrogen sorption isotherms up to 1 bar were measured using a Quantachrome Autosorb iQ-MP gas sorption analyzer at -196 °C. The CO<sub>2</sub> adsorption up to 1 bar was measured using a Quantachrome iSorb-HP gas sorption analyzer at 0 °C. Prior to the sorption experiments, the compounds were degassed at 120 °C for 12 h under dynamic vacuum. The UV-Vis absorption spectra in solution were recorded with a PerkinElmer LAMBDA 750 UV-Vis spectrophotometer. Fluorescence emission studies were carried out with a HORIBA JOBIN YVON Fluoromax-4 spectrofluorometer.

### 4.2.2 Synthesis of Ce-UiO-66-N<sub>3</sub> (1-N<sub>3</sub>)

A mixture of H<sub>2</sub>BDC-N<sub>3</sub> linker (44 mg, 213  $\mu\text{mol}$ ) in DMF (1.2 mL) and an aqueous solution of ammonium cerium(IV) nitrate (400  $\mu\text{L}$ , 0.5333 M) was sealed in a glass tube and heated using an aluminium block heater under magnetic stirring at 100 °C for 15 min. The light yellow precipitate was first washed with DMF (2  $\times$  2 mL) and then with acetone (4  $\times$  2 mL). The resulting solid was dried at 70 °C for 1 h in a conventional oven. The yield was 37 mg. FT-IR (KBr, cm<sup>-1</sup>): 3428 (br), 2927 (w), 2425 (w), 2210 (w), 2120 (vs), 1654 (s), 1582 (s), 1493 (m),

1403 (sh), 1381 (vs), 1277 (m), 1158 (w), 1103 (w), 945 (w), 896 (w), 793 (sh), 766 (s), 656 (w), 594 (m), 531 (s).

#### 4.2.3 Synthesis of Ce-UiO-66-NO<sub>2</sub> (2-NO<sub>2</sub>)

A mixture of H<sub>2</sub>BDC-NO<sub>2</sub> linker (45 mg, 213  $\mu$ mol) in DMF (1.2 mL) and an aqueous solution of ammonium cerium(IV) nitrate (400  $\mu$ L, 0.5333 M) was sealed in a glass tube and heated using an aluminium block heater under magnetic stirring at 100 °C for 15 min. The yellow precipitate was first washed with DMF (2  $\times$  2 mL) and then with acetone (4  $\times$  2 mL). The resulting solid was dried at 70 °C for 1 h in a conventional oven. The yield was 34 mg. FT-IR (KBr, cm<sup>-1</sup>): 3428 (br), 2927 (w), 1650 (sh), 1590 (s), 1530 (sh), 1493 (m), 1392 (vs), 1255 (w), 1124 (w), 1062 (w), 924 (w), 821 (w), 780 (w), 717 (w), 670 (w), 580 (m), 518 (m).

#### 4.2.4 Activation of the Compounds

The as-synthesized materials were activated in two steps. In the first step, the as-synthesized compound (100 mg) was solvent-extracted in methanol (200 mL) for 24 h. In the second step, the methanol-exchanged forms of **1-N<sub>3</sub>** and **2-NO<sub>2</sub>** were heated at 90 and 120 °C under vacuum for 3 and 12 h, respectively. The thermally activated samples will be designated as **1'-N<sub>3</sub>** and **2'-NO<sub>2</sub>** hereafter.

#### 4.2.5 Preparation of the Medium for Fluorescence Studies

Solid HEPES (0.2383 g) was dissolved in deionized water (100 mL) and pH of the medium was adjusted to 7.4 by using 0.5 N NaOH solution.

#### 4.2.6 Fluorescence Titration Experiments

In order to perform the fluorescence titration measurements, each (0.5 mg) of **1'-N<sub>3</sub>** and **2'-NO<sub>2</sub>** (1.35  $\mu$ mol of -N<sub>3</sub> and -NO<sub>2</sub> functionalities, respectively) was suspended in 2 mL of HEPES buffer (10 mM, pH 7.4) inside a quartz cuvette. For all the fluorescence measurements, the excitation wavelength ( $\lambda_{\text{ex}}$ ) was 334 nm and the emission spectra were recorded in the range of 344-650 nm. For recording the fluorescent turn-on responses of **1'-N<sub>3</sub>** and **2'-NO<sub>2</sub>** towards H<sub>2</sub>S, NaHS (10 equivalents with respect to the azide and nitro functionalities in **1'-N<sub>3</sub>** and **2'-NO<sub>2</sub>**, respectively) was added to the suspension and fluorescence spectra were recorded at a regular time interval (60 s) till saturation. The concentrations of each probe and NaHS in the

resulting suspensions were 0.11 and 6.6 mM, respectively. Similar experiments were also performed by replacing NaHS with other analytes such as glutathione, cysteine, alanine, serine, NaCl, NaBr, NaI, NaNO<sub>2</sub> and NaNO<sub>3</sub>. Moreover, a comparative fluorescence titration study was performed with Zr-based azide- and nitro-functionalized UiO-66 MOFs for revealing the effect of metal ions on H<sub>2</sub>S detection.

## 4.3 RESULTS AND DISCUSSIONS

### 4.3.1 Synthesis and Characterization

Both **1-N<sub>3</sub>** and **2-NO<sub>2</sub>** were synthesized by using similar synthetic procedures reported formerly for Ce-UiO-66-X MOFs.<sup>46</sup> The solvothermal reaction (under magnetic stirring at 100 °C for 15 min) of a mixture containing an aqueous solution of ammonium cerium(IV) nitrate and a solution of H<sub>2</sub>BDC-N<sub>3</sub> (for **1-N<sub>3</sub>**) or H<sub>2</sub>BDC-NO<sub>2</sub> (for **1-NO<sub>2</sub>**) linker in DMF resulted in light yellow crystalline solids of the title compounds.

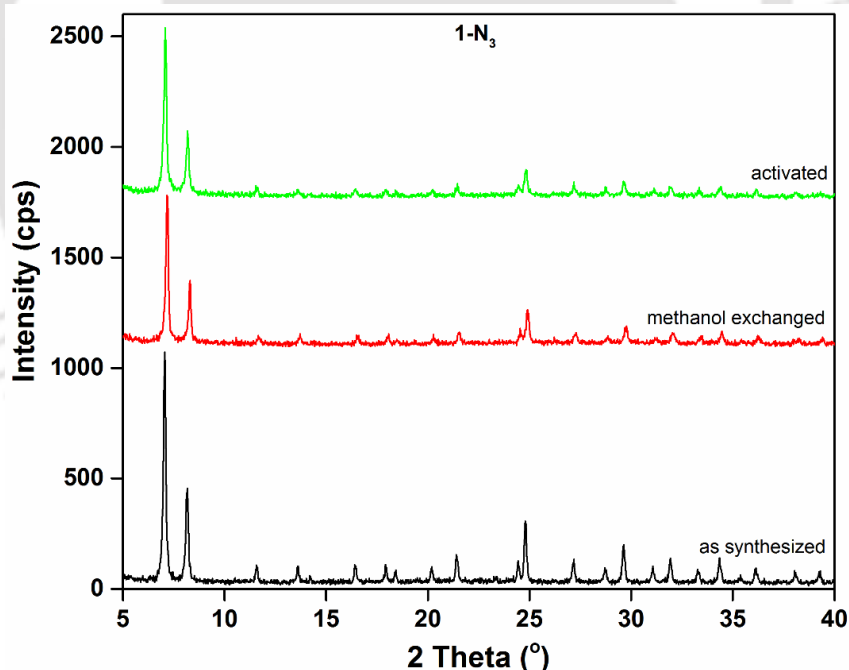


**Figure 4.1** XRPD patterns of **1-N<sub>3</sub>** in different forms: as-synthesized (black), methanol-exchanged (red) and activated at 90 °C (green).

The guest molecules encapsulated within the pores of the as-synthesized samples of **1-N<sub>3</sub>** and **2-NO<sub>2</sub>** were removed in a two-step activation procedure. At first, the occluded molecules

entrapped inside the pores were exchanged with easily removable methanol molecules by using the Soxhlet extraction process. In the second step, the methanol-exchanged samples were heated under vacuum to remove the methanol molecules from the pores. In this way, the thermally activated forms of the two compounds were achieved. Both as-synthesized and thermally activated forms of the compounds exhibited similar XRPD patterns (Figures 4.1 and 4.2). Thus, both compounds retained their structural integrity after the activation procedures.

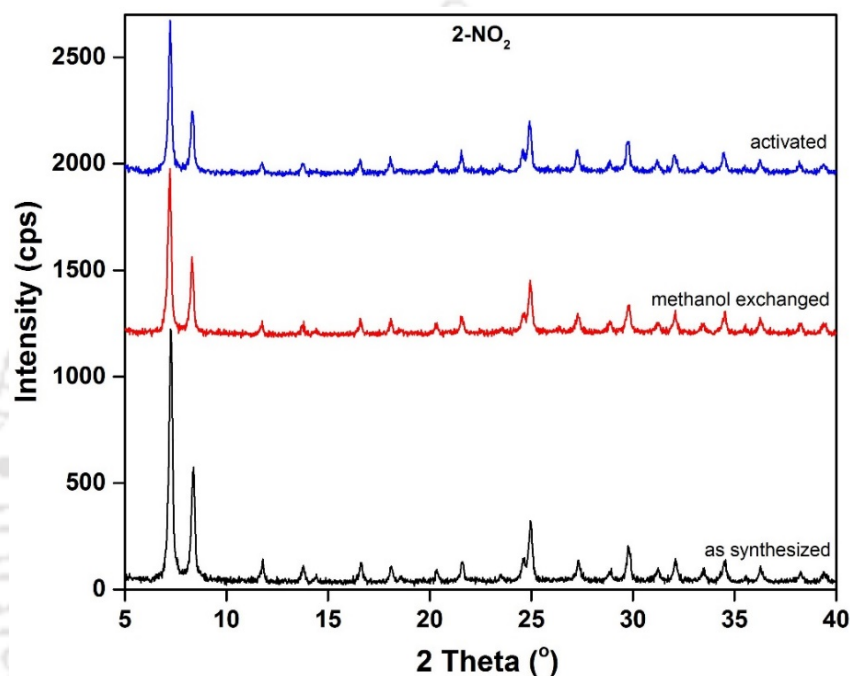


**Figure 4.2** XRPD patterns of 2-NO<sub>2</sub> in different forms: as-synthesized (black), methanol-exchanged (red) and activated at 90 °C (blue).

In the FT-IR spectra of the as-synthesized and thermally activated samples of 1-N<sub>3</sub> and 2-NO<sub>2</sub>, the asymmetric and symmetric –CO<sub>2</sub> stretching vibrations of the coordinated linker molecules are located in the regions 1580-1590 and 1380-1390 cm<sup>-1</sup>, respectively (Figures 4.3 and 4.4). The appearance of a strong peak at 2120 cm<sup>-1</sup> in the FT-IR spectra of the as-synthesized and activated samples of 1-N<sub>3</sub> can be assigned to the stretching of the azide functional group attached with the H<sub>2</sub>BDC-N<sub>3</sub> linker molecule (Figure 4.3).<sup>58</sup>

The experimental XRPD patterns of the as-synthesized samples of structurally related 1-N<sub>3</sub> and 2-NO<sub>2</sub> (Figure 4.5) are very similar, as expected. The unit cell parameters (Table 4.1) derived from the XRPD patterns are similar to the recently reported, isostructural Ce-UiO-66

material.<sup>46</sup> The values of the lattice parameters suggest that both compounds possess cubic structures. As described previously,<sup>46</sup> the 3D cubic frameworks of both compounds are constructed from  $[\text{Ce}_6\text{O}_4(\text{OH})_4]^{12+}$  building units, which are interconnected by the carboxylate groups of twelve linker molecules. The resulting microporous frameworks comprise larger octahedral (free diameter  $\sim 11 \text{ \AA}$ ) and smaller tetrahedral (free diameter  $\sim 8 \text{ \AA}$ ) cages.

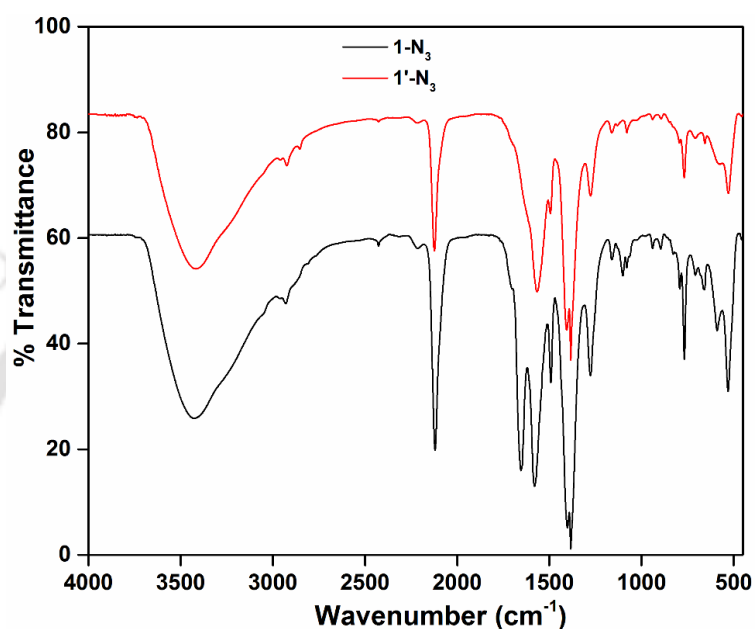


**Figure 4.3** FT-IR spectra of as-synthesized  $1\text{-N}_3$  (black) and activated  $1'\text{-N}_3$  (red).

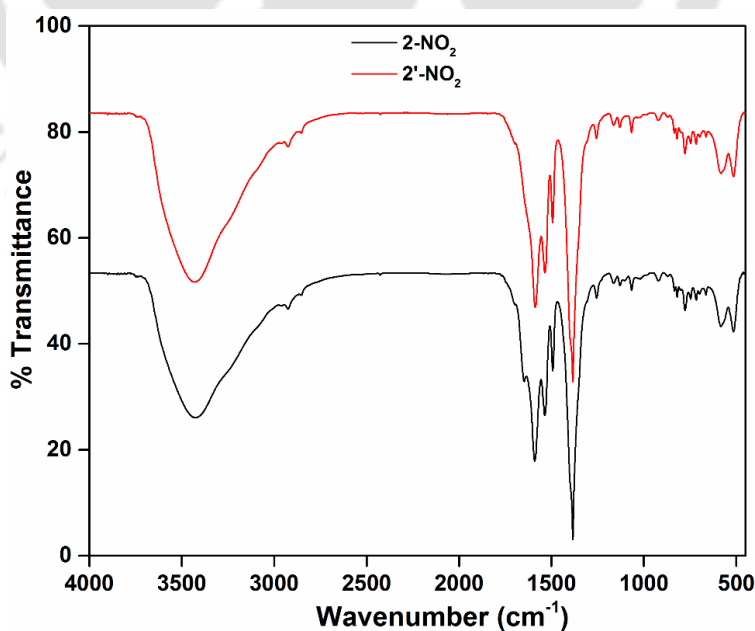


**Figure 4.4** FT-IR spectra of as-synthesized  $2\text{-NO}_2$  (black) and activated  $2'\text{-NO}_2$  (red).

**Table 4.1** Unit cell parameters of as-synthesized **1-N<sub>3</sub>** and **2-NO<sub>2</sub>** having cubic unit cells. The values are compared with those of the formerly reported Ce-UiO-66 and Ce-UiO-66-NO<sub>2</sub>.<sup>46</sup>

Compound	$a$ (Å)	$V$ (Å <sup>3</sup> )
<b>1-N<sub>3</sub></b>	21.492(12)	9927.5(6)
<b>1-NO<sub>2</sub></b>	21.464(7)	9889.4(13)
Ce-UiO-66	21.4727(3)	9900.6(4)
Ce-UiO-66-NO <sub>2</sub>	21.5194(2)	-

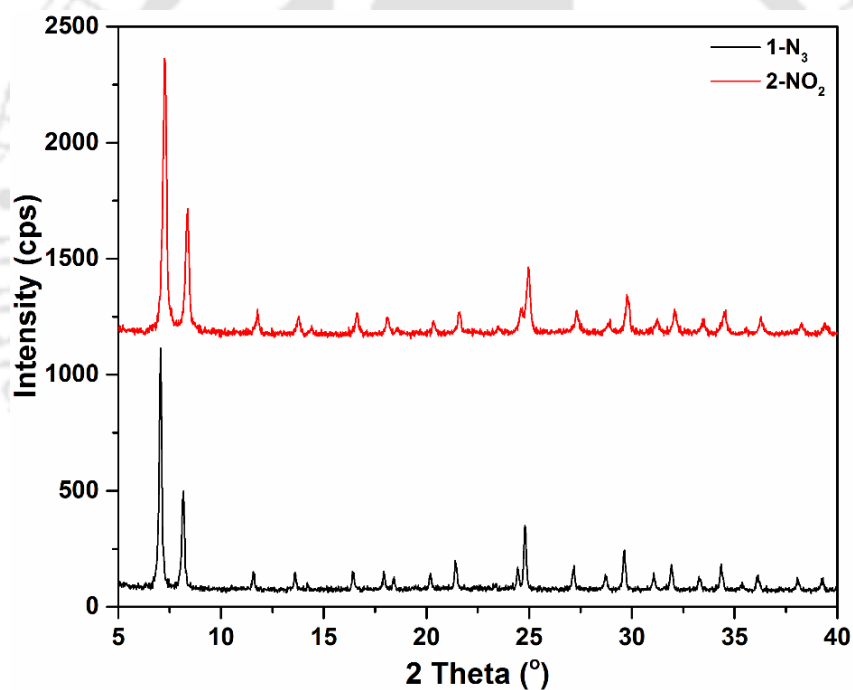


**Figure 4.5** Experimental XRPD patterns of the as-synthesized samples of **1-N<sub>3</sub>** (black) and **2-NO<sub>2</sub>** (red) measured at room temperature.

### 4.3.2 Thermal and Chemical Stability

In order to examine the thermal stability of **1-N<sub>3</sub>** and **2-NO<sub>2</sub>**, thermogravimetric analyses (TGA) were performed under air atmosphere in the temperature range of 25-650 °C at a heating rate of 5 °C min<sup>-1</sup>. The TG curves of the as-synthesized samples of **1-N<sub>3</sub>** and **2-NO<sub>2</sub>** (Figures 4.6 and 4.7) disclose that the materials are stable up to 200 and 300 °C, respectively. Therefore, **2-**

$\text{NO}_2$  has higher thermal stability as compared to  $1\text{-N}_3$ . The thermal stability of  $2\text{-NO}_2$  is same as that of the recently reported  $\text{Ce-UiO-66-NO}_2$ .<sup>65</sup>

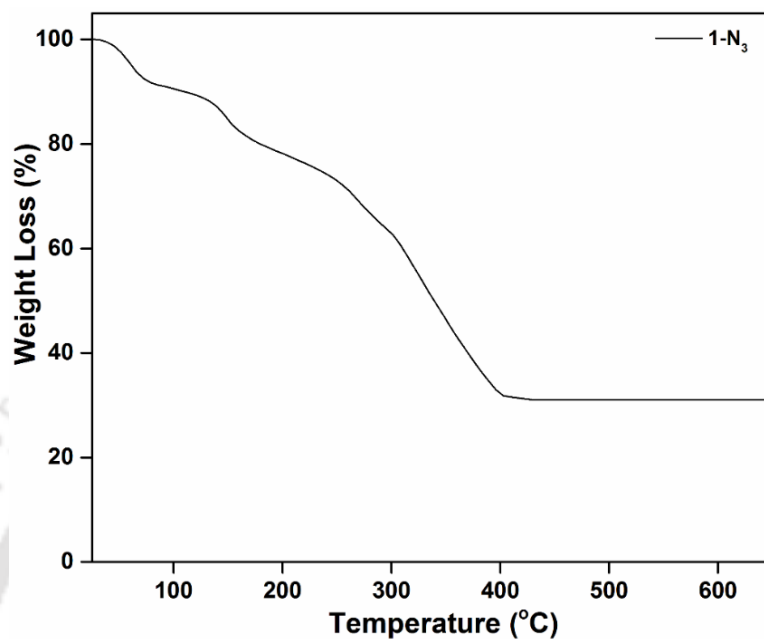


**Figure 4.6** TG curve of as-synthesized  $1\text{-N}_3$  recorded in an air atmosphere in the temperature range of 25-650 °C with a heating rate of 5 °C min<sup>-1</sup>.

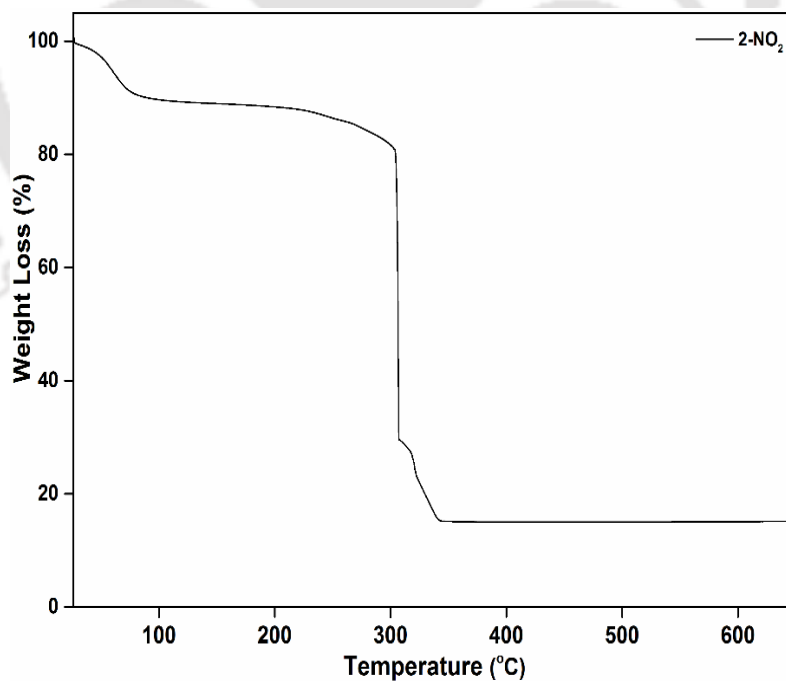


**Figure 4.7** TG curve of as-synthesized  $2\text{-NO}_2$  recorded in an air atmosphere in the temperature range of 25-650 °C with a heating rate of 5 °C min<sup>-1</sup>.

In order to check the chemical stability of  $1'-N_3$ , the material was stirred in water, methanol, ethanol, DMF, acetic acid, 1M HCl and 1M NaOH solutions. Then, the crystallinity of the filtered materials was examined by XRPD experiments (Figure 4.8). The crystallinity (and hence structural integrity) of the material was completely retained after treating with water, methanol, ethanol, DMF and acetic acid solutions. However, treatment of the material with 1M HCl solution led to significant loss of crystallinity. After treatment with 1M NaOH solution, the material lost its crystallinity and became completely amorphous. Therefore, the chemical stability of  $1'-N_3$  is comparable with the formerly reported Ce-UiO-66 compound.<sup>65</sup> It is worthy to note that both materials showed good stability in water (Figures 4.8 and 4.9). Based on this observation, the  $H_2S$  sensing experiments for both compounds were carried out in HEPES buffer (pH = 7.4).

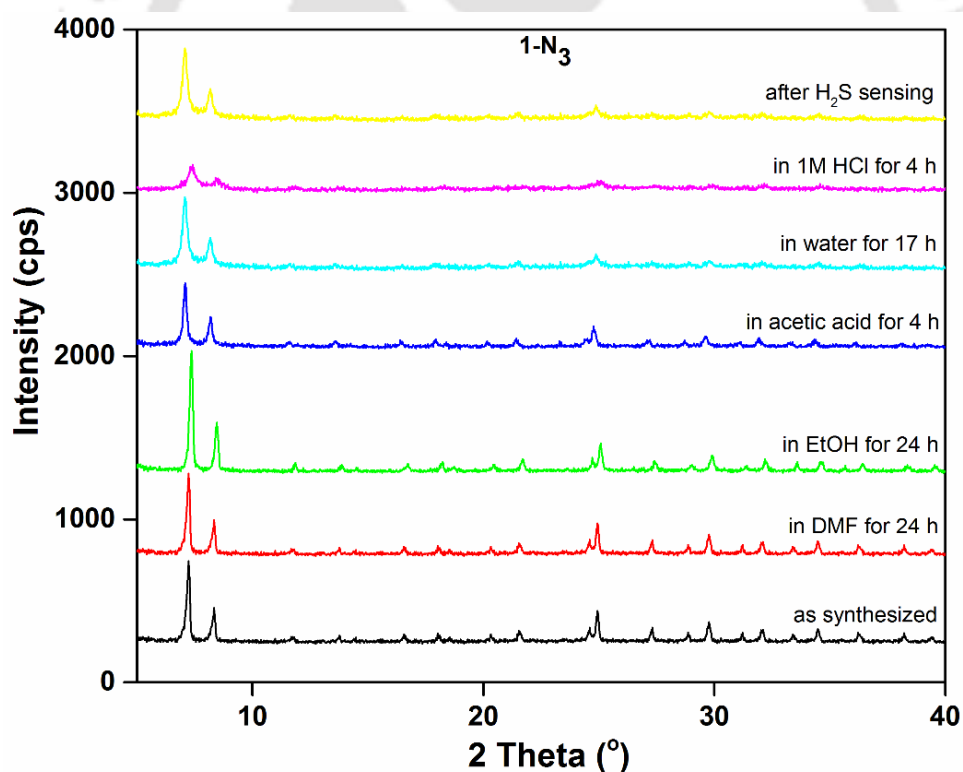


**Figure 4.8** XRPD patterns of  $1-N_3$  in different forms: as-synthesized (black), DMF (red), EtOH (green), acetic acid (blue), water (cyan), 1M HCl (pink) and after  $H_2S$  sensing experiment (yellow).

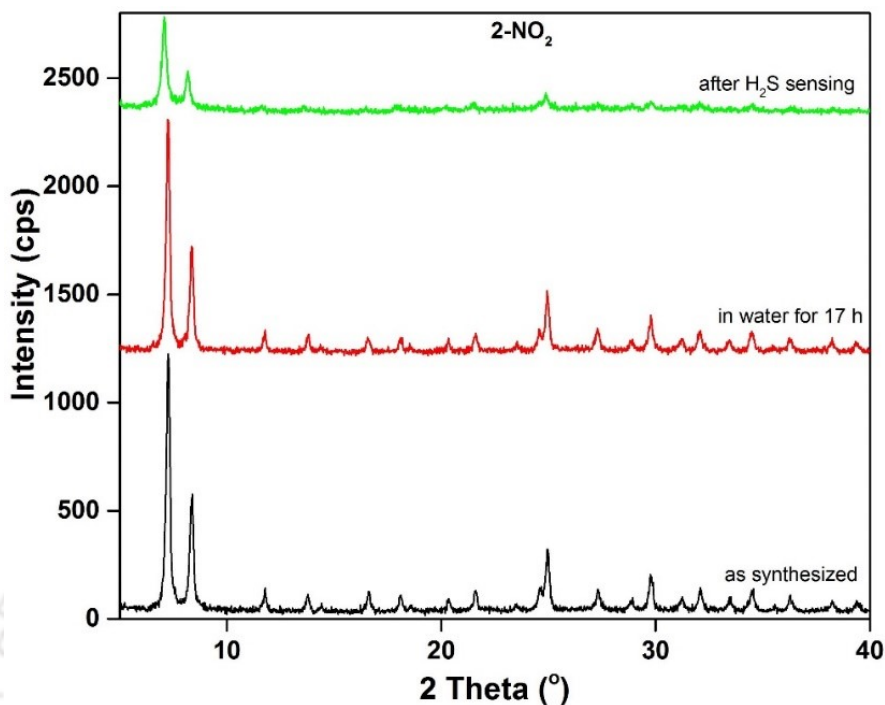


**Figure 4.9** XRPD patterns of 2-NO<sub>2</sub> in water (red) and after H<sub>2</sub>S sensing experiment (green).

#### 4.3.3 Fluorescence Turn-On Experiments: Sensing of H<sub>2</sub>S

Ce-based fluorescent turn-on probe for H<sub>2</sub>S detection has not been reported till today. On the other hand, UiO analogues have proven its usefulness in biological systems without causing any toxicity.<sup>59</sup> Encouraged by these facts, herein we have explored the application potentials of an azide- and a nitro-functionalized Ce-based UiO-66 material as fluorescent turn-on probes under physiological conditions (pH = 7.4).

In order to investigate the detection performances of 1'-N<sub>3</sub> and 2'-NO<sub>2</sub> towards H<sub>2</sub>S, fluorescent turn-on experiments were performed under physiological conditions by employing NaHS as the source of H<sub>2</sub>S. Both azide and nitro groups (attached with the linker molecules), which can effectively quench fluorescence, undergo reduction to amine when exposed to H<sub>2</sub>S. Thus, the azide- and nitro-functionalized Ce-UiO-66 compounds are post-synthetically transformed to the amine-functionalized Ce-UiO-66 material during the reaction-based sensing of H<sub>2</sub>S. The highly fluorescent amine-functionalized MOF is responsible for the fluorescent turn-on behaviour when excited at 334 nm. Owing to the presence of electron-withdrawing azide and nitro groups attached with the linker molecules, both 1'-N<sub>3</sub> and 2'-NO<sub>2</sub> exhibited very weak fluorescence and remained in the fluorescent turn-off state. For investigating of the turn-on

response of **1'-N<sub>3</sub>** and **2'-NO<sub>2</sub>** towards H<sub>2</sub>S, 10 equivalents of NaHS per azide/nitro group were added to the suspension of the compounds in HEPES buffer (pH = 7.4) and the fluorescence emission spectra were measured in a regular time interval (60 s). For **1'-N<sub>3</sub>**, there was nearly 7-fold increase in the fluorescence emission ( $\lambda_{em} = 429$  nm) intensity after 60 s and almost saturation of the fluorescence intensity was observed after 760 s (Figure 4.10). On the other hand, for Zr-UiO-66-N<sub>3</sub>, the addition of NaHS caused 4-fold increase in the fluorescence emission ( $\lambda_{em} = 429$  nm) intensity after 60 s and almost saturation of the fluorescence intensity was observed after 180 s (Figure 4.11). A very fast response for H<sub>2</sub>S detection was also observed for **2'-NO<sub>2</sub>**, showing ~16-fold increase in the fluorescence intensity ( $\lambda_{em} = 429$  nm) after 60 s and achieving saturation of the fluorescence intensity after 760 s (Figure 4.12). On the other hand, only 3-fold increase in the fluorescence emission ( $\lambda_{em} = 429$  nm) intensity after 60 s was observed for Zr-UiO-66-NO<sub>2</sub> and saturation of the fluorescence intensity was noticed after 480 s (Figure 4.13). The immediate turn-on of the fluorescence intensity after addition of NaHS renders **1'-N<sub>3</sub>** and **2'-NO<sub>2</sub>** as potential fluorescent sensor materials for the fast and real-time detection of H<sub>2</sub>S. It is worthy to note that the present compounds exhibited slightly slower response times towards H<sub>2</sub>S as compared to those of the previously reported<sup>32, 33, 42, 43, 58</sup> MOF-based sensor compounds (Table 4.2) but they showed higher fluorescent turn-on efficiency than their Zr-based counterparts.

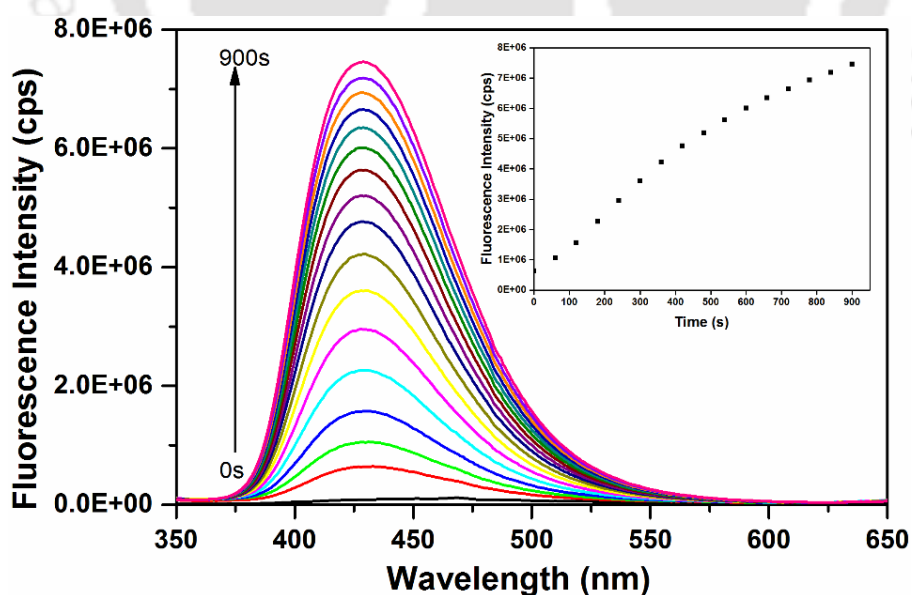


**Figure 4.10** Fluorescence turn-on response of **1'-N<sub>3</sub>** towards addition of NaHS at a regular time interval (60 s) up to 900 s. Inset: Time-dependence of the emission intensity at 429 nm.

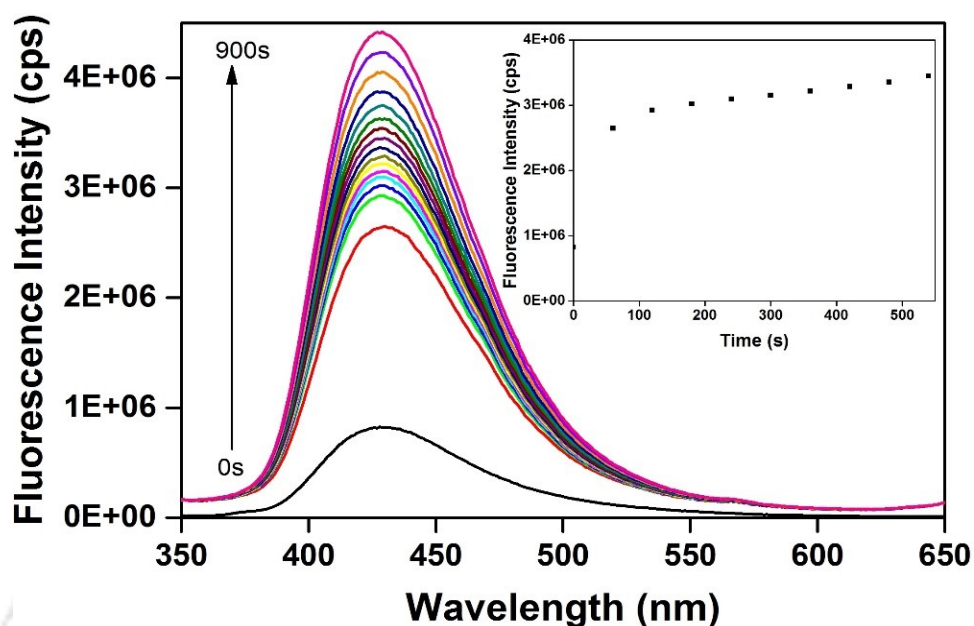


**Figure 4.11** Fluorescence turn-on response of Zr-UiO-66-N<sub>3</sub> towards addition of NaHS at a regular time interval (60 s) up to 900 s. Inset: Time-dependence of the emission intensity at 429 nm.

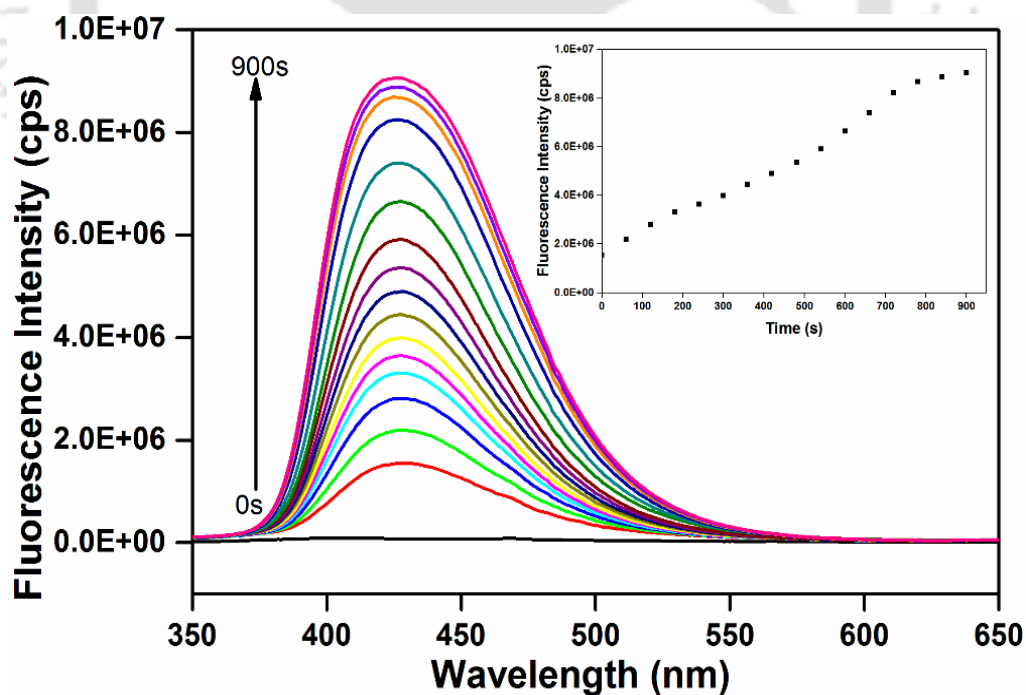


**Figure 4.12** Fluorescence turn-on response of 2'-NO<sub>2</sub> towards addition of NaHS at a regular time interval (60 s) up to 900 s. Inset: Time-dependence of the emission intensity at 429 nm.

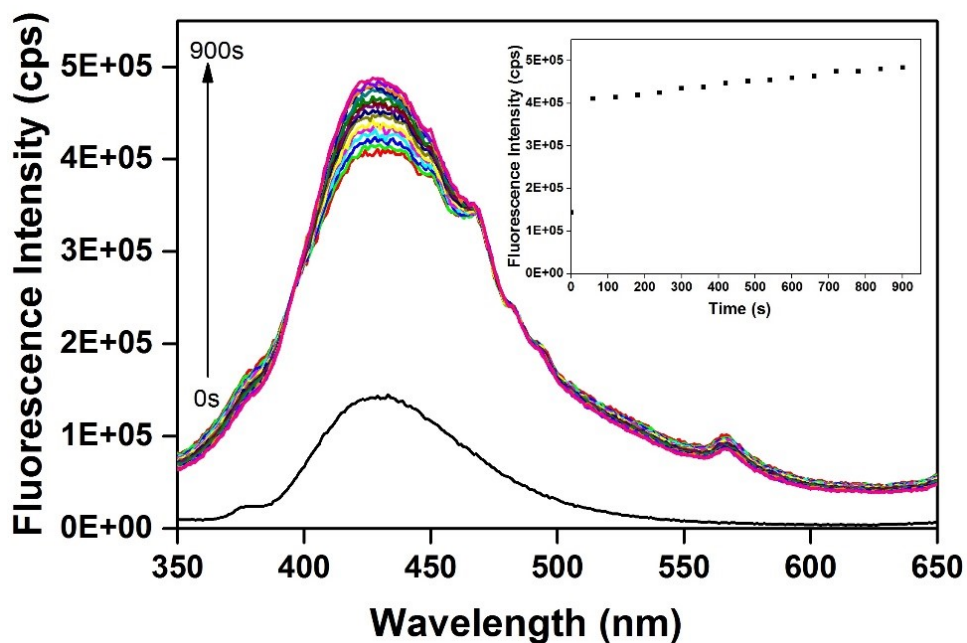


**Figure 4.13** Fluorescence turn-on response of Zr-UiO-66-NO<sub>2</sub> towards addition of NaHS at a regular time interval (60 s) up to 900 s. Inset: Time-dependence of the emission intensity at 429 nm.

**Table 4.2** Comparison of the response time, detection limit and analyte used for H<sub>2</sub>S detection with MOFs reported till date.

Sl. No.	MOF	Response time (s)	Detection Limit ( $\mu$ M)	Analyte	Ref.
1	Ce-UiO-66-N <sub>3</sub>	760	12.2	NaSH	This Work
2	Ce-UiO-66-NO <sub>2</sub>	760	34.84	NaSH	This Work
3	Zr-UiO-66-N <sub>3</sub>	180	176.7	NaSH	
4	Zr-UiO-66-NO <sub>2</sub>	480	95.4	NaSH	
5	IRMOF-3-N <sub>3</sub>	< 120	28.3	NaSH	33
6	Zr-UiO-66-NO <sub>2</sub>	$\approx$ 460	188	Na <sub>2</sub> S	32
7	Zr-UiO-66-N <sub>3</sub>	180	118	Na <sub>2</sub> S	58
8	MN-ZIF-90	-	-	-	43
9	Al-TCPP-Cu	-	-	-	42

For practical applications in biological systems, high selectivity towards the target analyte molecule over other interfering biomolecules (in order to avoid false responses) is a primary criterion for a fluorescence turn-on probe. In order to determine the selectivity of **1'-N<sub>3</sub>** and **2'-NO<sub>2</sub>** for H<sub>2</sub>S over other potentially interfering biomolecules (such as alanine, serine, cysteine and glutathione) and some common reducing anions (such as NaCl, NaBr, NaI, NaNO<sub>2</sub> and NaNO<sub>3</sub>), the fluorescence responses of the compounds towards these potentially interfering biological species were investigated. Figure 4.14 reveals that thiol-containing amino acids (such as cysteine and glutathione) and alanine also showed slight fluorescence turn-on response under identical conditions, whereas other amino acids and reducing anions showed negligible changes in the fluorescence intensity of **1'-N<sub>3</sub>**. On the other hand, no significant effect on the fluorescence intensity by any of these interfering biomolecules was observed for **2'-NO<sub>2</sub>** (Figure 4.15). It is worthy to note that the thiol-containing amino acids such as cysteine and glutathione are known to be responsible for the reduction of azide groups to amine functionalities leading to off-target H<sub>2</sub>S detection.<sup>53, 60</sup> We have also investigated the reducing behavior of (tris(2-carboxyethyl)phosphine) (TCEP), a common reductant in biological assays, towards **1'-N<sub>3</sub>** and **2'-NO<sub>2</sub>** (Figures 4.16 and 4.17).

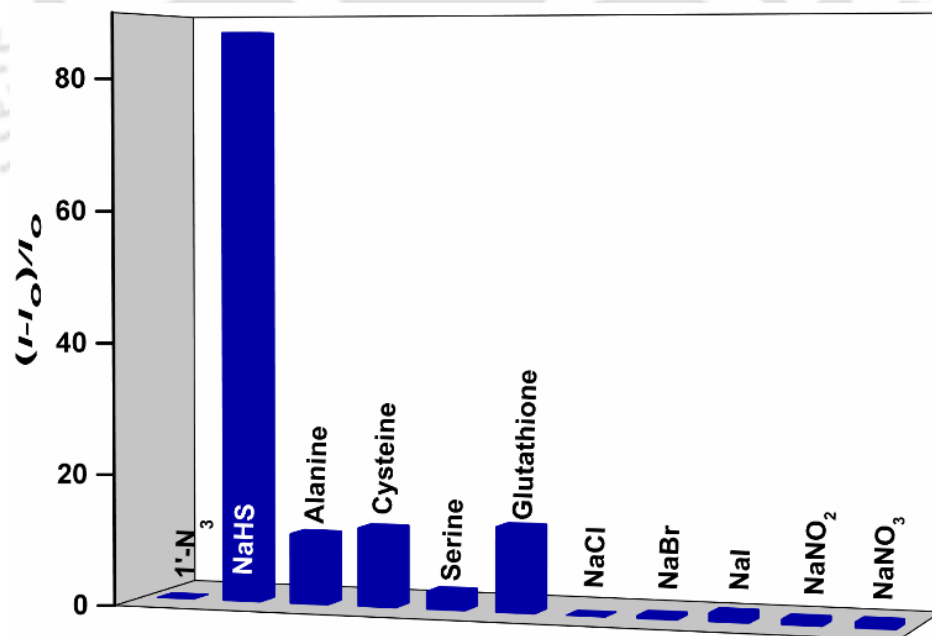


**Figure 4.14** Relative fluorescence response of **1'-N<sub>3</sub>** towards various analytes (10 equivalents per azide group) after 900 s of analyte addition.

It was found that the azide group was easily reduced to amine in presence of TCEP and hence showed fluorescence turn-on response when treated with  $1'-N_3$ . However,  $2'-NO_2$  still remained in fluorescence turn-off state even after treating with TCEP. Thus, it can be concluded that nitro group in  $2'-NO_2$  cannot be reduced by TCEP.

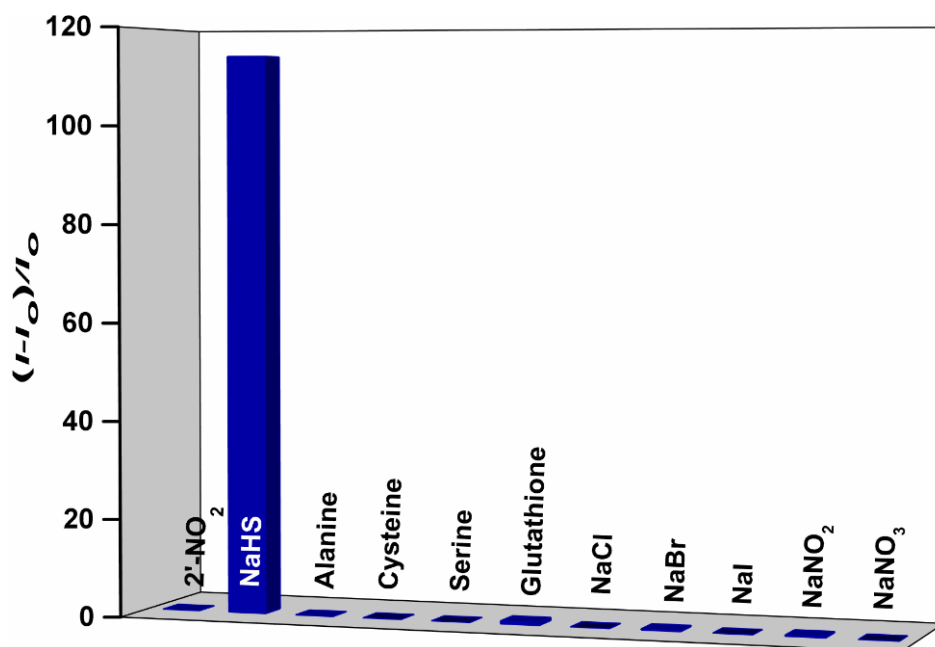


**Figure 4.15** Relative fluorescence response of  $2'-NO_2$  towards various analytes (10 equivalents per nitro group) after 900 s of analyte addition.

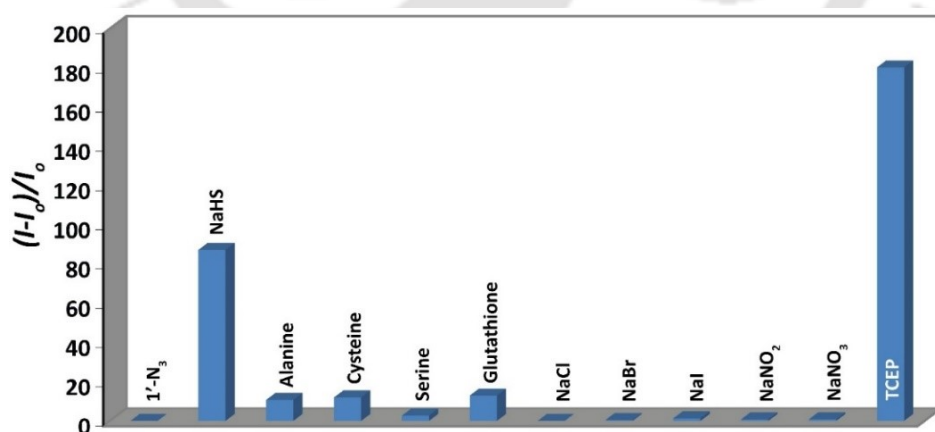


**Figure 4.16** Relative fluorescence response of  $1'-N_3$  towards TCEP (10 equivalents per azide group) after 900 s of analyte addition.

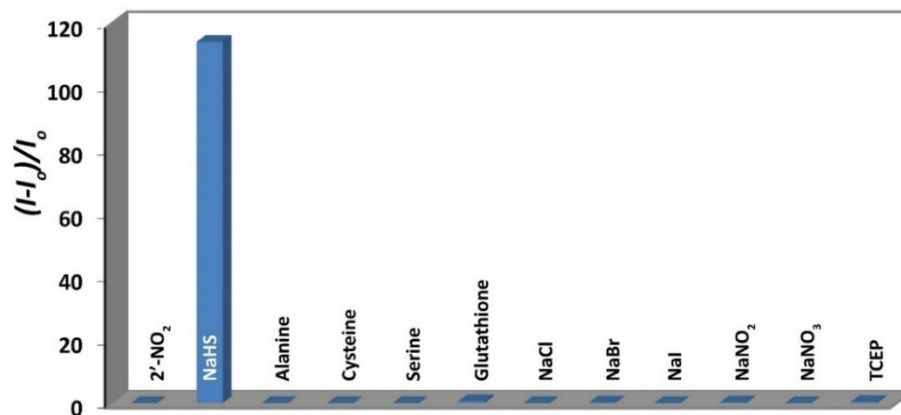


**Figure 4.17** Relative fluorescence response of 2'-NO<sub>2</sub> towards TCEP (10 equivalents per azide group) after 900 s of analyte addition.

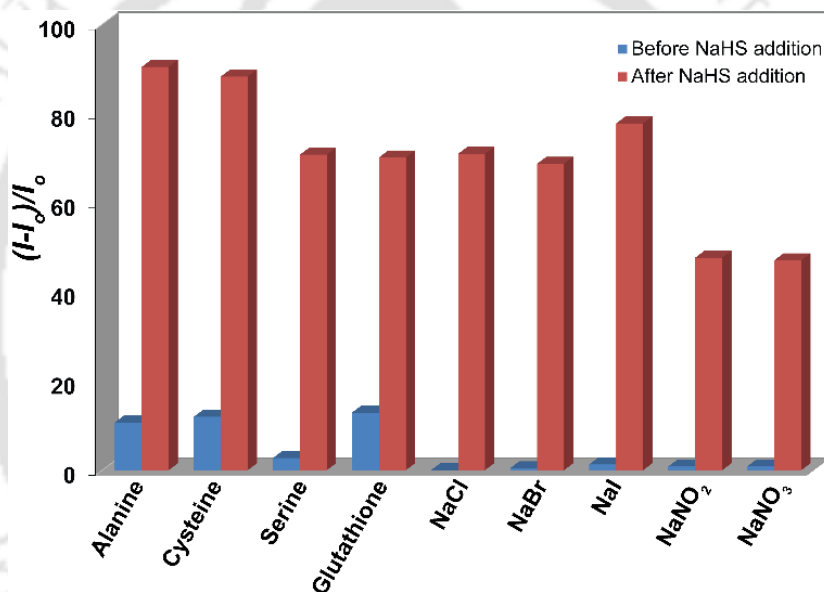


**Figure 4.18** Fluorescence turn-on response of probe 1'-N<sub>3</sub> at 429 nm in presence of a competing analyte (blue), followed by addition of NaHS to the solution containing the analyte (red).

An efficient fluorescence turn-on response of the sensor material in presence of other competing molecules is crucial for successful detection of H<sub>2</sub>S in complex biological systems. Therefore, the selective fluorescence turn-on responses of 1'-N<sub>3</sub> and 2'-NO<sub>2</sub> towards NaHS in presence of other interfering analytes were examined. In these experiments, 10 equivalents of NaHS were added to a HEPES-buffered solution (10 mM, pH = 7.4) containing the sensor material and the competing analyte (10 equivalents), and the fluorescence spectra were recorded after 15 min (Figures 4.18 and 4.19). Both of the sensor materials exhibited significant fluorescence turn-on responses towards H<sub>2</sub>S even in the presence of other potentially interfering

molecules. Thus, fast and selective detection of H<sub>2</sub>S was achieved without any interference from competing analytes, eluding off-target reactivity and false response. Except glutathione (for **2'-NO<sub>2</sub>**), all the competing molecules showed minimal interference with the detection of H<sub>2</sub>S. For **2'-NO<sub>2</sub>**, the presence of glutathione showed a detrimental effect on the fluorescence response towards H<sub>2</sub>S (Figure 4.19).

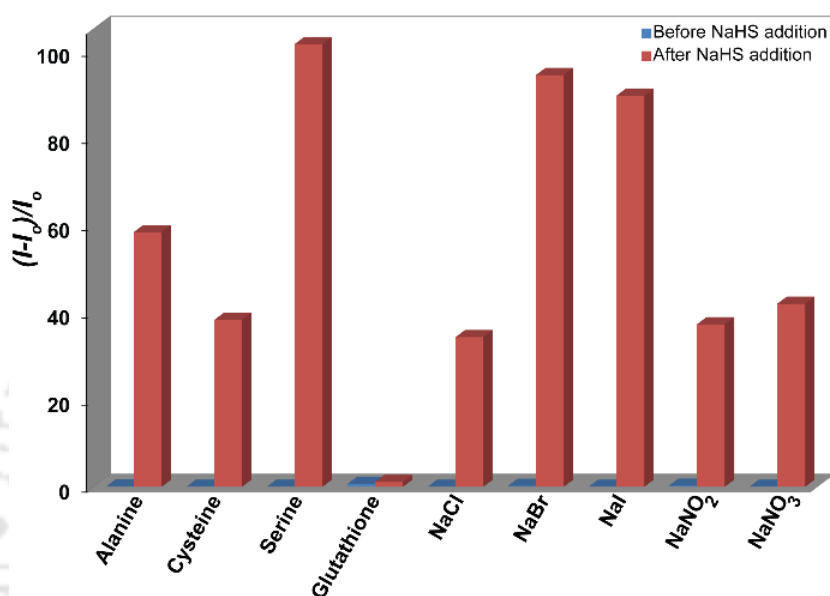


**Figure 4.19** Fluorescence turn-on response of probe **2'-NO<sub>2</sub>** at 429 nm in presence of a competing analyte (blue), followed by addition of NaHS to the solution containing the analyte (red).

For quantitative determination of the fluorescence responses of **1'-N<sub>3</sub>** and **2'-NO<sub>2</sub>** towards H<sub>2</sub>S, fluorometric titrations were carried out with different concentrations of NaHS (0 to 10 equivalents). Upon incremental addition of NaHS, the fluorescence emission intensities of both compounds increased gradually (Figures 4.20 and 4.21). The plots of the fluorescence intensity versus the concentration of **1'-N<sub>3</sub>** and **2'-NO<sub>2</sub>** are shown in the insets of Figures 4.20 and 4.21, respectively. Both of these plots disclose linear relationships. The slopes (S) of the linear curves have been calculated to be 545599 (for **1'-N<sub>3</sub>**) and 134778 (for **2'-NO<sub>2</sub>**). By following the standard equation (detection limit =  $3S_b/S$ , where  $S_b$  is the standard deviation for replicating detections of blank solutions)<sup>34</sup> for calculation of the detection limit, it has been found that the detection limits of **1'-N<sub>3</sub>** and **2'-NO<sub>2</sub>** towards H<sub>2</sub>S are 12.2  $\mu$ M and 34.8  $\mu$ M, respectively. The estimated detection limits towards H<sub>2</sub>S in the present work fall within the range of H<sub>2</sub>S concentration found in the biological systems.<sup>61, 62</sup> In contrast, the Zr-based counterpart of these

two MOFs have shown higher detection limits ( $176.7 \mu\text{M}$  for Zr-UiO-66- $\text{N}_3$  and  $95.4 \mu\text{M}$  for Zr-UiO-66- $\text{NO}_2$ ) (Figure 4.22 & 4.23) compared to  $1'\text{-N}_3$  and  $2'\text{-NO}_2$ . The detection limits of the present compounds are comparable with those of the formerly reported<sup>32, 33, 42, 43, 58</sup> MOF-based  $\text{H}_2\text{S}$  sensor materials (Table 4.2). It is noteworthy that both materials retained their crystallinity (and hence structural integrity) after the  $\text{H}_2\text{S}$  sensing experiments, which has been corroborated by the XRPD (Figures 4.8 and 4.9) experiments.

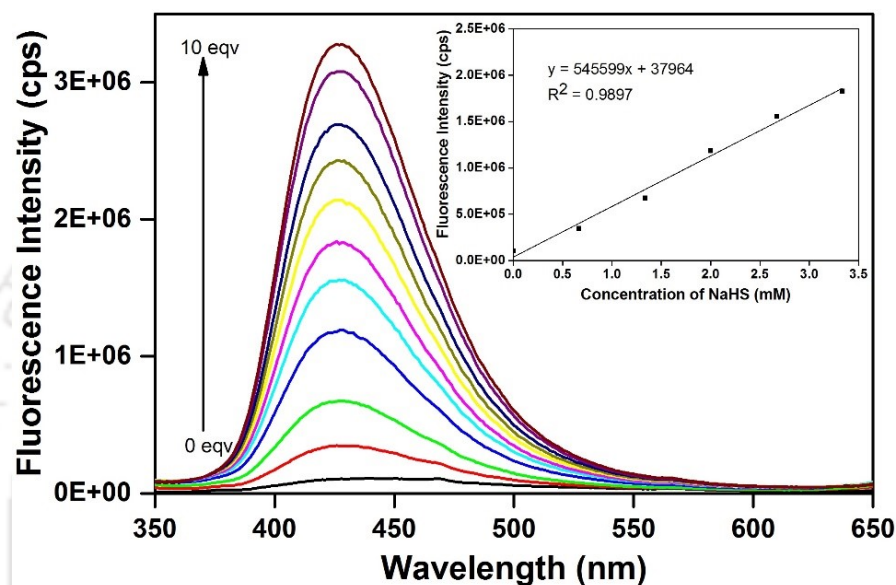


**Figure 4.20** Fluorescence turn-on response of  $1'\text{-N}_3$  with increasing concentrations of NaHS. All the experiments were carried out in HEPES buffer (10 mM, pH = 7.4).

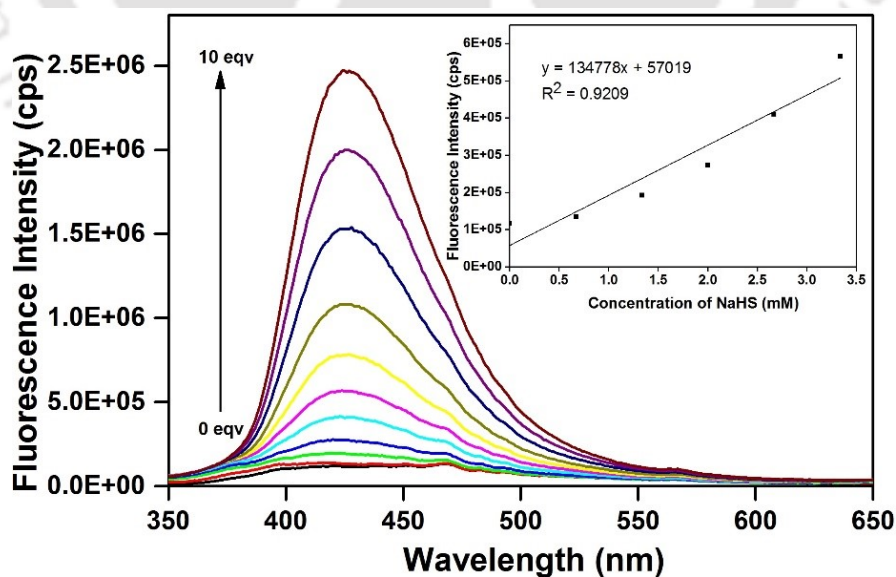


**Figure 4.21** Fluorescence turn-on response of  $2'\text{-NO}_2$  with increasing concentrations of NaHS. All the experiments were carried out in HEPES buffer (10 mM, pH = 7.4).

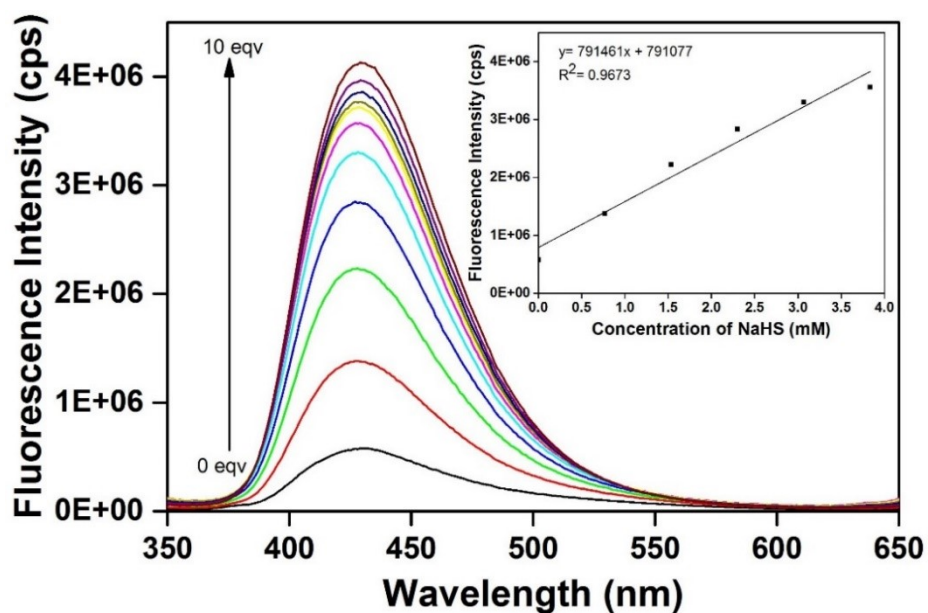


**Figure 4.22** Fluorescence turn-on response of Zr-UiO-66-N<sub>3</sub> with increasing concentrations of NaHS. All the experiments were carried out in HEPES buffer (10 mM, pH = 7.4).

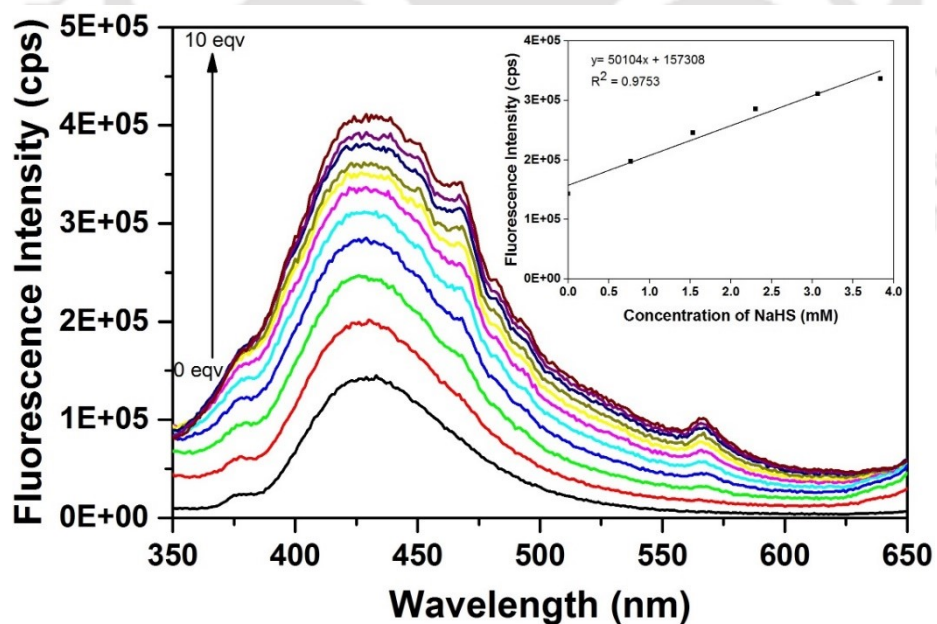


**Figure 4.23** Fluorescence turn-on response of Zr-UiO-66-NO<sub>2</sub> with increasing concentrations of NaHS. All the experiments were carried out in HEPES buffer (10 mM, pH = 7.4).

### 4.3.4 Recyclability Test

In order to investigate the recyclability of **1'-N<sub>3</sub>**, the material was recovered after every fluorescence titration experiment with 10 equivalents of NaHS by centrifugation, followed by washing several times with water. Recyclability test of **1'-N<sub>3</sub>** revealed that the material displayed a strong emission after the first cycle (when excited at 334 nm) before the addition of NaHS and almost negligible response was observed after the addition of NaHS (Figure 4.24). After the treatment with NaHS (during first cycle of use), the azide functional group of the material is permanently reduced to amine, which resulted in strong fluorescence emission before the addition of NaHS (during the second cycle of use). The same trend was also observed during the third cycle of fluorescence titration experiment. Thus, the material exhibited poor recyclability.

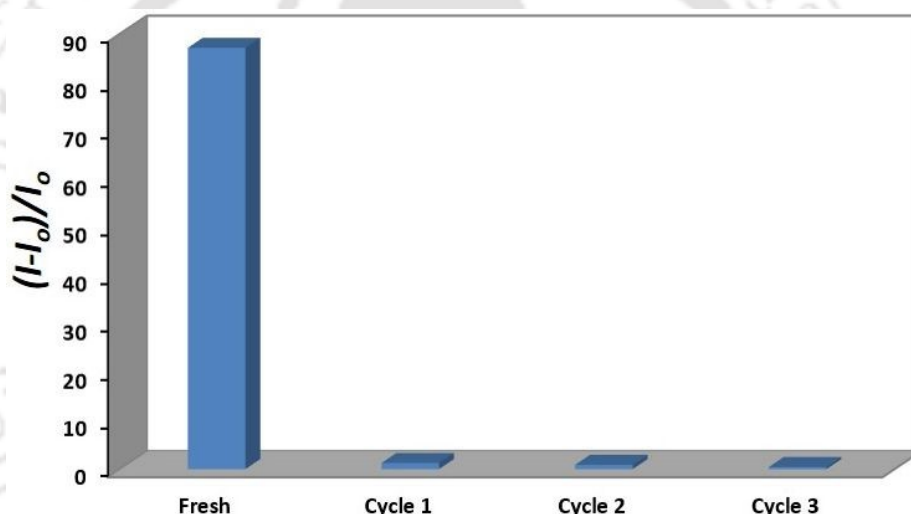


**Figure 4.24** Recyclability test for the fluorescence turn-on response of **1'-N<sub>3</sub>** towards NaHS.

### 4.3.5 Gas Adsorption Properties

N<sub>2</sub> adsorption analyses were performed with the thermally activated **1'-N<sub>3</sub>** and **2'-NO<sub>2</sub>**. The N<sub>2</sub> adsorption isotherms exhibit type-I isotherms (Figure 4.25). The calculated specific BET surface area of **1'-N<sub>3</sub>** (835 m<sup>2</sup> g<sup>-1</sup>) lies within the range of BET surface area of the recently reported Ce-UiO-66-X (X = -F, -CH<sub>3</sub>, -Cl and -NO<sub>2</sub>) compounds (727-1075 m<sup>2</sup> g<sup>-1</sup>; Table 4.3).<sup>65</sup> The specific BET surface area of **2'-NO<sub>2</sub>** (819 m<sup>2</sup> g<sup>-1</sup>) is slightly higher compared to that of the recently reported Ce-UiO-66-NO<sub>2</sub> compound (727 m<sup>2</sup> g<sup>-1</sup>).<sup>65</sup> At p/p<sub>0</sub> = 0.5, **1'-N<sub>3</sub>** and **2'-NO<sub>2</sub>** exhibit total micropore volumes of 0.44 and 0.43 cm<sup>3</sup> g<sup>-1</sup>, respectively.

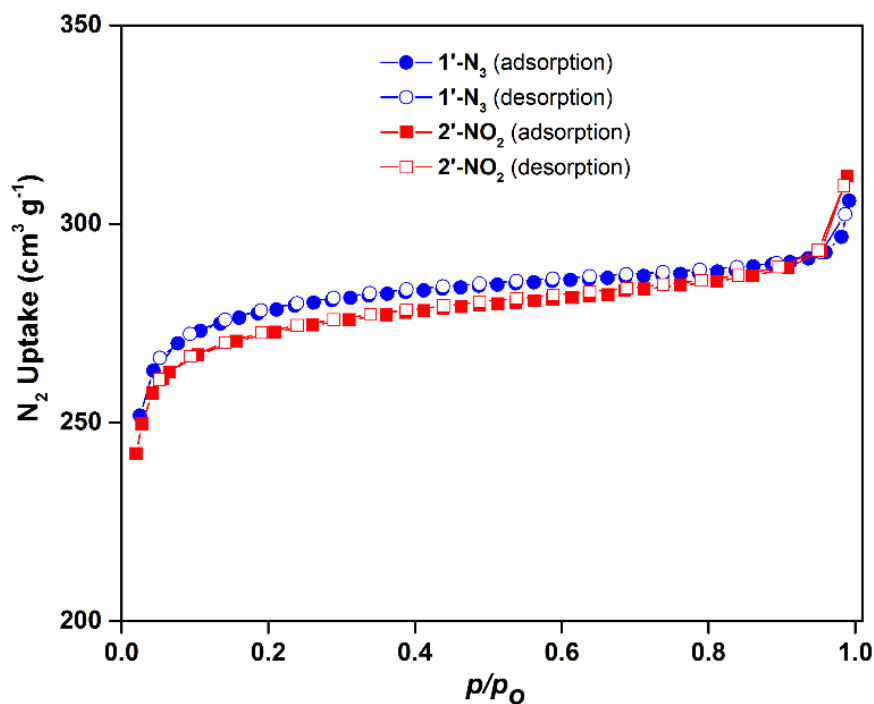


**Figure 4.25**  $\text{N}_2$  adsorption (solid symbols) and desorption (empty symbols) isotherms of the thermally activated  $1'\text{-N}_3$  (blue, circles) and  $2'\text{-NO}_2$  (red, squares) recorded at  $-196\text{ }^\circ\text{C}$ .

**Table 4.3** Specific BET surface areas and micropore volumes of thermally activated  $1'\text{-N}_3$  and  $2'\text{-NO}_2$ . The values are compared with those of the previously reported Ce-UiO-66 and Ce-UiO-66-X compounds.<sup>46</sup>

Compound	BET Surface Area ( $\text{m}^2\text{ g}^{-1}$ )	Micropore Volume ( $\text{cm}^3\text{ g}^{-1}$ )
$1\text{-N}_3$	835	0.44
$1\text{-NO}_2$	819	0.43
Ce-UiO-66	1282	0.50
Ce-UiO-66-F	1075	0.42
Ce-UiO-66- $\text{CH}_3$	985	0.39
Ce-UiO-66-Cl	770	0.31
Ce-UiO-66- $\text{NO}_2$	727	0.29

The  $\text{CO}_2$  adsorption measurements were performed with the thermally activated  $1'\text{-N}_3$  and  $2'\text{-NO}_2$  at  $0\text{ }^\circ\text{C}$  up to 1 bar. The  $\text{CO}_2$  adsorption isotherms (Figure 4.26) of both compounds

display type-I behavior in the pressure range from 0 to 1 bar. The CO<sub>2</sub> uptake values of **1'-N<sub>3</sub>** and **2'-NO<sub>2</sub>** at 1 bar are found to be 2.6 and 3.7 mmol g<sup>-1</sup>, respectively. These CO<sub>2</sub> adsorption capacities are among the highest values reported for isostructural, Zr-based UiO-66-X (X = –NO<sub>2</sub>, –NH<sub>2</sub>, –OH, –CH<sub>3</sub> and –(CH<sub>3</sub>)<sub>2</sub>) materials.<sup>63-65</sup>

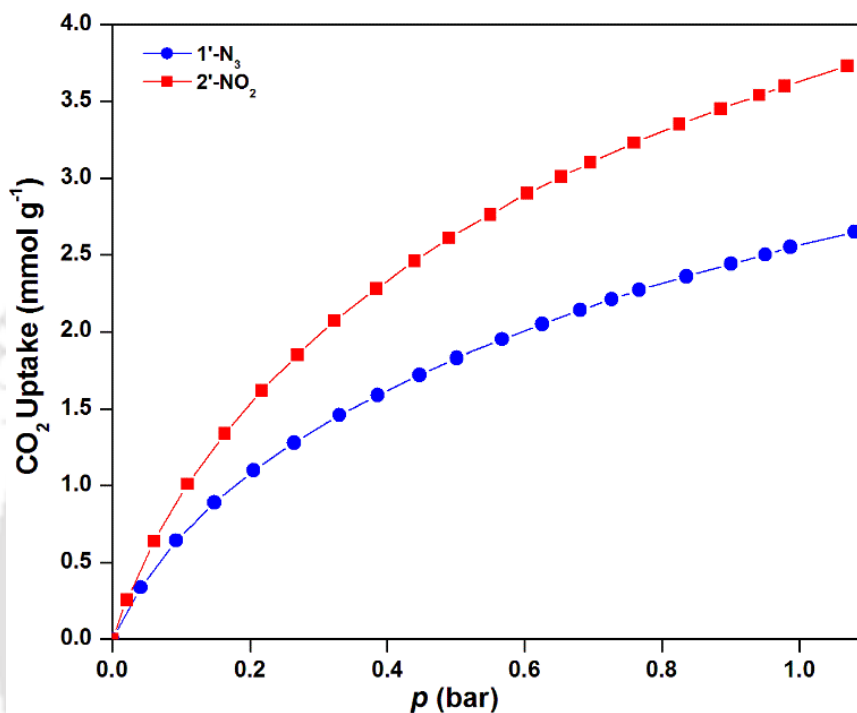


**Figure 4.26** Low-pressure CO<sub>2</sub> adsorption isotherms of the thermally activated **1'-N<sub>3</sub>** (blue, circles) and **2'-NO<sub>2</sub>** (red, squares) measured at 0 °C.

#### 4.4 CONCLUSIONS

A new (**1'-N<sub>3</sub>**) and an existing (**2'-NO<sub>2</sub>**) Ce(IV)-based MOF with UiO-66 framework topology have been employed for the first time as fluorescence turn-on probes for the detection of H<sub>2</sub>S under physiological conditions. Both compounds show significant potentials towards highly selective, sensitive (detection limits: 12.2 μM for **1'-N<sub>3</sub>** and 34.8 μM for **2'-NO<sub>2</sub>**) and fast detection of H<sub>2</sub>S. The detection performances (in terms of fold enhancement) of the Ce-based UiO-66 MOFs towards H<sub>2</sub>S are higher as compared to their Zr-based counterparts. Owing to their extraordinary selectivity towards sensing of H<sub>2</sub>S even in the presence of other potentially interfering biomolecules, these compounds could be promising candidates for the real-time monitoring of H<sub>2</sub>S in biological systems. Apart from the rapid, selective and sensitive detection

of H<sub>2</sub>S, both of these compounds can effectively adsorb considerable amounts CO<sub>2</sub> at 0 °C and in pressure range of 0 to 1 bar. Thus, they are also promising materials in the field of CO<sub>2</sub> capture.

#### 4.5 REFERENCES

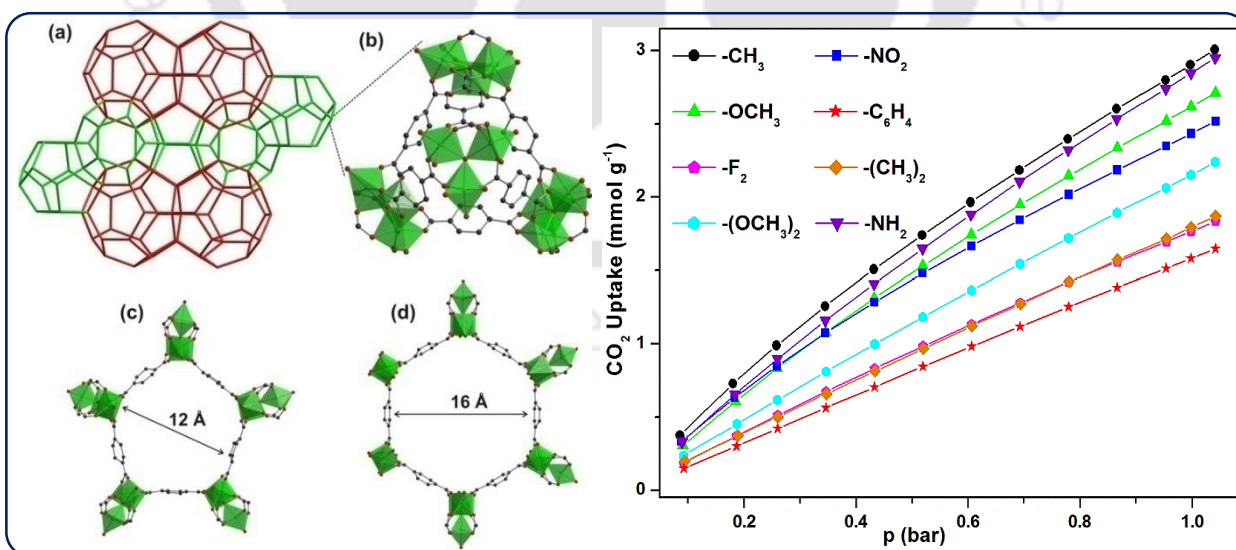
1. R. J. Reiffenstein, W. C. Hulbert and S. H. Roth, *Annu. Rev. Pharmacol. Toxicol.*, 1992, **32**, 109.
2. R. G. Hendrickson, A. Chang and R. J. Hamilton, *Am. J. Ind. Med.*, 2004, **45**, 346.
3. T. L. Guidotti, *Int. J. Toxicol.*, 2010, **29**, 569.
4. T. S. Bailey and M. D. Pluth, *J. Am. Chem. Soc.*, 2013, **135**, 16697.
5. R. Wang, *FASEB J.*, 2002, **16**, 1792.
6. D. Boehning and S. H. Snyder, *Annu. Rev. Neurosci.*, 2003, **26**, 105.
7. C. Szabo, *Nat. Rev. Drug Discovery*, 2007, **6**, 917.
8. L. Li, P. Rose and P. K. Moore, *Annu. Rev. Pharmacol. Toxicol.*, 2011, **51**, 169.
9. K. Tanizawa, *J. Biochem.*, 2011, **149**, 357.
10. G. Yang, L. Wu, B. Jiang, B. Yang, J. Qi, K. Cao, Q. Meng, A. K. Mustafa, W. Mu, S. Zhang, S. H. Snyder and R. Wang, *Science*, 2008, **322**, 587.
11. K. Abe and H. J. Kimura, *Neuroscience (Oxford)*, 1996, **16**, 1066.
12. L. Li, M. Bhatia, Y. Z. Zhu, Y. C. Zhu, R. D. Ramnath, Z. J. Wang, F. B. Anuar, M. Whiteman, M. Salto-Tellez and P. K. Moore, *FASEB J.*, 2005, **19**, 1196.
13. J. W. Calvert, S. Jha, S. Gundewar, W. J. Elrod, A. Ramachandran, C. B. Pattillo, C. G. Kevil and D. J. Lefer, *Circ. Res.*, 2009, **105**, 365.
14. A. Papapetropoulos, A. Pyriochou, Z. Altaany, G. Yang, A. Marazioti, Z. Zhou, M. G. Jeschke, L. K. Branski, D. N. Herndon, R. Wang and C. Szabó, *Proc. Natl. Acad. Sci. U.S.A.*, 2009, **106**, 21972.
15. G. Yang, L. Wu and R. Wang, *FASEB J.*, 2006, **20**, 553.
16. C. K. Nicholson and J. W. Calvert, *Pharmacol. Res.*, 2010, **62**, 289.
17. K. Eto, T. Asada, K. Arima, T. Makifuchi and H. Kimura, *Biochem. Biophys. Res. Commun.*, 2002, **293**, 1485.
18. P. Kamoun, M. C. Belardinelli, A. Chabli, K. Lallouchi and B. Chadeaux-Vekemans, *Am. J. Med. Genet. Sect. A.*, 2003, **116**, 310.
19. W. Yang, G. Yang, X. Jia, L. Wu and R. Wang, *J. Physiol.*, 2005, **569**, 519.

20. S. Fiorucci, E. Antonelli, A. Mencarelli, S. Orlandi, B. Renga, G. Rizzo, E. Distrutti, V. Shah and A. Morelli, *Hepatology*, 2005, **42**, 539.
21. C. Szabo, C. Coletta, C. Chao, K. Modis, B. Szczesny, A. Pa-papetropoulos and M. R. Hellmich, *Proc. Natl. Acad. Sci. USA*, 2013, **110**, 12474.
22. J. Furne, A. Saeed and M. D. Levitt, *Am. J. Physiol.*, 2008, **295**, 1479.
23. M. G. Choi, S. Cha, H. Lee, H. L. Jeon and S. K. Chang, *Chem. Commun.*, 2009, 7390.
24. M. M. F. Choi, *Analyst*, 1998, **123**, 1631.
25. N. S. Lawrence, J. Davis, L. Jiang, T. G. J. Jones, S. N. Davies and R. G. Compton, *Electroanalysis*, 2000, **18**, 1453.
26. M. Ishigami, K. Hiraki, K. Umemura, Y. Ogasawara, K. Ishii and H. Kimura, *Antioxid. Redox Signal.*, 2009, **11**, 205.
27. G.-J. Mao, T.-T. Wei, X. X. Wang, S. Huan, D.-Q. Lu, J. Zhang, X.-B. Zhang, W. Tan, G.-L. Shen and R.-Q. Yu, *Anal. Chem.*, 2013, **85**, 7875.
28. H. Peng, W. Chen, S. Burroughs and B. Wang, *Curr. Org. Chem.*, 2013, **17**, 641.
29. F. Yu, X. Hanab and L. Chen, *Chem. Commun.*, 2014, **50**, 12234.
30. C. Liu, J. Pan, S. Li, Y. Zhao, L. Y. Wu, C. E. Berkman, A. R. Whorton and M. Xian, *Angew. Chem. Int. Ed.*, 2011, **50**, 10327.
31. B. Ke, W. Wu, W. Liu, H. Liang, D. Gong, X. Hu and M. Li, *Anal. Chem.*, 2016, **88**, 592.
32. S. S. Nagarkar, A. V. Desai and S. K. Ghosh, *Chem. Eur. J.*, 2015, **21**, 9994.
33. X. Zhang, J. Zhang, Q. Hu, Y. Cui, Y. Yang and G. Qian, *Appl. Surf. Sci.*, 2015, **355**, 814.
34. A. R. Lippert, E. J. New and C. J. Chang, *J. Am. Chem. Soc.*, 2011, **133**, 10078.
35. L. A. Montoya and M. D. Pluth, *Chem. Commun.*, 2012, **48**, 4767.
36. S. Chen, Z.-j. Chen, W. Ren and H.-w. Ai, *J. Am. Chem. Soc.*, 2012, **134**, 9589.
37. S. K. Das, C. S. Lim, S. Y. Yang, J. H. Han and B. R. Cho, *Chem. Commun.*, 2012, **48**, 8395.
38. Q. Wan, Y. Song, Z. Li, X. Gao and H. Ma, *Chem. Commun.*, 2013, **49**, 502.
39. Z. Wu, Z. Li, L. Yang, J. Han and S. Han, *Chem. Commun.*, 2012, **48**, 10120.
40. Y. Jiang, Q. Wu and X. Chang, *Talanta*, 2014, **121**, 122.
41. H. Peng, Y. Cheng, C. Dai, A. L. King, B. L. Predmore, D. J. Lefter and B. Wang, *Angew. Chem. Int. Ed.*, 2011, **50**, 9672.

42. Y. Ma, H. Su, X. Kuang, X. Li, T. Zhang and B. Tang, *Anal. Chem.*, 2014, **86**, 11459.
43. H. Li, X. Feng, Y. Guo, D. Chen, R. Li, X. Ren, X. Jiang, Y. Dong and B. Wang, *Sci Rep.*, 2014, **4**, 1.
44. S. S. Nagarkar, A. V. Desai and S. K. Ghosh, *Chem. Commun.*, 2014, **50**, 8915.
45. O. Ayhan, I. L. Malaestean, A. Ellern, J. v. Leusen, S. G. Baca and P. Kögerler, *Cryst. Growth Des.*, 2014, **14**, 3541.
46. M. Lammert, M. T. Wharmby, S. Smolders, B. Bueken, A. Lieb, K. A. Lomachenko, D. D. Vos and N. Stock, *Chem. Commun.*, 2015, **51**, 12578.
47. F. Costantino, P. L. Gentili and N. Audebrand, *Inorg. Chem. Commun.*, 2009, **12**, 406.
48. N. A. Khan, M. M. Haque and S. H. Jhung, *Eur. J. Inorg. Chem.*, 2010, 4975.
49. P. R. Matthes and K. Müller-Buschbaum, *Z. Anorg. Allg. Chem.*, 2014, 2847.
50. V. S. Lin, W. Chen, M. Xian and C. J. Chang, *Chem. Soc. Rev.*, 2015, **44**, 4596.
51. F. Yu, X. Han and L. Chen, *Chem. Commun.*, 2014, **50**, 12234.
52. J. Li, C. Yin and F. Huo, *RSC Adv.*, 2015, **5**, 2191.
53. A. R. Lippert, *J. Inorg. BioChem.*, 2014, **133**, 136.
54. M. Kim, J. F. Cahill, Y. Su, K. A. Prather and S. M. Cohen, *Chem. Sci.*, 2012, **3**, 126.
55. W. Morris, W. E. Briley, E. Auyeung, M. D. Cabezas and C. A. Mirkin, *J. Am. Chem. Soc.*, 2014, **136**, 7261–7264.
56. A. Boultif and D. J. Louer, *J. Appl. Crystallogr.*, 1991, **24**, 987.
57. STOE WinXPOW version 2.11, Stoe & Cie GmbH, Darmstadt, Germany, 2005.
58. S. S. Nagarkar, T. Saha, A. V. Desai, P. Talukdar and S. K. Ghosh, *Sci Rep.*, 2014, **4**, 1.
59. P. Horcajada, R. Gref, T. Baati, P. K. Allan, G. Maurine, P. Couvreur, G. Ferey, R. Morris and C. Serre, *Chem. Rev.*, 2012, **112**, 1232.
60. K. Sasakura, K. Hanaoka, N. Shibuya, Y. Mikami, Y. Kimura, T. Komatsu, T. Ueno, T. Terai, H. Kimura and T. Nagano, *J. Am. Chem. Soc.*, 2011, **133**, 18003.
61. P. Wu, J. Zhang, S. Wang, A. Zhu and X. Hou, *Chem. Eur. J.*, 2014, **20**, 952.
62. L. Li, P. Rose and P. K. Moore, *Annu. Rev. Pharmacol. Toxicol.*, 2011, **51**, 169.
63. S. Biswas and P. V. D. Voort, *Eur. J. Inorg. Chem.*, 2013, 2154.
64. Y. Huang, W. Qin, Z. Li and Y. Li, *Dalton Trans.*, 2012, **41**, 9283.
65. H. Jasuja, J. Zang, D. S. Sholl and K. S. Walton, *J. Phys. Chem. C*, 2012, **116**, 23526.

## Synthesis and Gas Adsorption Properties of New Functionalized Al-MIL-101-X (X = -CH<sub>3</sub>, -NO<sub>2</sub>, -OCH<sub>3</sub>, -C<sub>6</sub>H<sub>4</sub>, -F<sub>2</sub>, -(CH<sub>3</sub>)<sub>2</sub>, -(OCH<sub>3</sub>)<sub>2</sub>) Materials

This chapter presents the facile synthesis, full characterization and gas adsorption properties of seven new functionalized Al-MIL-101-X (X = -CH<sub>3</sub>, -NO<sub>2</sub>, -OCH<sub>3</sub>, -C<sub>6</sub>H<sub>4</sub>, -F<sub>2</sub>, -(CH<sub>3</sub>)<sub>2</sub>, -(OCH<sub>3</sub>)<sub>2</sub>) materials. To confirm the phase purity of the materials, XRPD analysis, FT-IR spectroscopy, thermogravimetric and elemental analysis were performed. The thermally activated forms of all the materials show significant porosity, as revealed by the N<sub>2</sub> and CO<sub>2</sub> sorption analysis. The high thermal and moisture stability of the light-weight, non-toxic Al-MIL-101-X-CE materials along with the considerably high porosity would make them potential candidates for applications in gas storage and separation.

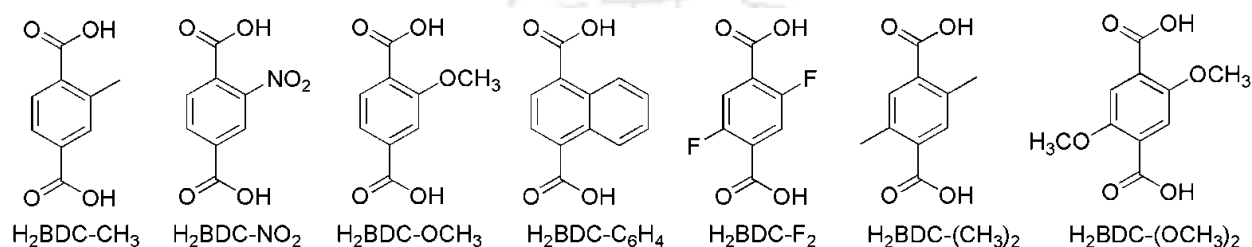


## 5.1 INTRODUCTION

Metal-organic frameworks (MOFs)<sup>1-6</sup> have been extensively used in a broad range of areas such as gas storage/separation,<sup>7-9</sup> heterogeneous catalysis<sup>10, 11</sup> and drug delivery<sup>12-15</sup> in the last two decades due to their highly crystalline and extremely porous nature. Although a wide variety of potential applications of MOFs in different fields have been largely explored, the development of air- and moisture-stable MOFs having usable functional organic sites is still a major challenge. The structures of some famous un-functionalized MOFs,<sup>16-19</sup> which have displayed potential applications in adsorption, separation or catalysis, collapse when exposed to moisture from air. This structural instability hampers their industrial applications. In order to improve their hydrolytic stabilities, hydrophobic functional groups (e.g., -F, -CH<sub>3</sub>, -OCF<sub>3</sub>, etc.)<sup>20-24</sup> have been introduced into their frameworks. Besides the employment of hydrophobic functional groups to the organic linkers, the incorporation of metal cations with higher oxidation states (e.g. Al(III),<sup>25, 26</sup> Cr(III),<sup>27</sup> Ti(IV),<sup>28</sup> Zr(IV),<sup>29</sup> etc.) has been found to be a promising strategy for achieving MOFs possessing reasonably higher physicochemical stabilities (moisture, thermal and acid-base).

The MIL-n (MIL = Material of the Institute Lavoisier) family of MOFs, originally developed by Ferey and coworkers, have exhibited high thermal and chemical stability as well as considerably high porosity.<sup>25-27</sup> The hydrolytically stable Cr(III)-based MIL-101 MOF, for example, displays high thermal stability above 400 °C and bears extraordinarily high surface area of 4100 m<sup>2</sup> g<sup>-1</sup>.<sup>27, 30</sup> Stock's and several other groups have reported single- and mixed-linker Cr-MIL-101 derivatives.<sup>30-39</sup> In addition to the parent and functionalized Cr-MIL-101-X (X = -H, -F, -Cl, -Br, -I, -CH<sub>3</sub>, -NO<sub>2</sub>, -NH<sub>2</sub>, -OH, -CO<sub>2</sub>H, -SO<sub>3</sub>H, etc.) compounds, hydrolytically stable Fe-MIL-101-X (X = -H, -Cl, -NH<sub>2</sub> and -(CH<sub>3</sub>)<sub>2</sub>) compounds were also reported in the literature.<sup>40, 41</sup> The synthesis of non- and amino-functionalized vanadium-based MIL-101 materials was reported by the groups of Van Der Voort<sup>42</sup> and Zou<sup>43</sup>. However, the vanadium MOF materials were found to be sensitive to air. In addition to the pristine and functionalized Cr(III), Fe(III) and V(III)-based MIL-101 materials, the synthesis, CO<sub>2</sub>/CH<sub>4</sub> separation and catalytic properties of Al-MIL-101-NH<sub>2</sub> compound possessing high thermal and chemical stability were also reported.<sup>26, 44, 45</sup> Although the Al-MIL-101 derivatives are expected to be light-weight, non-toxic, highly porous and stable against hydrolysis, yet the synthesis procedures of Al-MIL-101 derivatives

having any other functional group than amino are hitherto unknown. In this work, we wish to report on the synthesis, complete characterization, thermal stability as well as gas adsorption characteristics of seven new functionalized Al-MIL-101-X (X = -CH<sub>3</sub>, -NO<sub>2</sub>, -OCH<sub>3</sub>, -C<sub>6</sub>H<sub>4</sub>, -F<sub>2</sub>, -(CH<sub>3</sub>)<sub>2</sub>, -(OCH<sub>3</sub>)<sub>2</sub>) materials. The effect of the various attached functional groups (Scheme 5.1) on the thermal stability and gas adsorption performance of the resulting Al-MIL-101-X compounds has been investigated.



**Scheme 5.1** Structures of the functionalized terephthalic acid linker molecules H<sub>2</sub>BDC-X used for the preparation of the Al-MIL-101-X compounds.

## 5.2 EXPERIMENTAL SECTION

### 5.2.1 Materials and General Methods

The H<sub>2</sub>BDC-CH<sub>3</sub>,<sup>46</sup> H<sub>2</sub>BDC-OCH<sub>3</sub>,<sup>47</sup> H<sub>2</sub>BDC-F<sub>2</sub><sup>48</sup> and H<sub>2</sub>BDC-(OCH<sub>3</sub>)<sub>2</sub><sup>49</sup> ligands were synthesized by following previously published procedures. All other starting materials were of reagent grade and used as received from the commercial suppliers. Fourier transform infrared (FT-IR) spectra were recorded in the region of 440-4000 cm<sup>-1</sup> with a Perkin Elmer Spectrum Two FT-IR spectrometer. The following indications are used to characterize absorption bands: very strong (vs), strong (s), medium (m), weak (w), shoulder (sh) and broad (br). Thermogravimetric analysis (TGA) was performed with a Netzsch STA-409CD thermal analyzer in a temperature range of 25-600 °C under air atmosphere at a heating rate of 4 °C min<sup>-1</sup>. Ambient temperature X-Ray powder diffraction (XRPD) patterns were recorded on a Bruker D2 Phaser X-ray diffractometer (30 kV, 10 mA) or a Thermo Scientific ARL X'Tra diffractometer (40 kV, 40 mA), using Cu-Kα (λ = 1.5406 Å). Energy dispersive X-ray (EDX) analyses were carried out with a Hitachi S3400N SEM-EDX (SEM = scanning electron microscope) instrument. The nitrogen sorption isotherms up to 1 bar were measured using a Belsorp Mini apparatus at -196 °C. The carbon dioxide adsorption analyses were performed using a

Micromeritics TriStar 3000 analyzer at 0 °C. Prior to the sorption experiments, the compounds were degassed at 130 °C under vacuum for 24 h.

*Caution!* Perchlorate salt is potentially explosive and caution should be exercised when dealing with such material. However, the small quantities used in this study were not found to present a hazard.

The frequencies of FT-IR absorption bands for all the thermally activated Al-MIL-101-X compounds are presented in Tables 5.1.

### 5.2.2 Synthesis

#### **General Procedure for the Synthesis of the Al-MIL-101-X Materials by Solvothermal Method**

A mixture of  $\text{Al}(\text{ClO}_4)_3 \cdot 9\text{H}_2\text{O}$  and  $\text{H}_2\text{BDC-X}$  (50 mg) ligand with a 1:1 molar ratio (Table 5.2) in 2 mL of *N,N*-diethylformamide (DEF) was placed in a Pyrex tube (15 mL). The tube was sealed and heated in a preheated heating block to 130 °C, held at this temperature for a specific reaction time (Table 5.3), then cooled to room temperature spontaneously. The precipitate was collected by filtration using membrane filters, washed with acetone ( $2 \times 3$  mL) and dried in air. The compounds obtained by using the solvothermal method are denoted as Al-MIL-101-X-CE (CE = conventional electric) hereafter.

#### **General Procedure for the Synthesis of the Al-MIL-101-X Materials by Microwave Irradiation Method**

A mixture of  $\text{Al}(\text{ClO}_4)_3 \cdot 9\text{H}_2\text{O}$  and  $\text{H}_2\text{BDC-X}$  (50 mg) ligand with a 1:1 molar ratio (Table 5.1) in 2 mL of DEF was placed in a Pyrex tube (10 mL). The tube was sealed and heated in a microwave synthesizer (CEM, Discover S) to 170 °C at 150 W, held under these conditions for 10 min with stirring, then cooled to room temperature. The precipitate was collected by filtration using membrane filters, washed with acetone ( $2 \times 3$  mL) and dried in air. The compounds produced by using the microwave irradiation method are referred to as Al-MIL-101-X-MW (MW = microwave) hereafter.

**Table 5.1** Frequencies of infrared absorption bands<sup>[a]</sup> for the thermally activated forms of Al-MIL-101-X-CE compounds.

Compound	Infrared Absorption Frequencies (cm <sup>-1</sup> )
<b>1-CH<sub>3</sub></b>	3435 (br), 1598 (vs), 1496 (w), 1427 (vs), 1385 (sh), 1293 (w), 1265 (w), 1145 (w), 1122 (s), 1089 (sh), 1020 (w), 770 (m), 632 (m), 604 (sh), 539 (w)
<b>2-NO<sub>2</sub></b>	3424 (br), 1617 (vs), 1538 (m), 1505 (m), 1427 (vs), 1122 (s), 1094 (sh), 1020 (br), 835 (w), 780 (w), 752 (w), 599 (br), 484 (w)
<b>3-OCH<sub>3</sub></b>	3424 (br), 1603 (vs), 1501 (m), 1455 (sh), 1427 (vs), 1380 (sh), 1307 (w), 1251 (s), 1140 (w), 1122 (s), 1094 (sh), 1029 (m), 886 (w), 780 (s), 636 (m), 613 (m), 549 (sh), 479 (w)
<b>4-C<sub>6</sub>H<sub>4</sub></b>	3424 (br), 1607 (vs), 1515 (w), 1459 (sh), 1422 (s), 1385 (sh), 1265 (w), 1117 (m), 1104 (sh), 1020 (m), 867 (w), 789 (w), 664 (w), 613 (w)
<b>5-F<sub>2</sub></b>	3413 (br), 1630 (vs), 1542 (w), 1487 (m), 1445 (vs), 1413 (sh), 1380 (sh), 1367 (s), 1297 (w), 1191 (m), 1122 (m), 1029 (s), 900 (w), 807 (m), 780 (m), 599 (m), 544 (w)
<b>6-(CH<sub>3</sub>)<sub>2</sub></b>	3428 (br), 1700 (w), 1598 (vs), 1496 (w), 1436 (vs), 1380 (w), 1362 (w), 1288 (w), 1191 (w), 1122 (m), 1089 (sh), 1020 (sh), 988 (s), 914 (w), 794 (m), 761 (w), 669 (w), 627 (w), 585 (s), 470 (m)
<b>7-(OCH<sub>3</sub>)<sub>2</sub></b>	3432 (br), 1612 (vs), 1505 (w), 1459 (sh), 1422 (s), 1385 (sh), 1339 (w), 1265 (w), 1214 (m), 1122 (m), 1025 (m), 937 (m), 807 (m), 636 (m)
Al-MIL-101-NH <sub>2</sub>	3394 (br), 1621 (sh), 1584 (vs), 1496 (m), 1441 (vs), 1404 (sh), 1334 (sh), 1260 (sh), 1122 (s), 1089 (sh), 1020 (m), 775 (s), 618 (s), 553 (w)

<sup>[a]</sup> Abbreviations: s = strong; vs = very strong; m = medium, w = weak, sh = shoulder.

**Table 5.2** Amounts of  $\text{Al}(\text{ClO}_4)_3 \cdot 9\text{H}_2\text{O}$  and  $\text{H}_2\text{BDC-X}$  linkers used for the synthesis of the Al-MIL-101-X compounds via both solvothermal and microwave irradiation method.

Compound	Amount of $\text{Al}(\text{ClO}_4)_3 \cdot 9\text{H}_2\text{O}$		Amount of $\text{H}_2\text{BDC-X}$	
	mmol	mg	mmol	mg
<b>1-CH<sub>3</sub></b>	0.277	135	0.277	50
<b>2-NO<sub>2</sub></b>	0.236	115	0.236	50
<b>3-OCH<sub>3</sub></b>	0.255	126	0.255	50
<b>4-C<sub>6</sub>H<sub>4</sub></b>	0.232	113	0.232	50
<b>5-F<sub>2</sub></b>	0.247	121	0.247	50
<b>6-(CH<sub>3</sub>)<sub>2</sub></b>	0.257	126	0.257	50
<b>7-(OCH<sub>3</sub>)<sub>2</sub></b>	0.221	108	0.221	50
Al-MIL-101-NH <sub>2</sub>	0.276	135	0.276	50

**Table 5.3** Summary of the reaction times used for synthesizing the Al-MIL-101-X compounds by solvothermal method.

MOF	Reaction Time (h)
<b>1-CH<sub>3</sub></b>	5
<b>2-NO<sub>2</sub></b>	6
<b>3-OCH<sub>3</sub></b>	12
<b>4-C<sub>6</sub>H<sub>4</sub></b>	12
<b>5-F<sub>2</sub></b>	3
<b>6-(CH<sub>3</sub>)<sub>2</sub></b>	12
<b>7-(OCH<sub>3</sub>)<sub>2</sub></b>	5
Al-MIL-101-NH <sub>2</sub>	12

### 5.2.3 Activation of the As-Synthesized Al-MIL-101-X-CE Materials

All the as-synthesized Al-MIL-101-X materials, prepared by the solvothermal method, were activated in two steps. In the first step, the suspension of each material (0.2 g) in 30 mL methanol was placed in a Teflon-lined stainless steel autoclave and heated at 85 °C for 24 h in a conventional oven. In the second step, the white materials were collected by filtration and heated at 130 °C under dynamic vacuum for 24 h.

## 5.3 RESULTS AND DISCUSSIONS

### 5.3.1 Synthesis and Activation

The strategies used for the preparation of the functionalized Al-MIL-101-X materials were adopted from earlier reports on the  $M^{3+}/H_2BDC-X$  ( $M = Al, Cr, Fe$ ) system which resulted in MIL-53,<sup>25</sup> MIL-101 or CAU-1 (CAU = Christian-Albrechts-University)<sup>50</sup> phases depending on the synthesis parameters. It has been well-established in the literature<sup>51</sup> that MIL-101 corresponds to the kinetically stable phase, whereas MIL-53 belongs to the thermodynamically stable phase. Initially, the metastable phase of MOF-235 is observed, which is converted to MIL-53 or MIL-101 phases, depending on the reaction parameters.<sup>52</sup> MIL-101 and MIL-53 phases are formed at shorter and longer reaction times, respectively.<sup>50</sup> It has been suggested that the initially formed MIL-101 phase is transformed into MIL-53 phase when the reaction time is longer. Furthermore, the employment of higher reaction temperatures facilitates the formation of MIL-53 phase.<sup>43</sup> Thus, for the synthesis of the Al-MIL-101-X phases, we have employed shorter times (3-12 h) and moderate temperature (130 °C for Al-MIL-101-X-CE materials). We have avoided the use of polar, protic solvents (e.g.  $H_2O$ , methanol and ethanol), since these solvents in  $Al^{3+}/H_2BDC-X$  system leads to Al-MIL-53 or CAU-1 phases.<sup>50,52</sup> Thus, polar, aprotic solvents such as *N,N*-dimethylformamide (DMF), *N,N*-diethylformamide (DEF) and *N,N*-dimethylacetamide (DMA) have been employed for the synthesis of the Al-MIL-101-X materials. The nature of metal salt also plays determining role in synthesizing Al-MIL-53 and Al-MIL-101 phases. Synthesis using  $Al(NO_3)_3 \cdot 9H_2O$  causes the formation of Al-MIL-53 phase, irrespective of the solvent.<sup>26,50</sup> Hence, we have avoided this metal salt and limited our choice of metal salt to  $AlCl_3 \cdot 6H_2O$  and  $Al(ClO_4)_3 \cdot 9H_2O$ .

The procedures used for the synthesis of the functionalized Al-MIL-101-X compounds differ considerably from the formerly reported Al-MIL-101-NH<sub>2</sub> material.<sup>26,44</sup> For the optimization of the synthesis conditions of the Al-MIL-101-X materials, mixtures of aluminum salts [ $AlCl_3 \cdot 6H_2O$  and  $Al(ClO_4)_3 \cdot 9H_2O$ ] and  $H_2BDC-X$  linkers in all possible combinations were heated in polar amide solvents such as DMF, DEF and DMA. The molar ratio between the specific Al salt and the corresponding  $H_2BDC-X$  linker was kept constant at 1:1. Many of these combinations lead to the formation of Al-MIL-53-X materials. Interestingly, the reaction mixtures of  $Al(ClO_4)_3 \cdot 9H_2O$  and  $H_2BDC-X$  linkers having a molar ratio of 1:1 in DEF under

solvothermal conditions (130 °C) produced highly crystalline Al-MIL-101-X materials. The optimized reaction times varied from 3 to 12 h (Table 5.3). When the reactions were carried out for a longer time compared to the optimized reaction times, Al-MIL-53-X compounds were obtained. Similar effect of reaction time on the synthesis of metal-terephthalates (i.e., MIL-53 and MIL-101 phases) has been previously documented in the literature.<sup>51</sup> The synthesis procedures for the Al-MIL-101-X (X = -CH<sub>3</sub>, -NO<sub>2</sub>, -OCH<sub>3</sub>, -C<sub>6</sub>H<sub>4</sub>, -F<sub>2</sub>, -(CH<sub>3</sub>)<sub>2</sub>, -(OCH<sub>3</sub>)<sub>2</sub>) materials were highly reproducible. On the other hand, the attempts of synthesis of non-, fluoro- and chloro-functionalized Al-MIL-101 materials under the similar conditions yielded Al-MIL-53-X (X = -H, -F, -Cl) materials. The synthesis of the formerly reported<sup>26</sup> amino-functionalized Al-MIL-101 materials was accomplished under the presented solvothermal reaction conditions. We were able to prepare Al-MIL-101-NH<sub>2</sub> in only 12 h, compared to the report of Serra-Crespo et al.<sup>26</sup>, who have synthesized this material in 72 h. AlCl<sub>3</sub>·6H<sub>2</sub>O in DMF was used in the former synthesis procedure<sup>26</sup> of Al-MIL-101-NH<sub>2</sub>, whereas Al(ClO<sub>4</sub>)<sub>3</sub>·9H<sub>2</sub>O in DEF was employed in the presented preparation method. In both cases, the syntheses were carried out at 130 °C. It is worthy to note that Al-MIL-101-NH<sub>2</sub> material was also prepared by Hartmann et al.<sup>44</sup> These researchers have used a new approach, in which AlCl<sub>3</sub>·6H<sub>2</sub>O was added in a step-wise manner (total reaction time = 20.5 h) to the reaction mixture in DMF at 110 °C.

Since shorter reaction times were found to be suitable for the synthesis of the Al-MIL-101-X materials, preparation of the same materials were attempted by microwave irradiation method, which also requires shorter reaction times.<sup>53</sup> In fact, we were successful in synthesizing four of the presented Al-MIL-101-X (X = -CH<sub>3</sub>, -OCH<sub>3</sub>, -C<sub>6</sub>H<sub>4</sub>, -(OCH<sub>3</sub>)<sub>2</sub>) materials under identical microwave-assisted solvothermal conditions (170 °C, 10 min, 150 W). Similar to the solvothermal reactions with CE heating, the reaction mixtures of Al(ClO<sub>4</sub>)<sub>3</sub>·9H<sub>2</sub>O and H<sub>2</sub>BDC-X linkers with a molar ratio of 1:1 in DEF were used in the microwave irradiation method. Unfortunately, the crystallinity of the Al-MIL-101-X-MW materials (Figure 5.1) decreased considerably upon extended exposure to moisture from air. Due to the sensitivity of the as-synthesized Al-MIL-101-X-MW materials towards moisture, they were not activated in order to achieve permanent porosity. In contrast, the as-synthesized Al-MIL-101-X-CE materials were found to be relatively more stable in air and they were activated for gas adsorption studies.

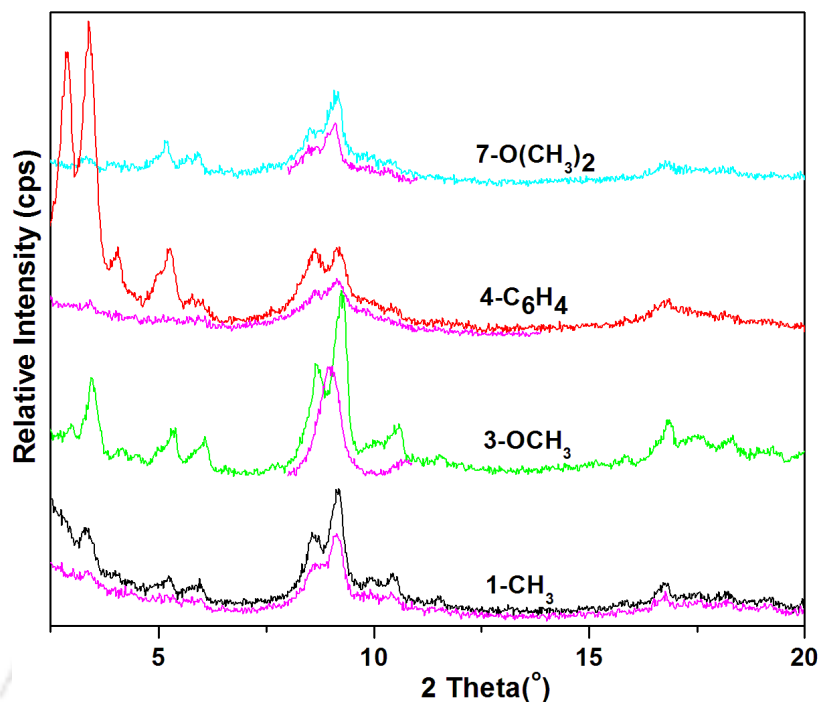


**Figure 5.1** XRPD patterns of the freshly synthesized Al-MIL-101-X-MW materials: **1-CH<sub>3</sub>** (black), **3-OCH<sub>3</sub>** (green), **4-C<sub>6</sub>H<sub>4</sub>** (red) and **7-(OCH<sub>3</sub>)<sub>2</sub>** (cyan). The XRPD patterns (magenta) of the same samples after exposure to air for 15 days are also shown.

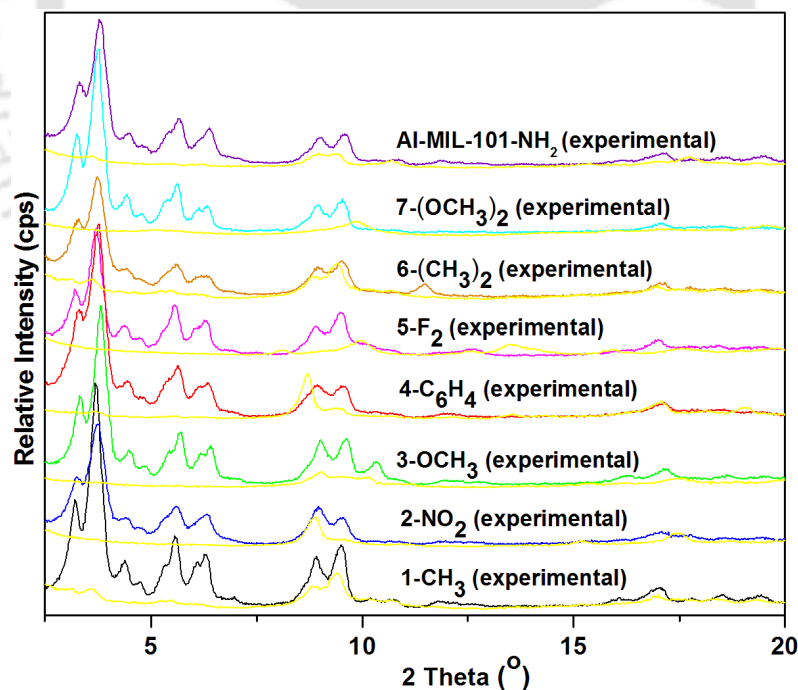


**Figure 5.2** XRPD patterns of the freshly synthesized Al-MIL-101-X-CE materials: **1-CH<sub>3</sub>** (black), **2-NO<sub>2</sub>** (blue), **3-OCH<sub>3</sub>** (green), **4-C<sub>6</sub>H<sub>4</sub>** (red), **5-F<sub>2</sub>** (magenta), **6-(CH<sub>3</sub>)<sub>2</sub>** (orange), **7-(OCH<sub>3</sub>)<sub>2</sub>** (cyan) and Al-MIL-101-NH<sub>2</sub> (violet). The XRPD patterns (yellow) of the same samples after stirring with water for 24 h are also shown.

The guest molecules encapsulated within the pores of the as-synthesized Al-MIL-101-X-CE materials were removed in a two-step activation procedure similar to that reported for the previously reported<sup>26</sup> Al-MIL-101-NH<sub>2</sub> material. In the first step, the guest molecules were exchanged with more volatile and thus easily removable methanol molecules by heating the as-synthesized compounds in methanol. In the second step, the methanol molecules were removed from the pores by heating the filtered materials at 130 °C under dynamic vacuum for 24 h in order to obtain the thermally activated materials. The thermally activated Al-MIL-101-X-CE materials were not sensitive towards moisture from air. However, the crystallinity (and hence structural integrity) of the samples deteriorated significantly when treated with water, as verified by the XRPD experiments (Figure 5.2). It is worthy to note that MIL-101 analogues of Fe(III)<sup>54</sup> and Al(III)<sup>44</sup> were formerly found to be unstable in water, whereas those of Cr(III)<sup>27</sup> possess high hydrothermal stability. Furthermore, the MIL-53 analogues of Fe(III),<sup>55</sup> Al(III)<sup>25</sup> and Cr(III)<sup>56</sup> are stable in water. The higher hydrothermal stability of MIL-53 analogues compared to the MIL-101 variants might be ascribed<sup>57</sup> to the sterically more shielded [MO<sub>6</sub>] inorganic building units (IBUs) of MIL-53 as compared to the open ones of MIL-101. Hence, except for Cr-MIL-101, the IBUs of Fe(III) and Al(III) analogues of MIL-101 are prone to attack by water. The hydrothermal stability of Cr-MIL-101 is typically attributed<sup>58</sup> to the considerably low exchange rates of the ligands with water because of the gain in energy by ligand field stabilization energy.

### 5.3.2 Structure Description

The experimental XRPD patterns of Al-MIL-101-X-CE and Al-MIL-101-X-MW compounds (Figure 5.3 and 5.4) are similar to the calculated XRPD pattern of un-functionalized Cr-MIL-101 exhibiting a cubic structure (Figure 5.5). Therefore, the Al-MIL-101-X materials are isostructural with Cr-MIL-101, which is also clear from the similarity between their XRPD patterns. The framework structures of Al-MIL-101-X materials are described here in brief, since the structure of Cr-MIL-101 (Figure 5.5) is already reported.<sup>27</sup> The structures of the as-synthesized Al-MIL-101-X materials are built up of trimeric oxo-centered [Al<sub>3</sub>(μ<sub>3</sub>-O)Cl(DEF)<sub>2</sub>]<sup>6+</sup> building blocks that contain [AlO<sub>6</sub>] octahedra. It is worthy to note that the formation of chloride anions by thermal decomposition of metal perchlorate salts has been previously reported in literature.<sup>59</sup> The trimeric building blocks are interconnected by the functionalized terephthalate ligands along the edges resulting in the formation of supertetrahedra

(ST). Further connection of the ST with each other in three-dimension leads to the augmented zeolite Mobil Thirty-Nine (MTN) type of framework.

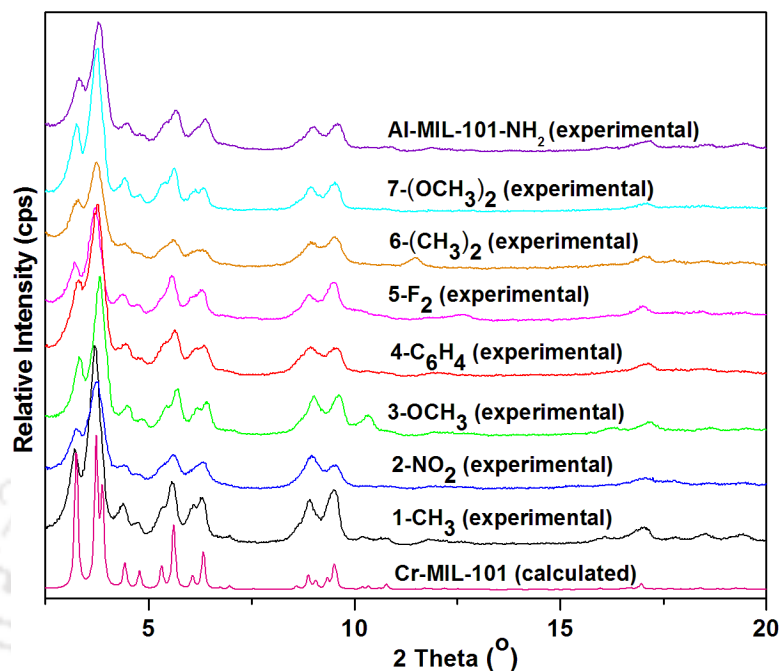


**Figure 5.3** Calculated XRPD pattern of Cr-MIL-101 (pink) and experimental XRPD patterns of the thermally activated 1-CH<sub>3</sub> (black), 2-NO<sub>2</sub> (blue), 3-OCH<sub>3</sub> (green), 4-C<sub>6</sub>H<sub>4</sub> (red), 5-F<sub>2</sub> (magenta), 6-(CH<sub>3</sub>)<sub>2</sub> (orange), 7-(OCH<sub>3</sub>)<sub>2</sub> (cyan) and Al-MIL-101-NH<sub>2</sub> (violet) synthesized by solvothermal method.

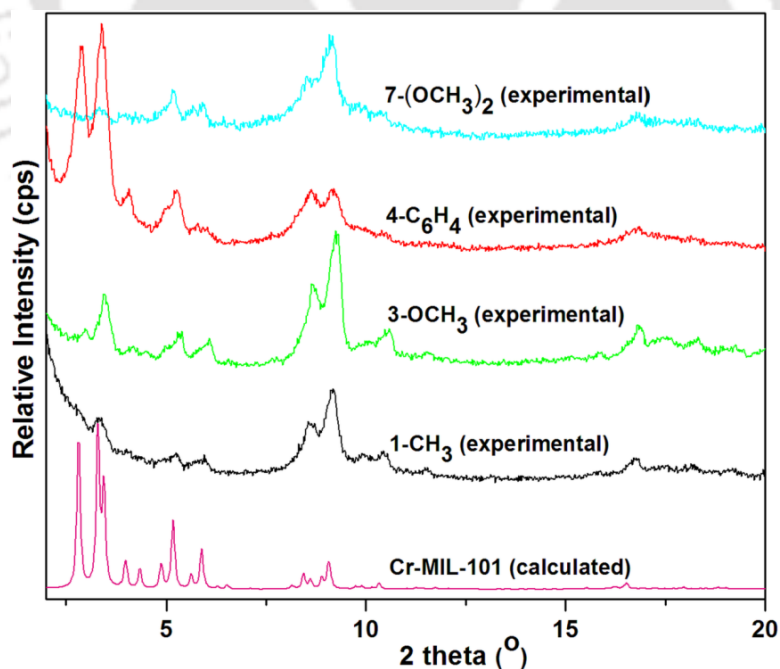


**Figure 5.4** Calculated XRPD pattern of Cr-MIL-101 (pink) and experimental XRPD patterns of the as-synthesized 1-CH<sub>3</sub> (black), 3-OCH<sub>3</sub> (green), 4-C<sub>6</sub>H<sub>4</sub> (red) and 7-(OCH<sub>3</sub>)<sub>2</sub> (cyan) synthesized by microwave irradiation method.

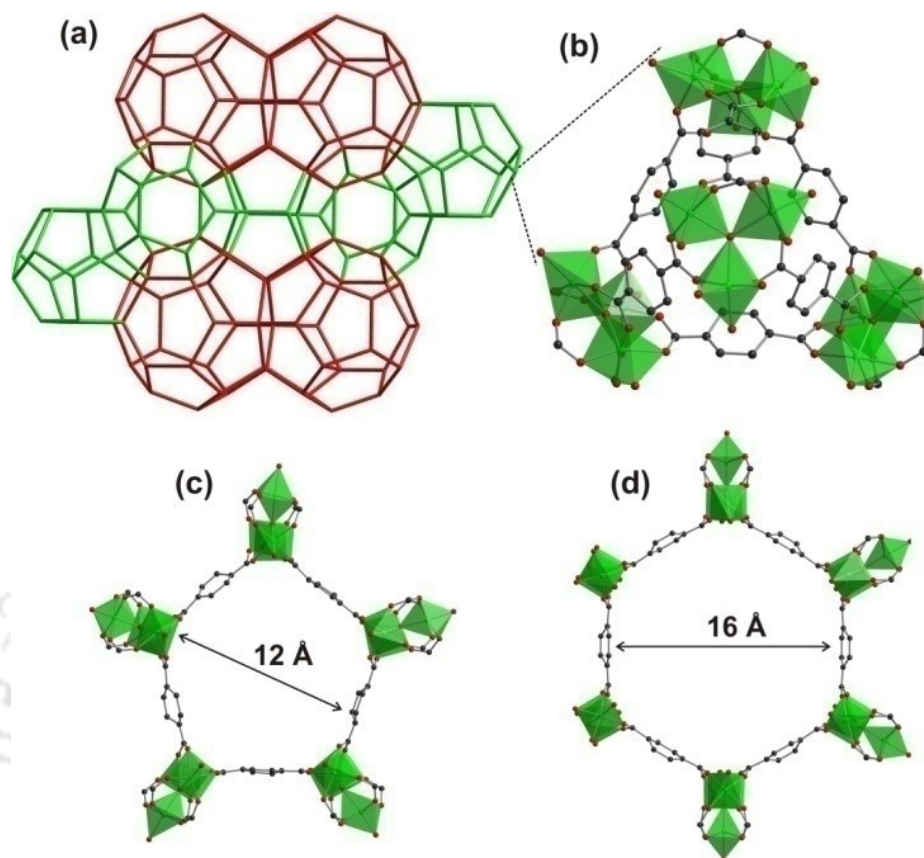


**Figure 5.5** (a) Framework structure of Cr-MIL-101 having MTN topology and containing smaller (green) and larger (red) mesoporous cages. The structure is constructed from (b) supertetrahedra (ST), which consist of trimeric oxido-centered  $[\text{Cr}_3(\mu_3\text{-O})(\text{F})(\text{H}_2\text{O})_2]^{6+}$  building blocks at the vertices interconnected by terephthalate ligands. The smaller and larger cages bear only pentagonal (c) or a combination of pentagonal (c) and hexagonal (d) windows, respectively. Color codes: Cr, green octahedra; C, gray; O, red. The MTN framework (a) and the portions of Cr-MIL-101 network (b-d) have been drawn by utilizing the atomic coordinates given in “Database of Zeolite Structures”<sup>60</sup> and ref. 27, respectively.

It is noteworthy that the labile coordination sites of the  $[\text{AlO}_6]$  octahedra in the as-synthesized Al-MIL-101-X materials are filled with the O-donor atoms from DEF molecules or chlorine atoms, rather than fluorine atoms or water molecules as in the case of Cr-MIL-101. The existence of such coordinated DEF molecules in the structures of the as-synthesized Al-MIL-101-X materials has been verified by IR spectroscopy and TG analyses (*cf.* Infrared Spectroscopy and Thermal Stability sections). The presence of coordinated chloride anions has been corroborated by energy dispersive X-ray (EDX) experiments (Figures 5.6 to 5.13). The frameworks comprise two types of mesoporous cages. The smaller cage is built up of 12 pentagonal rings possessing a free diameter of *ca.* 12 Å, and the accessible diameter of the cage

is *ca.* 29 Å. The larger cage consists of 12 pentagonal and 4 hexagonal rings with a free diameter of the hexagonal rings of *ca.* 16 Å and an accessible cage diameter of *ca.* 34 Å. The smaller and larger cages are composed of 20 and 28 ST, respectively. They are present in a ratio of 2:1.

It is worthy to mention that the molecular formula (i.e.,  $[\text{Al}_3\text{OCl}(\text{DEF})_2(\text{BDC-X})_3]$ ) of the as-synthesized Al-MIL-101-X materials have been assigned based on the fact that the existence of chloride anions and DEF molecules in 1:2 ratios will make the structures electrostatically neutral. The assignment of the molecular formulae of the as-synthesized materials by spectroscopic techniques (TG, EDX and IR) is tentative. This is due to the fact that the chloride anions or DEF molecules ascribed as coordinated ligands might also correspond to the guest species inside the pores. For example, the investigation of the structure of Al-MIL-100 by solid-state NMR spectroscopy disclosed that the pores also encapsulate different species such as nitrate, unreacted trimesic acid and water molecules.<sup>61</sup> It is noteworthy that the DMF molecules were found to serve as the coordinated ligands in the previously reported Al-MIL-101-NH<sub>2</sub> material.<sup>26</sup>

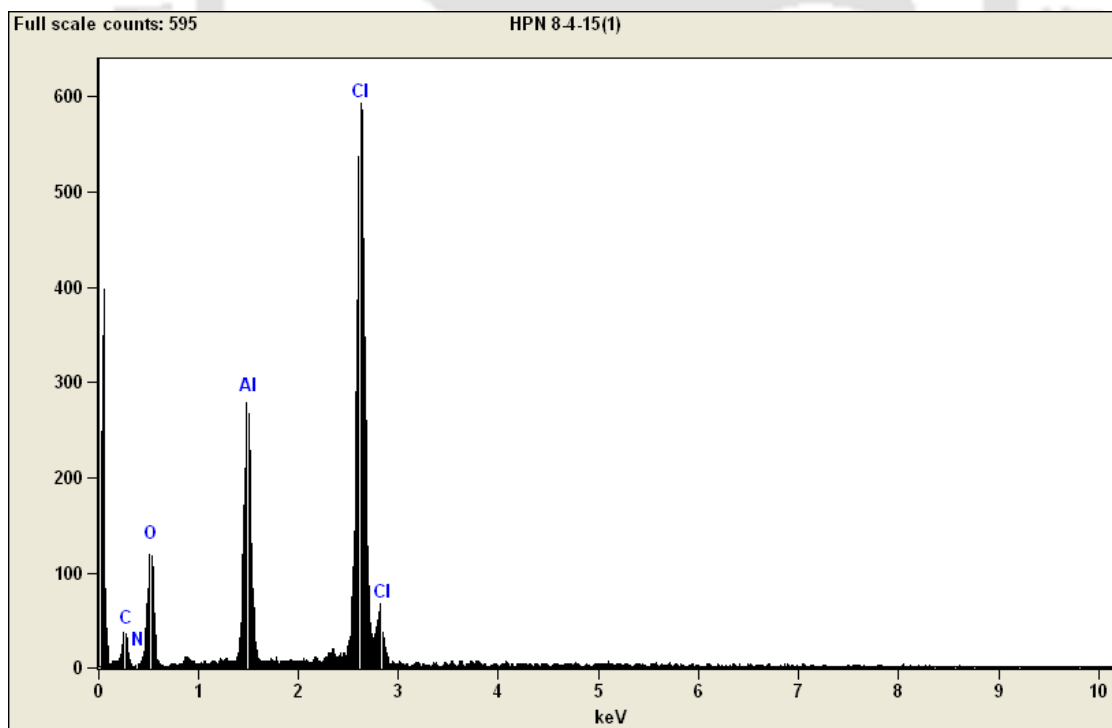


**Figure 5.6** EDX spectrum of thermally activated 1-CH<sub>3</sub>.

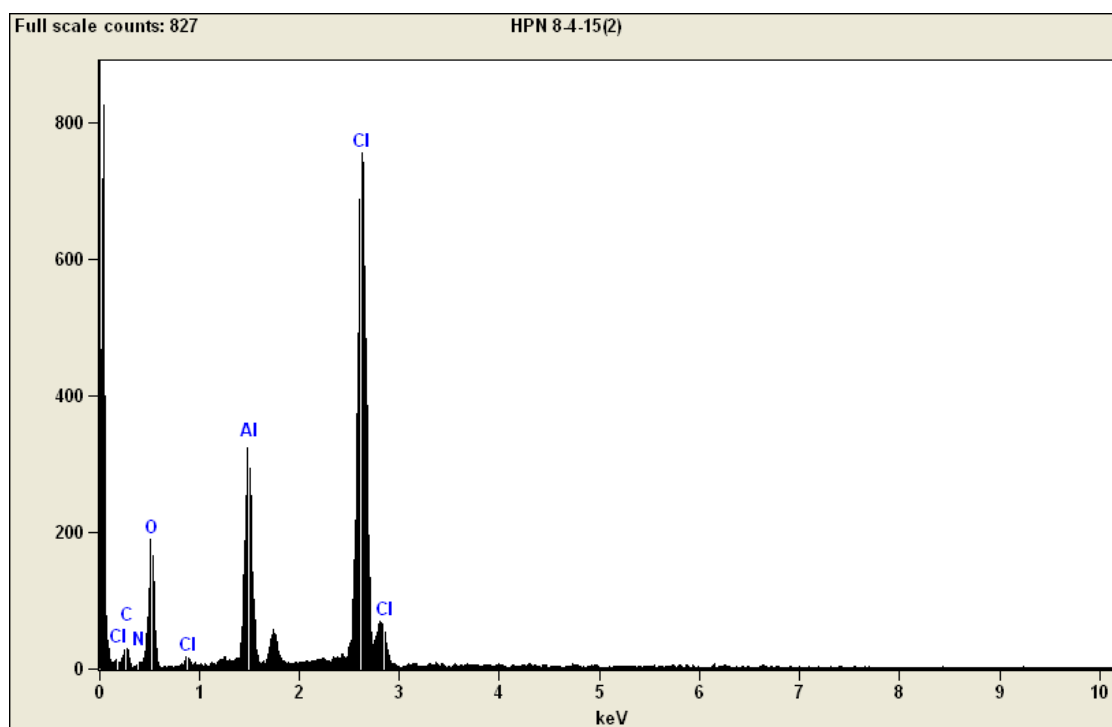


Figure 5.7 EDX spectrum of thermally activated 2-NO<sub>2</sub>.

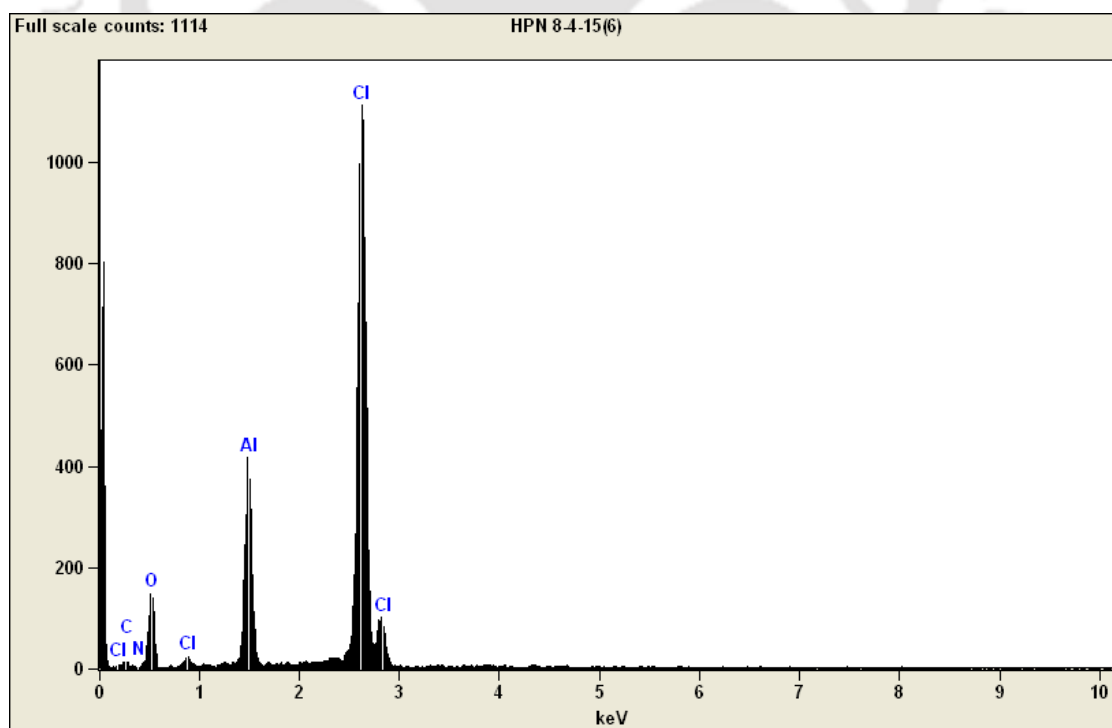


Figure 5.8 EDX spectrum of thermally activated 3-OCH<sub>3</sub>.

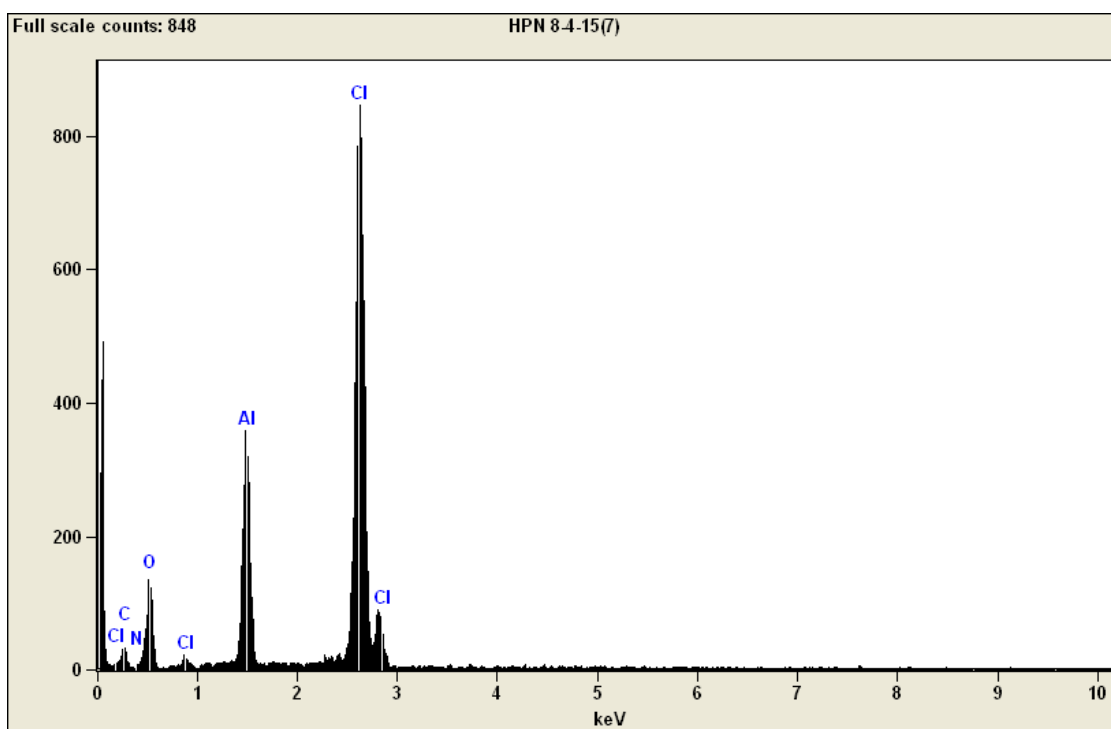


Figure 5.9 EDX spectrum of thermally activated 4-C<sub>6</sub>H<sub>4</sub>.

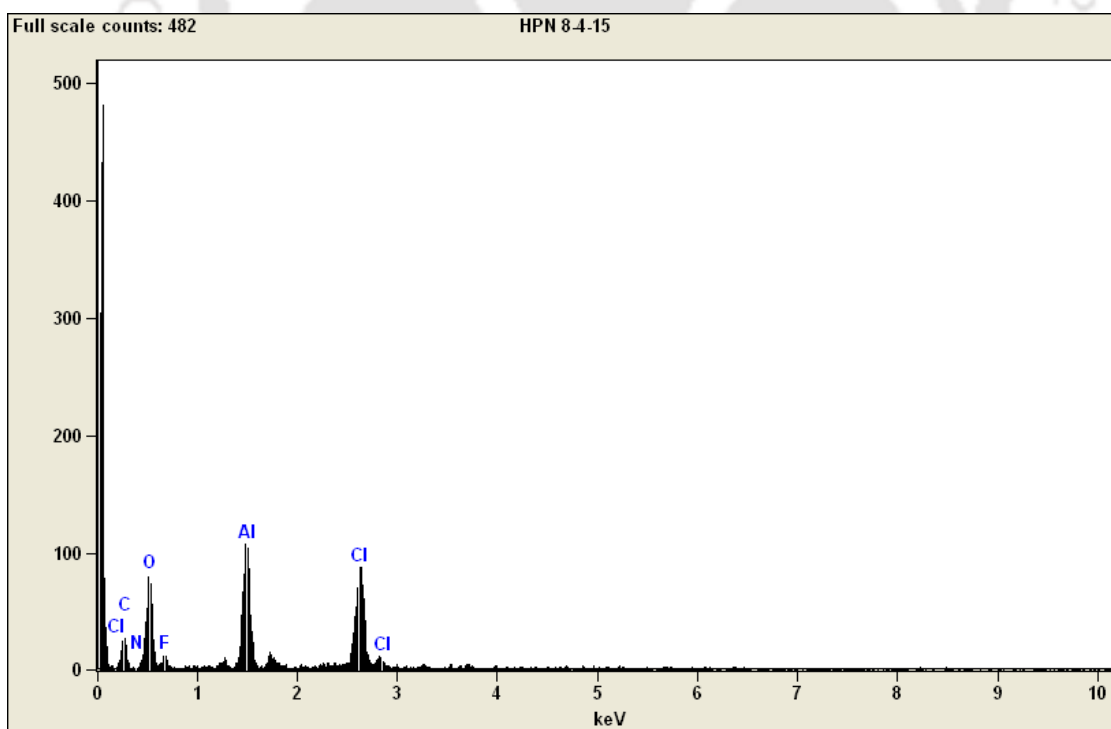


Figure 5.10 EDX spectrum of thermally activated 5-F<sub>2</sub>.

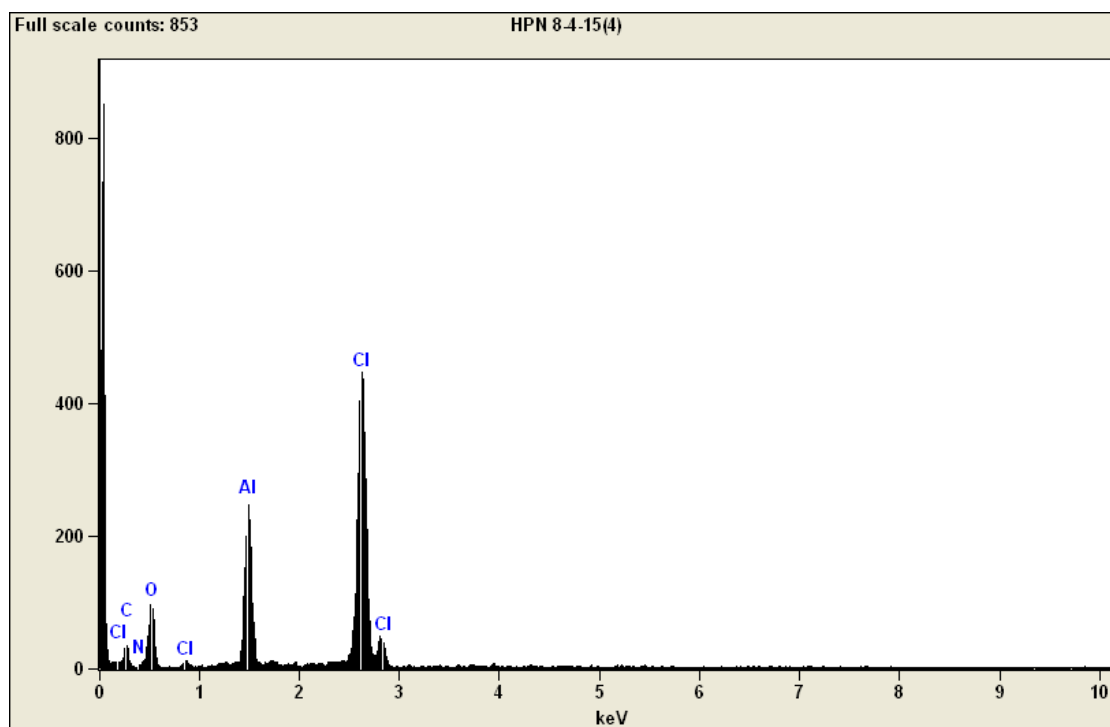


Figure 5.11 EDX spectrum of thermally activated 6-(CH<sub>3</sub>)<sub>2</sub>.

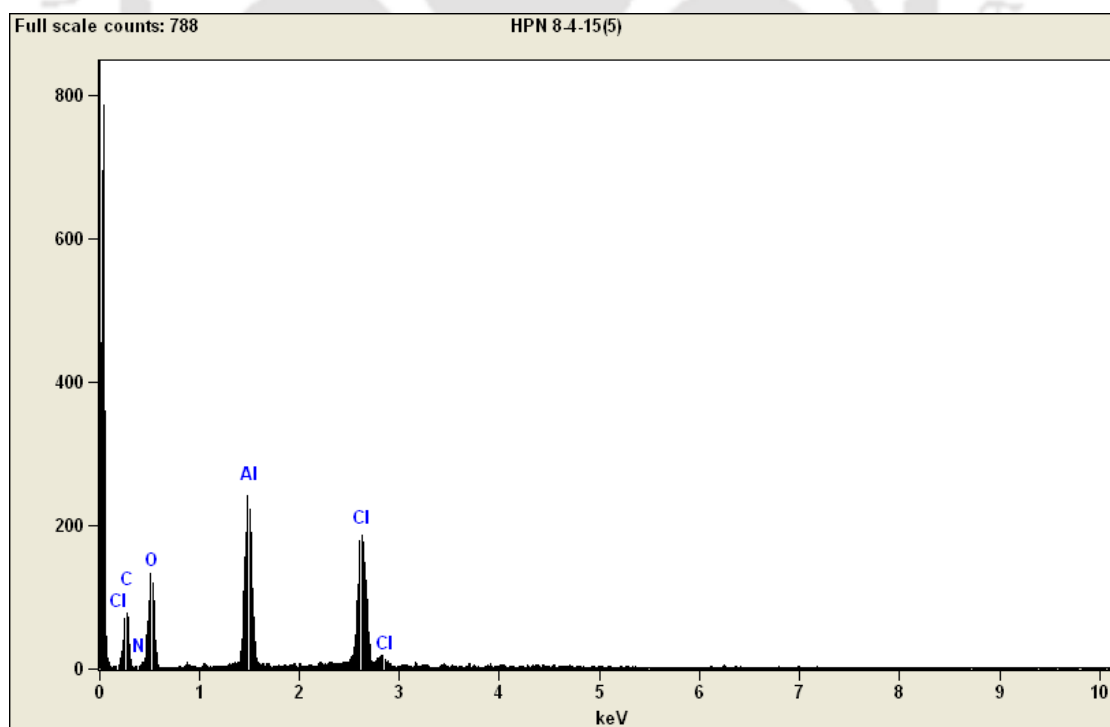
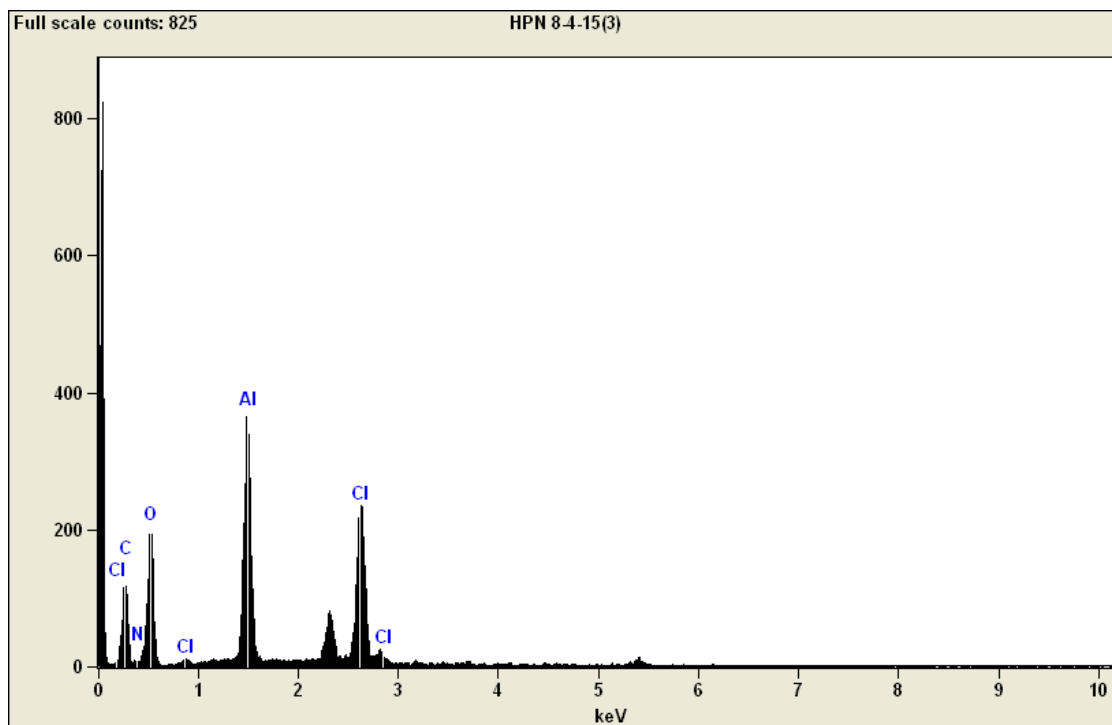


Figure 5.12 EDX spectrum of thermally activated 7-(OCH<sub>3</sub>)<sub>2</sub>.



**Figure 5.13** EDX spectrum of thermally activated Al-MIL-101-NH<sub>2</sub>.

The TG curves and FT-IR spectra of the thermally activated materials indicate that the coordinated DEF molecules are absent in the structures. Thus, we hypothesize the following: during the activation process, the coordinated DEF molecules have been exchanged with methanol molecules, which have been subsequently removed by heating. The thermally activated materials absorb water from air after cooling to room temperature. In this way, the activated Al-MIL-101-X materials incorporate coordinated H<sub>2</sub>O molecules in the structures and they bear tentative molecular formula of [Al<sub>3</sub>OCl(H<sub>2</sub>O)<sub>2</sub>(BDC-X)<sub>3</sub>.L<sub>x</sub>(H<sub>2</sub>BD-X)] (Table 5.4).

### 5.3.3 Infrared Spectroscopy

As expected, the FT-IR spectra of each of the Al-MIL-101-X material (Figures 5.14-5.16) are very similar, since all the materials are isostructural. In the FT-IR spectra of the thermally activated Al-MIL-101-X-CE materials, the strong absorption bands owing to the asymmetric and symmetric –CO<sub>2</sub> stretching vibrations of the coordinated terephthalate ligand molecules are located in regions 1595-1625 cm<sup>-1</sup> and 1420-1445 cm<sup>-1</sup>, respectively.<sup>62</sup>

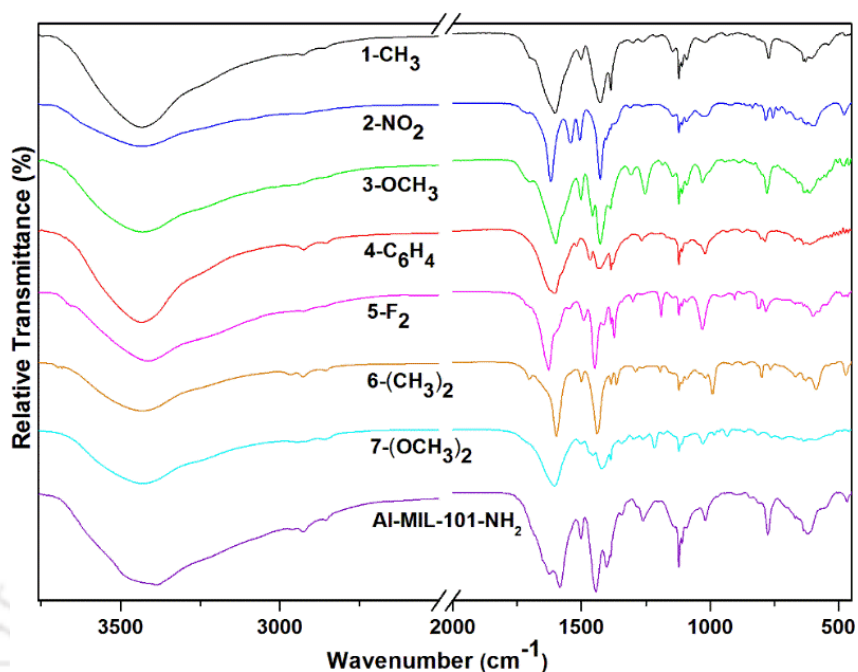


**Figure 5.14** FT-IR spectra of the thermally activated 1-CH<sub>3</sub> (black), 2-NO<sub>2</sub> (blue), 3-OCH<sub>3</sub> (green), 4-C<sub>6</sub>H<sub>4</sub> (red), 5-F<sub>2</sub> (magenta), 6-(CH<sub>3</sub>)<sub>2</sub> (orange), 7-(OCH<sub>3</sub>)<sub>2</sub> (cyan) and Al-MIL-101-NH<sub>2</sub> (violet) synthesized by solvothermal method.

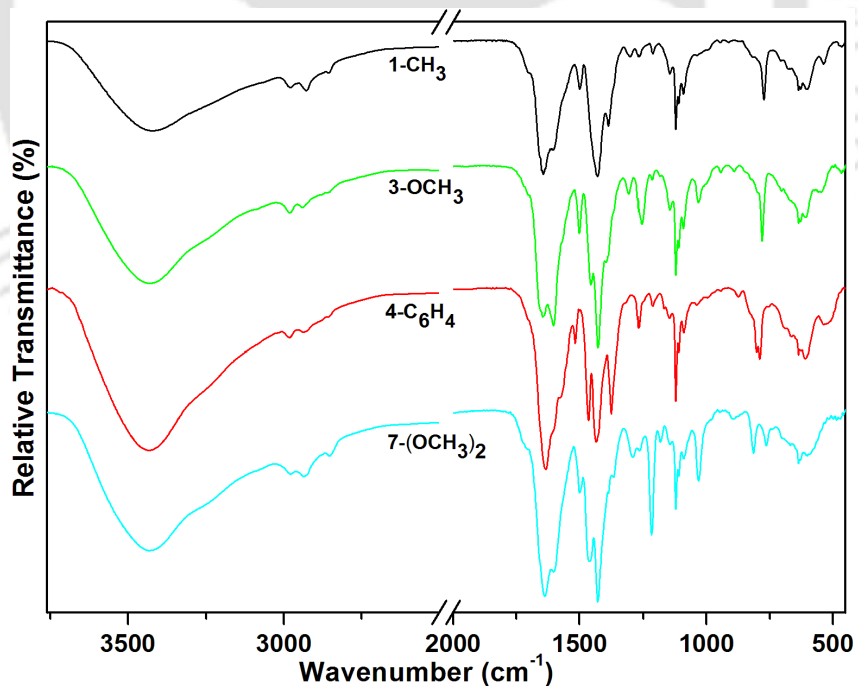


**Figure 5.15** FT-IR spectra of the thermally activated 1-CH<sub>3</sub> (black), 3-OCH<sub>3</sub> (green), 4-C<sub>6</sub>H<sub>4</sub> (red) and 7-(OCH<sub>3</sub>)<sub>2</sub> (cyan) synthesized by microwave irradiation method.

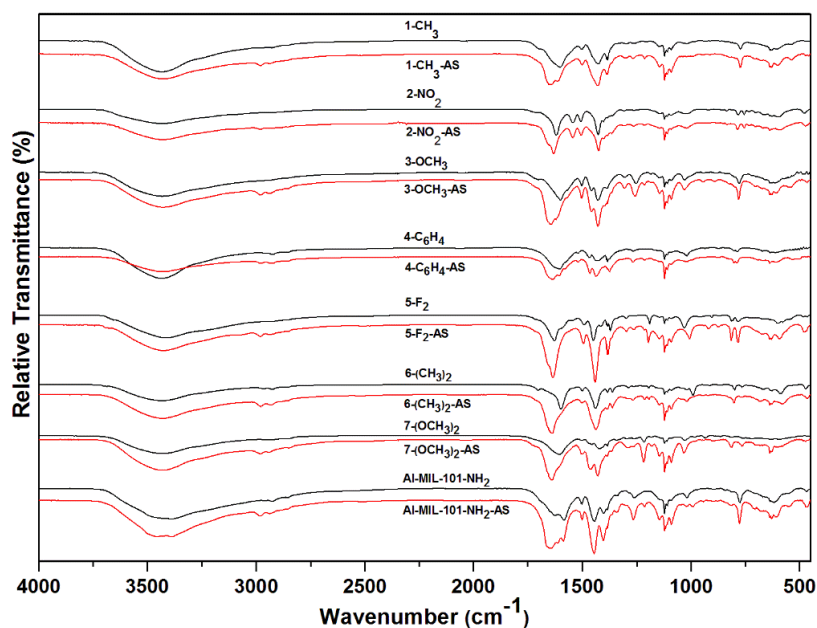


**Figure 5.16** Comparison among the FT-IR spectra of the as-synthesized (red) and thermally activated (black) Al-MIL-101-X materials synthesized by solvothermal method. AS = as-synthesized.

In the IR spectra of the as-synthesized materials, the carbonyl stretching vibrations of the coordinated DEF molecules show strong absorption bands in the region  $1625\text{--}1645\text{ cm}^{-1}$ , which are overlapped with the asymmetric  $\text{--CO}_2$  stretching vibrations of coordinated BDC-X molecules. The absorption bands for the occluded  $\text{H}_2\text{BDC-X}$  (especially for  $\text{--CO}_2\text{H}$  groups) and coordinated DEF molecules (particularly for carbonyl stretching vibrations) are very weak or absent in the IR spectra of the thermally activated materials, indicating almost complete removal of guest molecules from the pores of the materials.<sup>63</sup>

### 5.3.4 Thermal Stability

In order to investigate the thermal stability of all the Al-MIL-101-X materials, thermogravimetric analyses (Figure 5.17) were performed with the as-synthesized as well as thermally activated forms of the materials in air atmosphere. According to the TG analyses, all the materials are thermally stable up to  $260\text{--}430\text{ }^\circ\text{C}$ . This wide temperature range suggests that the various functional groups play great roles in determining thermal stability of all the Al-MIL-101-X materials. The thermal stability of the materials decreases in the following order: **4-C<sub>6</sub>H<sub>4</sub>** ( $430\text{ }^\circ\text{C}$ ) > **5-F<sub>2</sub>** ( $410\text{ }^\circ\text{C}$ ) > **1-CH<sub>3</sub>** ( $400\text{ }^\circ\text{C}$ ) > **6-(CH<sub>3</sub>)<sub>2</sub>** ( $370\text{ }^\circ\text{C}$ ) > **3-OCH<sub>3</sub>** ( $350\text{ }^\circ\text{C}$ ) > **2-NO<sub>2</sub>** ( $300\text{ }^\circ\text{C}$ ) > **7-(OCH<sub>3</sub>)<sub>2</sub>** ( $260\text{ }^\circ\text{C}$ ). In general, materials bearing less hydrophilic functional groups (e.g.  $\text{--C}_6\text{H}_4$ ,  $\text{--F}$  and  $\text{--CH}_3$ ) have shown higher thermal stability compared to those possessing

more hydrophilic functional groups, which is in agreement with an earlier report.<sup>64</sup> However, as pointed out by Makal et al.,<sup>64</sup> the standard TG experiment might not describe the thermal stability of a MOF compound precisely, since the thermal stability obtained from TGA and in-situ synchrotron XRPD thermal decomposition experiments were different in their studies. The highest thermal stability of **4-C<sub>6</sub>H<sub>4</sub>** is slightly higher than the un-functionalized Cr-MIL-101 compound, which decomposes above 400 °C.<sup>65</sup> The thermal stability of the previously reported Al-MIL-101-NH<sub>2</sub> material, which decomposes above 380 °C, lies within the range of thermal stability of the presented materials.<sup>26</sup>

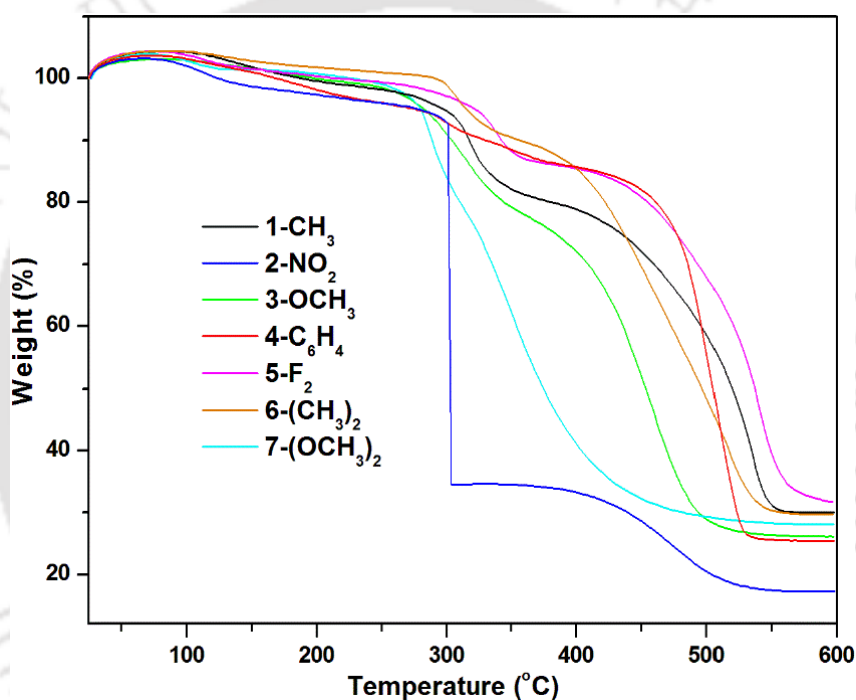


**Figure 5.17** TGA curves of the thermally activated **1-CH<sub>3</sub>** (black), **2-NO<sub>2</sub>** (blue), **3-OCH<sub>3</sub>** (green), **4-C<sub>6</sub>H<sub>4</sub>** (red), **5-F<sub>2</sub>** (magenta), **6-(CH<sub>3</sub>)<sub>2</sub>** (orange) and **7-(OCH<sub>3</sub>)<sub>2</sub>** (cyan) synthesized by solvothermal method. The TG analyses were performed in an air atmosphere.

In the TG traces of the as-synthesized Al-MIL-101-X materials, the first weight loss steps in the 50-200 °C range might be ascribed to the removal of occluded/coordinated water and DEF molecules. The second weight loss steps, which occur up to the decomposition temperatures, might be attributed to the removal of guest H<sub>2</sub>BDC-X molecules. Below the decomposition temperatures, the TG curves of the thermally activated (Figure 5.17) forms of all the materials (except **2-NO<sub>2</sub>** and **7-(OCH<sub>3</sub>)<sub>2</sub>**) exhibit one weight loss step in the 250-390 °C range due to the removal of occluded H<sub>2</sub>BDC-X molecules. The observed weight losses for the thermally

activated materials are in agreement with the calculated ones (Tables 5.4). The presence of guest functionalized terephthalic acid molecules in the pores of the thermally activated materials indicates incomplete activation of the materials.

**Table 5.4** Weight loss steps in TG curves for the thermally activated forms of Al-MIL-101-X-CE materials and their tentative molecular formula.

Compound	$L_x$ <sup>[a]</sup>	2 <sup>nd</sup> Weight Loss (%): Obs. / Cal.	Molecular Formula
<b>1-CH<sub>3</sub></b>	0.8	16.7/17.0	$[\text{Al}_3\text{OCl}(\text{H}_2\text{O})_2(\text{C}_9\text{H}_6\text{O}_4)_3] \cdot 0.8(\text{C}_9\text{H}_8\text{O}_4)$
<b>2-NO<sub>2</sub></b>	-	-	$[\text{Al}_3\text{OCl}(\text{H}_2\text{O})_2(\text{C}_8\text{H}_3\text{NO}_6)_3]$
<b>3-OCH<sub>3</sub></b>	0.9	19.3/19.0	$[\text{Al}_3\text{OCl}(\text{H}_2\text{O})_2(\text{C}_9\text{H}_6\text{O}_5)_3] \cdot 0.9(\text{C}_9\text{H}_8\text{O}_5)$
<b>4-C<sub>6</sub>H<sub>4</sub></b>	0.4	10.4/9.7	$[\text{Al}_3\text{OCl}(\text{H}_2\text{O})_2(\text{C}_{12}\text{H}_{10}\text{O}_4)_3] \cdot 0.4(\text{C}_{12}\text{H}_{12}\text{O}_4)$
<b>5-F<sub>2</sub></b>	0.6	13.4/13.6	$[\text{Al}_3\text{OCl}(\text{H}_2\text{O})_2(\text{C}_8\text{H}_2\text{F}_2\text{O}_4)_3] \cdot 0.6(\text{C}_8\text{H}_4\text{F}_2\text{O}_4)$
<b>6-(CH<sub>3</sub>)<sub>2</sub></b>	0.4	9.5/9.4	$[\text{Al}_3\text{OCl}(\text{H}_2\text{O})_2(\text{C}_{10}\text{H}_8\text{O}_4)_3] \cdot 0.5(\text{C}_{10}\text{H}_{10}\text{O}_4)$
<b>7-(OCH<sub>3</sub>)<sub>2</sub></b>	-	-	$[\text{Al}_3\text{OCl}(\text{H}_2\text{O})_2(\text{C}_{10}\text{H}_8\text{O}_6)_3]$

[a]  $L_x$  = No. of H<sub>2</sub>BDC-X Molecules Removed in 2<sup>nd</sup> Weight Loss Step

### 5.3.5 Gas Adsorption Properties

The N<sub>2</sub> sorption experiments performed with the thermally activated forms of all the Al-MIL-101-X-CE compounds exhibit type-I adsorption isotherms (Figure 5.18) with a small step in the adsorption curves at  $p/p_0 = 0.2$ . These two steps were previously attributed to the different fillings of the cavities. Only the supertetrahedra (ST) are filled at very low relative pressures ( $p/p_0 < 0.05$ ), whereas the medium ( $p/p_0 = 0.15$ ) and the larger ( $p/p_0 = 0.20$ ) cavities are filled as the relative pressures increase.<sup>66</sup> These types of shapes of the adsorption isotherms have been formerly reported in the literature for the M-MIL-101-X (M = Cr, Fe, V and Al) materials.<sup>12, 26, 27, 30-44, 67</sup> The specific BET surface areas (Table 5.5) were determined from the N<sub>2</sub> adsorption isotherms. They reveal significant porosities, which are lower compared to those of the unfunctionalized Cr-MIL-101 material.<sup>27</sup> The value of BET surface area is highest for **1-CH<sub>3</sub>** among the functionalized Al-MIL-101-X materials. The BET surface areas of the materials decrease in the order: **1-CH<sub>3</sub>** > Al-MIL-101-NH<sub>2</sub> > **3-OCH<sub>3</sub>** > **7-(OCH<sub>3</sub>)<sub>2</sub>** > **2-NO<sub>2</sub>** ≈ **6-(CH<sub>3</sub>)<sub>2</sub>** > **4-C<sub>6</sub>H<sub>4</sub>** > **5-F<sub>2</sub>**. In most cases, the mono-functionalized Al-MIL-101-X materials have displayed higher BET surface area values compared to those of the di-functionalized variants, as expected. In general, the observed BET surface area values of the compounds are in agreement with the size of the attached functional groups. The discrepancies between the experimental and expected

(based on the size or steric dimension of the functional groups)<sup>68</sup> BET surface area values for some materials might be attributed to the incomplete activation of the materials. It is worthy to note that the BET surface area of the Al-MIL-101-NH<sub>2</sub> material (2230 m<sup>2</sup> g<sup>-1</sup>) is significantly lower compared to the report of Hartmann et al. (3099 m<sup>2</sup> g<sup>-1</sup>),<sup>44</sup> but it is slightly higher compared to the value reported by Serra-Crespo et al. (2100 m<sup>2</sup> g<sup>-1</sup>).<sup>26</sup>

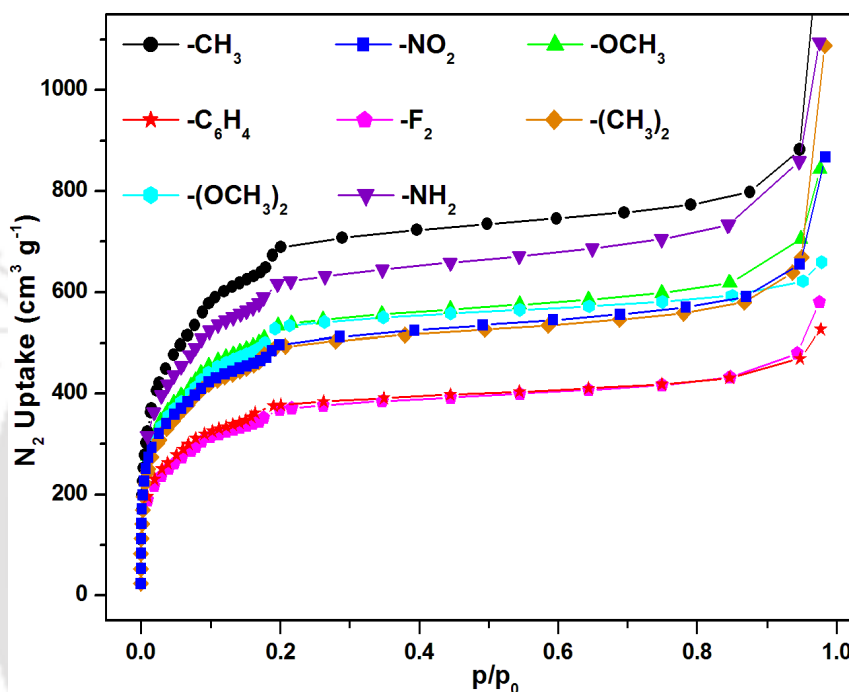


**Figure 5.18** N<sub>2</sub> adsorption isotherms of the thermally activated **1-CH<sub>3</sub>** (black, circles), **2-NO<sub>2</sub>** (blue, squares), **3-OCH<sub>3</sub>** (green, triangles), **4-C<sub>6</sub>H<sub>4</sub>** (red, stars), **5-F<sub>2</sub>** (magenta, pentagons), **6-(CH<sub>3</sub>)<sub>2</sub>** (orange, rotated squares), **7-(OCH<sub>3</sub>)<sub>2</sub>** (cyan, hexagons) and Al-MIL-101-NH<sub>2</sub> (violet, upside-down triangles) synthesized by solvothermal method. The adsorption curves were recorded at -196 °C.

**Table 5.5** Specific BET surface areas of the Al-MIL-101-X materials synthesized by solvothermal method.

MOF	BET Surface Area (m <sup>2</sup> g <sup>-1</sup> )	MOF	BET Surface Area (m <sup>2</sup> g <sup>-1</sup> )
<b>1-CH<sub>3</sub></b>	2398	<b>5-F<sub>2</sub></b>	1328
<b>2-NO<sub>2</sub></b>	1725	<b>6-(CH<sub>3</sub>)<sub>2</sub></b>	1728
<b>3-OCH<sub>3</sub></b>	1928	<b>7-(OCH<sub>3</sub>)<sub>2</sub></b>	1906
<b>4-C<sub>6</sub>H<sub>4</sub></b>	1350	Al-MIL-101-NH <sub>2</sub>	2230

The CO<sub>2</sub> adsorption experiments were performed with the thermally activated Al-MIL-101-X-CE materials at 0 °C up to 1 bar. As shown in Figure 5.19, the CO<sub>2</sub> adsorption isotherms of all the compounds follow type-I behavior in the pressure range from 0 to 1 bar. The CO<sub>2</sub> uptake values (mmol g<sup>-1</sup>) of the materials at 1 bar (i.e. p/p<sub>0</sub> = 0.3) decrease in the order: **1-CH<sub>3</sub>** (3.0) > Al-MIL-101-NH<sub>2</sub> (2.9) > **3-OCH<sub>3</sub>** (2.7) > **2-NO<sub>2</sub>** (2.5) > **7-(OCH<sub>3</sub>)<sub>2</sub>** (2.2) > **6-(CH<sub>3</sub>)<sub>2</sub>** (1.9) > **5-F<sub>2</sub>** (1.8) > **4-C<sub>6</sub>H<sub>4</sub>** (1.6). In comparison, the N<sub>2</sub> adsorption capacities at p/p<sub>0</sub> = 0.3 follow the same sequence as that of the specific surface areas. Hence, at p/p<sub>0</sub> = 0.3, the order of CO<sub>2</sub> uptake values does not completely match with that of N<sub>2</sub> adsorption capacities. This fact suggests that the CO<sub>2</sub> adsorption capacities of the Al-MIL-101-X materials are dependent on both the size and nature of the attached functional groups. The size of the functional groups determines the specific surface areas, whereas the nature of attached functional groups governs the nature of framework-CO<sub>2</sub> interactions.

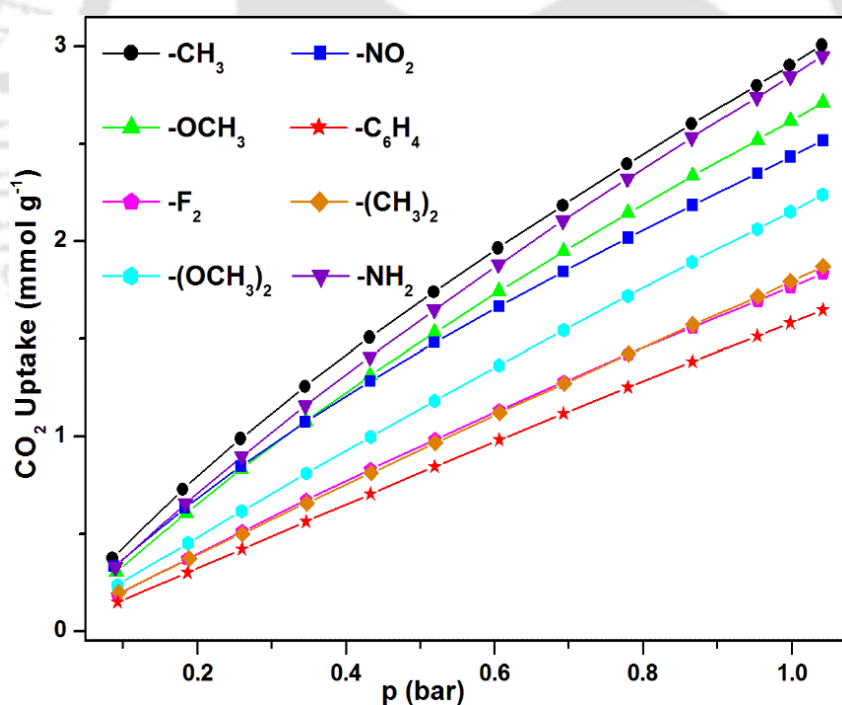


**Figure 5.19** CO<sub>2</sub> adsorption isotherms of the thermally activated **1-CH<sub>3</sub>** (black, circles), **2-NO<sub>2</sub>** (blue, squares), **3-OCH<sub>3</sub>** (green, triangles), **4-C<sub>6</sub>H<sub>4</sub>** (red, stars), **5-F<sub>2</sub>** (magenta, pentagons), **6-(CH<sub>3</sub>)<sub>2</sub>** (orange, rotated squares), **7-(OCH<sub>3</sub>)<sub>2</sub>** (cyan, hexagons) and Al-MIL-101-NH<sub>2</sub> (violet, upside-down triangles) synthesized by solvothermal method. The adsorption curves were measured at 0 °C.

## 5.4 CONCLUSIONS

We have presented the facile synthesis, full characterization and gas adsorption properties of seven new functionalized Al-MIL-101-X (X = -CH<sub>3</sub>, -NO<sub>2</sub>, -OCH<sub>3</sub>, -C<sub>6</sub>H<sub>4</sub>, -F<sub>2</sub>, -(CH<sub>3</sub>)<sub>2</sub>, -(OCH<sub>3</sub>)<sub>2</sub>) materials. The seven new materials along with the formerly reported Al-MIL-101-NH<sub>2</sub> compound were prepared by employing stoichiometric mixtures of Al(ClO<sub>4</sub>)<sub>3</sub>·9H<sub>2</sub>O and H<sub>2</sub>BDC-X linkers in DEF under similar solvothermal conditions (130 °C, 3-12 h) with conventional electric (CE) heating. The Al-MIL-101-X materials with X = -CH<sub>3</sub>, -OCH<sub>3</sub>, -C<sub>6</sub>H<sub>4</sub> and -(OCH<sub>3</sub>)<sub>2</sub> were also prepared under identical microwave-assisted solvothermal conditions (170 °C, 10 min, 150 W) by employing similar reaction mixtures as those used during the syntheses with CE heating. Thus, a significant reduction in the reaction time was observed in the microwave irradiation method as compared to the solvothermal technique. The phase purity of the materials was verified by XRPD analysis, FT-IR spectroscopy, thermogravimetric and elemental analysis. All the Al-MIL-101-X materials showed high thermal stability up to 260-430 °C in an air atmosphere. The thermally activated forms of all the materials show significant porosity, as disclosed by the N<sub>2</sub> (S<sub>BET</sub> in the range of 1328-2398 m<sup>2</sup> g<sup>-1</sup>) and CO<sub>2</sub> (uptake values in the range of 1.6-3.0 mmol g<sup>-1</sup> at 0 °C and 1 bar) sorption analysis. The N<sub>2</sub> adsorption capacities of the materials are dependent on the size of the attached functional groups. On the other hand, the CO<sub>2</sub> uptake values of the materials are dependent on both the size and nature of attached functional groups, resulting in various CO<sub>2</sub>-framework interactions. The high thermal and moisture stability of the light-weight, non-toxic Al-MIL-101-X-CE materials along with the considerably high porosity would make them potential candidates for applications in gas storage and separation.

## 5.5 REFERENCES

1. Themed issue on MOFs: *Chem. Soc. Rev.*, 2009, **38**, 1201.
2. Special issue on MOFs: *Chem. Rev.*, 2012, **112**, 673.
3. Themed issue on MOFs: *Chem. Soc. Rev.*, 2014, **43**, 5415.
4. O. M. Yaghi, M. O’Keeffe, N. W. Ockwig, H. K. Chae, M. Eddaoudi and J. Kim, *Nature*, 2003, **423**, 705.
5. G. Férey, *Chem. Soc. Rev.*, 2008, **37**, 191.
6. S. Kitagawa, R. Kitaura and S. Noro, *Angew. Chem. Int. Ed.*, 2004, **43**, 2334.

7. J. R. Li, R. J. Kuppler and H. C. Zhou, *Chem. Soc. Rev.*, 2009, **38**, 1477.
8. L. J. Murray, M. Dinca and J. R. Long, *Chem. Soc. Rev.*, 2009, **38**, 1294.
9. L. Hamon, P. L. Llewellyn, T. Devic, A. Ghoufi, G. Clet, V. Guillermin, G. D. Pirngruber, G. Maurin, C. Serre, G. Driver, W. van Beek, E. Jolimaître, A. Vimont, M. Daturi and G. Férey, *J. Am. Chem. Soc.*, 2009, **131**, 17490.
10. J. Lee, O. K. Farha, J. Roberts, K. A. Scheidt, S. T. Nguyen and J. T. Hupp, *Chem. Soc. Rev.*, 2009, **38**, 1450.
11. L. Ma, C. Abney and W. Lin, *Chem. Soc. Rev.*, 2009, **38**, 1248.
12. K. M. L. Taylor-Pashow, J. Della Rocca, Z. G. Xie, S. Tran and W. Lin, *J. Am. Chem. Soc.*, 2009, **131**, 14261.
13. P. Horcajada, T. Chalati, C. Serre, B. Gillet, C. Sebrie, T. Baati, J. F. Eubank, D. Heurtaux, P. Clayette, C. Kreuz, J. S. Chang, Y. K. Hwang, V. Marsaud, Y.-N. Bories, L. Cynober, S. Gil, G. Férey, P. Couvreur and R. Gref, *Nat. Mater.*, 2010, **9**, 172.
14. M. Vallet-Regí, F. Balasch and D. Arcos, *Angew. Chem. Int. Ed.*, 2007, **46**, 7548.
15. P. Horcajada, C. Serre, M. Vallet-Regí, M. Sebban, F. Taulelle and G. Férey, *Angew. Chem. Int. Ed.*, 2006, **45**, 5974.
16. L. M. Huang, H. T. Wang, J. X. Chen, Z. B. Wang, J. Y. Sun, D. Y. Zhao and Y. S. Yan, *Microporous Mesoporous Mater.*, 2003, **58**, 105.
17. J. A. Greathouse and M. D. Allendorf, *J. Am. Chem. Soc.*, 2006, **128**, 10678.
18. Y. Li and R. T. Yang, *Langmuir*, 2007, **23**, 12937.
19. S. S. Kaye, A. Dailly, O. M. Yaghi and J. R. Long, *J. Am. Chem. Soc.*, 2007, **129**, 14176.
20. D. Ma, Y. Li and Z. Li, *Chem. Commun.*, 2011, **47**, 7377.
21. T. Wu, L. Shen, M. Luebbers, C. Hu, Q. Chen, Z. Ni and R. I. Masel, *Chem. Commun.*, 2010, **46**, 6120.
22. C. Yang, X. P. Wang and M. A. Omary, *J. Am. Chem. Soc.*, 2007, **129**, 15454.
23. S. Biswas, T. Remy, S. Couck, D. Denysenko, G. Rampelberg, J. F. M. Denayer, D. Volkmer, C. Detavernier and P. Van Der Voort, *Phys.Chem. Chem. Phys.*, 2013, **15**, 3552.
24. S. Biswas, S. Couck, D. Denysenko, A. Bhunia, M. Grzywa, J. F. M. Denayer, D. Volkmer, C. Janiak and P. Van Der Voort, *Microporous Mesoporous Mater.*, 2013, **181**, 175.

25. T. Loiseau, C. Serre, C. Huguenard, G. Fink, F. Taulelle, M. Henry, T. Bataille and G. Férey, *Chem.–Eur. J.*, 2004, **10**, 1373.
26. P. Serra-Crespo, E. V. Ramos-Fernandez, J. Gascon and F. Kapteijn, *Chem. Mater.*, 2011, **23**, 2565.
27. G. Férey, C. Mellot-Draznieks, C. Serre, F. Millange, J. Dutour, S. Surble and I. Margiolaki, *Science*, 2005, **309**, 2040.
28. M. Dan-Hardi, C. Serre, T. Frot, L. Rozes, G. Maurin, C. Sanchez and G. Férey, *J. Am. Chem. Soc.*, 2009, **131**, 10857.
29. J. H. Cavka, S. Jakobsen, U. Olsbye, N. Guillou, C. Lamberti, S. Bordiga and K. P. Lillerud, *J. Am. Chem. Soc.*, 2008, **130**, 13850.
30. M. Lammert, S. Bernt, F. Vermoortele, D. E. De Vos and N. Stock, *Inorg. Chem.*, 2013, **52**, 8521.
31. A. Klinkebiel, N. Reimer, M. Lammert, N. Stock and U. Luning, *Chem. Commun.*, 2014, **50**, 9306.
32. P. A. Szilagyi, I. Weinrauch, J. Juan-Alcañiz, P. Serra-Crespo, A. Grzech, H. Oh, M. de Respinis, B. J. Trzesniewski, F. Kapteijn, R. van de Krol, H. Geerlings, J. Gascon, M. Hirscher and B. Dam, *J. Phys. Chem. C*, 2014, **118**, 19572.
33. S. Bernt, V. Guillerme, C. Serre and N. Stock, *Chem. Commun.*, 2011, **47**, 2838.
34. D. Jiang, L. L. Keenan, A. D. Burrows and K. J. Edler, *Chem. Commun.*, 2012, **48**, 12053.
35. J. Juan-Alcañiz, R. Gielisse, A. B. Lago, E. V. Ramos-Fernandez, P. Serra-Crespo, T. Devic, N. Guillou, C. Serre, F. Kapteijn and J. Gascon, *Catal. Sci. Technol.*, 2013, **3**, 2311.
36. G. Akiyama, R. Matsuda, H. Sato, A. Hori, M. Takata and S. Kitagawa, *Microporous Mesoporous Mater.*, 2012, **157**, 89.
37. G. Akiyama, R. Matsuda, H. Sato, M. Takata and S. Kitagawa, *Adv. Mater.*, 2011, **23**, 3294.
38. F. L. Morel, M. Ranocchiari and J. A. van Bokhoven, *Ind. Eng. Chem. Res.*, 2014, **53**, 9120.
39. M. G. Goesten, K. B. Sai Sankar Gupta, E. V. Ramos-Fernandez, H. Khajavi, J. Gascon and F. Kapteijn, *CrystEngComm*, 2012, **14**, 4109.

40. B. Wu, X. Lin, L. Ge, L. Wu and T. Xu, *Chem. Commun.*, 2013, **49**, 143.
41. P. Horcajada, H. Chevreau, D. Heurtaux, F. Benyettou, F. Salles, T. Devic, A. Garcia-Marquez, C. Yu, H. Lavrard, C. L. Dutson, E. Magnier, G. Maurin, E. Elkaim and C. Serre, *Chem. Commun.*, 2014, **50**, 6872.
42. S. Biswas, S. Couck, M. Grzywa, J. F. M. Denayer, D. Volkmer and P. Van Der Voort, *Eur. J. Inorg. Chem.*, 2012, 2481.
43. F. Carson, J. Su, A. E. Platero-Prats, W. Wan, Y. Yun, L. Samain and X. Zou, *Cryst. Growth Des.*, 2013, **13**, 5036.
44. M. Hartmann and M. Fischer, *Microporous Mesoporous Mater.*, 2012, **164**, 38.
45. R. Srirambalaji, S. Hong, R. Natarajan, M. Yoon, R. Hota, Y. Kim, Y. H. Ko and K. Kim, *Chem. Commun.*, 2012, **48**, 11650.
46. T. Devic, P. Horcajada, C. Serre, F. Salles, G. Maurin, B. Moulin, D. Heurtaux, G. Clet, A. Vimont, J.-M. Greneche, B. Le Ouay, F. Moreau, E. Magnier, Y. Filinchuk, J. Marrot, J.-C. Lavalley, M. Daturi and G. Ferey, *J. Am. Chem. Soc.*, 2010, **132**, 1127.
47. Y. Chen, L. Chen, W. Zhou, D. Zha, D. Zhou, F. Bai and M. Wan, *Synth. Met.*, 2009, **159**, 1649.
48. M. Kuwabara, A. Murakami, K. Fukunishi, M. Nomura and H. Yamanaka, *J. Fluorine Chem.*, 1989, **42**, 105.
49. S. Henke, A. Schneemann, S. Kapoor, R. Winter and R. A. Fischer, *J. Mater. Chem.*, 2012, **22**, 909.
50. T. Ahnfeldt, N. Guillou, D. Gunzelmann, I. Margiolaki, T. Loiseau, G. Ferey, J. Senker and N. Stock, *Angew. Chem. Int. Ed.*, 2009, **48**, 5163.
51. N. A. Khan, J. W. Jun and S. H. Jung, *Eur. J. Inorg. Chem.*, 2010, 1043.

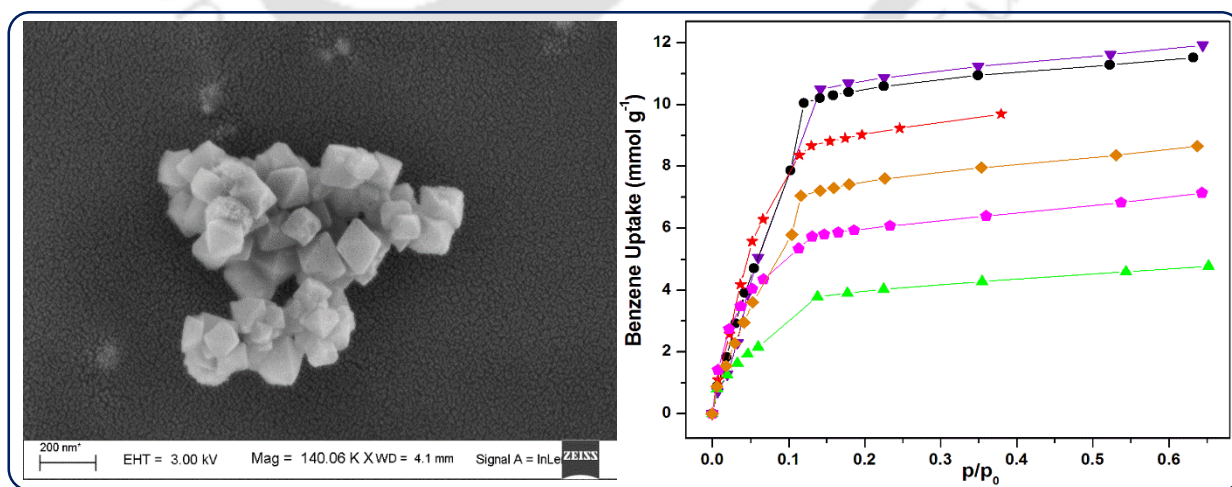
- 
52. E. Stavitski, M. Goesten, J. Juan-Alcaniz, A. Martinez-Joaristi, P. Serra-Crespo, A. V. Petukhov, J. Gascon and F. Kapteijn, *Angew. Chem. Int. Ed.*, 2011, **50**, 9624.
53. N. Stock and S. Biswas, *Chem. Rev.*, 2012, **112**, 933.
54. S. Bauer, C. Serre, T. Devic, P. Horcajada, J. Marrot, G. Férey and N. Stock, *Inorg. Chem.*, 2008, **47**, 7568.
55. T. R. Whitfield, X. Wang, L. Liu and A. Jacobson, *Solid State Sci.*, 2005, **7**, 1096.
56. C. Serre, F. Millange, C. Thouvenot, M. Nogues, G. Marsolier, D. Louer and G. Férey, *J. Am. Chem. Soc.*, 2002, **124**, 13519.
57. T. Wittmann, R. Siegel, N. Reimer, W. Milius, N. Stock and J. Senker, *Chem. Eur. J.*, 2015, **21**, 314.
58. M. Bosch, M. Zhang and H.-C. Zhou, *Adv. Chem.*, 2014, **2014**, 1.
59. A. K. Galwey and M. E. Brown, *Thermal Decomposition of Ionic Solids*, Elsevier, Amsterdam, 1999.
60. <http://www.iza-structure.org/databases/>.
61. M. Haouas, C. Volkringer, T. Loiseau, G. Férey and F. Taulelle, *Phys. Chem. C*, 2011, **115**, 17934.
62. T. Loiseau, C. Serre, C. Huguenard, F. T. G. Fink, M. Henry, T. Bataille and G. Férey, *Phys. Chem. Chem. Phys.*, 2004, **10**, 1373.
63. S. Biswas, T. Ahnfeldt and N. Stock, *Inorg. Chem.*, 2011, **50**, 9518.
64. T. A. Makal, X. Wang and H.-C. Zhou, *Cryst. Growth Des.*, 2013, **13**, 4760.
65. J. Juan-Alcañiz, E. V. Ramos-Fernandez, U. Lafont, J. Gascon and F. Kapteijn, *J. Catal.*, 2010, **269**, 229.

66. D.-Y. Hong, Y. K. Hwang, C. Serre, G. Ferey and J. S. Chang, *Adv. Funct. Mater.*, 2009, **19**, 1537.
67. C. Scherb, J. J. Williams, F. Hinterholzinger, S. Bauer, N. Stock and T. Bein, *J. Mater. Chem.*, 2011, **21**, 14849.
68. P. Horcajada, F. Salles, S. Wuttke, T. Devic, D. Heurtaux, G. Maurin, A. Vimont, M. Daturi, O. David, E. Magnier, N. Stock, Y. Filinchuk, D. Popov, C. Riekkel, G. Ferey and C. Serre, *J. Am. Chem. Soc.*, 2011, **133**, 17839.



## Synthesis, Characterization and Sorption Properties of Functionalized Cr-MIL-101-X (X = -F, -Cl, -Br, -CH<sub>3</sub>, -C<sub>6</sub>H<sub>4</sub>, -F<sub>2</sub>, -(CH<sub>3</sub>)<sub>2</sub>) Materials

This chapter presents the hydrothermal synthesis, complete characterization and sorption behavior of functionalized Cr-MIL-101-X (X = -F, -Cl, -Br, -CH<sub>3</sub>, -C<sub>6</sub>H<sub>4</sub>, -F<sub>2</sub>, -(CH<sub>3</sub>)<sub>2</sub>) materials. All of the functionalized compounds except Cr-MIL-101-C<sub>6</sub>H<sub>4</sub> were obtained by reacting the mixtures of CrO<sub>3</sub>, H<sub>2</sub>BDC-X linkers, conc. HCl and water. On the other hand, the Cr-MIL-101-X compounds with X = -Cl, -Br and -C<sub>6</sub>H<sub>4</sub> were synthesized in a shorter reaction times. The phase purity of the materials is confirmed by a combination of XRPD analysis, DRIFT spectroscopy and thermogravimetric analysis. TG analyses shows that all the Cr-MIL-101-X compounds exhibit high thermal stability up to 270-300 °C in an air atmosphere. All the thermally activated materials exhibit significant porosity, as verified by the N<sub>2</sub>, CO<sub>2</sub> and benzene sorption analyses. The high thermal and hydrolytic stability as well as noticeably high porosity would make the Cr-MIL-101-X compounds as potential candidates for applications in gas/liquid storage and separation.

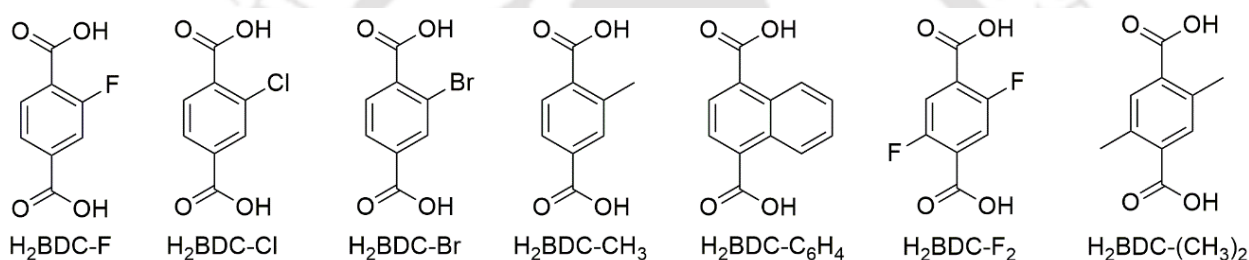


## 6.1 INTRODUCTION

Synthesis of air- and moisture-stable MOF materials possessing effective functional organic sites is still a major challenge for their applications in industry. Several famous unfunctionalized MOF compounds<sup>1-4</sup> showing promising applications in adsorption, separation or catalysis suffer from low physicochemical stabilities (moisture, thermal, acid-base), which hinder their industrial applications. In order to increase the hydrolytic stabilities, several hydrophobic functional groups (e.g., -F, -CH<sub>3</sub>, -OCF<sub>3</sub>, etc.)<sup>5-9</sup> have been integrated into their frameworks. In addition, MOFs possessing relatively higher physicochemical stabilities have been attained through the employment of metal cations having higher oxidation states than divalent cations (e.g. Al(III),<sup>10, 11</sup> Cr(III),<sup>12</sup> Ti(IV),<sup>13</sup> Zr(IV),<sup>14</sup> etc.). Among several approaches that have been employed so far for increasing the water stability of MOFs, ligand functionalization is the most widely employed strategy.<sup>15, 16</sup>

Ferey's group introduced the MIL-n (MIL = Material of the Institute Lavoisier) series of MOFs that exhibited not only high thermal and chemical stability but also surprisingly high porosity.<sup>10-12, 17</sup> For example, the Cr(III)-based MOF material represented as MIL-101, which is stable in air, water and acidic conditions, shows high thermal stability up to 275 °C.<sup>12, 18</sup> This material possesses extremely high BET surface area of 4100 m<sup>2</sup> g<sup>-1</sup>.<sup>12</sup> The incorporation of various functional groups into the frameworks of Cr(III), Fe(III) and Al(III)-based MIL-101 materials was carried out by several research groups. The functionalized (single- and mixed-linker) Cr-MIL-101-X (X = -H, -F, -Cl, -Br, -I, -CH<sub>3</sub>, -NO<sub>2</sub>, -NH<sub>2</sub>, -OH, -CO<sub>2</sub>H, -SO<sub>3</sub>H, etc.) compounds were documented in the literature by the groups of Stock, Kitagawa and several others.<sup>18-28</sup> Moreover, Xu's group reported on the preparation of highly proton conductive membrane materials with the hydrolytically stable Fe-MIL-101-NH<sub>2</sub> compound.<sup>29</sup> The V-MIL-101 and V-MIL-101-NH<sub>2</sub> materials, which were separately documented in the literature by the groups of Van Der Voort<sup>30</sup> and Zou,<sup>31</sup> were found to be sensitive to air. The group of Gascon reported on the CO<sub>2</sub>/CH<sub>4</sub> separation and catalytic activities of the Al-MIL-101-NH<sub>2</sub> material, which showed high thermal and chemical stability.<sup>11, 32, 33</sup> Recently, a report has been published by our group on the facile synthesis (by both conventional and microwave irradiation method) and gas adsorption behavior of seven new functionalized Al-MIL-101-X (X = -CH<sub>3</sub>, -NO<sub>2</sub>, -OCH<sub>3</sub>, -C<sub>6</sub>H<sub>4</sub>, -F<sub>2</sub>, -(CH<sub>3</sub>)<sub>2</sub>, -(OCH<sub>3</sub>)<sub>2</sub>) materials.<sup>34</sup> Inspired by the above-mentioned distinctive

and advantageous properties of the pristine and functionalized Cr-MIL-101 materials, we have introduced several new functional groups into the framework of Cr-MIL-101. In this chapter, we wish to present the synthesis, thorough characterization, thermal stability as well as gas/vapor adsorption features of seven functionalized Cr-MIL-101-X (X = -F, -Cl, -Br, -CH<sub>3</sub>, -C<sub>6</sub>H<sub>4</sub>, -F<sub>2</sub>, -(CH<sub>3</sub>)<sub>2</sub>) compounds. A systematic study on the influence of the different functional groups (Scheme 1) on the thermal stability as well as gas/vapor adsorption characteristics of the Cr-MIL-101-X materials has been carried out. Although some of these functionalized Cr-MIL-101-X (X = -F, -Cl, -Br, -CH<sub>3</sub>, -(CH<sub>3</sub>)<sub>2</sub>) materials have been recently reported, they were prepared by employing different synthesis conditions compared to those presented in this chapter.<sup>19, 28</sup> Moreover, the effect of the functional groups on the thermal stability and gas/vapor sorption properties of the functionalized Cr-MIL-101-X materials was not evaluated.



**Scheme 6.1** Structures of the functionalized terephthalic acid linkers H<sub>2</sub>BDC-X used for the synthesis of the Cr-MIL-101-X materials.

## 6.2 EXPERIMENTAL SECTION

### 6.2.1 Materials and General Methods

The H<sub>2</sub>BDC-F,<sup>35</sup> H<sub>2</sub>BDC-Cl,<sup>35</sup> H<sub>2</sub>BDC-CH<sub>3</sub>,<sup>35</sup> and H<sub>2</sub>BDC-F<sub>2</sub><sup>36</sup> ligands were synthesized as described previously. All other starting materials were of reagent grade and used as received from the commercial suppliers. Diffuse-reflectance infrared Fourier transform (DRIFT) spectra were carried out with a Thermo Nicolet 6700 FTIR spectrometer equipped with a nitrogen-cooled MCT detector and a KBr beam splitter. The DRIFT cell was connected to a vacuum manifold. The following indications are used to characterize absorption bands: very strong (vs), strong (s), medium (m), weak (w), shoulder (sh) and broad (br). Thermogravimetric analyses (TGA) were carried out with a Netzsch STA-409CD thermal analyzer in a temperature range of 25-600 °C under air atmosphere at a heating rate of 4 °C min<sup>-1</sup>. Ambient temperature X-Ray powder diffraction (XRPD) patterns were measured on a Thermo Scientific ARL X'Tra

diffractometer (40 kV, 40 mA), using Cu-K $\alpha$  ( $\lambda = 1.5406 \text{ \AA}$ ). The nitrogen sorption isotherms up to 1 bar were recorded using a Belsorp Mini apparatus at  $-196 \text{ }^\circ\text{C}$ . The carbon dioxide adsorption measurements were carried out using a Micromeritics TriStar 3000 analyzer at  $0 \text{ }^\circ\text{C}$ . The vapor phase isotherms of benzene at  $50 \text{ }^\circ\text{C}$  were measured by the gravimetric method using a microbalance of VTI Corporation. The compounds were degassed at  $160 \text{ }^\circ\text{C}$  under vacuum for 18 h prior to the sorption experiments. The surface morphology of the as-synthesized Cr-MIL-101-X materials was investigated by Field Emission Scanning Electron Microscope (FESEM) using a Zeiss (Gemini) instrument or by SEM using Hitachi S3400N equipment.

The frequencies of infrared absorption bands for all the Cr-MIL-101-X compounds are presented in Table 6.1. The weights of the samples used for the TG and adsorption analyses are summarized in Table 6.2. The synthesis of Cr-MIL-101 was carried out according to a formerly published procedure.<sup>37</sup> The routine characterization measurements (XRPD, TGA, IR spectroscopy and N<sub>2</sub> sorption analysis) were carried out in order to verify its purity.

**Table 6.1** Frequencies of infrared absorption bands<sup>[a]</sup> for the thermally activated forms of Cr-MIL-101-X compounds.

Compound	Infrared Absorption Frequencies (cm <sup>-1</sup> )
<b>1-F</b>	1630 (vs), 1498 (s), 1417 (vs), 1392 (sh), 1315 (w), 1289 (m), 1162 (w), 1089 (w), 1064 (w), 988 (w), 958 (w), 843 (m), 805 (w), 770 (s)
<b>2-Cl</b>	1631 (vs), 1489 (m), 1404 (vs), 1281 (w), 1251 (w), 1162 (w), 1056 (m), 907 (w), 834 (w), 770 (vs)
<b>3-Br</b>	1630 (vs), 1545 (m), 1498 (m), 1421 (vs), 1281 (w), 1162 (w), 1064 (w), 992 (w), 839 (m), 805 (w), 770 (s), 728 (w), 702 (w)
<b>4-CH<sub>3</sub></b>	1617 (vs), 1498 (s), 1408 (vs), 1378 (sh), 1204 (w), 1162 (w), 1098 (w), 864 (w), 839 (w), 762 (s), 719 (w)
<b>5-C<sub>6</sub>H<sub>4</sub></b>	1617(vs), 1464 (s), 1426 (vs), 1370 (vs), 1264 (s), 1213 (m), 1162 (m), 1030 (w), 919 (w), 851 (w), 834 (w), 787 (s), 740 (w)
<b>6-F<sub>2</sub></b>	1630 (vs), 1511 (w), 1485 (w), 1426 (vs), 1374 (vs), 1289 (s), 1196 (m), 1153 (w), 941 (w), 911 (w)
<b>7-(CH<sub>3</sub>)<sub>2</sub></b>	1613 (vs), 1536 (sh), 1493 (w), 1421 (vs), 1383 (sh), 1358 (s), 1289 (w), 1191 (m), 1153 (m), 919 (m), 860 (w), 796 (s), 753 (m)
Cr-MIL-101	1630 (vs), 1511 (s), 1404 (vs), 1162 (m), 1022 (s), 881 (w), 834 (m), 813 (sh), 749 (s), 719 (w)

<sup>[a]</sup> Abbreviations: s = strong; vs = very strong; m = medium, w = weak, sh = shoulder.

**Table 6.2** Weights of the samples used for the TG and adsorption analyses.

Compound	Weight (mg)			
	TGA	N <sub>2</sub> adsorption	CO <sub>2</sub> adsorption	Benzene adsorption
<b>1-F</b>	17.438	28.3	36.1	9.772650
<b>2-Cl</b>	12.611	32.3	30.6	-
<b>3-Br</b>	12.805	26.8	73.4	9.892967
<b>4-CH<sub>3</sub></b>	10.479	24	29.1	9.799967
<b>5-C<sub>6</sub>H<sub>4</sub></b>	11.345	22.4	32.9	8.994550
<b>6-F<sub>2</sub></b>	9.89	28.3	33.9	10.027800
<b>7-(CH<sub>3</sub>)<sub>2</sub></b>	12.233	40.8	63.8	-
Cr-MIL-101	-	29.1	36.5	9.902467

### 6.2.2 Synthesis

General Procedure for the Synthesis of Cr-MIL-101-X Compounds with X = -F, -Cl, -Br, -CH<sub>3</sub>, -F<sub>2</sub> and -(CH<sub>3</sub>)<sub>2</sub>: A mixture of CrO<sub>3</sub> (125 mg, 1.25 mmol), H<sub>2</sub>BDC-X linker (1.25 mmol), water (5 mL) and conc. HCl (0.15 mL, 4.89 mmol) was placed in a 50 mL Teflon-lined stainless steel autoclave and heated at 180 °C for 144 h in a conventional oven. After cooling to room temperature, the green materials were collected by filtration using membrane filters, washed with acetone (3 × 5 mL) and dried in air. The yields of the Cr-MIL-101-X compounds were: - F, 280 mg; -Cl, 285 mg; -Br, 350 mg; -CH<sub>3</sub>, 295 mg; -F<sub>2</sub>, 300 mg; -(CH<sub>3</sub>)<sub>2</sub>, 305 mg.

Synthesis of Cr-MIL-101-C<sub>6</sub>H<sub>4</sub>: A mixture of CrCl<sub>3</sub>·6H<sub>2</sub>O (266 mg, 1.00 mmol) and H<sub>2</sub>BDC-C<sub>6</sub>H<sub>4</sub> linker (216 mg, 1.00 mmol) in water (5 mL) was placed in a 50 mL Teflon-lined stainless steel autoclave and heated at 180 °C for 12 h in a conventional oven. After cooling to room temperature, the green materials were collected by filtration using filter papers, washed with acetone (3 × 5 mL) and dried in air. The yield was 255 mg.

Alternative Synthesis of Cr-MIL-101-Cl: A mixture of CrCl<sub>3</sub>·6H<sub>2</sub>O (266 mg, 1.00 mmol) and H<sub>2</sub>BDC-Cl linker (200 mg, 1.00 mmol) in water (5 mL) was placed in a 50 mL Teflon-lined stainless steel autoclave and heated at 180 °C for 12 h in a conventional oven. After cooling to room temperature, the green materials were collected by filtration using filter papers, washed with acetone (3 × 5 mL) and dried in air. The yield was 215 mg.

Alternative Synthesis of Cr-MIL-101-Br: A mixture of  $\text{Cr}(\text{NO}_3)_3 \cdot 9\text{H}_2\text{O}$  (400 mg, 1.00 mmol) and  $\text{H}_2\text{BDC-Br}$  linker (245 mg, 1.00 mmol) in water (5 mL) was placed in a 50 mL Teflon-lined stainless steel autoclave and heated at 210 °C for 18 h in a conventional oven. After cooling to room temperature, the green materials were collected by filtration using filter papers, washed with acetone ( $3 \times 5$  mL) and dried in air. The yield was 310 mg.

### 6.2.3 Activation of the As-Synthesized Cr-MIL-101-X Compounds

All the as-synthesized Cr-MIL-101-X compounds were activated in a three-step activation process. At first, the suspension of each compound (0.2 g) in 20 mL DMF was placed in a Teflon-lined stainless steel autoclave and heated at 155 °C for 24 h in a conventional oven. In the second step, the filtered solids were suspended in ethanol (30 ml) and heated at 100 °C for 24 h in a conventional oven. In the third step, the green compounds were collected by filtration and heated at 160 °C under dynamic vacuum for 18 h.

## 6.3 RESULTS AND DISCUSSIONS

### 6.3.1 Synthesis and Activation

Six of the Cr-MIL-101-X ( $X = -\text{F}$ ,  $-\text{Cl}$ ,  $-\text{Br}$ ,  $-\text{CH}_3$ ,  $-\text{F}_2$  and  $-(\text{CH}_3)_2$ ) materials were prepared by a general synthesis approach. The reaction conditions for the synthesis of these materials are different compared to that employed in the literature for few other functionalized Cr-MIL-101-X compounds.<sup>19, 24, 25, 28</sup> Indeed, the reaction of a mixture of  $\text{CrO}_3$ ,  $\text{H}_2\text{BDC-X}$  ligand, conc. HCl and water with a molar ratio of 1:1:3.9:222.2 at 180 °C for 144 h led to the formation of highly crystalline Cr-MIL-101-X materials. It is noteworthy that the preparation of the chloro- and bromo-functionalized Cr-MIL-101 materials under similar synthetic conditions has recently been demonstrated by the Stock group.<sup>19</sup> Furthermore, the synthesis of the Cr-MIL-101- $(\text{CH}_3)_2$  compound under similar reaction conditions has been very recently reported by Kitagawa's group.<sup>28</sup> The Cr-MIL-101- $\text{C}_6\text{H}_4$  material could not be synthesized by the above-mentioned general synthetic method. It was prepared by the reaction of a stoichiometric mixture of  $\text{CrCl}_3 \cdot 6\text{H}_2\text{O}$  and  $\text{H}_2\text{BDC-C}_6\text{H}_4$  in water at 180 °C for 12 h. Compared to the 120 h of reaction time as described in ref.19, the chloro- and bromo-functionalized Cr-MIL-101 compounds could also be synthesized in only 12 and 18 h, respectively. In these cases, the synthesis conditions for the Cr-MIL-101-Cl material were similar to those of the presented Cr-MIL-101- $\text{C}_6\text{H}_4$  compound.

On the other hand, the Cr-MIL-101-Br material was prepared by the reaction conditions that were formerly employed for the preparation of the parent Cr-MIL-101 material.<sup>37</sup> The FESEM and SEM images (Figures 6.1 (a)-6.1 (i)) of as-synthesized Cr-MIL-101-X (X= 1-F, 2-Cl, 3-Br, 4-CH<sub>3</sub>, 5-C<sub>6</sub>H<sub>4</sub>, 6-F<sub>2</sub> and 7-(CH<sub>3</sub>)<sub>2</sub>) materials confirm that the compounds were formed in homogeneous crystallite phases and there is almost no sign of amorphous phase in the samples.

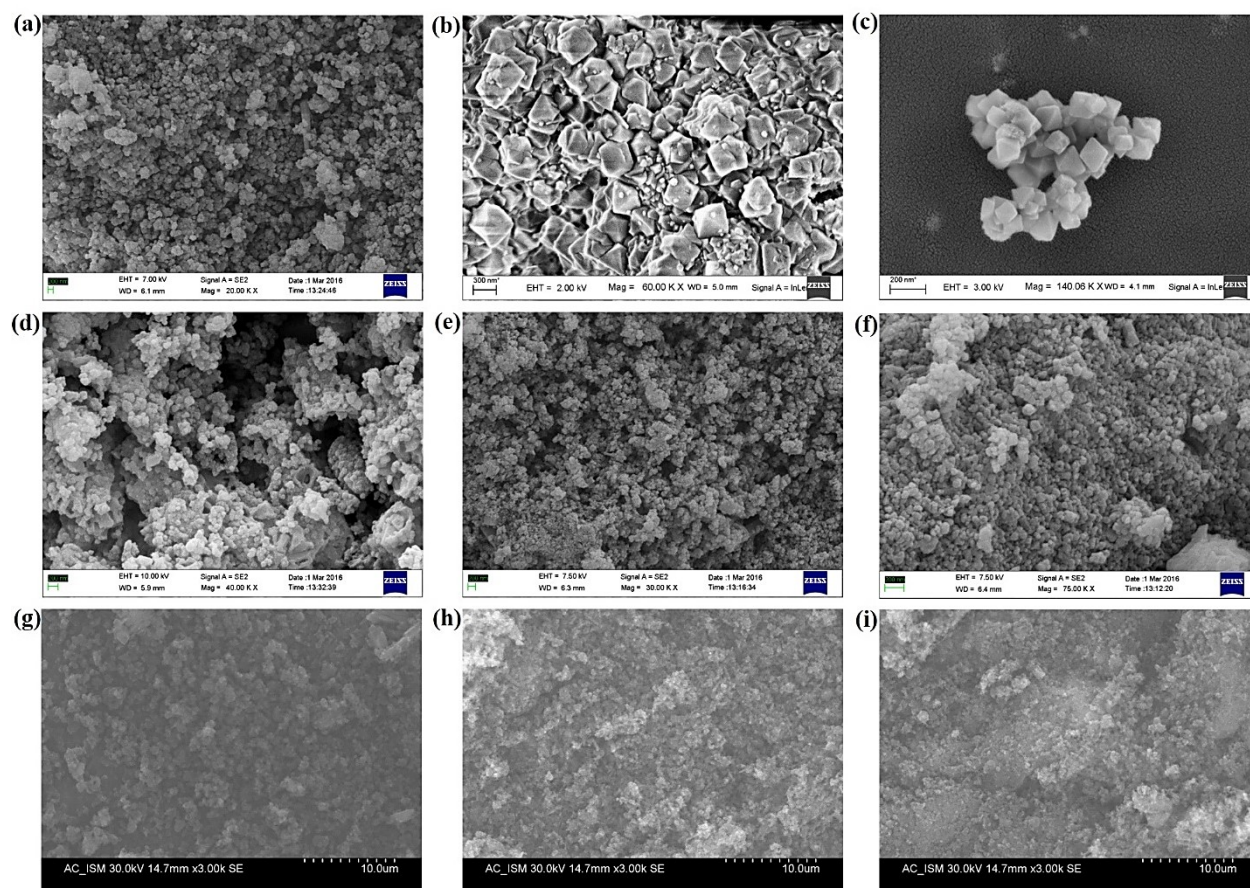


**Figure 6.1** FESEM images for (a) 1-F, (b) 2-Cl (6d), (c) 3-Br (6d), (d) 4-CH<sub>3</sub>, (e) 5-C<sub>6</sub>H<sub>4</sub>, (f) 7-(CH<sub>3</sub>)<sub>2</sub> and SEM images for (g) 6-F<sub>2</sub>, (h) Cr-MIL-101-Br (18h), (i) Cr-MIL-101-Cl (12h).

The removal of the guest molecules encapsulated within the pores of the as-synthesized Cr-MIL-101-X materials was accomplished in a three-step activation method similar to that reported in the literature<sup>38</sup> for the pristine Cr-MIL-101 material. At first, the guest molecules were exchanged by heating the as-synthesized materials in a polar solvent such as DMF. In the second step, the exchange of the DMF molecules was performed with more volatile and thus easily removable ethanol molecules by heating the DMF-exchanged materials in ethanol. In the

third step, the ethanol molecules were removed from the cavities by heating the ethanol-exchanged materials under vacuum, leading to the empty-pore forms of the materials.

### 6.3.2 Structure Description

The experimental XRPD patterns of the functionalized Cr-MIL-101-X materials (Figure 6.2) are similar with the calculated XRPD pattern of parent Cr-MIL-101 exhibiting a cubic structure (Figure 6.3). The Cr-MIL-101-X materials are thus isostructural with Cr-MIL-101, which is also obvious from the similarity between their XRPD patterns. Since the structure of Cr-MIL-101 (Figure 6.3) is already reported in the literature,<sup>12</sup> a brief description of the framework structures of Cr-MIL-101-X materials is presented here.<sup>39</sup>

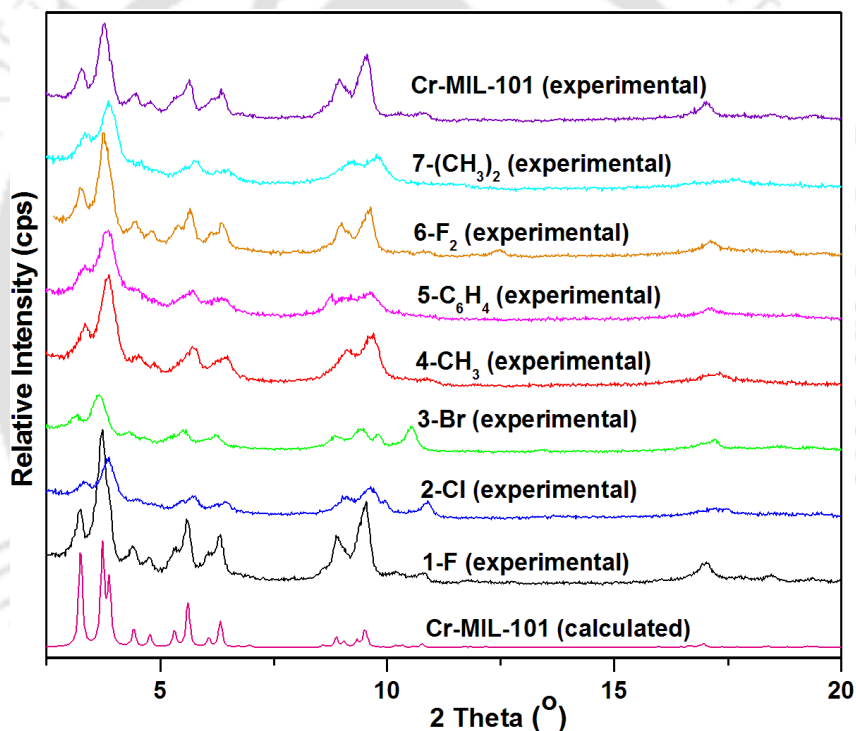


**Figure 6.2** Calculated XRPD pattern of Cr-MIL-101 (pink) and experimental XRPD patterns of the thermally activated **1-F** (black), **2-Cl** (blue), **3-Br** (green), **4-CH<sub>3</sub>** (red), **5-C<sub>6</sub>H<sub>4</sub>** (magenta), **6-F<sub>2</sub>** (orange), **7-(CH<sub>3</sub>)<sub>2</sub>** (cyan) and Cr-MIL-101 (violet).

The structures of Cr-MIL-101-X materials are constructed from trimeric oxo-centered  $[\text{Cr}_3(\mu_3\text{-O})\text{Cl}(\text{H}_2\text{O})_2]^{6+}$  building units that are composed of  $[\text{CrO}_5\text{Cl}]$  octahedra. The trimeric building units are interconnected by the functionalized terephthalate ligands along the edges, resulting in the formation of supertetrahedra (ST). Further connection of the ST with each other in three-dimension leads to the augmented zeolite Mobil Thirty-Nine (MTN) type of framework.

The frameworks are composed of two types of mesoporous cages. The smaller cage is constructed from 12 pentagonal rings bearing a free diameter of *ca.* 12 Å, and the accessible diameter of the cage is *ca.* 29 Å. The larger cage is built up of 12 pentagonal and 4 hexagonal rings possessing a free diameter of the hexagonal rings of *ca.* 16 Å and an accessible cage diameter of *ca.* 34 Å. The smaller and larger cages, that are present in a ratio of 2:1, consist of 20 and 28 ST, respectively.

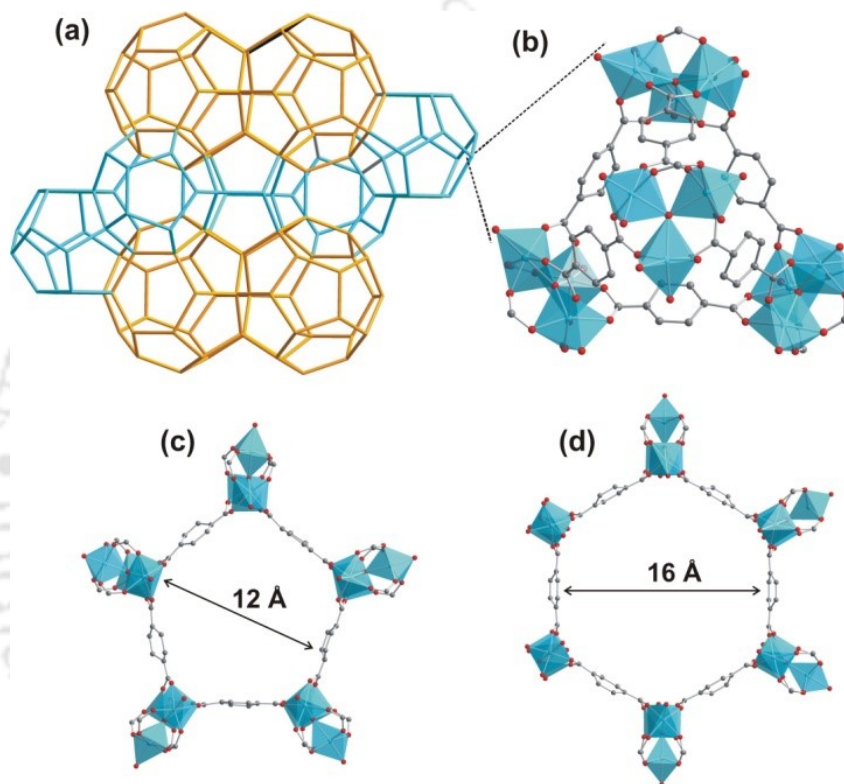


**Figure 6.3** (a) MTN topological framework structure of Cr-MIL-101 having smaller (blue) and larger (orange) mesoporous cages. The structure is constructed from (b) supertetrahedra (ST), which comprise trimeric oxido-centered  $[\text{Cr}_3(\mu_3\text{-O})(\text{F})(\text{H}_2\text{O})_2]^{6+}$  building blocks at the vertices cross-linked by terephthalate linkers. The smaller and larger cages possess only pentagonal (c) or a combination of pentagonal (c) and hexagonal (d) windows, respectively. Color codes: Cr, blue octahedra; C, gray; O, red. The MTN framework (a) and the parts of Cr-MIL-101 network (b-d) have been drawn by using the atomic coordinates provided in “Database of Zeolite Structures”<sup>40</sup> and ref.12, respectively.

### 6.3.3 DRIFT Analysis

The DRIFT spectra of the Cr-MIL-101-X materials (Figure 6.4) show high similarity with each other, as expected. The DRIFT spectra of the functionalized Cr-MIL-101-X materials also bear resemblance with that of the pristine Cr-MIL-101 material. In the DRIFT spectra of the thermally activated Cr-MIL-101-X materials, the strong absorption bands due to the asymmetric

and symmetric  $-\text{CO}_2$  stretching vibrations of the coordinated terephthalate ligand molecules are observed in the regions  $1613\text{--}1630\text{ cm}^{-1}$  and  $1404\text{--}1425\text{ cm}^{-1}$ , respectively.<sup>41,42</sup> In the DRIFT spectra, the absorption bands for the protonated guest  $\text{H}_2\text{BDC-X}$  molecules are very weak or absent. This fact suggests that almost complete removal of guest molecules from the pores of the Cr-MIL-101-X materials has occurred.

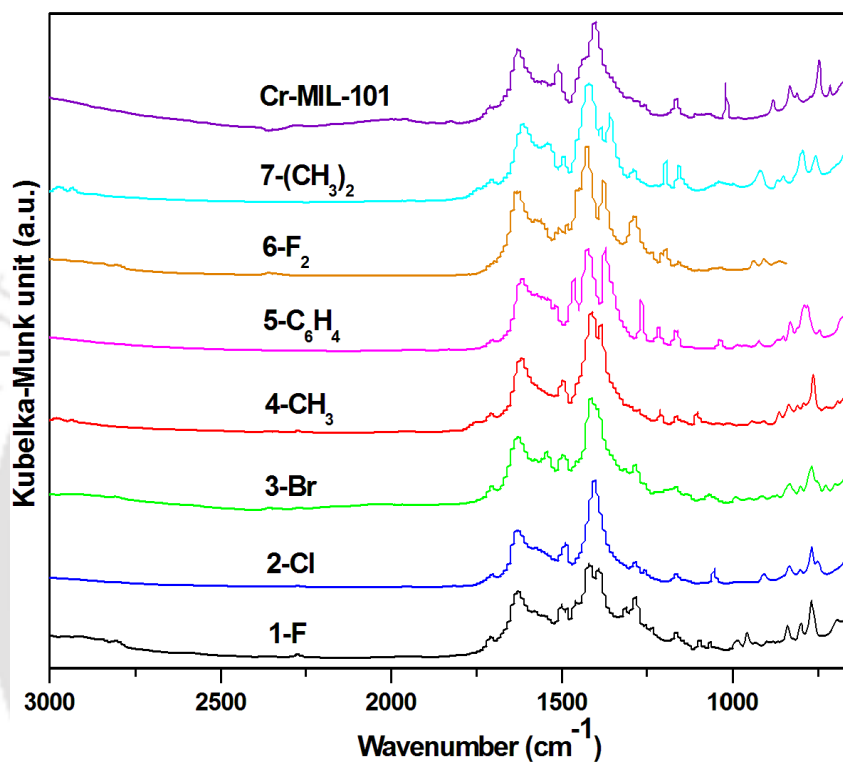


**Figure 6.4** DRIFT spectra of the thermally activated **1-F** (black), **2-Cl** (blue), **3-Br** (green), **4-CH<sub>3</sub>** (red), **5-C<sub>6</sub>H<sub>4</sub>** (magenta), **6-F<sub>2</sub>** (orange), **7-(CH<sub>3</sub>)<sub>2</sub>** (cyan) and Cr-MIL-101 (violet).

### 6.3.4 Thermal Stability

In order to investigate the thermal stability of all the Cr-MIL-101-X materials, thermogravimetric analyses (Figure 6.5) were carried out with the thermally activated forms of the materials in air atmosphere. According to the results of the TG analyses, all the materials are thermally stable up to  $270\text{--}300\text{ }^\circ\text{C}$ . This narrow temperature range indicates that the various functional groups do not play significant roles in determining the thermal stability of the Cr-MIL-101-X materials. The decreasing order of the thermal stability of the materials is **5-C<sub>6</sub>H<sub>4</sub>** ( $300\text{ }^\circ\text{C}$ ) > **2-Cl** ( $280\text{ }^\circ\text{C}$ )  $\approx$  **7-(CH<sub>3</sub>)<sub>2</sub>** ( $280\text{ }^\circ\text{C}$ ) > **1-F** ( $270\text{ }^\circ\text{C}$ )  $\approx$  **3-Br** ( $270\text{ }^\circ\text{C}$ )  $\approx$  **4-CH<sub>3</sub>** ( $270\text{ }^\circ\text{C}$ )  $\approx$  **6-F<sub>2</sub>** ( $270\text{ }^\circ\text{C}$ ). The highest thermal stability of **5-C<sub>6</sub>H<sub>4</sub>** is slightly higher than the pristine Cr-MIL-101 material, which shows thermal stability up to  $275\text{ }^\circ\text{C}$ .<sup>12</sup> In literature, it has been stated

that hydrophobicity increases the thermal stability of MOFs, but there is no clear evidence. Therefore, we cannot assign the highest thermal stability of Cr-MIL-101-C<sub>6</sub>H<sub>4</sub> to its hydrophobicity. It is worthy to note that the recently reported Al-MIL-101-C<sub>6</sub>H<sub>4</sub> material exhibited the highest thermal stability among the functionalized Al-MIL-101-X (X = -CH<sub>3</sub>, -NO<sub>2</sub>, -OCH<sub>3</sub>, -C<sub>6</sub>H<sub>4</sub>, -F<sub>2</sub>, -(CH<sub>3</sub>)<sub>2</sub>, -(OCH<sub>3</sub>)<sub>2</sub>) compounds.<sup>34</sup> Below the decomposition temperatures, the TG curves of the thermally activated forms of all the materials do not exhibit any weight loss step owing to the removal of guest (solvent or H<sub>2</sub>BDC-X ligand) molecules. The absence of occluded molecules in the pores of the thermally activated materials verifies complete activation of the materials.

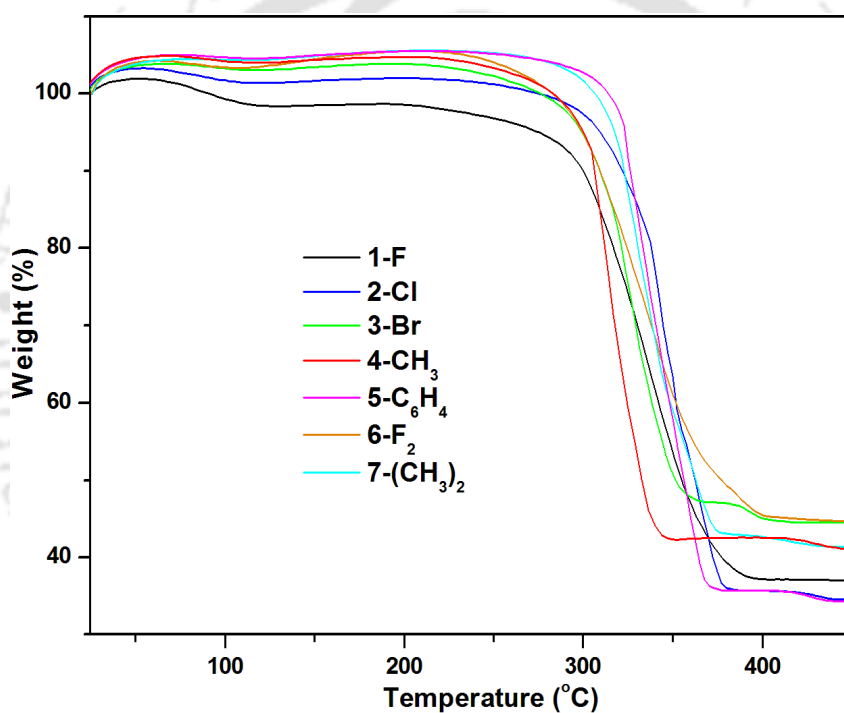


**Figure 6.5** TG curves of the thermally activated **1-F** (black), **2-Cl** (blue), **3-Br** (green), **4-CH<sub>3</sub>** (red), **5-C<sub>6</sub>H<sub>4</sub>** (magenta), **6-F<sub>2</sub>** (orange) and **7-(CH<sub>3</sub>)<sub>2</sub>** measured in an air atmosphere.

### 6.3.5 Sorption Properties

N<sub>2</sub> sorption measurements were performed with the thermally activated forms of all the Cr-MIL-101-X materials. All the materials display type-I N<sub>2</sub> adsorption isotherms (Figure 6.6). A small step is observed in the adsorption curves at  $p/p_0 = 0.2$ . The occurrence of these two steps in the adsorption isotherms was formerly ascribed to the different fillings of the cages. At very low relative pressures ( $p/p_0 < 0.05$ ), only the supertetrahedra (ST) are filled. As the relative pressures increase, the medium ( $p/p_0 = 0.15$ ) and the larger ( $p/p_0 = 0.20$ ) cages are filled.<sup>43</sup> The

adsorption isotherms possessing similar shapes have been previously reported in the literature for the M-MIL-101-X (M = Cr, Fe, V and Al) materials.<sup>11, 12, 18-32, 44, 45</sup> The specific BET surface areas (Table 6.3) were derived from the N<sub>2</sub> adsorption isotherms. The values of BET surface areas disclose substantial porosities, which are considerably lower compared to that of the parent Cr-MIL-101 material.<sup>12, 18, 25</sup> Among the presented functionalized Cr-MIL-101-X materials, the highest value of BET surface area is observed for **4-CH<sub>3</sub>**. The BET surface areas of the materials decrease in the order: Cr-MIL-101 > **4-CH<sub>3</sub>** > **1-F** > **6-F<sub>2</sub>** > **2-Cl** > **7-(CH<sub>3</sub>)<sub>2</sub>** > **5-C<sub>6</sub>H<sub>4</sub>** > **3-Br**.

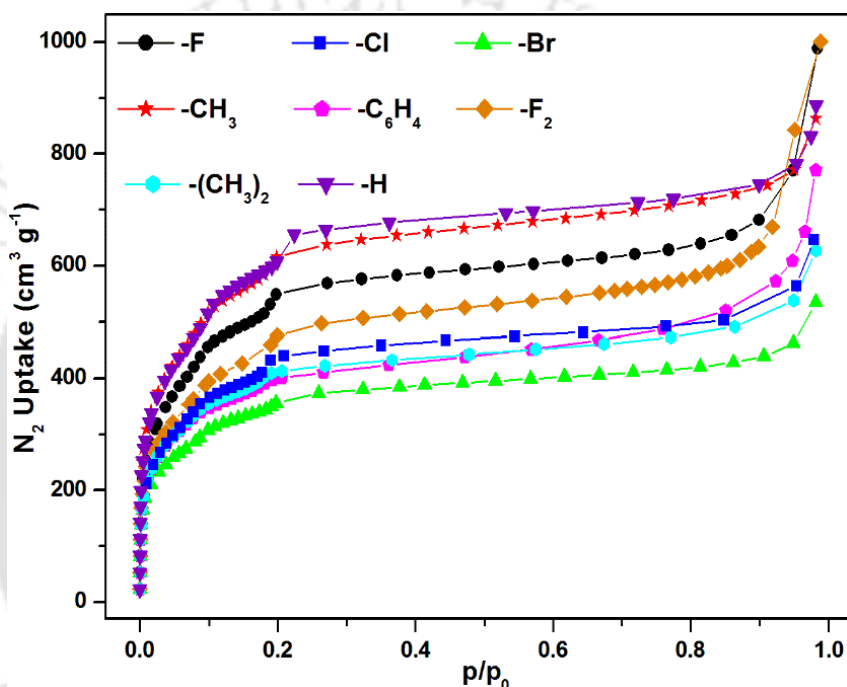


**Figure 6.6** N<sub>2</sub> adsorption isotherms of the thermally activated **1-F** (black, circles), **2-Cl** (blue, squares), **3-Br** (green, triangles), **4-CH<sub>3</sub>** (red, stars), **5-C<sub>6</sub>H<sub>4</sub>** (magenta, pentagons), **6-F<sub>2</sub>** (orange, rotated squares), **7-(CH<sub>3</sub>)<sub>2</sub>** (cyan, hexagons) and Cr-MIL-101 (violet, upside-down triangles) measured at -196 °C.

The CO<sub>2</sub> adsorption measurements were carried out with the thermally activated Cr-MIL-101-X materials at 0 °C up to 1 bar. All the Cr-MIL-101-X materials display type-I CO<sub>2</sub> adsorption isotherms (Figure 6.7) in the pressure range of 0-1 bar. The decreasing order of the CO<sub>2</sub> adsorption capacities (mmol g<sup>-1</sup>) of the materials at 1 bar (i.e. p/p<sub>0</sub> = 0.3) is **1-F** (2.9) > Cr-MIL-101 (2.2) > **4-CH<sub>3</sub>** (2.0) ≈ **6-F<sub>2</sub>** (2.0) > **5-C<sub>6</sub>H<sub>4</sub>** (1.8) ≈ **7-(CH<sub>3</sub>)<sub>2</sub>** (1.8) > **2-Cl** (1.8) > **3-Br** (1.7). In comparison, the N<sub>2</sub> adsorption capacities at p/p<sub>0</sub> = 0.3 shows the same trend as that of the specific BET surface areas. Therefore, at p/p<sub>0</sub> = 0.3, the sequence of CO<sub>2</sub> uptake values differs from that of the N<sub>2</sub> adsorption capacities.

**Table 6.3** Specific BET Surface Areas of the Cr-MIL-101-X materials determined from the N<sub>2</sub> Adsorption Isotherms.

Compound	BET Surface Area (m <sup>2</sup> g <sup>-1</sup> )	Micropore Volume (cm <sup>3</sup> g <sup>-1</sup> ) <sup>[a]</sup>	CO <sub>2</sub> uptake at 1 bar (mmol g <sup>-1</sup> )	C <sub>6</sub> H <sub>6</sub> uptake at p/p <sub>0</sub> = 0.35 (molecules per unit cell)	Ref.
<b>1-F</b>	1899 <sup>[b]</sup>	0.92	2.9	139.5	This work
	2282 <sup>[c]</sup>	1.20	-	-	19
<b>2-Cl</b>	1556 <sup>[b]</sup>	0.75	1.8	-	This work
	1720 <sup>[c]</sup>	0.87	-	-	19
<b>3-Br</b>	1273 <sup>[b]</sup>	0.62	1.7	66.2	This work
	1631 <sup>[c]</sup>	0.87	-	-	19
<b>4-CH<sub>3</sub></b>	2135 <sup>[b]</sup>	1.04	2	119.5	This work
	1467 <sup>[c]</sup>	0.68	-	-	19
<b>5-C<sub>6</sub>H<sub>4</sub></b>	1413 <sup>[b]</sup>	0.68	1.8	90.5	This work
<b>6-F<sub>2</sub></b>	1647 <sup>[b]</sup>	0.82	-	-	This work
<b>7-(CH<sub>3</sub>)<sub>2</sub></b>	1452 <sup>[b]</sup>	0.69	1.8	-	This work
	2127 <sup>[b]</sup>	-	-	-	28
Cr-MIL-101	2172 <sup>[b]</sup>	1.07	2.2	132.9	This work
	2367-4100	2.0(1) <sup>[d]</sup>	-	-	12, 46, 25

<sup>[a]</sup> Micropore volume determined at p/p<sub>0</sub> = 0.5; <sup>[b]</sup> Specific BET surface area estimated in the p/p<sub>0</sub> range of 0.05-0.1; <sup>[c]</sup> Specific BET surface area estimated using the Rouquerol method.<sup>47</sup>; <sup>[d]</sup> Determined using the Dubinin-Radushkevich equation.

The CO<sub>2</sub> adsorption capacities of the mono- and di-fluorinated Cr-MIL-101 compounds at 1 bar deserve special attentions as the employment of the fluorinated ligands in MOFs increases the CO<sub>2</sub> uptake capacity.<sup>48-50</sup> The mono-fluorinated **1-F** shows the highest CO<sub>2</sub> uptake value at 1 bar, although it bears lower BET surface area compared to those of un-functionalized Cr-MIL-101 and **4-CH<sub>3</sub>**. Similarly, the CO<sub>2</sub> adsorption capacity of the di-fluorinated **6-F<sub>2</sub>** equals to that of **4-CH<sub>3</sub>**, despite the fact that the BET surface area of the former is considerably lower compared to that of the latter. Thus, the fluorination of the pore walls inside the framework enhances the CO<sub>2</sub> uptake of Cr-MIL-101. Similar effect of the attached fluorine groups in enhancing the CO<sub>2</sub> adsorption capacities of the un-functionalized MOFs has been previously documented in the literature.<sup>48-50</sup> All these observations suggest that both the size and the nature of the attached functional groups determine the CO<sub>2</sub> uptake values of the Cr-MIL-101-X materials. The values of the specific BET surface areas are dependent on the size of the attached

functional groups, whereas the nature of framework-CO<sub>2</sub> interactions is governed by the nature of the attached functional groups.

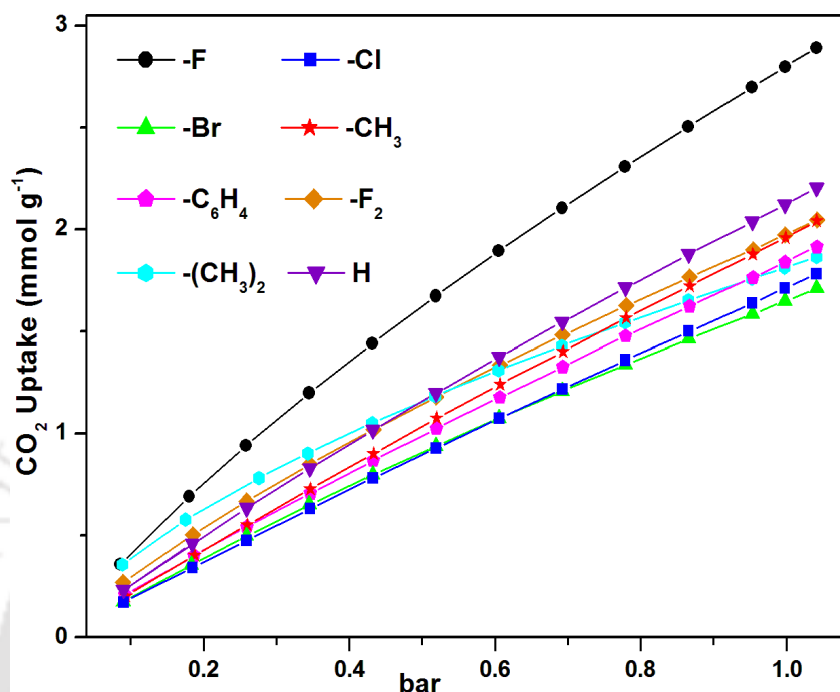


**Figure 6.7** CO<sub>2</sub> adsorption isotherms of the thermally activated **1-F** (black, circles), **2-Cl** (blue, squares), **3-Br** (green, triangles), **4-CH<sub>3</sub>** (red, stars), **5-C<sub>6</sub>H<sub>4</sub>** (magenta, pentagons), **6-F<sub>2</sub>** (orange, rotated squares), **7-(CH<sub>3</sub>)<sub>2</sub>** (cyan, hexagons) and Cr-MIL-101 (violet, upside-down triangles) measured at 0 °C.

Although the fluorination has been demonstrated to enhance the CO<sub>2</sub> adsorption capacity of Cr-MIL-101, it should be noted that specific BET surface area of the material decreases with increase in the number of attached –F groups. The observed CO<sub>2</sub> uptake is also dependent on the specific BET surface area, apart from the extent of fluorination. Thus, the CO<sub>2</sub> adsorption capacity of **1-F** at 1 bar is higher than **6-F<sub>2</sub>** (which is in agreement with their specific BET surface areas), although the reverse is expected from the degree of fluorination (i.e., the number of attached –F groups per linker molecule).

The Cr-MIL-101 material has formerly been demonstrated to show high benzene adsorption capacities due to the high packing efficiency and strong  $\pi$ -interaction of benzene with the adsorption sites in the framework.<sup>44</sup> Inspired by this fact, we have measured benzene adsorption isotherms with the Cr-MIL-101-X materials at 50 °C. The benzene adsorption isotherms (Figure 6.8) display type-I behavior with a small step at  $p/p_0 = 0.12$ . Similar to the N<sub>2</sub> adsorption isotherms, the presence of these two steps in the benzene adsorption isotherms might

be related to the different filling of the cages.<sup>49</sup> The benzene adsorption capacities (molecules per unit cell) of the materials at  $p/p_0 = 0.35$  decrease in the order: **1-F** (139.5) > Cr-MIL-101 (132.9) > **4-CH<sub>3</sub>** (119.5) > **6-F<sub>2</sub>** (107.04) > **5-C<sub>6</sub>H<sub>4</sub>** (90.5) > **3-Br** (66.2). The benzene uptake value (132.9 molecules per unit cell at 50 °C and  $p/p_0 = 0.6$ ) of the un-functionalized Cr-MIL-101 material is lower compared to that reported in the literature (229.6 molecules per unit cell at 32 °C and  $p/p_0 = 0.6$ ). Considering that the unit cell of Cr-MIL-101 consists of a total of 24 cages (16 smaller and 8 larger cages),<sup>51</sup> the descending order of benzene adsorption capacities (molecules per cage) at  $p/p_0 = 0.35$  becomes **1-F** (5.8) > Cr-MIL-101 (5.5) > **4-CH<sub>3</sub>** (5.0) > **6-F<sub>2</sub>** (4.5) > **5-C<sub>6</sub>H<sub>4</sub>** (3.8) > **3-Br** (2.8). Interestingly, the mono-fluorinated **1-F** displays the highest benzene uptake value at  $p/p_0 = 0.35$ , despite the fact that it has lower BET surface area compared to those of un-functionalized Cr-MIL-101 and **4-CH<sub>3</sub>**. Since benzene is a nonpolar molecule, this observation can be assigned to the higher hydrophobicity of the fluorine-functionalized Cr-MIL-101 as compared to the non- and methyl-functionalized Cr-MIL-101. Similar trend in hydrophobicity between the methyl-functionalized and fluorinated frameworks has been documented in the literature for highly hydrophobic nickel MOFs possessing bi-pyrazolate linkers.<sup>52</sup>

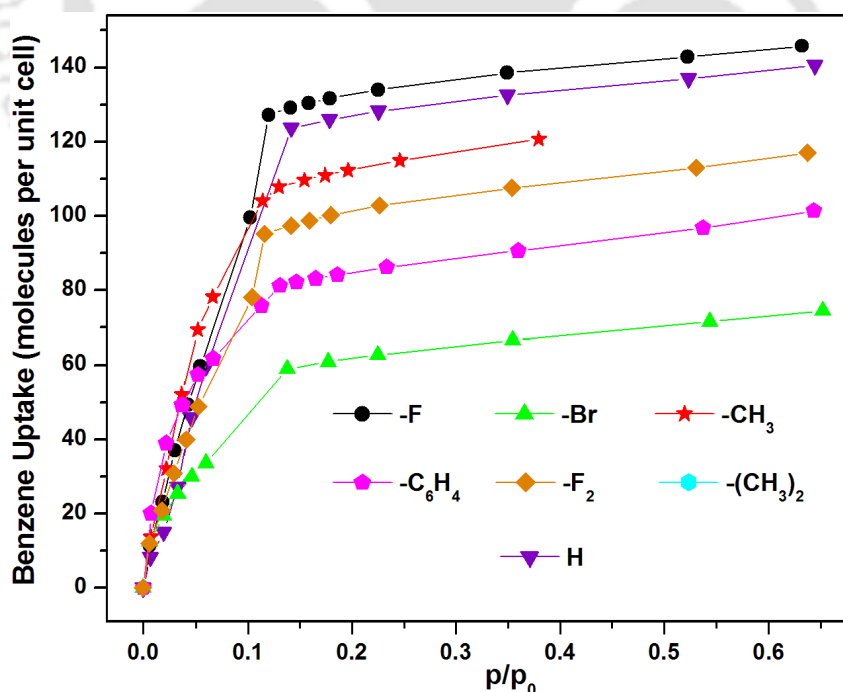


**Figure 6.8** Benzene adsorption isotherms of the thermally activated **1-F** (black, circles), **3-Br** (green, triangles), **4-CH<sub>3</sub>** (red, stars), **5-C<sub>6</sub>H<sub>4</sub>** (magenta, pentagons), **6-F<sub>2</sub>** (orange, rotated squares) and Cr-MIL-101 (violet, upside-down triangles) recorded at 50 °C.

## 6.4 CONCLUSIONS

The hydrothermal synthesis, thorough characterization and sorption properties of functionalized Cr-MIL-101-X (X = -F, -Cl, -Br, -CH<sub>3</sub>, -C<sub>6</sub>H<sub>4</sub>, -F<sub>2</sub>, -(CH<sub>3</sub>)<sub>2</sub>) materials have been demonstrated. A general synthetic approach was employed for the preparation of all of the functionalized Cr-MIL-101-X materials except Cr-MIL-101-C<sub>6</sub>H<sub>4</sub>. In this approach, the highly crystalline materials were obtained by reacting the mixtures of CrO<sub>3</sub>, H<sub>2</sub>BDC-X ligands, conc. HCl and water with a molar ratio of 1:1:3.9:222.2 at 180 °C for 144 h. In sharp contrast to the 144 h of reaction time, three of the Cr-MIL-101-X materials with X = -Cl, -Br and -C<sub>6</sub>H<sub>4</sub> could be prepared in considerably shorter reaction times (12-18 h at 180-210 °C). The main advantage of the alternative synthesis method described herein for **2-Cl** and **3-Br** compared to the previously reported synthesis procedure is that the present method (12 h and 18 h for **2-Cl** and **3-Br**, respectively) involves shorter reaction times than the previous procedure (120 h for each compound). However, the **2-Cl** and **3-Br** prepared by the alternative method exhibit relatively lower crystallinity and specific BET surface areas compared to the materials synthesized by the previous procedure. The phase purity of the materials was verified by a combination of XRPD measurements, DRIFT spectroscopy and thermogravimetric analysis. As corroborated by the TG analyses, all the Cr-MIL-101-X materials exhibit high thermal stability up to 270-300 °C in an air atmosphere. All the thermally activated materials exhibit significant porosity, as confirmed by the N<sub>2</sub> ( $S_{\text{BET}}$  in the 1273-2135 m<sup>2</sup> g<sup>-1</sup> range), CO<sub>2</sub> (uptake values in the 1.7-2.9 mmol g<sup>-1</sup> range at 0 °C and 1 bar) and benzene (adsorption capacities in the 66.2-139.5 molecules per unit cell range at 50 °C and p/p<sub>0</sub> = 0.35) sorption experiments. The N<sub>2</sub> uptake values of the materials are dependent on the size of the grafted functional groups. On the other hand, their CO<sub>2</sub> and benzene adsorption capacities are dependent both on the size and the nature of attached functional groups, leading to different adsorptive-framework interactions. Specifically, the mono- and di-fluorinated Cr-MIL-101 materials exhibited enhanced CO<sub>2</sub> adsorption capacities. Furthermore, Cr-MIL-101-F showed higher benzene uptake value compared to the non- and methyl-functionalized Cr-MIL-101, suggesting that the fluorination induced more hydrophobicity in Cr-MIL-101 as compared to the methylation. The high thermal and hydrolytic stability as well as remarkably high porosity would make the Cr-MIL-101-X materials as potential candidates for applications in gas/liquid storage and separation.

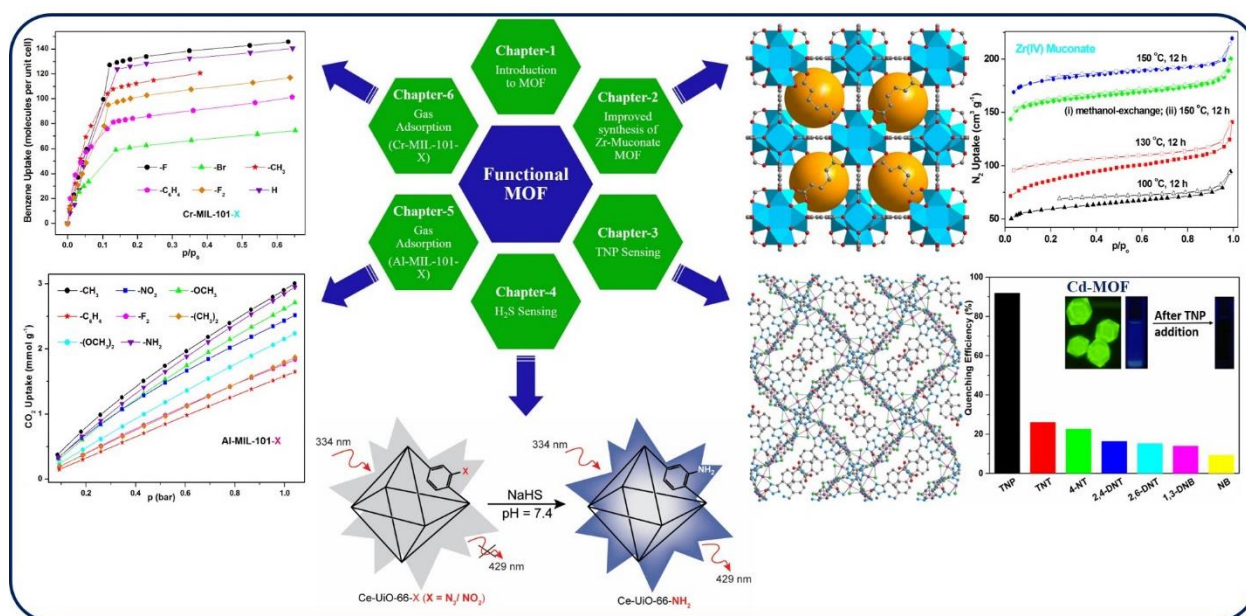
## 6.5 REFERENCES

1. L. M. Huang, H. T. Wang, J. X. Chen, Z. B. Wang, J. Y. Sun, D. Y. Zhao and Y. Yan, *Microporous Mesoporous Mater.*, 2003, **58**, 105.
2. J. A. Greathouse and M. D. Allendorf, *J. Am. Chem. Soc.*, 2006, **128**, 10678.
3. Y. Li and R. T. Yang, *Langmuir*, 2007, **23**, 12937.
4. S. S. Kaye, A. Dailly, O. M. Yaghi and J. R. Long, *J. Am. Chem. Soc.*, 2007, **129**, 14176.
5. D. Ma, Y. Li and Z. Li, *Chem. Commun.*, 2011, **47**, 7377.
6. T. Wu, L. Shen, M. Luebbbers, C. Hu, Q. Chen, Z. Ni and R. I. Masel, *Chem. Commun.*, 2010, **46**, 6120.
7. C. Yang, X. P. Wang and M. A. Omary, *J. Am. Chem. Soc.*, 2007, **129**, 15454.
8. S. Biswas, T. Remy, S. Couck, D. Denysenko, G. Rampelberg, J. F. M. Denayer, D. Volkmer, C. Detavernier and P. V. D. Voort, *Phys.Chem. Chem. Phys.*, 2013, **15**, 3552.
9. S. Biswas, S. Couck, D. Denysenko, A. Bhunia, M. Grzywa, J. F. M. Denayer, D. Volkmer, C. Janiak and P. V. D. Voort, *Microporous Mesoporous Mater.*, 2013, **181**, 175.
10. T. Loiseau, C. Serre, C. Huguenard, G. Fink, F. Taulelle, M. Henry, T. Bataille and G. Férey, *Chem.–Eur. J.*, 2004, **10**, 1373.
11. P. Serra-Crespo, E. V. Ramos-Fernandez, J. Gascon and F. Kapteijn, *Chem. Mater.*, 2011, **23**, 2565.
12. G. Férey, C. Mellot-Draznieks, C. Serre, F. Millange, J. Dutour, S. Surble and I. Margiolaki, *Science*, 2005, **309**, 2040.
13. M. Dan-Hardi, C. Serre, T. Frot, L. Rozes, G. Maurin, C. Sanchez and G. Férey, *J. Am. Chem. Soc.*, 2009, **131**, 10857.
14. J. H. Cavka, S. Jakobsen, U. Olsbye, N. Guillou, C. Lamberti, S. Bordiga and K. P. Lillerud, *J. Am. Chem. Soc.*, 2008, **130**, 13850.
15. M. Bosch, M. Zhang and H.-C. Zhou, *Adv. Chem.*, 2014, 1.
16. N. C. Burtch, H. Jasuja and K. S. Walton, *Chem. Rev.*, 2014, **114**, 10575.
17. K. Barthelet, D. Riou and G. Férey, *Chem. Commun.*, 2002, 1492.
18. S. Bernt, V. Guillermin, C. Serre and N. Stock, *Chem. Commun.*, 2011, **47**, 2838.
19. M. Lammert, S. Bernt, F. Vermoortele, D. E. De Vos and N. Stock, *Inorg. Chem.*, 2013, **52**, 8521.
20. A. Klinkebiel, N. Reimer, M. Lammert, N. Stock and U. Luning, *Chem. Commun.*, 2014, **50**, 9306.

21. P. A. Szilagy, I. Weinrauch, J. Juan-Alcañiz, P. Serra-Crespo, A. Grzech, H. Oh, M. de Respinis, B. J. Trzesniewski, F. Kapteijn, R. van de Krol, H. Geerlings, J. Gascon, M. Hirscher and B. Dam, *J. Phys. Chem. C*, 2014, **118**, 19572.
22. D. Jiang, L. L. Keenan, A. D. Burrows and K. J. Edler, *Chem. Commun.*, 2012, **48**, 12053.
23. J. Juan-Alcaniz, R. Gielisse, A. B. Lago, E. V. Ramos-Fernandez, P. Serra-Crespo, T. Devic, N. Guillou, C. Serre, F. Kapteijn and J. Gascon, *Catal. Sci. Technol.*, 2013, **3**, 2311.
24. G. Akiyama, R. Matsuda, H. Sato, A. Hori, M. Takata and S. Kitagawa, *Microporous Mesoporous Mater.*, 2012, **157**, 89.
25. G. Akiyama, R. Matsuda, H. Sato, M. Takata and S. Kitagawa, *Adv. Mater.*, 2011, **23**, 3294.
26. F. L. Morel, M. Ranocchiari and J. A. van Bokhoven, *Ind. Eng. Chem. Res.*, 2014, **53**, 9120.
27. M. G. Goesten, K. B. Sai Sankar Gupta, E. V. Ramos-Fernandez, H. Khajavi, J. Gascon and F. Kapteijn, *CrystEngComm*, 2012, **14**, 4109.
28. G. Akiyama, R. Matsuda, H. Sato and S. Kitagawa, *Chem. Asian J.*, 2014, **9**, 2772.
29. B. Wu, X. Lin, L. Ge, L. Wu and T. Xu, *Chem. Commun.*, 2013, **49**, 143.
30. S. Biswas, S. Couck, M. Grzywa, J. F. M. Denayer, D. Volkmer and P. Van Der Voort, *Eur. J. Inorg. Chem.*, 2012, 2481.
31. F. Carson, J. Su, A. E. Platero-Prats, W. Wan, Y. Yun, L. Samain and X. Zou, *Cryst. Growth Des.*, 2013, **13**, 5036.
32. M. Hartmann and M. Fischer, *Microporous Mesoporous Mater.*, 2012, **164**, 38.
33. R. Srirambalaji, S. Hong, R. Natarajan, M. Yoon, R. Hota, Y. Kim, Y. H. Ko and K. Kim, *Chem. Commun.*, 2012, **48**, 11650.
34. A. Buragohain, P. V. D. Voort and S. Biswas, *Microporous Mesoporous Mater.*, 2015, **215**, 91.
35. T. Devic, P. Horcajada, C. Serre, F. Salles, G. Maurin, B. Moulin, D. Heurtaux, G. Clet, A. Vimont, J.-M. Greneche, B. Le Ouay, F. Moreau, E. Magnier, Y. Filinchuk, J. Marrot, J.-C. Lavalley, M. Daturi and G. Férey, *J. Am. Chem. Soc.*, 2010, **132**, 1127.
36. M. Kuwabara, A. Murakami, K. Fukunishi, M. Nomura and H. Yamanaka, *J. Fluorine Chem.*, 1989, **42**, 105.
37. L. Bromberg, Y. Diao, H. Wu, S. A. Speakman and T. A. Hatton, *Chem. Mater.*, 2012, **24**, 1664.
38. I. Y. Skobelev, A. B. Sorokin, K. A. Kovalenko, V. P. Fedin and O. A. Kholdeeva, *J. Catal.*, 2013, **298**, 61.

39. R. Banerjee, H. Furukawa, D. Britt, C. Knobler, M. O’Keeffe and O. M. Yaghi, *J. Am. Chem. Soc.*, 2009, **131**, 3875.
40. <http://www.iza-structure.org/databases/>.
41. S. Biswas, T. Ahnfeldt and N. Stock, *Inorg. Chem.*, 2011, **50**, 9518.
42. T. Loiseau, C. Serre, C. Huguenard, F. T. G. Fink, M. Henry, T. Bataille and G. Férey, *Chem. Eur. J.*, 2004, **10**, 1373.
43. D.-Y. Hong, Y. K. Hwang, C. Serre, G. Férey and J. S. Chang, *Adv. Funct. Mater.*, 2009, **19**, 1537.
44. K. M. L. Taylor-Pashow, J. D. Rocca, Z. G. Xie, S. Tran and W. Lin, *J. Am. Chem. Soc.*, 2009, **131**, 14261.
45. C. Scherb, J. J. Williams, F. Hinterholzinger, S. Bauer, N. Stock and T. Bein, *J. Mater. Chem.*, 2011, **21**, 14849.
46. S. Bernt, V. Guillermin, C. Serre and N. Stock, *Chem. Commun.*, 2011, **47**, 2838.
47. J. Rouquerol, P. Llewellyn and F. Rouquerol, *Stud. Surf. Sci. Catal.*, 2007, **160**, 49.
48. D.-S. Zhang, Z. Chang, Y.-F. Li, Z.-Y. Jiang, Z.-H. Xuan, Y.-H. Zhang, J.-R. Li, Q. Chen, T.-L. Hu and X.-H. Bu, *Sci. Rep.*, 2013, **3**, 3312.
49. H.-H. Wang, T.-T. Guo, D. Xie, Z.-Q. Bai, L. Hou and Y.-Y. Wang, *Eur. J. Inorg. Chem.*, 2015, **2015**, 5773.
50. L. Hou, W.-J. Shi, Y.-Y. Wang, Y. Guo, C. Jin and Q.-Z. Shi, *Chem. Commun.*, 2011, **47**, 5464.
51. P. Horcajada, C. Serre, M. Vallet-Regí, M. Sebban, F. Taulelle and G. Férey, *Angew. Chem. Int. Ed.*, 2006, **45**, 5974.
52. N. M. Padial, E. Q. Procopio, C. Montoro, E. Lopez, J. E. Oltra, V. Colombo, A. Maspero, N. Masciocchi, S. Galli, I. Senkowska, S. Kaskel, E. Barea and J. A. R. Navarro, *Angew. Chem.*, 2013, **125**, 8448.

## CONCLUSIONS AND OUTLOOK



The work presented in this thesis demonstrates that the functionalization of MOFs is a promising strategy to enhance the physicochemical stability (air, water, acid-base, heat, etc.) as well as gas storage and separation properties of the resulting MOFs. The attached functional groups can act as interaction sites for specific gas molecules (during gas adsorption) and analytes (during fluorescence sensing), thus increasing the selectivity of the MOF material towards the target gas molecule or analyte. Therefore, the functionalized MOFs can be employed for the separation of gas mixtures. Furthermore, they can be utilized for the selective fluorimetric detection of a target analyte in the presence of potentially interfering analytes.

In Chapter 2, an improved synthesis procedure for the preparation of the formerly reported Zr(IV) *trans,trans*-muconate framework material is presented. Instead of using non-commercial Zr<sub>6</sub>-methacrylate oxocluster as the metal source, the same MOF material was successfully synthesized by using commercially available ZrCl<sub>4</sub> as the Zr source. During the synthesis, small amounts of H<sub>2</sub>O or conc. HCl were used as additives in DMF. The influence of ZrCl<sub>4</sub>/additive molar ratio on the crystallinity of the materials has been systematically examined. According to the thermogravimetric analyses, the two materials are stable up to ~250 °C in N<sub>2</sub> atmosphere. As

confirmed by the XRPD analyses, both of the materials are unstable in acetic acid, 1M HCl and 1M NaOH solutions. The crystallinity of the materials deteriorated slowly when they were exposed to water as well as moisture (from air), suggesting gradual structural collapse of the framework over time. The effect of activation temperature on the BET surface area of the materials was also examined. As corroborated by the N<sub>2</sub> sorption measurements, the optimally activated material exhibited BET surface area of 557 m<sup>2</sup> g<sup>-1</sup>, which is lower than the isostructural UiO-66 (950 m<sup>2</sup> g<sup>-1</sup>) but it is close to the literature value (705 m<sup>2</sup> g<sup>-1</sup>) of Zr(IV) muconate. Owing to its moderate physicochemical stability and significant porosity, the material is a potential candidate in the field of gas storage and separation.

The successful solvothermal synthesis of strongly fluorescent 3D Cd(II)-based MOF incorporating a highly  $\pi$ -conjugated amide-functionalized ditopic tetrazolate-based organic ligand is presented in Chapter 3. Selective detection of explosive 2,4,6-trinitrophenol (TNP) by activated material with a very high rate of response was confirmed by the steady-state fluorescence titration experiments. It was observed that the selective detection of TNP was also possible in presence of other potentially interfering nitroaromatic explosives. The detection limit of the material for the sensing of TNP was estimated to be  $1.87 \times 10^{-7}$  M (42.84 ppb), which is comparable with other MOF-based fluorescence sensors reported until today. The recyclability experiments indicate high photostability and reusability of the compound for long-term in-field detection of nitroaromatic explosive materials. The combination of experimental and theoretical results provides indications in favor of both energy and electron transfer mechanisms for the highest quenching efficiency of TNP. Moreover, the enhanced selectivity of the material for sensing of TNP can be instinctively assigned to the existence of electrostatic interactions between the N-H moiety of the ligand and the hydroxyl group of TNP. The outstanding sensing performance renders the material as a promising sensing device for the real-world detection of TNP.

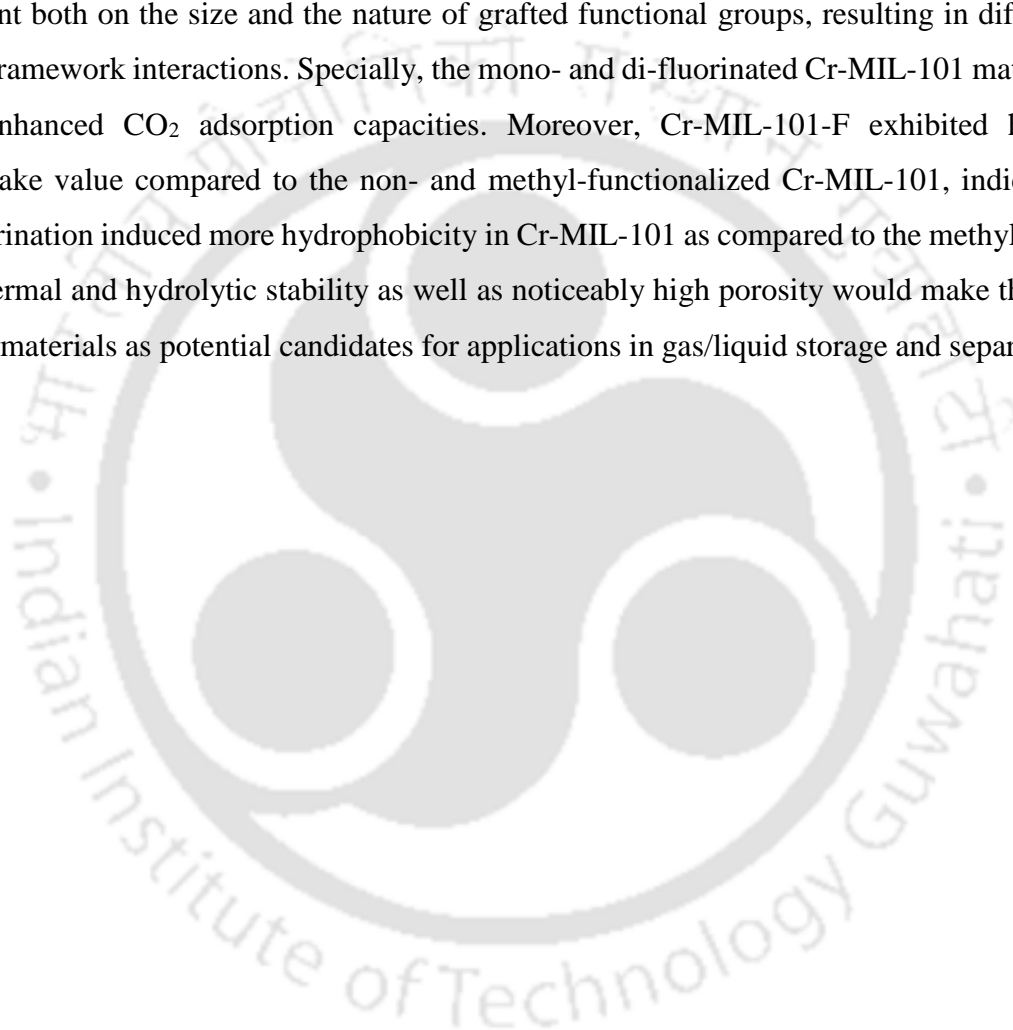
In Chapter 4, a new azide- and an existing nitro-functionalized Ce(IV)-based MOF with UiO-66 framework topology have been presented for the first time as fluorescence turn-on probes for the detection of H<sub>2</sub>S under physiological conditions. Both materials demonstrated promising potentials towards highly selective, sensitive (detection limits: 12.2  $\mu$ M for azide-functionalized mof and 34.8  $\mu$ M for nitro-functionalized MOF) and rapid detection of H<sub>2</sub>S. It was observed that the Ce-based UiO-66 MOFs exhibited improved fluorescence response towards H<sub>2</sub>S than their Zr-

based counterparts. Owing to their extraordinary selectivity towards sensing of H<sub>2</sub>S even in the presence of other potentially interfering biomolecules, these materials could be promising candidates for the real-time monitoring of H<sub>2</sub>S in biological systems. Besides the fast, selective and sensitive detection of H<sub>2</sub>S, both of these materials can effectively adsorb considerable amounts CO<sub>2</sub> at 0 °C and in pressure range of 0 to 1 bar. As a result, they are also excellent materials in the field of CO<sub>2</sub> capture.

The facile synthesis, complete characterization and gas adsorption properties of seven new functionalized Al-MIL-101-X (X = -CH<sub>3</sub>, -NO<sub>2</sub>, -OCH<sub>3</sub>, -C<sub>6</sub>H<sub>4</sub>, -F<sub>2</sub>, -(CH<sub>3</sub>)<sub>2</sub>, -(OCH<sub>3</sub>)<sub>2</sub>) materials are demonstrated in Chapter 5. The seven new materials along with the formerly reported Al-MIL-101-NH<sub>2</sub> compound were prepared by using stoichiometric mixtures of Al(ClO<sub>4</sub>)<sub>3</sub>·9H<sub>2</sub>O and H<sub>2</sub>BDC-X linkers in DEF under similar solvothermal conditions (130 °C, 3-12 h) with conventional electric heating. The Al-MIL-101-X materials with X = -CH<sub>3</sub>, -OCH<sub>3</sub>, -C<sub>6</sub>H<sub>4</sub> and -(OCH<sub>3</sub>)<sub>2</sub> were also prepared under identical microwave-assisted solvothermal conditions (170 °C, 10 min, 150 W). A substantial reduction in the reaction time was observed in the microwave irradiation method as compared to the solvothermal technique. It was observed that Al-MIL-101-X materials can sustain up to 260-430 °C in an air atmosphere. The thermally activated forms of all the materials showed significant porosity, as revealed by the N<sub>2</sub> (S<sub>BET</sub> in the range of 1328-2398 m<sup>2</sup> g<sup>-1</sup>) and CO<sub>2</sub> (uptake values in the range of 1.6-3.0 mmol g<sup>-1</sup> at 0 °C and 1 bar) sorption analysis. The N<sub>2</sub> adsorption capacities of the materials are reliant on the size of the attached functional groups, whereas the CO<sub>2</sub> uptake values of the materials are dependent on both the size and nature of attached functional groups, resulting in various CO<sub>2</sub>-framework interactions. The high thermal and moisture stability of the light-weight, non-toxic Al-MIL-101-X materials along with the significantly high porosity would make them potential candidates for applications in gas storage and separation.

Chapter 6 demonstrates the hydrothermal synthesis, complete characterization and sorption properties of functionalized Cr-MIL-101-X (X = -F, -Cl, -Br, -CH<sub>3</sub>, -C<sub>6</sub>H<sub>4</sub>, -F<sub>2</sub>, -(CH<sub>3</sub>)<sub>2</sub>) materials. All of the functionalized compounds except Cr-MIL-101-C<sub>6</sub>H<sub>4</sub> were obtained by reacting the mixtures of CrO<sub>3</sub>, H<sub>2</sub>BDC-X linkers, conc. HCl and water with a molar ratio of 1:1:3.9:222.2 at 180 °C for 144 h. On the other hand, the Cr-MIL-101-X materials with X = -Cl, -Br and -C<sub>6</sub>H<sub>4</sub> was synthesized in a shorter reaction times (12-18 h at 180-210 °C). According to the TG analyses,

all the Cr-MIL-101-X materials exhibit high thermal stability up to 270-300 °C in an air atmosphere. All the thermally activated materials displayed significant porosity, as verified by the N<sub>2</sub> ( $S_{\text{BET}}$  in the 1273-2135 m<sup>2</sup> g<sup>-1</sup> range), CO<sub>2</sub> (uptake values in the 1.7-2.9 mmol g<sup>-1</sup> range at 0 °C and 1 bar) and benzene (adsorption capacities in the 66.2-139.5 molecules per unit cell range at 50 °C and  $p/p_0 = 0.35$ ) sorption measurements. The N<sub>2</sub> uptake values of the materials are dependent on the size of the attached functional groups whereas, their CO<sub>2</sub> and benzene adsorption capacities are dependent both on the size and the nature of grafted functional groups, resulting in different adsorptive-framework interactions. Specially, the mono- and di-fluorinated Cr-MIL-101 materials displayed enhanced CO<sub>2</sub> adsorption capacities. Moreover, Cr-MIL-101-F exhibited higher benzene uptake value compared to the non- and methyl-functionalized Cr-MIL-101, indicating that the fluorination induced more hydrophobicity in Cr-MIL-101 as compared to the methylation. The high thermal and hydrolytic stability as well as noticeably high porosity would make the Cr-MIL-101-X materials as potential candidates for applications in gas/liquid storage and separation.



1/9/2017

RightsLink Printable License

**ROYAL SOCIETY OF CHEMISTRY LICENSE  
TERMS AND CONDITIONS**

Jan 09, 2017

This Agreement between Amlan Buragohain ("You") and Royal Society of Chemistry ("Royal Society of Chemistry") consists of your license details and the terms and conditions provided by Royal Society of Chemistry and Copyright Clearance Center.

License Number	4024780022078
License date	Jan 09, 2017
Licensed Content Publisher	Royal Society of Chemistry
Licensed Content Publication	Chemical Communications (Cambridge)
Licensed Content Title	Fluorescent metal-organic framework for selective sensing of nitroaromatic explosives
Licensed Content Author	Bappaditya Gole, Arun Kumar Bar, Partha Sarathi Mukherjee
Licensed Content Date	Oct 13, 2011
Licensed Content Volume Number	47
Licensed Content Issue Number	44
Type of Use	Thesis/Dissertation
Requestor type	academic/educational
Portion	figures/tables/images
Number of figures/tables/images	1
Format	print and electronic
Distribution quantity	5
Will you be translating?	no
Order reference number	
Title of the thesis/dissertation	Development of functional Metal Organic Frameworks for gas storage and fluorescence sensing application
Expected completion date	Feb 2017
Estimated size	200
Customer Tax ID	IN7086652502
Requestor Location	Amlan Buragohain Department of Chemistry, Lab No. CHL 203 IIT Guwahati Amingaon Guwahati, 781039 India Attn: Amlan Buragohain
Customer VAT ID	IN7086652502
Billing Type	Invoice
Billing Address	Amlan Buragohain Department of Chemistry, Lab No. CHL 203 IIT Guwahati

<https://s100.copyright.com/CustomAdmin/PLF.jsp?ref=39a15e89-b835-4cfd-b161-56386563bff7>

1/4

1/9/2017

RightsLink Printable License

Amingaon  
Guwahati, India 781039  
Attn: Amlan Buragohain

Total 0.00 USD

#### Terms and Conditions

This License Agreement is between {Requestor Name} ("You") and The Royal Society of Chemistry ("RSC") provided by the Copyright Clearance Center ("CCC"). The license consists of your order details, the terms and conditions provided by the Royal Society of Chemistry, and the payment terms and conditions.

#### RSC / TERMS AND CONDITIONS

##### INTRODUCTION

The publisher for this copyrighted material is The Royal Society of Chemistry. By clicking "accept" in connection with completing this licensing transaction, you agree that the following terms and conditions apply to this transaction (along with the Billing and Payment terms and conditions established by CCC, at the time that you opened your RightsLink account and that are available at any time at .

##### LICENSE GRANTED

The RSC hereby grants you a non-exclusive license to use the aforementioned material anywhere in the world subject to the terms and conditions indicated herein. Reproduction of the material is confined to the purpose and/or media for which permission is hereby given.

##### RESERVATION OF RIGHTS

The RSC reserves all rights not specifically granted in the combination of (i) the license details provided by your and accepted in the course of this licensing transaction; (ii) these terms and conditions; and (iii) CCC's Billing and Payment terms and conditions.

##### REVOCATION

The RSC reserves the right to revoke this license for any reason, including, but not limited to, advertising and promotional uses of RSC content, third party usage, and incorrect source figure attribution.

##### THIRD-PARTY MATERIAL DISCLAIMER

If part of the material to be used (for example, a figure) has appeared in the RSC publication with credit to another source, permission must also be sought from that source. If the other source is another RSC publication these details should be included in your RightsLink request. If the other source is a third party, permission must be obtained from the third party. The RSC disclaims any responsibility for the reproduction you make of items owned by a third party.

##### PAYMENT OF FEE

If the permission fee for the requested material is waived in this instance, please be advised that any future requests for the reproduction of RSC materials may attract a fee.

##### ACKNOWLEDGEMENT

The reproduction of the licensed material must be accompanied by the following acknowledgement:

Reproduced ("Adapted" or "in part") from {Reference Citation} (or Ref XX) with permission of The Royal Society of Chemistry.

If the licensed material is being reproduced from New Journal of Chemistry (NJC), Photochemical & Photobiological Sciences (PPS) or Physical Chemistry Chemical Physics (PCCP) you must include one of the following acknowledgements:

For figures originally published in NJC:

Reproduced ("Adapted" or "in part") from {Reference Citation} (or Ref XX) with permission of The Royal Society of Chemistry (RSC) on behalf of the European Society for Photobiology, the European Photochemistry Association and the RSC.

For figures originally published in PPS:

Reproduced ("Adapted" or "in part") from {Reference Citation} (or Ref XX) with permission of The Royal Society of Chemistry (RSC) on behalf of the Centre National de la Recherche Scientifique (CNRS) and the RSC.

<https://s100.copyright.com/CustomerAdmin/PLF.jsp?ref=39a15e89-b835-4cfd-b161-56386563bf7>

2/4

1/9/2017

RightsLink Printable License

For figures originally published in PCCP:  
 Reproduced (“Adapted” or “in part”) from {Reference Citation} (or Ref XX) with  
 permission of the PCCP Owner Societies.

#### HYPERTEXT LINKS

With any material which is being reproduced in electronic form, you must include a  
 hypertext link to the original RSC article on the RSC’s website. The recommended form for  
 the hyperlink is <http://dx.doi.org/10.1039/DOI> suffix, for example in the link  
<http://dx.doi.org/10.1039/b110420a> the DOI suffix is ‘b110420a’. To find the relevant DOI  
 suffix for the RSC article in question, go to the Journals section of the website and locate the  
 article in the list of papers for the volume and issue of your specific journal. You will find  
 the DOI suffix quoted there.

#### LICENSE CONTINGENT ON PAYMENT

While you may exercise the rights licensed immediately upon issuance of the license at the  
 end of the licensing process for the transaction, provided that you have disclosed complete  
 and accurate details of your proposed use, no license is finally effective unless and until full  
 payment is received from you (by CCC) as provided in CCC's Billing and Payment terms  
 and conditions. If full payment is not received on a timely basis, then any license  
 preliminarily granted shall be deemed automatically revoked and shall be void as if never  
 granted. Further, in the event that you breach any of these terms and conditions or any of  
 CCC's Billing and Payment terms and conditions, the license is automatically revoked and  
 shall be void as if never granted. Use of materials as described in a revoked license, as well  
 as any use of the materials beyond the scope of an unrevoked license, may constitute  
 copyright infringement and the RSC reserves the right to take any and all action to protect its  
 copyright in the materials.

#### WARRANTIES

The RSC makes no representations or warranties with respect to the licensed material.

#### INDEMNITY

You hereby indemnify and agree to hold harmless the RSC and the CCC, and their  
 respective officers, directors, trustees, employees and agents, from and against any and all  
 claims arising out of your use of the licensed material other than as specifically authorized  
 pursuant to this licence.

#### NO TRANSFER OF LICENSE

This license is personal to you or your publisher and may not be sublicensed, assigned, or  
 transferred by you to any other person without the RSC's written permission.

#### NO AMENDMENT EXCEPT IN WRITING

This license may not be amended except in a writing signed by both parties (or, in the case  
 of “Other Conditions, v1.2”, by CCC on the RSC's behalf).

#### OBJECTION TO CONTRARY TERMS

You hereby acknowledge and agree that these terms and conditions, together with CCC's  
 Billing and Payment terms and conditions (which are incorporated herein), comprise the  
 entire agreement between you and the RSC (and CCC) concerning this licensing transaction,  
 to the exclusion of all other terms and conditions, written or verbal, express or implied  
 (including any terms contained in any purchase order, acknowledgment, check endorsement  
 or other writing prepared by you). In the event of any conflict between your obligations  
 established by these terms and conditions and those established by CCC's Billing and  
 Payment terms and conditions, these terms and conditions shall control.

#### JURISDICTION

This license transaction shall be governed by and construed in accordance with the laws of  
 the District of Columbia. You hereby agree to submit to the jurisdiction of the courts located  
 in the District of Columbia for purposes of resolving any disputes that may arise in  
 connection with this licensing transaction.

#### LIMITED LICENSE

The following terms and conditions apply to specific license types:

<https://s100.copyright.com/CustomAdmin/PLF.jsp?ref=39a15e89-b835-4cfd-b161-56386563bfff7>

3/4

1/9/2017

RightsLink Printable License

**Translation**

This permission is granted for non-exclusive world English rights only unless your license was granted for translation rights. If you licensed translation rights you may only translate this content into the languages you requested. A professional translator must perform all translations and reproduce the content word for word preserving the integrity of the article.

**Intranet**

If the licensed material is being posted on an Intranet, the Intranet is to be password-protected and made available only to bona fide students or employees only. All content posted to the Intranet must maintain the copyright information line on the bottom of each image. You must also fully reference the material and include a hypertext link as specified above.

**Copies of Whole Articles**

All copies of whole articles must maintain, if available, the copyright information line on the bottom of each page.

**Other Conditions**

v1.2

Gratis licenses (referencing \$0 in the Total field) are free. Please retain this printable license for your reference. No payment is required.

If you would like to pay for this license now, please remit this license along with your payment made payable to "COPYRIGHT CLEARANCE CENTER" otherwise you will be invoiced within 48 hours of the license date. Payment should be in the form of a check or money order referencing your account number and this invoice number {Invoice Number}.

Once you receive your invoice for this order, you may pay your invoice by credit card.

Please follow instructions provided at that time.

**Make Payment To:**

Copyright Clearance Center

Dept 001

P.O. Box 843006

Boston, MA 02284-3006

For suggestions or comments regarding this order, contact Rightslink Customer Support: [customercare@copyright.com](mailto:customercare@copyright.com) or +1-855-239-3415 (toll free in the US) or +1-978-646-2777.

**Questions? [customercare@copyright.com](mailto:customercare@copyright.com) or +1-855-239-3415 (toll free in the US) or +1-978-646-2777.**

1/26/2017

RightsLink Printable License

**JOHN WILEY AND SONS LICENSE  
TERMS AND CONDITIONS**

Jan 26, 2017

This Agreement between Amlan Buragohain ("You") and John Wiley and Sons ("John Wiley and Sons") consists of your license details and the terms and conditions provided by John Wiley and Sons and Copyright Clearance Center.

License Number	4036570702965
License date	Jan 26, 2017
Licensed Content Publisher	John Wiley and Sons
Licensed Content Publication	Chemistry - A European Journal
Licensed Content Title	A Fluorescent Sensor for Highly Selective Detection of Nitroaromatic Explosives Based on a 2D, Extremely Stable, Metal–Organic Framework
Licensed Content Author	Shu-Ran Zhang, Dong-Ying Du, Jun-Sheng Qin, Shao-Juan Bao, Shun-Li Li, Wen-Wen He, Ya-Qian Lan, Ping Shen, Zhong-Min Su
Licensed Content Date	Feb 27, 2014
Licensed Content Pages	6
Type of use	Dissertation/Thesis
Requestor type	University/Academic
Format	Print and electronic
Portion	Figure/table
Number of figures/tables	1
Original Wiley figure/table number(s)	Figure 3 (b)
Will you be translating?	No
Title of your thesis / dissertation	Development of functional Metal Organic Frameworks for gas storage and fluorescence sensing application
Expected completion date	Feb 2017
Expected size (number of pages)	200
Requestor Location	Amlan Buragohain Department of Chemistry, Lab No. CHL 203 IIT Guwahati Amingaon Guwahati, 781039 India Attn: Amlan Buragohain
Publisher Tax ID	EU826007151
Customer VAT ID	IN7086652502
Billing Type	Invoice
Billing Address	Amlan Buragohain Department of Chemistry, Lab No. CHL 203 IIT Guwahati Amingaon

<https://s100.copyright.com/AppDispatchServlet>

1/5

1/26/2017

RightsLink Printable License

Guwahati, India 781039  
 Attn: Amlan Buragohain

Total 0.00 USD

Terms and Conditions

### TERMS AND CONDITIONS

This copyrighted material is owned by or exclusively licensed to John Wiley & Sons, Inc. or one of its group companies (each a "Wiley Company") or handled on behalf of a society with which a Wiley Company has exclusive publishing rights in relation to a particular work (collectively "WILEY"). By clicking "accept" in connection with completing this licensing transaction, you agree that the following terms and conditions apply to this transaction (along with the billing and payment terms and conditions established by the Copyright Clearance Center Inc., ("CCC's Billing and Payment terms and conditions"), at the time that you opened your RightsLink account (these are available at any time at <http://myaccount.copyright.com>).

#### Terms and Conditions

- The materials you have requested permission to reproduce or reuse (the "Wiley Materials") are protected by copyright.
- You are hereby granted a personal, non-exclusive, non-sub licensable (on a stand-alone basis), non-transferable, worldwide, limited license to reproduce the Wiley Materials for the purpose specified in the licensing process. This license, **and any CONTENT (PDF or image file) purchased as part of your order**, is for a one-time use only and limited to any maximum distribution number specified in the license. The first instance of republication or reuse granted by this license must be completed within two years of the date of the grant of this license (although copies prepared before the end date may be distributed thereafter). The Wiley Materials shall not be used in any other manner or for any other purpose, beyond what is granted in the license. Permission is granted subject to an appropriate acknowledgement given to the author, title of the material/book/journal and the publisher. You shall also duplicate the copyright notice that appears in the Wiley publication in your use of the Wiley Material. Permission is also granted on the understanding that nowhere in the text is a previously published source acknowledged for all or part of this Wiley Material. Any third party content is expressly excluded from this permission.
- With respect to the Wiley Materials, all rights are reserved. Except as expressly granted by the terms of the license, no part of the Wiley Materials may be copied, modified, adapted (except for minor reformatting required by the new Publication), translated, reproduced, transferred or distributed, in any form or by any means, and no derivative works may be made based on the Wiley Materials without the prior permission of the respective copyright owner. **For STM Signatory Publishers clearing permission under the terms of the [STM Permissions Guidelines](#) only, the terms of the license are extended to include subsequent editions and for editions in other languages, provided such editions are for the work as a whole in situ and does not involve the separate exploitation of the permitted figures or extracts**, You may not alter, remove or suppress in any manner any copyright, trademark or other notices displayed by the Wiley Materials. You may not license, rent, sell, loan, lease, pledge, offer as security, transfer or assign the Wiley Materials on a stand-alone basis, or any of the rights granted to you hereunder to any other person.
- The Wiley Materials and all of the intellectual property rights therein shall at all times remain the exclusive property of John Wiley & Sons Inc, the Wiley Companies, or

<https://s100.copyright.com/AppDispatchServlet>

2/5

1/26/2017

RightsLink Printable License

their respective licensors, and your interest therein is only that of having possession of and the right to reproduce the Wiley Materials pursuant to Section 2 herein during the continuance of this Agreement. You agree that you own no right, title or interest in or to the Wiley Materials or any of the intellectual property rights therein. You shall have no rights hereunder other than the license as provided for above in Section 2. No right, license or interest to any trademark, trade name, service mark or other branding ("Marks") of WILEY or its licensors is granted hereunder, and you agree that you shall not assert any such right, license or interest with respect thereto

- NEITHER WILEY NOR ITS LICENSORS MAKES ANY WARRANTY OR REPRESENTATION OF ANY KIND TO YOU OR ANY THIRD PARTY, EXPRESS, IMPLIED OR STATUTORY, WITH RESPECT TO THE MATERIALS OR THE ACCURACY OF ANY INFORMATION CONTAINED IN THE MATERIALS, INCLUDING, WITHOUT LIMITATION, ANY IMPLIED WARRANTY OF MERCHANTABILITY, ACCURACY, SATISFACTORY QUALITY, FITNESS FOR A PARTICULAR PURPOSE, USABILITY, INTEGRATION OR NON-INFRINGEMENT AND ALL SUCH WARRANTIES ARE HEREBY EXCLUDED BY WILEY AND ITS LICENSORS AND WAIVED BY YOU.
- WILEY shall have the right to terminate this Agreement immediately upon breach of this Agreement by you.
- You shall indemnify, defend and hold harmless WILEY, its Licensors and their respective directors, officers, agents and employees, from and against any actual or threatened claims, demands, causes of action or proceedings arising from any breach of this Agreement by you.
- IN NO EVENT SHALL WILEY OR ITS LICENSORS BE LIABLE TO YOU OR ANY OTHER PARTY OR ANY OTHER PERSON OR ENTITY FOR ANY SPECIAL, CONSEQUENTIAL, INCIDENTAL, INDIRECT, EXEMPLARY OR PUNITIVE DAMAGES, HOWEVER CAUSED, ARISING OUT OF OR IN CONNECTION WITH THE DOWNLOADING, PROVISIONING, VIEWING OR USE OF THE MATERIALS REGARDLESS OF THE FORM OF ACTION, WHETHER FOR BREACH OF CONTRACT, BREACH OF WARRANTY, TORT, NEGLIGENCE, INFRINGEMENT OR OTHERWISE (INCLUDING, WITHOUT LIMITATION, DAMAGES BASED ON LOSS OF PROFITS, DATA, FILES, USE, BUSINESS OPPORTUNITY OR CLAIMS OF THIRD PARTIES), AND WHETHER OR NOT THE PARTY HAS BEEN ADVISED OF THE POSSIBILITY OF SUCH DAMAGES. THIS LIMITATION SHALL APPLY NOTWITHSTANDING ANY FAILURE OF ESSENTIAL PURPOSE OF ANY LIMITED REMEDY PROVIDED HEREIN.
- Should any provision of this Agreement be held by a court of competent jurisdiction to be illegal, invalid, or unenforceable, that provision shall be deemed amended to achieve as nearly as possible the same economic effect as the original provision, and the legality, validity and enforceability of the remaining provisions of this Agreement shall not be affected or impaired thereby.
- The failure of either party to enforce any term or condition of this Agreement shall not constitute a waiver of either party's right to enforce each and every term and condition of this Agreement. No breach under this agreement shall be deemed waived or excused by either party unless such waiver or consent is in writing signed by the party granting such waiver or consent. The waiver by or consent of a party to a breach of

<https://s100.copyright.com/AppDispatchServlet>

3/5

1/26/2017

RightsLink Printable License

any provision of this Agreement shall not operate or be construed as a waiver of or consent to any other or subsequent breach by such other party.

- This Agreement may not be assigned (including by operation of law or otherwise) by you without WILEY's prior written consent.
- Any fee required for this permission shall be non-refundable after thirty (30) days from receipt by the CCC.
- These terms and conditions together with CCC's Billing and Payment terms and conditions (which are incorporated herein) form the entire agreement between you and WILEY concerning this licensing transaction and (in the absence of fraud) supersedes all prior agreements and representations of the parties, oral or written. This Agreement may not be amended except in writing signed by both parties. This Agreement shall be binding upon and inure to the benefit of the parties' successors, legal representatives, and authorized assigns.
- In the event of any conflict between your obligations established by these terms and conditions and those established by CCC's Billing and Payment terms and conditions, these terms and conditions shall prevail.
- WILEY expressly reserves all rights not specifically granted in the combination of (i) the license details provided by you and accepted in the course of this licensing transaction, (ii) these terms and conditions and (iii) CCC's Billing and Payment terms and conditions.
- This Agreement will be void if the Type of Use, Format, Circulation, or Requestor Type was misrepresented during the licensing process.
- This Agreement shall be governed by and construed in accordance with the laws of the State of New York, USA, without regards to such state's conflict of law rules. Any legal action, suit or proceeding arising out of or relating to these Terms and Conditions or the breach thereof shall be instituted in a court of competent jurisdiction in New York County in the State of New York in the United States of America and each party hereby consents and submits to the personal jurisdiction of such court, waives any objection to venue in such court and consents to service of process by registered or certified mail, return receipt requested, at the last known address of such party.

#### **WILEY OPEN ACCESS TERMS AND CONDITIONS**

Wiley Publishes Open Access Articles in fully Open Access Journals and in Subscription journals offering Online Open. Although most of the fully Open Access journals publish open access articles under the terms of the Creative Commons Attribution (CC BY) License only, the subscription journals and a few of the Open Access Journals offer a choice of Creative Commons Licenses. The license type is clearly identified on the article.

##### **The Creative Commons Attribution License**

The [Creative Commons Attribution License \(CC-BY\)](#) allows users to copy, distribute and transmit an article, adapt the article and make commercial use of the article. The CC-BY license permits commercial and non-

##### **Creative Commons Attribution Non-Commercial License**

The [Creative Commons Attribution Non-Commercial \(CC-BY-NC\) License](#) permits use, distribution and reproduction in any medium, provided the original work is properly cited and is not used for commercial purposes.(see below)

1/26/2017

RightsLink Printable License

**Creative Commons Attribution-Non-Commercial-NoDerivs License**

The [Creative Commons Attribution Non-Commercial-NoDerivs License](#) (CC-BY-NC-ND) permits use, distribution and reproduction in any medium, provided the original work is properly cited, is not used for commercial purposes and no modifications or adaptations are made. (see below)

**Use by commercial "for-profit" organizations**

Use of Wiley Open Access articles for commercial, promotional, or marketing purposes requires further explicit permission from Wiley and will be subject to a fee.

Further details can be found on Wiley Online Library

<http://olabout.wiley.com/WileyCDA/Section/id-410895.html>

**Other Terms and Conditions:**

**v1.10 Last updated September 2015**

Questions? [customercare@copyright.com](mailto:customercare@copyright.com) or +1-855-239-3415 (toll free in the US) or +1-978-646-2777.





1/26/2017

RightsLink Printable License

**ROYAL SOCIETY OF CHEMISTRY LICENSE  
TERMS AND CONDITIONS**

Jan 26, 2017

This Agreement between Amlan Buragohain ("You") and Royal Society of Chemistry ("Royal Society of Chemistry") consists of your license details and the terms and conditions provided by Royal Society of Chemistry and Copyright Clearance Center.

License Number	4036571137531
License date	Jan 26, 2017
Licensed Content Publisher	Royal Society of Chemistry
Licensed Content Publication	Chemical Communications (Cambridge)
Licensed Content Title	A fluorescent metal-organic framework for highly selective detection of nitro explosives in the aqueous phase
Licensed Content Author	Sanjog S. Nagarkar,Aamod V. Desai,Sujit K. Ghosh
Licensed Content Date	May 16, 2014
Licensed Content Volume Number	50
Licensed Content Issue Number	64
Type of Use	Thesis/Dissertation
Requestor type	academic/educational
Portion	figures/tables/images
Number of figures/tables/images	1
Format	print and electronic
Distribution quantity	5
Will you be translating?	no
Order reference number	
Title of the thesis/dissertation	Development of functional Metal Organic Frameworks for gas storage and fluorescence sensing application
Expected completion date	Feb 2017
Estimated size	200
Customer Tax ID	IN7086652502
Requestor Location	Amlan Buragohain Department of Chemistry, Lab No. CHL 203 IIT Guwahati Amingaon Guwahati, 781039 India Attn: Amlan Buragohain
Customer VAT ID	IN7086652502
Billing Type	Invoice
Billing Address	Amlan Buragohain Department of Chemistry, Lab No. CHL 203 IIT Guwahati

<https://s100.copyright.com/AppDispatchServlet>

1/4

1/26/2017

RightsLink Printable License

Amingaon  
Guwahati, India 781039  
Attn: Amlan Buragohain

Total 0.00 USD

#### Terms and Conditions

This License Agreement is between {Requestor Name} ("You") and The Royal Society of Chemistry ("RSC") provided by the Copyright Clearance Center ("CCC"). The license consists of your order details, the terms and conditions provided by the Royal Society of Chemistry, and the payment terms and conditions.

#### RSC / TERMS AND CONDITIONS

##### INTRODUCTION

The publisher for this copyrighted material is The Royal Society of Chemistry. By clicking "accept" in connection with completing this licensing transaction, you agree that the following terms and conditions apply to this transaction (along with the Billing and Payment terms and conditions established by CCC, at the time that you opened your RightsLink account and that are available at any time at .

##### LICENSE GRANTED

The RSC hereby grants you a non-exclusive license to use the aforementioned material anywhere in the world subject to the terms and conditions indicated herein. Reproduction of the material is confined to the purpose and/or media for which permission is hereby given.

##### RESERVATION OF RIGHTS

The RSC reserves all rights not specifically granted in the combination of (i) the license details provided by your and accepted in the course of this licensing transaction; (ii) these terms and conditions; and (iii) CCC's Billing and Payment terms and conditions.

##### REVOCATION

The RSC reserves the right to revoke this license for any reason, including, but not limited to, advertising and promotional uses of RSC content, third party usage, and incorrect source figure attribution.

##### THIRD-PARTY MATERIAL DISCLAIMER

If part of the material to be used (for example, a figure) has appeared in the RSC publication with credit to another source, permission must also be sought from that source. If the other source is another RSC publication these details should be included in your RightsLink request. If the other source is a third party, permission must be obtained from the third party. The RSC disclaims any responsibility for the reproduction you make of items owned by a third party.

##### PAYMENT OF FEE

If the permission fee for the requested material is waived in this instance, please be advised that any future requests for the reproduction of RSC materials may attract a fee.

##### ACKNOWLEDGEMENT

The reproduction of the licensed material must be accompanied by the following acknowledgement:

Reproduced ("Adapted" or "in part") from {Reference Citation} (or Ref XX) with permission of The Royal Society of Chemistry.

If the licensed material is being reproduced from New Journal of Chemistry (NJC), Photochemical & Photobiological Sciences (PPS) or Physical Chemistry Chemical Physics (PCCP) you must include one of the following acknowledgements:

For figures originally published in NJC:

Reproduced ("Adapted" or "in part") from {Reference Citation} (or Ref XX) with permission of The Royal Society of Chemistry (RSC) on behalf of the European Society for Photobiology, the European Photochemistry Association and the RSC.

For figures originally published in PPS:

Reproduced ("Adapted" or "in part") from {Reference Citation} (or Ref XX) with permission of The Royal Society of Chemistry (RSC) on behalf of the Centre National de la Recherche Scientifique (CNRS) and the RSC.

<https://s100.copyright.com/AppDispatchServlet>

2/4

1/26/2017

RightsLink Printable License

For figures originally published in PCCP:  
Reproduced (“Adapted” or “in part”) from {Reference Citation} (or Ref XX) with  
permission of the PCCP Owner Societies.

#### HYPERTEXT LINKS

With any material which is being reproduced in electronic form, you must include a  
hypertext link to the original RSC article on the RSC’s website. The recommended form for  
the hyperlink is <http://dx.doi.org/10.1039/DOI> suffix, for example in the link  
<http://dx.doi.org/10.1039/b110420a> the DOI suffix is ‘b110420a’. To find the relevant DOI  
suffix for the RSC article in question, go to the Journals section of the website and locate the  
article in the list of papers for the volume and issue of your specific journal. You will find  
the DOI suffix quoted there.

#### LICENSE CONTINGENT ON PAYMENT

While you may exercise the rights licensed immediately upon issuance of the license at the  
end of the licensing process for the transaction, provided that you have disclosed complete  
and accurate details of your proposed use, no license is finally effective unless and until full  
payment is received from you (by CCC) as provided in CCC's Billing and Payment terms  
and conditions. If full payment is not received on a timely basis, then any license  
preliminarily granted shall be deemed automatically revoked and shall be void as if never  
granted. Further, in the event that you breach any of these terms and conditions or any of  
CCC's Billing and Payment terms and conditions, the license is automatically revoked and  
shall be void as if never granted. Use of materials as described in a revoked license, as well  
as any use of the materials beyond the scope of an unrevoked license, may constitute  
copyright infringement and the RSC reserves the right to take any and all action to protect its  
copyright in the materials.

#### WARRANTIES

The RSC makes no representations or warranties with respect to the licensed material.

#### INDEMNITY

You hereby indemnify and agree to hold harmless the RSC and the CCC, and their  
respective officers, directors, trustees, employees and agents, from and against any and all  
claims arising out of your use of the licensed material other than as specifically authorized  
pursuant to this licence.

#### NO TRANSFER OF LICENSE

This license is personal to you or your publisher and may not be sublicensed, assigned, or  
transferred by you to any other person without the RSC's written permission.

#### NO AMENDMENT EXCEPT IN WRITING

This license may not be amended except in a writing signed by both parties (or, in the case  
of “Other Conditions, v1.2”, by CCC on the RSC's behalf).

#### OBJECTION TO CONTRARY TERMS

You hereby acknowledge and agree that these terms and conditions, together with CCC's  
Billing and Payment terms and conditions (which are incorporated herein), comprise the  
entire agreement between you and the RSC (and CCC) concerning this licensing transaction,  
to the exclusion of all other terms and conditions, written or verbal, express or implied  
(including any terms contained in any purchase order, acknowledgment, check endorsement  
or other writing prepared by you). In the event of any conflict between your obligations  
established by these terms and conditions and those established by CCC's Billing and  
Payment terms and conditions, these terms and conditions shall control.

#### JURISDICTION

This license transaction shall be governed by and construed in accordance with the laws of  
the District of Columbia. You hereby agree to submit to the jurisdiction of the courts located  
in the District of Columbia for purposes of resolving any disputes that may arise in  
connection with this licensing transaction.

#### LIMITED LICENSE

The following terms and conditions apply to specific license types:

1/26/2017

RightsLink Printable License

**Translation**

This permission is granted for non-exclusive world English rights only unless your license was granted for translation rights. If you licensed translation rights you may only translate this content into the languages you requested. A professional translator must perform all translations and reproduce the content word for word preserving the integrity of the article.

**Intranet**

If the licensed material is being posted on an Intranet, the Intranet is to be password-protected and made available only to bona fide students or employees only. All content posted to the Intranet must maintain the copyright information line on the bottom of each image. You must also fully reference the material and include a hypertext link as specified above.

**Copies of Whole Articles**

All copies of whole articles must maintain, if available, the copyright information line on the bottom of each page.

**Other Conditions**

v1.2

Gratis licenses (referencing \$0 in the Total field) are free. Please retain this printable license for your reference. No payment is required.

If you would like to pay for this license now, please remit this license along with your payment made payable to "COPYRIGHT CLEARANCE CENTER" otherwise you will be invoiced within 48 hours of the license date. Payment should be in the form of a check or money order referencing your account number and this invoice number {Invoice Number}.

Once you receive your invoice for this order, you may pay your invoice by credit card.

Please follow instructions provided at that time.

**Make Payment To:**

Copyright Clearance Center

Dept 001

P.O. Box 843006

Boston, MA 02284-3006

For suggestions or comments regarding this order, contact Rightslink Customer Support: [customercare@copyright.com](mailto:customercare@copyright.com) or +1-855-239-3415 (toll free in the US) or +1-978-646-2777.

**Questions? [customercare@copyright.com](mailto:customercare@copyright.com) or +1-855-239-3415 (toll free in the US) or +1-978-646-2777.**

1/26/2017

RightsLink Printable License

**ROYAL SOCIETY OF CHEMISTRY LICENSE  
TERMS AND CONDITIONS**

Jan 26, 2017

This Agreement between Amlan Buragohain ("You") and Royal Society of Chemistry ("Royal Society of Chemistry") consists of your license details and the terms and conditions provided by Royal Society of Chemistry and Copyright Clearance Center.

License Number	4036580336638
License date	Jan 26, 2017
Licensed Content Publisher	Royal Society of Chemistry
Licensed Content Publication	New Journal of Chemistry
Licensed Content Title	Guest-induced reversible structural transitions and concomitant on/off luminescence switching of an Eu(iii) metal-organic framework and its application in detecting picric acid
Licensed Content Author	Ao Li,Liang Li,Zhi Lin,Lin Song,Zi-Hao Wang,Qiang Chen,Tao Yang,Xin-Hui Zhou,Hong-Ping Xiao,Xiu-Ju Yin
Licensed Content Date	Jan 16, 2015
Licensed Content Volume Number	39
Licensed Content Issue Number	3
Type of Use	Thesis/Dissertation
Requestor type	academic/educational
Portion	figures/tables/images
Number of figures/tables/images	1
Format	print and electronic
Distribution quantity	5
Will you be translating?	no
Order reference number	
Title of the thesis/dissertation	Development of functional Metal Organic Frameworks for gas storage and fluorescence sensing application
Expected completion date	Feb 2017
Estimated size	200
Customer Tax ID	IN7086652502
Requestor Location	Amlan Buragohain Department of Chemistry, Lab No. CHL 203 IIT Guwahati Amingaon Guwahati, 781039 India Attn: Amlan Buragohain
Customer VAT ID	IN7086652502
Billing Type	Invoice
Billing Address	

<https://s100.copyright.com/AppDispatchServlet>

1/4

1/26/2017

RightsLink Printable License

Amlan Buragohain  
Department of Chemistry, Lab No. CHL 203  
IIT Guwahati  
Amingaon  
Guwahati, India 781039  
Attn: Amlan Buragohain

Total 0.00 USD

#### Terms and Conditions

This License Agreement is between {Requestor Name} ("You") and The Royal Society of Chemistry ("RSC") provided by the Copyright Clearance Center ("CCC"). The license consists of your order details, the terms and conditions provided by the Royal Society of Chemistry, and the payment terms and conditions.

#### RSC / TERMS AND CONDITIONS

##### INTRODUCTION

The publisher for this copyrighted material is The Royal Society of Chemistry. By clicking "accept" in connection with completing this licensing transaction, you agree that the following terms and conditions apply to this transaction (along with the Billing and Payment terms and conditions established by CCC, at the time that you opened your RightsLink account and that are available at any time at .

##### LICENSE GRANTED

The RSC hereby grants you a non-exclusive license to use the aforementioned material anywhere in the world subject to the terms and conditions indicated herein. Reproduction of the material is confined to the purpose and/or media for which permission is hereby given.

##### RESERVATION OF RIGHTS

The RSC reserves all rights not specifically granted in the combination of (i) the license details provided by your and accepted in the course of this licensing transaction; (ii) these terms and conditions; and (iii) CCC's Billing and Payment terms and conditions.

##### REVOCATION

The RSC reserves the right to revoke this license for any reason, including, but not limited to, advertising and promotional uses of RSC content, third party usage, and incorrect source figure attribution.

##### THIRD-PARTY MATERIAL DISCLAIMER

If part of the material to be used (for example, a figure) has appeared in the RSC publication with credit to another source, permission must also be sought from that source. If the other source is another RSC publication these details should be included in your RightsLink request. If the other source is a third party, permission must be obtained from the third party. The RSC disclaims any responsibility for the reproduction you make of items owned by a third party.

##### PAYMENT OF FEE

If the permission fee for the requested material is waived in this instance, please be advised that any future requests for the reproduction of RSC materials may attract a fee.

##### ACKNOWLEDGEMENT

The reproduction of the licensed material must be accompanied by the following acknowledgement:

Reproduced ("Adapted" or "in part") from {Reference Citation} (or Ref XX) with permission of The Royal Society of Chemistry.

If the licensed material is being reproduced from New Journal of Chemistry (NJC), Photochemical & Photobiological Sciences (PPS) or Physical Chemistry Chemical Physics (PCCP) you must include one of the following acknowledgements:

For figures originally published in NJC:

Reproduced ("Adapted" or "in part") from {Reference Citation} (or Ref XX) with permission of The Royal Society of Chemistry (RSC) on behalf of the European Society for Photobiology, the European Photochemistry Association and the RSC.

For figures originally published in PPS:

1/26/2017

RightsLink Printable License

Reproduced (“Adapted” or “in part”) from {Reference Citation} (or Ref XX) with permission of The Royal Society of Chemistry (RSC) on behalf of the Centre National de la Recherche Scientifique (CNRS) and the RSC.

For figures originally published in PCCP:

Reproduced (“Adapted” or “in part”) from {Reference Citation} (or Ref XX) with permission of the PCCP Owner Societies.

#### HYPERTEXT LINKS

With any material which is being reproduced in electronic form, you must include a hypertext link to the original RSC article on the RSC’s website. The recommended form for the hyperlink is <http://dx.doi.org/10.1039/DOI> suffix, for example in the link <http://dx.doi.org/10.1039/b110420a> the DOI suffix is ‘b110420a’. To find the relevant DOI suffix for the RSC article in question, go to the Journals section of the website and locate the article in the list of papers for the volume and issue of your specific journal. You will find the DOI suffix quoted there.

#### LICENSE CONTINGENT ON PAYMENT

While you may exercise the rights licensed immediately upon issuance of the license at the end of the licensing process for the transaction, provided that you have disclosed complete and accurate details of your proposed use, no license is finally effective unless and until full payment is received from you (by CCC) as provided in CCC's Billing and Payment terms and conditions. If full payment is not received on a timely basis, then any license preliminarily granted shall be deemed automatically revoked and shall be void as if never granted. Further, in the event that you breach any of these terms and conditions or any of CCC's Billing and Payment terms and conditions, the license is automatically revoked and shall be void as if never granted. Use of materials as described in a revoked license, as well as any use of the materials beyond the scope of an unrevoked license, may constitute copyright infringement and the RSC reserves the right to take any and all action to protect its copyright in the materials.

#### WARRANTIES

The RSC makes no representations or warranties with respect to the licensed material.

#### INDEMNITY

You hereby indemnify and agree to hold harmless the RSC and the CCC, and their respective officers, directors, trustees, employees and agents, from and against any and all claims arising out of your use of the licensed material other than as specifically authorized pursuant to this licence.

#### NO TRANSFER OF LICENSE

This license is personal to you or your publisher and may not be sublicensed, assigned, or transferred by you to any other person without the RSC's written permission.

#### NO AMENDMENT EXCEPT IN WRITING

This license may not be amended except in a writing signed by both parties (or, in the case of “Other Conditions, v1.2”, by CCC on the RSC's behalf).

#### OBJECTION TO CONTRARY TERMS

You hereby acknowledge and agree that these terms and conditions, together with CCC's Billing and Payment terms and conditions (which are incorporated herein), comprise the entire agreement between you and the RSC (and CCC) concerning this licensing transaction, to the exclusion of all other terms and conditions, written or verbal, express or implied (including any terms contained in any purchase order, acknowledgment, check endorsement or other writing prepared by you). In the event of any conflict between your obligations established by these terms and conditions and those established by CCC's Billing and Payment terms and conditions, these terms and conditions shall control.

#### JURISDICTION

This license transaction shall be governed by and construed in accordance with the laws of the District of Columbia. You hereby agree to submit to the jurisdiction of the courts located in the District of Columbia for purposes of resolving any disputes that may arise in connection with this licensing transaction.

<https://s100.copyright.com/AppDispatchServlet>

3/4

1/26/2017

RightsLink Printable License

**LIMITED LICENSE**

The following terms and conditions apply to specific license types:

**Translation**

This permission is granted for non-exclusive world English rights only unless your license was granted for translation rights. If you licensed translation rights you may only translate this content into the languages you requested. A professional translator must perform all translations and reproduce the content word for word preserving the integrity of the article.

**Intranet**

If the licensed material is being posted on an Intranet, the Intranet is to be password-protected and made available only to bona fide students or employees only. All content posted to the Intranet must maintain the copyright information line on the bottom of each image. You must also fully reference the material and include a hypertext link as specified above.

**Copies of Whole Articles**

All copies of whole articles must maintain, if available, the copyright information line on the bottom of each page.

**Other Conditions**

v1.2

Gratis licenses (referencing \$0 in the Total field) are free. Please retain this printable license for your reference. No payment is required.

If you would like to pay for this license now, please remit this license along with your payment made payable to "COPYRIGHT CLEARANCE CENTER" otherwise you will be invoiced within 48 hours of the license date. Payment should be in the form of a check or money order referencing your account number and this invoice number {Invoice Number}.

Once you receive your invoice for this order, you may pay your invoice by credit card.

Please follow instructions provided at that time.

**Make Payment To:**

Copyright Clearance Center

Dept 001

P.O. Box 843006

Boston, MA 02284-3006

For suggestions or comments regarding this order, contact Rightslink Customer Support: [customercare@copyright.com](mailto:customercare@copyright.com) or +1-855-239-3415 (toll free in the US) or +1-978-646-2777.

**Questions? [customercare@copyright.com](mailto:customercare@copyright.com) or +1-855-239-3415 (toll free in the US) or +1-978-646-2777.**

**Journal Articles:**

1. **A. Buragohain**, S. Couck, P. Van Der Voort, J. F. M. Denayer, S. Biswas, *Synthesis, Characterization and Sorption Properties of Functionalized Cr-MIL-101-X (X = -F, -Cl, -Br, -CH<sub>3</sub>, -C<sub>6</sub>H<sub>4</sub>, -F<sub>2</sub>, -(CH<sub>3</sub>)<sub>2</sub>) Materials*; **J. Solid State Chem.**, 2016, 238, 195.
2. **A. Buragohain**, S. Biswas, *Cerium based azide- and nitro-functionalized UiO-66 frameworks as turn-on fluorescent probes for the sensing of hydrogen sulphide*; **CrystEngComm**, 2016, 18, 4374.
3. **A. Buragohain**, M. Yousufuddin, M. Sarma, and S. Biswas, *3D Luminescent Amide-Functionalized Cadmium Tetrazolate Framework for Selective Detection of 2,4,6-Trinitrophenol*; **Cryst. Growth Des.**, 2016, 16, 842.
4. **A. Buragohain**, P. Van Der Voort, S. Biswas, *Facile Synthesis and Gas Adsorption Behavior of New Functionalized Al-MIL-101-X (X = -CH<sub>3</sub>, -NO<sub>2</sub>, -OCH<sub>3</sub>, -C<sub>6</sub>H<sub>4</sub>, -F<sub>2</sub>, -(CH<sub>3</sub>)<sub>2</sub>, -(OCH<sub>3</sub>)<sub>2</sub>) Materials*; **Microporous Mesoporous Mater.**, 2015, 215, 91.
5. **A. Buragohain**, S. Biswas, *Improved Synthesis of Zirconium (IV) Muconate Metal-Organic Framework: Characterization, Stability and Gas Sorption Properties*; **Eur. J. Inorg. Chem.**, 2015, 2463.

**Conferences Attended:****Poster Presentations**

1. **Amlan Buragohain** and Shyam Biswas, '*Selective detection of 2,4,6-trinitrophenol by newly designed 3D luminescent amide-functionalized Cadmium tetrazolate framework*'. Poster presented at UGC-SAP National Conference on Contemporary Developments in Chemical Sciences (CDCS)-2015, Nov 23-24, 2015, Tezpur University, India.
2. **Amlan Buragohain** and Shyam Biswas, '*Improved Synthesis of Zirconium(IV) Muconate Metal-Organic Framework: Characterization, Stability and Sorption Properties*'. Poster presented at Frontiers in Chemical Sciences (FICS) National Conference, Dec 04-06, 2014, IIT Guwahati, India.

